Evaluation of New Methods for Source Apportionment Using Real-Time Continuous Monitoring Instruments

October 2010

Produced cooperatively by
The Puget Sound Clean Air Agency and the University of Washington

Funded by United States Environmental Protection Agency and the Puget Sound Clean Air Agency under Grant Agreement XA96066801

Project Manager
Kathy Himes Strange and Mike Gilroy
Puget Sound Clean Air Agency
1904 Third Avenue, Suite 105
Seattle, WA 98101

Principal Investigator
Michael Yost, PhD
University of Washington
1959 NE Pacific St., HSB F225
Seattle, WA 98195

pscleanair.org
Puget Sound Clean Air Agency

SCHOOL OF PUBLIC HEALTH
UNIVERSITY of WASHINGTON

EPA
United States
Environmental Protection
Agency

Acknowledgments and Contact

We would like to thank the EPA for funding this valuable work. We also would like to acknowledge the efforts made by the University of Washington including Dr. Tim Larson, Dr. Mike Yost, Dr. Chris Simpson, and Dr. Yinhai Wang and their staff Jake Braden, Eric Coker, Cole Fitzpatrick, Sashidharan Komandur, Gretchen Onstad, Yu Runze, Maria Tchong-French, and Rob Crampton.

The entire monitoring group at the Puget Sound Clean Air Agency pitched in to make this project a success under the leadership of Erik Saganic and Matt Harper.

For more information about this report, please contact Erik Saganic at (206) 689-4003, eriks@pscleanair.org.

Table of Contents

List of Figures

List of Tables

Executive Summary

With funding from a US EPA grant, the Puget Sound Clean Air Agency and the University of Washington evaluated a number of novel methods to estimate diesel emissions and to characterize diesel sources, including vehicles and marine vessels.

Diesel particulate matter (DPM) remains the largest contributor to potential cancer risk in the Puget Sound area and many areas nationally.[42] Thus far, no direct way to monitor diesel emissions exists. Estimates of DPM are highly uncertain and require expensive and lengthy sampling schedules (up to 3 years). Additionally, traditional positive matrix factorization (PMF) based on speciation sampling cannot distinguish unique diesel sources.

Using hourly $PM_{2.5}$, non-methane hydrocarbon, and aethalometer data, a source apportionment model was developed and applied to a diesel impacted site (Seattle Duwamish). In this effort, we applied PMF to hourly continuous data to distinguish 7 source related factors. Illustrating the complex nature of DPM, these multiple source contributions create a multifaceted set of factors that relate PM, hydrocarbons, and different types of mobile sources.

Using hourly hydrocarbon data, we characterized three distinct features related to motor vehicle emissions: "High Load Diesel", "Gasoline/LPG" and "Idling/Crankcase Diesel". In addition, we associated a factor with combustion exhaust and fuel evaporative emissions described as "Fueling/Port Operations". Highly time resolved hydrocarbon data demonstrated significant potential to successfully resolve different vehicle sources, such as gasoline, truck, and marine emissions.

Two wood smoke features, one with higher gas concentrations, "Wood Smoke 1", and one with higher particle concentrations, "Wood Smoke 2", were identified. These factors show that the source contribution to PM at the site is due to many sources, and reflects a variety of factors other than the nearby highway and industrial activities. The "Wood Smoke 1" factor accounts for ~60% of the total benzene concentration. This benzene contribution complements our recent air toxics study which identified wood smoke impacted sites had the highest concentrations of benzene in the Puget Sound region.[42]

Source-related factors at the Seattle Duwamish site derived from PMF 3.0 based on hourly measurements of n-alkanes and selected fine particle metrics.

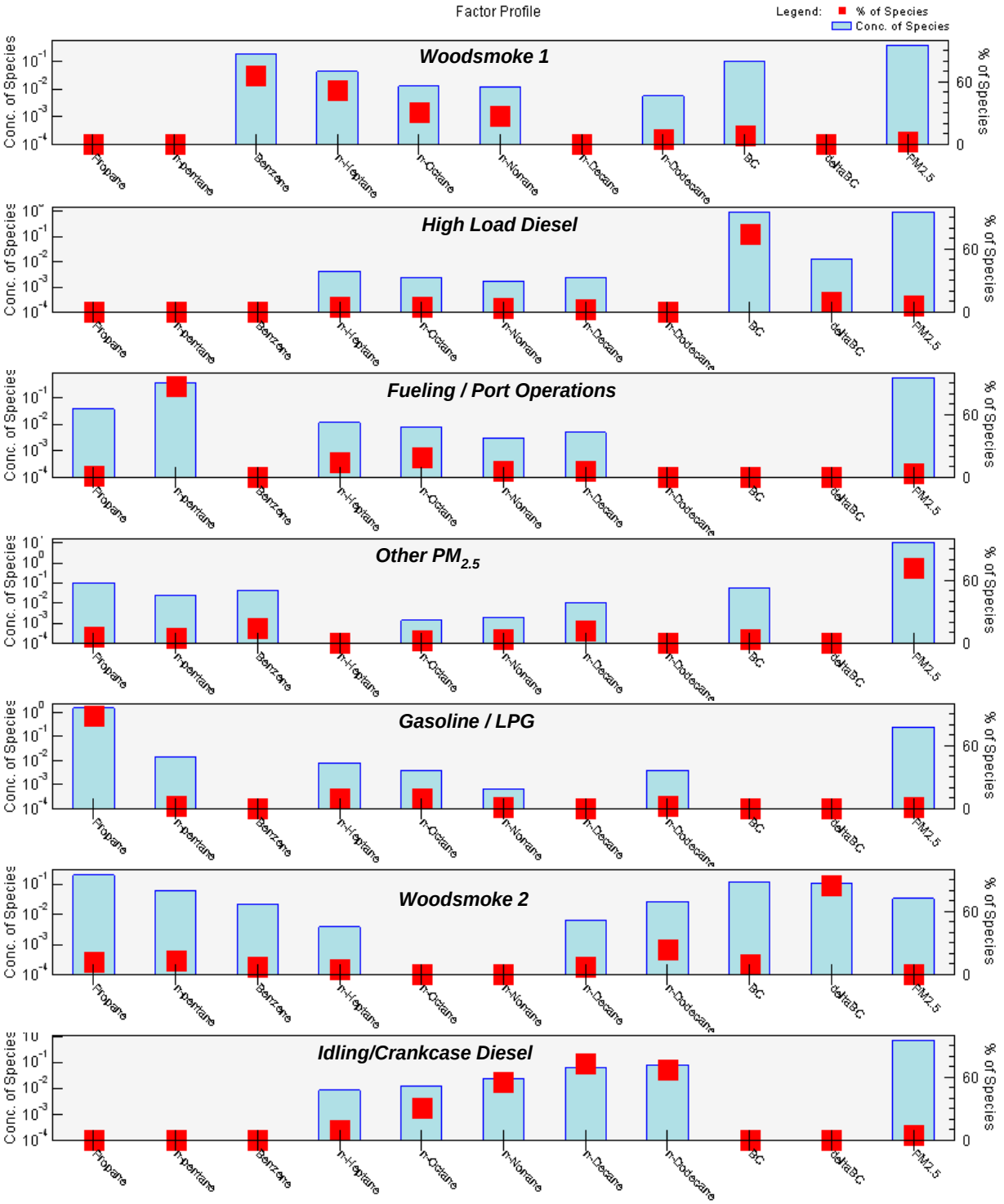

The 1057 hourly measurements were collected over four different sampling periods in 2009: 1/28–2/6, 3/29–4/9, 5/6-5/26, and 7/30-8/11.

The PMF source factors account for more than 94% of the variability in PM, but a substantial portion of the PM is not highly associated with hydrocarbon traffic sources. Therefore, most of the PM was found in the "Other $PM_{2.5}$" factor, which included the majority of the variance.

A marker for diesel exhaust (1-nitropyrene) was successfully linked to both truck traffic and the hourly PMF "High Load Diesel" factor. This study is the first to measure nitro-polycyclic aromatic hydrocarbons (NPAHs) in ambient PM in the Seattle area. 1-nitropyrene has been proposed as a molecular marker for diesel particulate matter (DPM) since it is by far the most abundant NPAH in DPM, while being much less abundant in PM derived from other sources.[1]

The measurements reported herein support the use of 1-nitropyrene (1-NP) as a molecular marker for diesel particulate matter. 1-NP was measured in PM collected on readily available, post-weighed Teflon filters using standard $PM_{2.5}$ Federal Reference Method (FRM) sampling methods.

1-NP levels showed a significant association with heavy truck counts on SR-99, and the weekday to weekend ratio of 1-NP concentrations paralleled the weekday to weekend ratio of heavy truck counts. 1-NP was also significantly associated with other traffic derived air pollutants including 1,3-butadiene, acetaldehyde, benzene, black carbon, elemental carbon, and naphthalene. Additionally, 1-NP was associated with the "High Load Diesel" source feature from the hourly PMF results.

Box Plots of 1-nitropyrene (pg/m^3) and "Heavy Trucks" on Weekends versus Weekdays

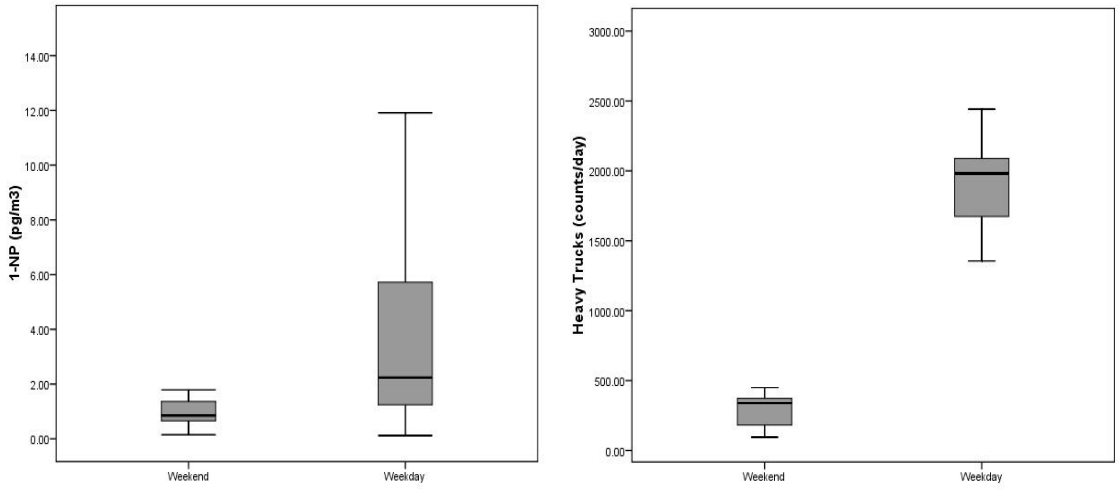

A multivariate analysis showed that volatile organic compounds (VOC) data can identify source markers for vehicles and other sources. This analysis also demonstrated additional relationships to the hourly PMF analysis. Based on multiple linear regression analysis, a subset of the VOC data was found to have statistically significant associations with hourly $PM_{2.5}$, truck traffic, and passenger vehicle traffic. The data generated by the real-time monitoring instruments consisted of 61 different variables observed on an hourly basis; more than 40 of these were VOC species retrieved from a gas chromatogram typically used in EPA ozone precursor analysis. A multivariate analysis showed that the VOC data can provide a source marker for vehicles and other sources, and this is associated with both truck (and car) traffic and $PM_{2.5}$ levels at the site.

The multivariate analysis identified many species that also appeared in the PMF analysis to apportion $PM_{2.5}$. This lends considerable weight to the reliability of the PMF analysis, which identified several vehicle-related sources for PM at the site. The data set selected for this analysis mainly comes from the non-heating season, which emphasized traffic-related impacts, in keeping with the aims of the study. A more comprehensive analysis with the inclusion of the 1 in 6 speciation data collected across all seasons may be warranted.

Remote monitoring of marine traffic to estimate diesel impacts is feasible with existing data sources and tools. AIS logging was shown to be particularly useful for collecting information on ship movements and activities. With appropriate linkage to other data sources, passive AIS data collection can be used to estimate emissions from ship traffic and to classify ships by size and activities. The demonstration modeling project, showed that in principle it was possible to track a vessel both in transit and in port, and model the emissions during this entire time. This approach to monitoring ship traffic offers an attractive and relatively low cost means of estimating marine emissions, but further validation of the modeling results is needed.

Direct monitoring of ship emissions with LIDAR was conducted, and successful data collection was obtained for ships docked at the Port of Seattle from a significant distance. Although many attempts were made to capture ships in transit, this proved very difficult and was unsuccessful because of the rapid movements of the ships and the difficulty of deploying the portable LIDAR system in time to observe ships once notification was received that they were underway. The study showed that direct observations of ships in transit with LIDAR would require a much more intensive sampling effort, and would require a long-term field deployment of this equipment for monitoring.

A new method for processing Photochemical Assessment Monitoring Stations (PAMS) Ozone Precursor Analyzer data was developed. An indirect benefit of this project was the introduction of a new process to align spectral data from the gas chromatographs used in the PAMS network. The procedure uses a software package (LineUp, InfoMetrix Inc) to align the chromatograms that typically drift with slight temperature and/or carrier gas pressure changes. These aligned files can then be batch processed, also in an automated manner, by the chromatography software package to identify and quantify VOCs present in the samples. This procedure dramatically reduced the amount of analyst time required to process the hourly GC data. Automation of the alignment process also has the advantage of removing potential for operator error or subjective operator identification of the peaks. This automated alignment procedure should prove especially useful to the EPA PAMS network operators, that use gas chromatography to measure 40+ VOCs on an hourly timescale.

Example of an alignment result for 5 consecutive spectra.

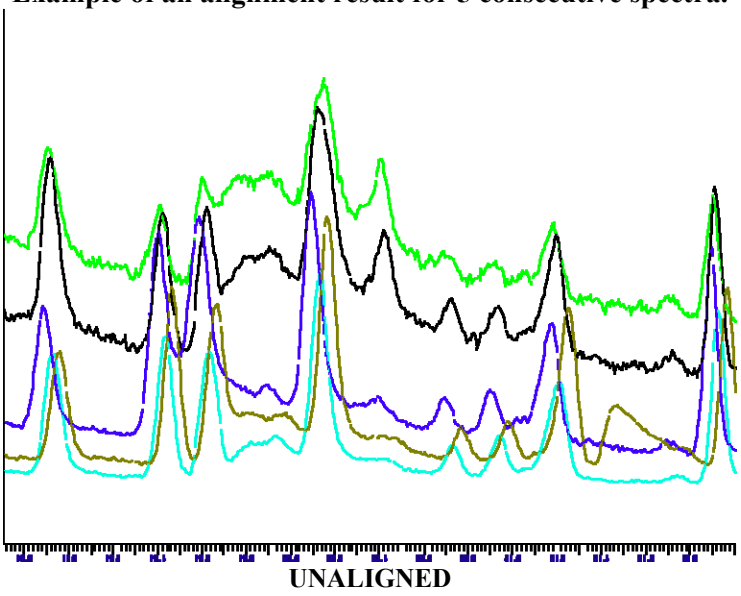

UNALIGNED

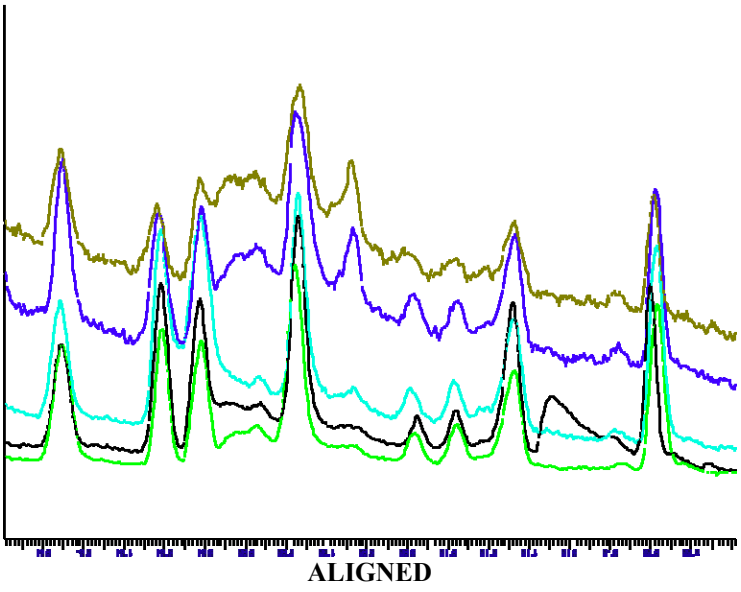

ALIGNED

The use of Open Path Fourier Transform Infrared Spectroscopy (OP-FTIR) for resolving gasoline and diesel emissions proved difficult. The OP-FTIR had unanticipated equipment failures contributed to reduced data collection during the study and only the May study period was selected for analysis. The instrument was able to measure ambient CO and CH_4 at the site, with 5 minute time resolution. After removing the methane features from the May dataset, the residual non-methane hydrocarbon feature was too small to provide reliable data for classifying gas and diesel vehicle signatures using a simple algorithm based on the C-H stretch spectrum.

Site access restrictions limited the beam path for the FTIR to only 71 meters, which was much shorter than desired (> 200 m). In addition, the beam path could only be located perpendicular to and some distance back from the roadway, rather than running across the highway or parallel to traffic. This configuration probably contributed to reduced roadway hydrocarbons in the beam, and coupled with the limited path length resulted in insufficient signal for the non-methane hydrocarbon analysis.

However, the study did demonstrate that this method was not very robust for measurements at ambient concentrations. The instrument could have had more optimal conditions, but it may still not prove successful at ambient concentrations.

A preliminary analysis combining hourly data with speciation data from 24 hour samples also offered very limited data. A preliminary analysis also was conducted to combine the hourly data with the 1 in 6 speciation data from 24 hour samples, along with other markers such as levoglucosan. This analysis indicated that the "other PM" source had major factors related to OC rich, 1-nitropyrene rich fuel oil and secondary aerosol sources.

These data are limited because there is very little overlap (~10 days) in the two data sets. This makes it difficult to compare these results directly with the results of the PMF apportionment based on the hourly data. Also given the relatively sparse $PM_{2.5}$ speciation data at this site (~ 60 days) we cannot readily identify all possible source-related features influencing the daily $PM_{2.5}$ speciation data.

Processing of additional time periods for the hourly GC data to provide more overlap with the speciation data would strengthen the source apportionment of this other $PM_{2.5}$ data. The current results suggest there may be value in evaluating a source apportionment approach that combines both the multiple linear regression analysis and PMF. The multiple linear regression analysis would be used to pre-select variables for subsequent inclusion in the PMF model.

1. Introduction

Diesel particulate matter (DPM) has been identified as one of the top air toxics of concern in the Puget Sound area. Puget Sound Clean Air Agency (the Agency) studies have highlighted diesel particulate matter as the most significant air toxic, with up to 75% of the potential cancer risk attributed to this pollutant.[2] Estimates of ambient DPM exposures have been based primarily on receptor modeling results taken from monitoring data at the Seattle Beacon Hill site, operated by the Washington State Department of Ecology (Ecology). However, these estimates vary depending upon the type of speciated data (Interagency Monitoring of Protected Visual Environments [IMPROVE] vs. Chemical Speciation Network [CSN]), the sample period of interest, and the specific algorithm used in the positive matrix factorization (PMF) model. The inconsistent apportionment results indicate that diesel and gasoline aerosol fractions are poorly understood, underscoring the inadequacies of relying on the Seattle Beacon Hill site (a residential site) alone to drive our understanding of air toxics in other areas where impacts likely are higher.

Numerous urban receptor modeling studies, such as Scheff et al[3] in Chicago, have apportioned the sources of non-methane hydrocarbons in urban air to distinguish mobile source contributions. Watson[4] provided a comprehensive review of the studies done prior to 2001. A number of the more recent studies have used EPA's chemical mass balance (CMB) model to distinguish vehicle exhaust contributions from other volatile organic compound (VOC) sources like gasoline evaporative losses and stationary sources [5,6,7,8,9,10,11,12,13] while other studies have employed multivariate receptor models to obtain both source-related features and associated source contributions.[14,15,16,17,18,19,20,21,22,23,31,32]

PMF and Unmix are statistical algorithms that solve the chemical mass balance model as a factor analysis problem without requiring prior source profiles as inputs.[38] Many studies have reported separate contribution estimates to total measured VOCs from heavy-duty and light-duty vehicle exhaust, using PMF,[31,33] Unmix,[32] CMB,[25,30,31,32] multivariate receptor models,[34] or by direct correlation with traffic information.[24,25]

This study undertook a multifaceted approach to better understand diesel emissions. New source apportionment models using multiple data sources were developed and applied to a site impacted

primarily by both gasoline and diesel vehicle traffic. In this effort, we attempted to use gas-phase hydrocarbon concentrations measured with a gas chromatograph (GC), 1-nitropyrene (1-NP) measurements on filters, measured car and truck traffic data, aethalometer data, existing CSN speciation data, and Fourier transform infrared spectroscopy (FTIR).

One objective of this study was to develop mobile source apportionment models based on the continuous non-methane hydrocarbon (NMHC) measurements provided from the gas chromatograph. In addition, these data were compared with on-site traffic monitoring data and traditional filter sampling methods in an attempt to validate this monitoring tool. The availability of hourly source profile monitoring provides an increased temporal resolution for evaluating diesel exhaust and gasoline vehicle impacts for more accurate apportionment of mobile sources.

A second aim of the study was to combine the NMHC apportionment methods developed here with traditional 24-hour filter and other sampler data to provide a more complete source apportionment picture of all particulate sources. This approach combines the short term NMHC assessment with the more traditional 24-hour measurements of air toxics which accounts for a very broad range of particulate sources, and improve apportionment of both mobile and stationary (including natural) particulate sources.

An additional approach to understanding area diesel sources was to monitor maritime activities. Real concern exists in understanding the areas in the Puget Sound region that are impacted by port activities and direct maritime diesel emissions. For these areas, determining the onshore impact from maritime vessels at sea would be helpful. Meteorological conditions that result in the largest diesel emission concentrations could be identified to better understand diesel exhaust exposure.

Therefore, an additional objective of the study was to use LIDAR (light detection and ranging), which is an optical remote sensing technology that measures properties of scattered light of a distant target, to directly monitor diesel emissions from maritime sources. Making these observations under a variety of wind conditions, and combining these observations with data on ship traffic and modeling, we can determine how these sources could impact populated regions.

We also developed an interface that collects information on commercial ship traffic from the Automatic Identification System (AIS), an automated tracking system used on ships and by Vessel Traffic Services (VTS) for identifying and locating vessels by electronically exchanging data with other nearby ships and VTS stations. This interface can be used to monitor activities of commercial ships in Puget Sound. We demonstrate that the AIS data can be combined with a dispersion model to predict impacts of marine emissions on air quality in the Seattle area.

This study also evaluated the use of an open-path Fourier transform infrared spectrometer (FTIR) for the apportionment of ambient concentrations of gasoline and diesel emissions. The FTIR has been used as a proven method for source testing for hazardous pollutants, and would be useful tool if it were successful.[26]

2. Site Description and Methods Overview

2.1. Seattle Duwamish Monitoring Site

The Seattle Duwamish monitoring site has been in place since 1971 in the heart of the Duwamish industrial valley. Before 2005, the site was in the parking lot across E. Marginal Way from the Federal Center South property. Since 2005, the site has been located on the property of the WA state liquor control board warehouse facility. The site is a neighborhood scale site that is representative of South Seattle neighborhoods and ambient exposure in the industrial valley. The site is influenced by a very complex mixture of mobile sources, marine sources, industrial sources, winter home heating wood smoke, and other pollution sources. The site is 80 meters west of E. Marginal Way (Highway 99), which is a main arterial for many large haul trucks as well as service vehicles, and personal automobiles. This monitoring site consistently has the highest annual average $PM_{2.5}$ concentration of any other monitoring site in Washington, but is below the federal annual standard, indicating that the area is in attainment of the current fine particle NAAQS levels.

The Seattle monitoring site was chosen to primarily gain perspective on diesel emission estimates and understanding from previously conducted source apportionment analyses. As a purpose was to develop monitoring methods that have shown potential to differentiate diesel particulate matter from other sources, the Seattle Duwamish site's industrial exposure was well suited for analysis. The pollutants monitored are summarized below in Table 2.1.

Data collected here included continuous fine particulate matter (PM) data, speciated fine particle data (metals, ions, and carbonaceous compounds), continuous aethalometer black carbon (BC) and ultraviolet carbon (UV), Federal Reference Method (FRM) $PM_{2.5}$ filters, which were then analyzed for levoglucosan content and 1-nitropyrene content, and meteorological data. Additionally, air toxics data from canisters (volatile organic compounds), PUF sample media (polycyclic organic hydrocarbons), DNPH tubes (carbonyl compounds), MIMS mobile monitoring data (volatile organic compounds), gas chromatograph data (non-methane hydrocarbons), Fourier transform infrared spectroscopy (hydrocarbons), and total particle bound polycyclic aromatic hydrocarbons were collected. Automatic Identification System data was used to collect ship tracking information. As needed, collocated samplers collected data for quality assurance purposes for assessing accuracy and precision.

Table 2.1 List of methods monitored at the Seattle Duwamish fixed site

Method	**Major Toxic Species (other species were analyzed based on the available suite of the analysis)**
1 in 3 or 1 in 6 day, 24-hour sampling for $PM_{2.5}$ by Federal Reference Method	$PM_{2.5}$ (24-hour)
1 in 6 day, 24-hour sampling for $PM_{2.5}$ by Federal Reference Method	1-Nitropyrene Levoglucosan
1 in 6 day, 24-hour sampling speciation by URG3000N and Met One SASS	Carbon compounds Ions Metals (60 total species)
Tapered element oscillating microbalance (TEOM) with filter dynamic measurement system (FDMS)	$PM_{2.5}$ (Hourly)
$PM_{2.5}$ continuous aethalometer	Black Carbon Channel (Absorption 880 nm) UV Channel (Absorption 370 nm)
Hourly gas sampling by Gas Chromatography – Flame Ionization Detector (GC-FID)	Propane Hexane Benzene n-Dodecane 46 other gas phase species
Hourly FTIR Fourier Transform infrared	Carbon monoxide Methane Water Attempted C-H stretches from hydrocarbons
LIDAR (Light Detection And Ranging)	Ship plume spatial light scattering
Hourly traffic counts by loop and video detection	Traffic counts in several different bins
Meteorological parameters	Wind direction Wind speed Temperature Relative humidity Ambient pressure
Automatic Identification System	Ship tracking information including location, speed, and other ship identifiers.

2.2. Monitoring Methods

During the course of this study, where possible, we used existing equipment and methods that have become standards in the EPA NATTS (National Air Toxics Trends Network) and UATMP (Urban Air Toxics Monitoring Program). The following summarizes each monitoring method used during the study. The Quality Assurance Project Plan provides detailed descriptions of the methods used.

2.2.1 Gas Chromatograph (GC)

Non-methane hydrocarbons (NMHC) are monitored routinely in the Photochemical Assessment Monitoring Stations (PAMS) network. In this study, the same guidance and procedures were used. A detailed description of sampling for NMHC samples has been described in the *Perkin Elmer GC Manual for Ozone Precursor Analysis*.[27] Additional resources include the EPA *Technical Assistance Document for Sampling and Analysis of Ozone Precursors* and the EPA *PAMS Implementation Manual*.[28] Additionally, the data validation process was outlined in the Quality Assurance Project Plan for this project.

The instrument system used to sample the NMHCs is an automatic thermal desorber (ATD) coupled to a gas chromatograph equipped with a flame ionization detector (FID). The manufacturer is Perkin Elmer with model numbers ATD 300 and GC Clarus 500.

The instrument sampling design had a stainless steel probe with insulation and heat-tape set to ~40ºC to avoid summer condensation in the probe. An EPA certified PAMS calibration gas cylinder was also installed to perform 1-point calibrations on the instrument and routine daily checks. EPA PAMS certified gas was used through this study period. The system was equipped with a Nafion dryer to draw most moisture out of the sample prior to entering the instrument. The instrument sampled at a rate of 50 mL/min for 40 minute collection times for each hour. Sampling occurred hourly. Hydrogen was used as the carrier gas and FID fuel. Zero-air dried with Drierite/5Å molecular sieves was used for the FID fuel, Nafion dryer, and cold trap purge. Table 2.2 provides design and performance specifications for this method. Data was collected and analyzed until it was deemed to be representative. The sample undergoes a split into a BP1 column for 6 to 12 carbon compounds, and a PLOT column for 2 to 6 carbon compounds. A full list of the analytes measured with the GC can be found in Table 2.2.1 below. The instrument operated continuously for almost a full year at the site, and a portion of that data series was selected for post-acquisition processing and incorporation into the source apportionment analysis. The sampling dates used for the study are listed in Table 2.2.2. These dates were chosen to target high pollution data during multiple seasons.

Table 2.2: Non-Methane Hydrocarbon Sampling Specifications

Equipment	Frequency	Acceptance Criteria	Reference
General Specifications			
Probe Type		Stainless Steel, 1/4"	TO-15
Probe Heating Temp		Width	
Carrier Gas Flow		40ºC ± 10ºC	Vendor Spec.
FID Fuel Flow Rate		5 mL/min	Vendor Spec.
Nafion Dryer Flow		~ 90 mL/min	Vendor Spec.
Rate	–	~ 250 mL/min	Vendor Spec.
Min Carrier Gas		~ 500 psi	Vendor Spec.
Pressure		99.995%	Vendor Spec.
Hydrogen Purity		~ 1.6 L/min	Vendor Spec.
Zero-Air Flow Rate		< 0.1 ppm Hydrocarbons	Vendor Spec.
Zero-Air Purity		-50ºC Dew Point	
Cal Gas Accuracy		10%	Gas Vendor Spec.
Sampler Performance Specifications			
Sample Flow Rate		50mL/min	
Flow Regulation		1mL/min	Vendor Spec.
Flow Rate Precision		1mL/min	Vendor Spec.
TD Leak Check	Hourly	0 psi	Vendor Spec.
Calibration Check	Daily	>5ppbv, ±50%	Regions I, II, III PAMS
		Results > 1ppbv reported	Regions I, II, III PAMS
Time Accuracy		< 5 minute error	

Table 2.2.1: Compounds measured hourly by the GC-FID. Items labeled with (*) were used in the source apportionment analysis.

PLOT Column Compounds (C2-C6)	BP-1 Column Compounds (C6-C12)
Propane*	n-Hexane
Propylene	3-Methylpentane
Isobutane	Methylcyclopentane
n-Butane*	2,4-Dimethylpentane
t-2-Butene	Benzene*
1-Butene	Cyclohexane
c-2-Butene	2-Methylhexane*
Isopentane	2,3-Dimethylpentane
n-Pentane*	3-Methylhexane
t-2-Pentene	2,2,4-Trimethylpentane
1-Pentene	n-Heptane*
c-2-Pentene	Methylcyclohexane
2,2-Dimethylbutane	2,3,4-Trimethylpentane
Isoprene	Toluene*
	2-Methylheptane
	3-Methylheptane
	n-Octane*
	Ethylbenzene*
	m & p-Xylene*
	Styrene
	o-Xylene
	n-Nonane*
	Isopropylbenzene
	n-Propylbenzene
	1,3,5-Trimethylbenzene
	o-Ethyltoluene
	1,2,4-Trimethylbenzene
	n-Decane*
	1,2,3-Trimethylbenzene*
	m-Diethylbenzene
	p-Diethylbenzene
	n-Undecane
	n-Dodecane*

Table 2.2.2 Data periods used for study.

Analyzed Periods	Start	End
Period 1:	01/28/09 0:00	02/06/09 23:00
Period 2:	03/29/09 15:00	04/09/09 15:00
Period 3:	05/06/09 18:00	05/27/09 0:00
Period 4:	07/30/09 01:00	08/12/09 0:00

2.2.2 Open path Fourier transform infrared spectroscopy (OP-FTIR)

Open path Fourier transform infrared spectroscopy has proven to be useful for quantification of numerous gaseous species including many air toxics. EPA's FTIR Open Path Guidance document provides a detailed description of this technique. The IR spectrum captures all detectable contaminants having a dipole moment over the beam path. As described in EPA compendium method TO-16, quantification of multiple VOC species is possible using Beer's Law and multivariate techniques.

Prior to this study, a preliminary method was developed to apportion hydrocarbon emissions observed with OP-FTIR due to diesel fuel or gasoline fuel vehicles. In summary, compounds found in diesel on average have more unsaturated hydrocarbons and have higher energy C-H stretches on the IR spectrum. Gasoline has more saturated hydrocarbons and lower energy C-H stretches:

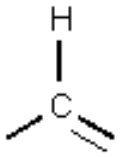

(C-H Absorption ~ 3000 cm^{-1})

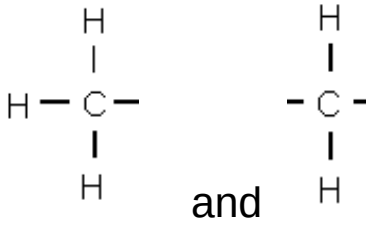

and

(C-H Absorption ~ 2850cm^{-1})

An OP-FTIR collected 400 spectra from 15 vehicles, five powered by diesel engine and the others by gasoline. The hydrocarbon C-H band from 2850 cm^{-1} to 3000 cm^{-1} was analyzed to distinguish the two classes of engines. The C-H region was divided into 30 sub-bands of 6 cm^{-1} resolution for analyses. Discriminant function analysis correctly classified 100% of the training set spectra (n=200) and 98% of the validation set (n=200). Altering the band resolution or signal-to-noise did not significantly decrease the model prediction ability; the model still correctly classified vehicles until the noise was approximately equal to the peak signal.

We hoped to apply this model to ambient air concentrations near the Seattle Duwamish site, which is located on state highway 99 and has substantial car and truck traffic. This model would be useful in proportioning both diesel and gasoline contributions in ambient air.

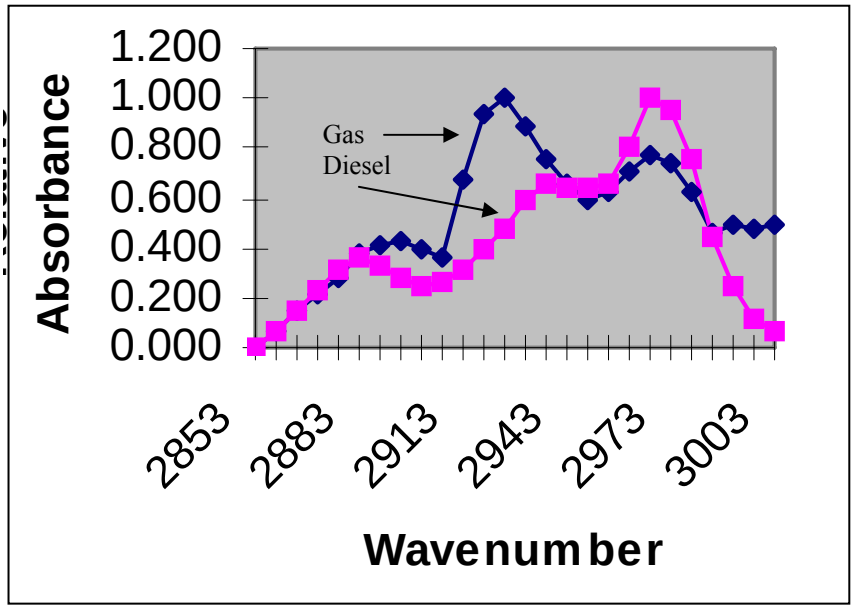

Figure 2.2.1: Gas vs. Diesel Normalized Peak Height

Successful classification of the 2 vehicle groups depends on hydrocarbon signatures from each type. The basis of the classification is shown graphically in a peak height normalized plot (Fig. 2.2.1) of all vehicles by fuel type. Figure 2.2.1 shows significant differences in the C-H bands of emissions from vehicles from the different fuel classes (gas and diesel). The diesel peak falls at 2925cm^{-1} and the gasoline peak around 2967cm^{-1}. Each point on the X axis of this plot represents a variable in the classification model. The diesel apportionment method described here depends only on the relative shape of C-H profiles, not the spectra of individual components. Since more than 30 hydrocarbon compounds contribute to the C-H region, this approach avoids the problem of missing data that occurs when using individual chemical species. The weighted model score gives a probability of classification into either diesel or gasoline vehicle for a spectrum. An ensemble of spectra over many vehicles may be interpreted as the proportion of diesel or gasoline vehicle contribution to the hydrocarbon signature.

2.2.3 $PM_{2.5}$ Continuous Instrumentation

Continuous $PM_{2.5}$ data collection occurred at the Seattle Duwamish site using the TEOM-FDMS (tapered element oscillating microbalance with filter dynamics measurement system). The TEOM-FDMS samples air through an impactor to aerodynamically isolate $PM_{2.5}$. The air sample goes through a filter that is on an oscillating tube. As the weight of the filter increases, the

instrument measures the change in frequency due to the increased mass on the filter. The mass is divided by the sample volume to obtain $PM_{2.5}$ in micrograms per cubic meter of ambient air. Through the use of the filter dynamic measurement system, the volume of pollution mass which is volatile is also measured and added to the fraction of $PM_{2.5}$ to obtain a more accurate measurement.

Black carbon channel and the ultraviolet (UV) channel measurements were made using a dual channel Aethalometer. The Aethalometer takes a sample of air and passes it through a glass fiber filter tape. The tape is measured continuously for light absorbance at both 880 nm (BC), and 370 nm (UV). The light absorbance is calibrated to micrograms per cubic meter using a standard proprietary equation.

2.2.4 Vehicle Traffic

Traffic volumes change significantly over time and location. Traffic sensors are needed to capture real-time traffic variations. Inductance loop detectors have been widely deployed in the central Puget Sound region. There is a loop detector station about every half mile on mainline lanes and freeway ramps in the Greater Seattle area.[29] About half of these are dual-loop detectors, measuring speed and classified vehicle volume data. Vehicles are classified based on their lengths, and assigned to one of the following four bins: (a) Bin 1, passenger cars and other smaller vehicles (length <26 ft); (b) Bin 2, single-unit trucks and vehicles pulling trailers (26 ft to 39 ft); (c) Bin 3, combination trucks and buses (39 ft to 65 ft); and (d) Bin 4, multi-trailer trucks (length greater than 65 ft). Archived loop-detector data of 20-second intervals can be downloaded from the Traffic Data Acquisition and Distribution (TDAD) website to support this project.

For the selected study location at the Duwamish site, classified traffic volumes were collected from an innovative wireless magnetic detector system installed in the roadway. These small (4" diameter) sensors detect disturbance of the earth's magnetic field caused by the presence of a vehicle, and use wireless technology to transmit the information to a nearby access point. The sensors can be easily imbedded into the roadway and provide a reliable and low-cost alternative to traditional dual-loop inductive detectors. Algorithms were applied to estimate long vehicle volumes (Bins 2, 3 & 4) from single-loop measurements at this site.[30,31] Loop detectors are subject to various malfunctions and a different method is needed to support air quality

considerations.[32,33,34] We also used the Video-based Vehicle Detection and Classification (VVDC) system developed by the Smart Transportation Applications and Research Laboratory (STAR Lab) at the University of Washington to demonstrate an alternative means for collecting traffic data from traffic cameras. The system was applied to extract bin volumes from video images at an intersection where loop detectors also were present to validate the traffic counts. The VVDC system was tested under different traffic and environmental conditions and achieved exceptional results in both vehicle detection and classification: the accuracy for vehicle detection was above 97% and the total truck count error was lower than 9%.[35] This innovative traffic data collection effort enhances the quality of diesel truck volume data which are critical inputs to evaluate the air toxics models developed in this study.

2.2.5 PMF Modeling

Although most receptor-based source apportionment modeling has been focused on apportioning the sources of fine particles, some applications have examined the sources of other pollutants. Following the initial work of Scheff et al.[36] in Chicago, numerous urban receptor modeling studies have apportioned the sources of non-methane hydrocarbons in urban air. Watson[37] provides a comprehensive review of the studies done prior to 2001.

To date, however, we know of no attempts to combine VOC and particle measurements in a single receptor model. Here we attempt to do so using a highly time-resolved data set. The data consists of simultaneous hourly data of selected VOCs, $PM_{2.5}$, and light absorption coefficient measured at two different wavelengths in order to obtain hourly estimates of selected $PM_{2.5}$ source contributions. Standard positive matrix factorization (EPA's PMF3.0) was applied to selected species in the hourly data set.

To distinguish diesel PM from other motor-vehicle related PM, we used hourly concentrations of selected n-alkanes and benzene from the data set described in Chapter 4. We also included a limited set of hourly fine particle measures, including $PM_{2.5}$, black carbon, and "delta carbon". This latter variable is based on the difference in light absorption values at two different wavelengths and its ambient concentration is claimed to be dominated by wood smoke rather than vehicle exhaust[38]. We chose to use estimated uncertainties in the PMF model based upon MDL and percent uncertainty. The values are shown in Table 2.2.3 below. The hourly concentrations for the selected hydrocarbons were based upon daily calibrations.

The intent of including the PM metrics was not to apportion all the sources of PM; it was to apportion the PM associated with heavy and light duty vehicles. Our approach has the advantage of including $PM_{2.5}$ measurements directly in the model without the complications associated with the use of $PM_{2.5}$ as well as its sub-component species in the same model. Given that motor vehicles are not the major source of $PM_{2.5,}$ there is by definition one feature representing the "other" sources of $PM_{2.5}$ that are not correlated with these selected species.

We address the question of "other" sources of $PM_{2.5}$ by comparing the sources derived from the apportionment of the hourly observations at this location with those derived from daily $PM_{2.5}$ speciation data. A limitation of this approach is that the hourly and daily data sets do not overlap very much. There are only 10 days in which we have simultaneous measurements of both daily $PM_{2.5}$ species and hourly VOC and particle data. Another limitation is the relative small number of available daily data with which to base a PMF model. To address this latter issue, we combined the available daily 1-nitropyrene and levoglucosan measurements, where available, and with the standard EPA speciation data. In all, there were 61 days of available $PM_{2.5}$ speciation data from this site that were collected between 11/08 and 10/09. During this period, there were 41 days of 1-NP data and 61 days of levoglucosan data. We ran the PMF model with the option of replacing these missing data on a given day with the median of the observed values over all days rather than eliminating the given day from the analysis. We used measurement specific uncertainties in this model as provided in the data set.

Table 2.2.3: Detection Limits and Measurement Uncertainties for the hourly data used in the PMF model

Species	Minimum Detection Limit[1]	Percent Uncertainty
Propane	0.02	8.0
n-pentane	0.02	10.2
Benzene	0.02	8.6
n-Heptane	0.02	7.6
n-Octane	0.02	8.7
n-Nonane	0.02	18.0
n-Decane	0.02	31.9
n-Dodecane	0.02	78.8
Black Carbon	0.10	10.0
delta Carbon	0.10	20.0
$PM_{2.5}$	1.0	5.0

[1]units are ppbv for hydrocarbons, $\mu g/m^3$ for particle metrics

2.2.6 Monitoring Ship Traffic with Automated Identification System (AIS) and Light Detection and Ranging (LIDAR)

We assessed maritime emissions using a combination of data sources, including real-time shipping traffic monitoring, LIDAR (Light Detection and Ranging), and meteorology. These data sources provide a comprehensive view of maritime emissions and their potential contribution to air quality in the region.

The U.S. Coast Guard in 2004 required all ships (> 65 ft) and towing vessels (> 26 ft) in the Puget Sound to be equipped with a vessel Automatic Identification System (AIS). The AIS provides voiceless navigation information exchange between vessels and onshore traffic centers in near real-time. This data is available for public access using a dedicated transponder or via the internet. Figure 2.2.4 displays the AIS study zone for the Seattle region, divided into equal sized study zones (4 km^2).

Much like a highway, shipping lanes on waterways can be viewed as transport corridors and emission factors can be applied for the shipping traffic. The AIS provides vessel identifying data such as call sign, name, "IMO" identification number, dimensions, draft, cargo type, destination, and accurate navigation information such as latitude/longitude position, course, and speed. In particular the IMO number can be linked to detailed information on ship size, tonnage, age, and engine horsepower and propulsion system. The AIS data and study zones will be used to calculate counts of ship “legs”, where a ship enters and exits a zone, as well as total number of hours in the zone and average speed in the zone, defined by ship type and size.

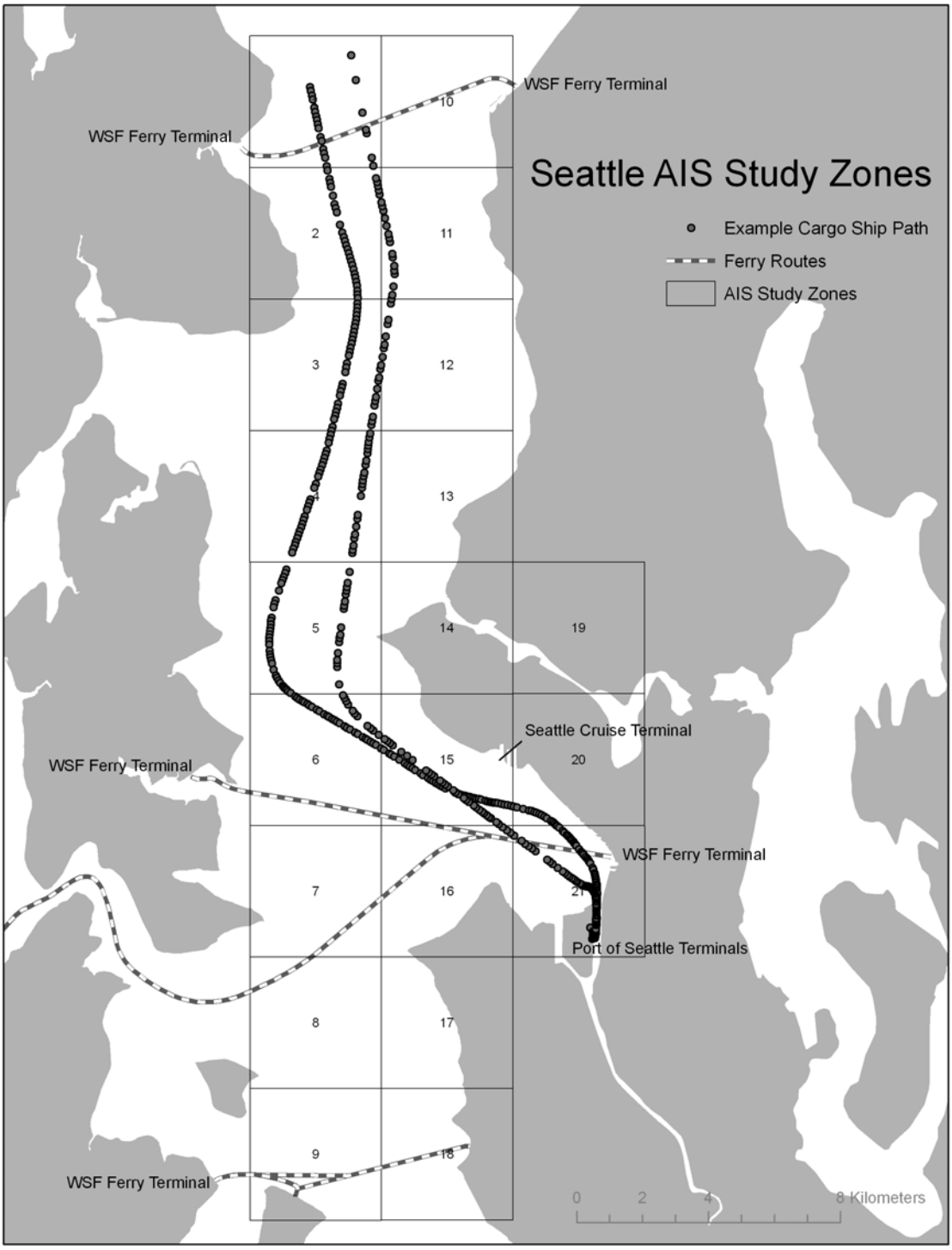

Figure 2.2.2: Seattle AIS Marine Emission Study Zone

LIDAR is an optical remote sensing technology that measures properties of scattered light to find range and/or other information of a distant target. LIDAR uses laser light pulses that are backscattered by aerosols in the atmosphere along the beam path and detected with a telescope and sensitive detector. The round-trip travel time for the pulse measures the distance to the aerosols. The intensity of the backscatter is proportional to the particle number density and the optical cross section. Scanning the light beam over a certain direction and elevation can provide a map of the aerosol density over a region of sky. With the LIDAR, we attempted to get acquire ship plumes in transit with backscattering information to better understand and model ship emissions.

Monitoring of ship aerosol emissions was done using a LIDAR provided by the University of Washington's Optical Remote Sensing Lab. The UW-LIDAR is an Orca photonics LRS-50 instrument mounted on a 2-axis computer-scanner and retrofitted with an Nd:YAG laser operated at 355nm. The UW-LIDAR produces 6 ns light pulses at 15Hz with a peak power of 1.6 MW sampled in 30m pixels. By operating in the UV, the LIDAR has high sensitivity for detecting fine aerosols (>0.2 um), and is eye-safe at all ranges.

The LIDAR was placed to observe harbor island traffic and ships traveling into the port of Seattle. Particle emissions from ships were measured in a one-month long campaign to assess the feasibility of measuring particle emissions and plume direction during routine operations.

3. Gas Chromatograph Peak Aligning Process

Gas chromatography has been used extensively in the PAMS network throughout the country to measure VOCs on an hourly timescale. However, there are extensive resources currently used in staff time to integrate and summarize the vast amounts of data. Additionally, the instruments are very sensitive to ambient temperature changes and agencies must control for large external temperatures swings for field shelters. If external factors vary too greatly, the retention times can drift significantly, thus requiring additional staff time for the data processing.

During this study, we developed a procedure to automate the process of aligning chromatograms. We produced a framework for a more standardized approach towards identifying and aligning known compounds in the gas chromatography time series, minimizing the requirement for recalibration and reprocessing.

Overall, for our internal process, we estimate that staff time spent on analysis was reduced by more than half with the development of this method of aligning chromatograms. Time savings for other organizations may vary depending on their data quality and internal processes, however this alignment method would likely increase efficiencies elsewhere as well.

3.1. Methods

The primary component of the method uses LineUp™ software from InfoMetrix, Inc. (Bothell, WA). The software aligns a gas chromatogram to a reference chromatogram of the user's choice. The peaks align laterally with a user assigned number of segments and the use of InfoMetrix proprietary algorithms.

The instrument was run hourly, with one hour a day run using an EPA PAMS calibration gas cylinder with identified concentrations for quality assurance checks, and to calibrate the instrument as necessary. The bulk of the GC methodology is found in Chapter 2.2.1 above.

3.1.1. Data Binning

For the purpose of analysis, data was divided into suitable bin sizes. This was primarily constrained by computing capacity available. A 10 day period was used as a 'bin' to simplify data handling, and often the GC datasets were interrupted in these timescales due to routine maintenance. Each bin was analyzed separately with their own respective calibrations.

3.1.2. Alignment of Data: Selection of a suitable reference file

To arrive at the best choice for a reference file, we considered a number of plausible approaches. One approach was to choose a reference file from the entire set of data (calibrant as well as sample files) through visual inspection by an expert (qualitative measures of similarity). The main downside in this approach is the variability in the expert judgment. Moreover, this approach prevents comparison of data from different sources due to the variability between experts.
A quantitative measure of similarity that can be reliably computed was another approach used that would allow for standardization and objectivity. Hence, we considered quantitative measures of similarity that would choose a reference file amongst all the calibrant and sample files. Mahalanobis distance is a widely used measure for similarity between a known and unknown dataset. It is based on correlations between variables by which different patterns can be identified and analyzed. It differs from Euclidean distance in that it takes into account the correlations of the data set and is scale-invariant, i.e. not dependent on the scale of measurements. Pirouette (also InfoMetrix Inc.) is commercially available software that can identify the file (one hour of sample data or a calibrant file) that is most similar to all the others.[39] This is determined by the file that gives the smallest value for the Mahalanobis distance.[40]

When the reference file was selected from the entire set of calibrant and sample files, the file with the smallest Mahalanobis distance was invariably a sample file. This is understandable since the number of sample files far exceeded the number of calibrant files. Additionally, the calibrant files often were higher in concentration and were also significantly different than sample files regarding the number of compounds present and the concentrations ratios of those compounds. Moreover, based on the measure of similarity, there were two distinct clusters that formed, one for the calibrant files and the other the sample files. Unfortunately, as the calibrant files concentrations were generally so much higher, it was more difficult to align calibrant files to

sample files, than it was sample files to calibrant files. Therefore, we modified our approach to choose a reference file using Mahalanobis distance only from the set of calibrant files.

3.1.3. Alignment of Data: Alignment to the reference file

Once the choice of the reference file was made, the automated graphic alignment tool LineUp was employed to align the data files to the reference file. As TotalChrom (Perkin Elmer) was used for data processing, raw files (the default file-type generated by TotalChrom) were required to be converted into a suitable file format for using LineUp. After processing in LineUp, the aligned files then needed to be reconverting back into a format compatible with TotalChrom. TotalChrom has the features necessary to do the conversion.

The biggest advantage of using LineUp is it provides for a standardized approach for reducing the variability in retention times completely independent of the user.[41] The peaks of these aligned files are identified and quantified according to a standardized time series of gas chromatography data to identify known and unknown compounds on the GC time series. This can be done by feeding the standardized time series into a method file hosted in TotalChrom. Using this approach the names and concentrations of all of the compounds in the time series across all data can be assigned in a single automated step, dramatically reducing the amount of analyst-time that is typically required to identify and quantify the VOCs. It is also free of the variability that can occur if the same steps were carried out manually.

3.2. Result of Data Alignment

Shown in Figure 3.1 are the Mahalanobis distances for the calibration checks for 01/28/09-02/06/10.

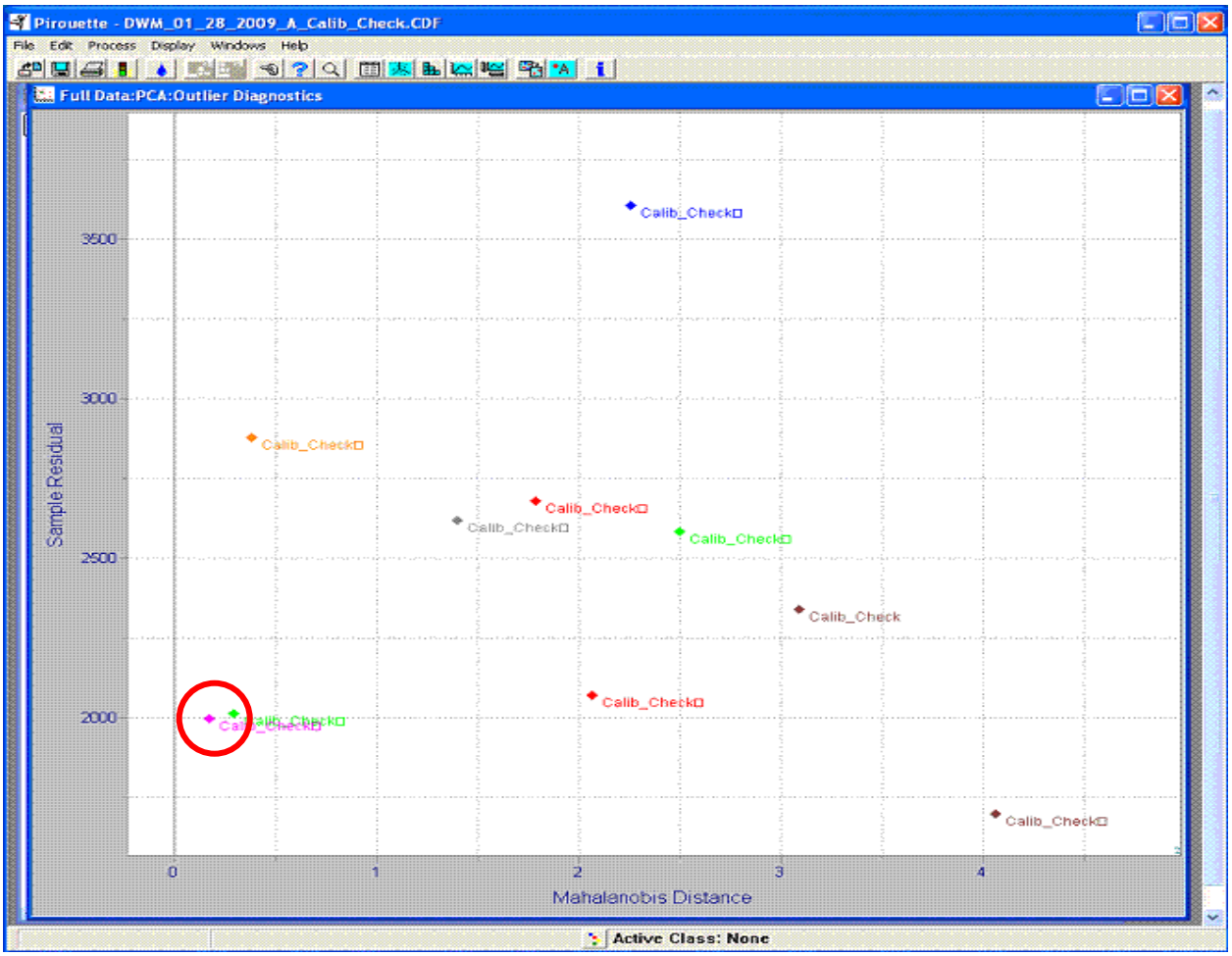

Figure 3.1: Pirouette™ software Mahalanobis distances example plotted for the BP-1 column calibration checks.

Based on Figure 3.1 above, the reference file chosen for the alignment is contained within the circled pink dot. It was the calibration check for 01/30/09. This reference file was used to align all calibration checks and samples in the BP-1 column.

Figure 3.2 below demonstrates the before and after results of using LineUp and the reference calibration file to align 5 samples:

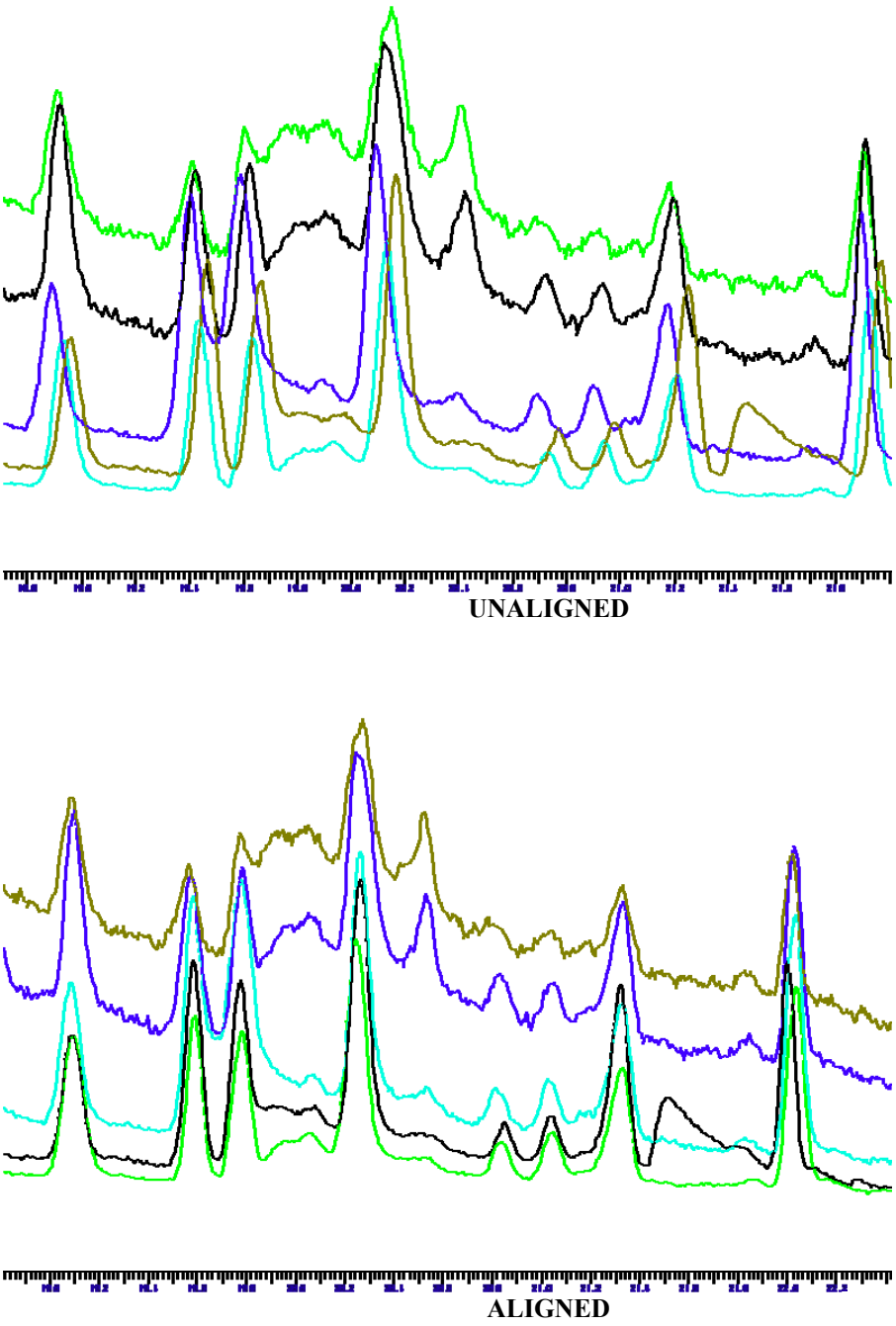

Figure 3.2: Example of an alignment result for 5 consecutive spectra and 9 peaks on 03/10/09 BP-1 Column.

Recoveries of calibration checks were calculated over the time periods that were analyzed to assess each parameter for quality assurance purposes. Figure 3.3 below demonstrates the quality of the data. Recoveries after alignment and the integration process were in the range 60-130%

(within the study's original data quality objectives). The percent recovery was calculated with the following formula:

% *Recovery* = (concentration of compound recovered/concentration of compound in cylinder) x 100.

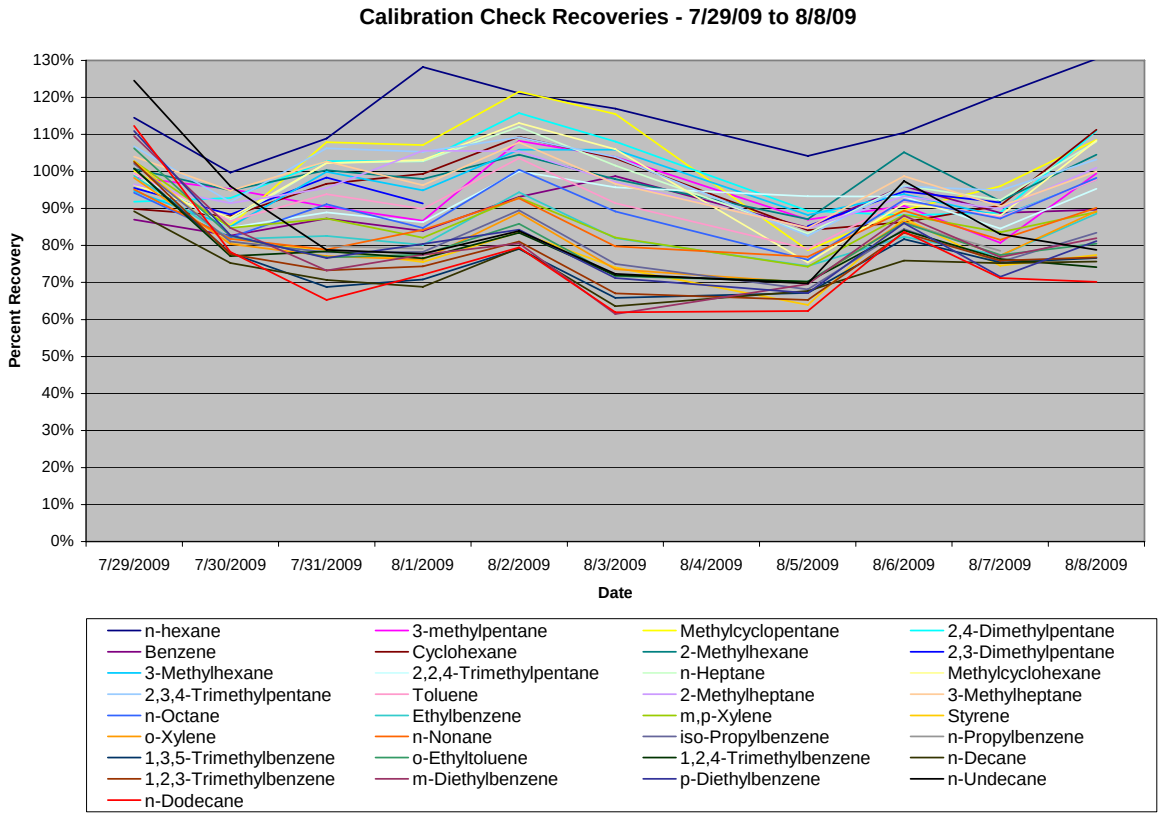

Figure 3.3: Data Quality: Calibration Recoveries Example

For 9 to 12 carbon compounds, the BP-1 column occasionally had higher recoveries than the 130% criteria allowed, and these results were invalidated accordingly. However, this was not due to the alignment process, but to the adhering of the larger compounds to the GC column. Most often compounds with 9-12 carbons had poor recoveries following larger concentrations (including calibrations).

4. Results from OP-FTIR, GC-FID, and $PM_{2.5}$ Continuous Instrumentation

This chapter characterizes and summarizes the data to give the reader a perspective on what was collected. For this study, 61 different parameters were measured on an hourly basis. A list of these variables is provided in Table 2.2.1 and summarized in Appendix A. Not all variables were available at all times, but most data did meet the data quality objective for data completion in our Quality Assurance Plan, with the exception of the OP-FTIR (discussed in section 4.1 below). The hourly data was paired with traffic observations to form an evaluation data set, spanning the period from 29 March to 11 August 2009.

The investigators used multivariate stepwise linear regression to identify the most significant observed variables accounting for the variation in both $PM_{2.5}$ observations and truck traffic observations. Rather than simply summarizing traffic and $PM_{2.5}$ data, the analysis team found the multivariate stepwise regression technique more useful. This analysis was complementary to the PMF analysis described in Chapter 5 which was conducted to apportion the hourly PM and VOC observations to different sources. The variables identified in the regression analysis, which were also recognized as important contributors in the PMF analysis, showed a consistent picture of factors impacting the site. To reiterate, two independent analytical methods (multivariate stepwise linear regression and PMF analysis) were used and yielded common conclusions.

4.1. OP-FTIR

An OP-FTIR instrument was deployed at the Duwamish site for approximately 10 months. A 71 meter beam path was set up near the monitoring site. We attempted to have retro-reflector access across the roadway, but were unable to resolve placement issues with the neighboring property owner. This resulted in a less than optimal beam path as shown in Figure 4.1 below.

Figure 4.1: Aerial view of the Duwamish site, showing placement of the FTIR beam path.

Four months of spectral data were collected and archived, as noted in Table 2.1, with weekly checks of signal intensity and instrument integrity. In March of 2009, a decline in signal intensity was noted and traced to a failing cryogenic cooler for the IR detector in the instrument. However, no funds were reserved for the cryogenic cooler repair. The cooler eventually failed in May of 2009, resulting in a data gap between 5/19/09 - 9/13/09 while replacement equipment was procured. This did not meet our goal for data completeness. The replacement instrument was put into service on 9/13/09 and collected additional data until 11/2009. Only this earlier data set was analyzed in this report, since it contained the time periods that overlapped with the periods selected for analysis of the NMHC-GC data collected at the site. The data analysis period was in May of 2009.

Initial data processing consisted of quantifying carbon monoxide (CO) and methane (CH_4) in the data series logged at the site, and examining the C-H stretch residual. To refine the spectrum for further analysis, concentrations of small molecules like water, CO, and CH_4 are estimated first. The estimated signals are then subtracted from the spectrum.

Examples of the CO and CH_4 time series results are shown in Figures 4.2 and 4.3 below. These data have high time resolution, reflecting the 5-minute averaging time for each spectrum in the series.

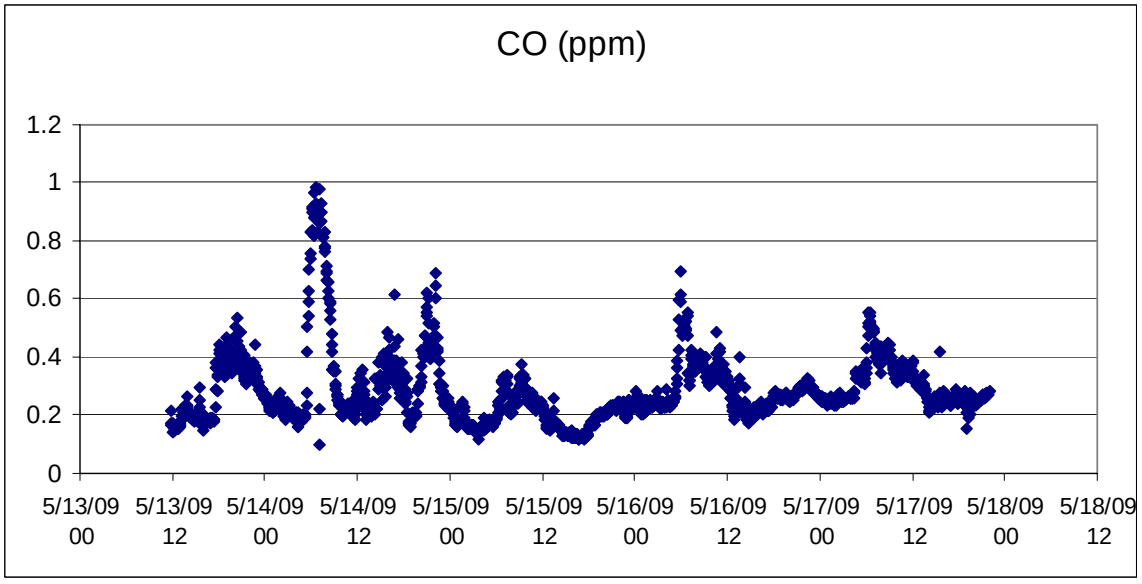

Figure 4.2: Five minute CO data collected at the Duwamish site by OP-FTIR

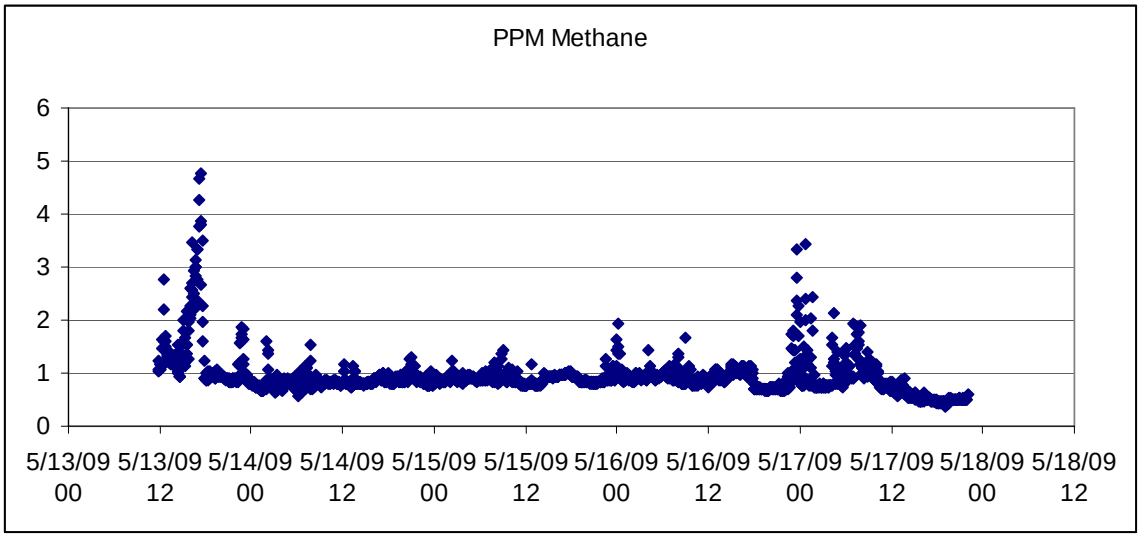

Figure 4.3: Five minute Methane data collected at the Duwamish site by OP-FTIR.

Although CH_4 and CO could be retrieved from the data, no C-H features remained above 3 times the noise equivalent absorbance (NEA) in that region of the spectrum. This made application of the C-H classification model too unreliable for use in the combined PMF analysis.

Efforts to improve the residuals through longer averaging up to a 1-hour period were unsuccessful. The residual NEA was elevated in this data due to the declining detector performance prior to the failure, although the main degradation was on the maximum signal strength and not NEA directly. However, the instrument performance was sufficient to meet the QA objectives for the period prior to the failure, so valid data was collected during at least part of the study. However, this data has been flagged due to the degraded maximum signal strength.

FTIR monitoring proved to be a significant challenge. Data from FTIR in this application was only useful in limited ways (in evaluating short time period resolution CO and CH_4 concentrations). Specific lessons learned are listed below:

- Cryogenic cooler repair and replacement must be anticipated.
- Open path should include source level concentrations if possible.

Regardless, FTIR data analysis remains very challenging and the limitations of this monitoring period neither supported nor rejected the hypothesis that the proposed C-H classification model could be effectively used in combined PMF analysis.

4.2. Seasonal and Weekly Variability of $PM_{2.5}$, BC, and Benzene

Figure 4.4 below shows a box and whisker plot of the hourly $PM_{2.5}$ observations, separated on a monthly and weekly time scale. The monthly variation is considerably larger than the day-to-day variation on a weekly scale, suggesting that season plays a significant role in the PM levels at the site. An analysis of variance[42] indicates that significant ($p < 0.05$) variation occurs on daily, weekly and monthly time scales and the variability between months is about 4 times as large as the day-to-day variation within a week. Since seasonal variability is the larger factor, our analysis focused on the time period where peak traffic impacts were likely to dominate the pollution matrix (minimizing the confounding effect of wood smoke sources in the model). Data from March, April, May, July, and August were used.

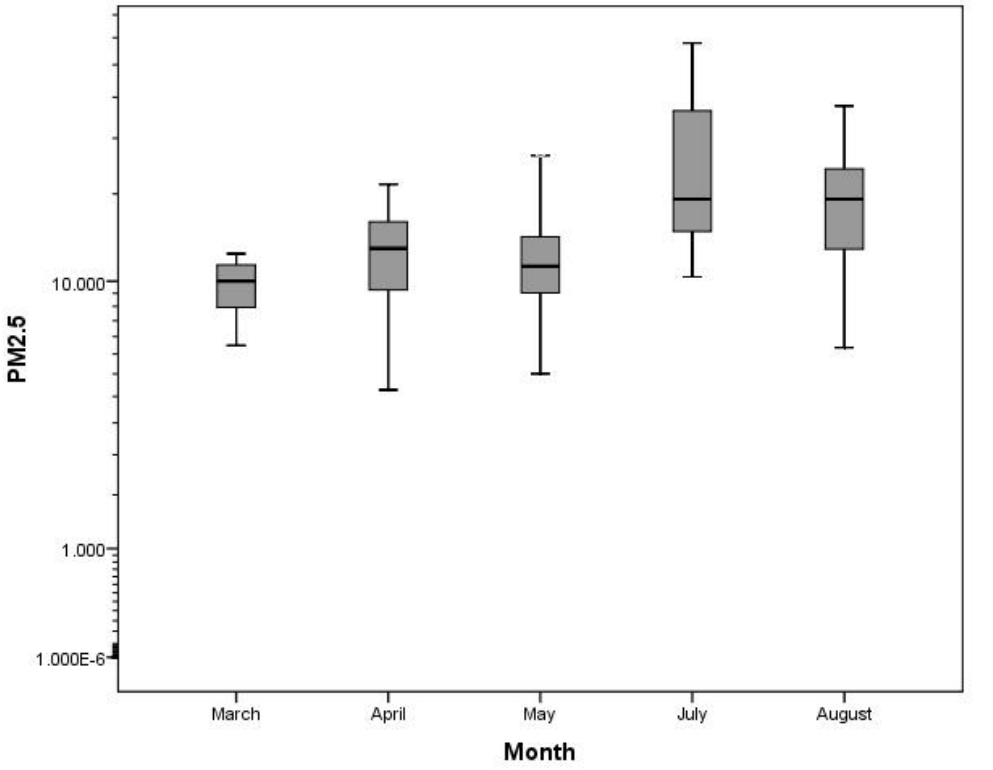

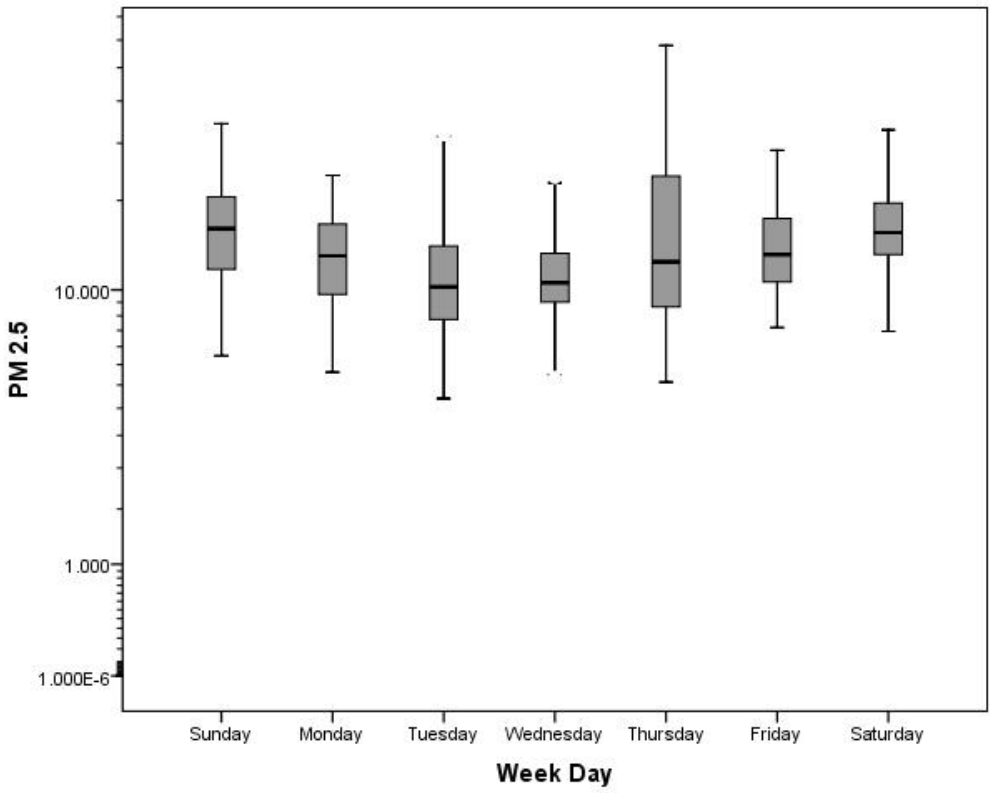

Figure 4.4: Box and whisker plot of hourly $PM_{2.5}$ values, by month and day of observation.

It was most useful to compare the $PM_{2.5}$ data with pollutant measurements which were closely linked to traffic sources. Figure 4.5 below shows a box and whisker plot of the hourly black carbon observations on a monthly and weekly time scale. Unlike $PM_{2.5}$ which has many sources, black carbon is more closely correlated with soot and diesel emissions (and not confounded by wood smoke sources during the months analyzed). In contrast to the $PM_{2.5}$ data, the monthly variability in black carbon is about the same as the day-to-day variability, suggesting that months within the March to August season play a much smaller role in the variability of this pollutant at the site. An analysis of variance indicates that variability between months is only about 1.6 times larger than day-to-day variation within a week.

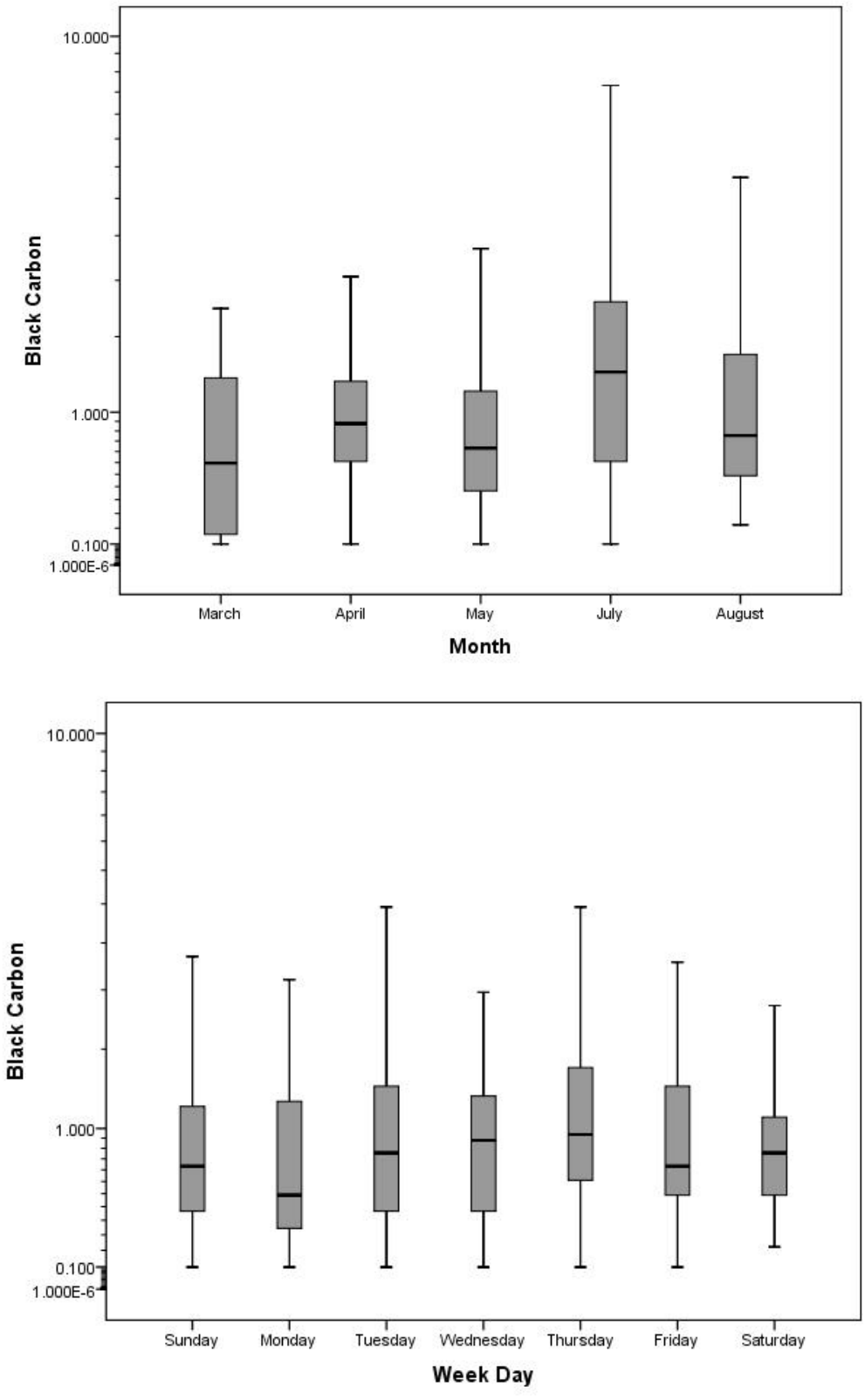

Figure 4.5: Box and whisker plot of hourly black carbon values, by month and day of observation.

Benzene is another measured hydrocarbon species that deserves attention both because of the strong association with wood smoke and because of its health risk. Benzene is a human carcinogen that nationally ranks highly among air toxics that potentially contribute to cancer risk. Benzene levels across month and week day are shown in Figure 4.6. Although the variation both between months and between days in a week is significant, the pattern changes over the months of observation. This is illustrated by the inset plot, which shows that the day to day changes in benzene change substantially between the cooler spring and warmer summer months. This likely is due to a variable such as meteorology, but it could possibly reflect the changing contribution from wood burning sources in cooler periods, to more traffic dominated sources in the summer. There is not enough evidence in this investigation to determine the cause with a high degree of certainty.

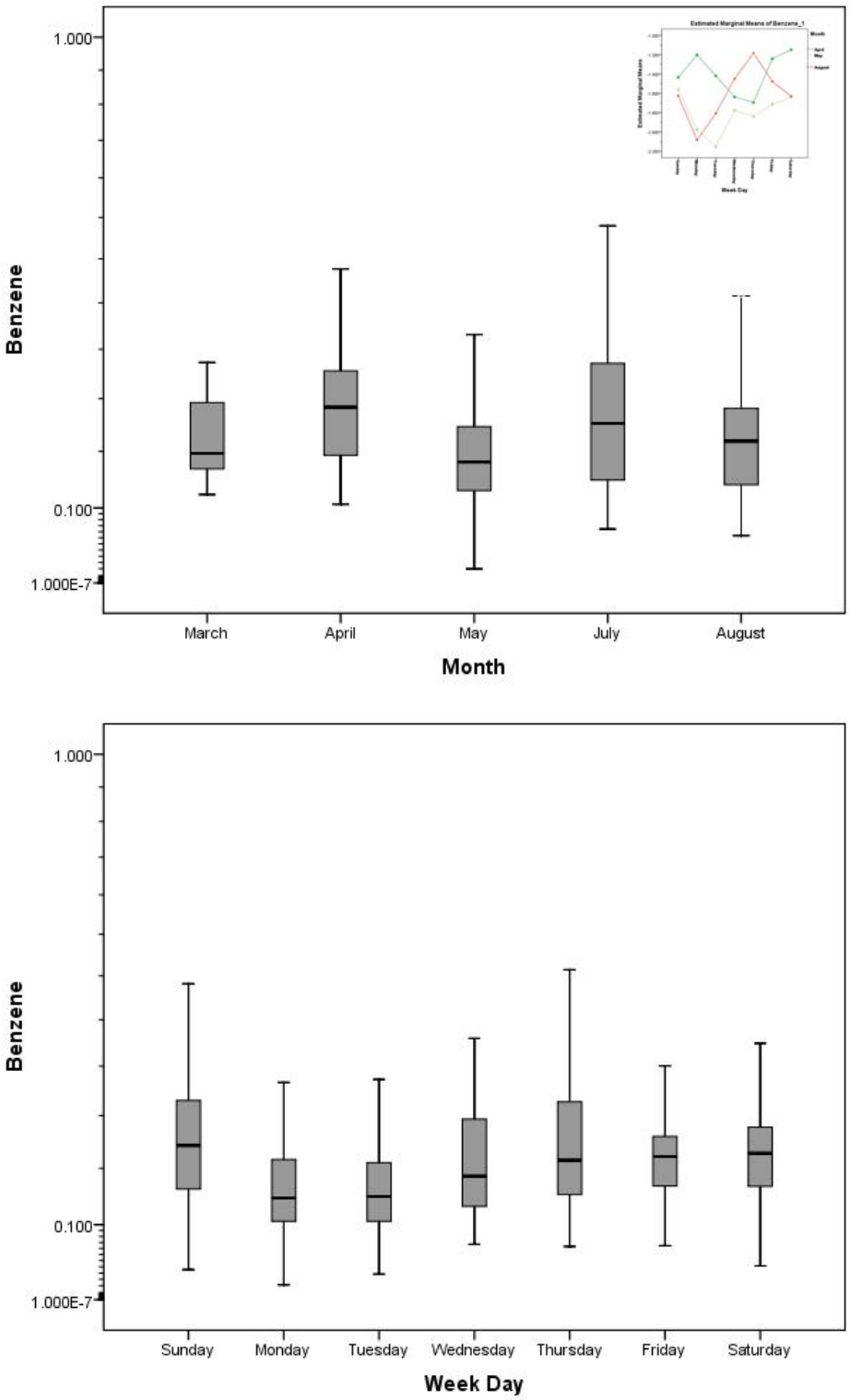

Figure 4.6: Box and whisker plot of hourly benzene values, by month and day of observation. The inset plot shows the pattern of expected values (marginal means) of ANOVA by weekday and month.

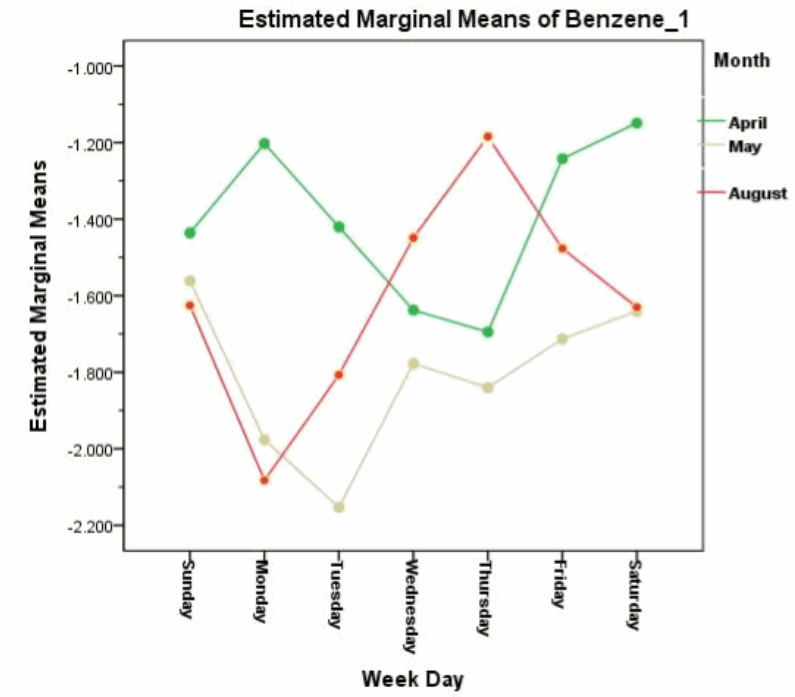

Inset Plot

4.3. Multivariate Associations with $PM_{2.5}$ and Vehicle Traffic

Given the large number of variables, it was deemed ineffective to conduct a univariate analysis on each analyte; such an approach also would miss important interrelationships in the measurements. Therefore, a multivariate analysis was used to screen the measurements and assess associations with both $PM_{2.5}$ and measured traffic variables at the site. A multiple linear regression model was used for this screening.

To explore an association with particulate concentrations, a stepwise regression model was implemented using $PM_{2.5}$ as the dependent variable and the other measurements as candidate independent variables. Histograms for all the measured data were first examined to determine if they were approximately normally distributed. All the variables exhibited a typical log-normal pattern with significant right-skewing and were log transformed to improve the distribution. The stepwise procedure was set with $p < 0.07$ to enter a variable into the model, and $p > 0.15$ to remove a variable from the model. After the stepwise analysis, a final reduced model was created, removing any variables with $p > 0.05$. The results of the reduced model were then ranked to assess the magnitude of the influence of individual variables in the model. Overall,

variables in the reduced model were able to explain 69% of the variance in the hourly $PM_{2.5}$ levels. The results of this analysis are shown in Table 4.1.

Table 4.1: Multivariate regression results for association between measurements and $PM_{2.5}$. Values shown in the upper panel (green) have a positive association with $PM_{2.5}$; values in the lower panel (rose) have a negative association with $PM_{2.5}$. The independent variables within each panel are ranked in order of decreasing correlation with the PM concentrations. Variables shown in bold type also were identified with factors in the PMF analysis of hourly $PM_{2.5}$.

Dependent Variable: $PM_{2.5}$ TEOM FDMS R2adj. =0.69	Unstandardized Coefficients	Std. Error	Standardized Coefficients		Sig.
	B		Beta	t	
(Constant)	2.789	.097		28.617	.000
Benzene	.405	.026	.497	15.288	.000
UV Channel (Delta BC)	.214	.049	.443	4.368	.000
n-Decane	.138	.018	.304	7.678	.000
Styrene	.102	.020	.199	5.159	.000
LAGS (Black Carbon, 1)	.075	.017	.157	4.357	.000
2,2-Dimethylbutane	.070	.017	.149	4.128	.000
3-Methylheptane	.074	.018	.129	4.067	.000
Cyclohexane	.061	.019	.120	3.148	.002
trans-2-Pentene	.047	.022	.084	2.123	.034
LAGS (n-Butane, 2)	.033	.011	.083	3.119	.002
Truck Fraction	.405	.153	.067	2.655	.008
2,3-Dimethylpentane	-.163	.027	-.285	-6.108	.000
Black Carbon	-.127	.049	-.265	-2.598	.010
2,4-Dimethylpentane	-.107	.021	-.164	-5.009	.000
2-Methylheptane	-.072	.017	-.137	-4.172	.000
Isopentane	-.037	.011	-.126	-3.521	.000
1,2,4-Trimethylbenzene	-.054	.025	-.120	-2.191	.029
Ethylbenzene	-.063	.023	-.118	-2.791	.005
1-Pentene	-.067	.020	-.109	-3.419	.001
n-Heptane	-.054	.024	-.103	-2.255	.024
Propylene	-.051	.024	-.072	-2.108	.035

As noted earlier, some variables display both seasonal and weekly patterns of variation, which could potentially mask or confound associations with measured variables. To account for these possible effects, variable differences across time were explored in the regression analysis. A series of time-lagged variables was created by back-shifting a time series of hourly measurements by 1 or 2 lag periods. A lag 1 back-shift operation refers to using the measurement from one hour before the original measurement. These back-shifted variables also were included in the stepwise analysis described earlier. Entering lagged variables into the regression model allows us to add autoregressive terms to the analysis that account for correlations between the various measurements over time (first and second-order autocorrelation)[43]. An example of one such variable is LAGS (n-Butane, 2) that appears in Table 4.1, which denotes the n-butane measurements lagged by 2 hours. The interpretation of this lagged variable is that n-butane measured 2 hours earlier has a significant influence on $PM_{2.5}$ in the current hour. This illustrates

the complex interrelationship of the variables; n-butane along with propane are associated with factor 3 in the PMF analysis (fueling/port operations) which is attributed to warehouses, loading facilities and LPG refueling facilities in the area. This lagged variable in the regression analysis may indicate that trucks or other transport vehicles are being loaded or unloaded in earlier time periods, and then later contribute to PM in the area when these vehicles resume travel on nearby roadways.

A second multivariate analysis was conducted to assess the association of the measurements with vehicle traffic. Specifically, the classified vehicle counts logged on the major roadway (highway 99) near the site were used as an indicator of traffic impacts. The variable truck fraction, which is the proportion of trucks in the total vehicle counts, was used to assess associations with other parameters. Truck fraction was computed for bins (3+4)/total (heavy trucks) and bins (2+3+4)/total (all trucks), and both gave similar results in the analysis (see section 2.2.4 for a description of bin categories). Using truck fraction as the dependent variable, the stepwise analysis described earlier was repeated, along with the reduced model and ranked assessment of the significant variables. The purpose of this analysis is to identify significant associations between truck traffic and the measured hydrocarbon species, rather than to predict truck traffic from the observations. Approximately 50% of the variance in the hourly truck fraction could be explained by the variables in the model. The results for this analysis applied to all trucks are shown in Table 4.2 below.

Table 4.2: Multivariate regression results for association between measurements and truck traffic. Truck traffic is modeled as the proportion of trucks (bins 2-4) in the total traffic. Values shown in the upper panel (green) have a positive association with truck traffic; values in the lower panel (rose) have a negative association with truck traffic. The independent variables within each panel are ranked in order of decreasing correlation with the truck traffic. Variables shown in bold type also were identified with factors in the PMF analysis of Hourly PM.

Dependent Variable: Truck Fraction R^2 adj. =.502	Unstandardized Coefficients	Std. Error	Standardized Coefficients		Sig.
	B		Beta	t	
(Constant)	.258	.013		19.663	.000
LAGS (Propane, 2)	.026	.004	.298	6.596	.000
Black Carbon	.017	.003	.221	5.205	.000
LAGS(Black Carbon, 2)	.015	.004	.190	4.268	.000
LAGS(Black Carbon, 1)	.011	.004	.143	2.606	.009
trans-2-Pentene	.012	.003	.126	3.781	.000
m-Diethylbenzene	.011	.004	.124	3.009	.003
LAGS (Propane, 1)	.010	.004	.110	2.320	.021
2-Methylhexane	.006	.004	.071	1.605	.109
LAGS (n-Butane, 2)	-.019	.003	-.292	-6.025	.000
Isobutane	-.014	.004	-.186	-3.815	.000
LAGS (n-Butane, 1)	-.012	.004	-.174	-3.169	.002
2,2,4-Trimethylpentane	-.012	.004	-.156	-2.941	.003
n-Decane	-.010	.003	-.137	-3.236	.001
2,3,4-Trimethylpentane	-.011	.003	-.128	-3.193	.001
UV Channel (Delta BC)	-.047	.010	-.126	-4.667	.000

The regression model in Table 4.2 indicates that propane measurements and black carbon are the most important features in the data set in relation to truck traffic at the site. Both variables have a significant association with truck traffic; the association with propane is lagged over a 1-2 hour time period, which is consistent with the idea that propane emissions are linked to warehouse activities a few hours earlier, and later reflected in increased traffic on the major roadway near the site. The black carbon emissions appear both as current and lagged associations; this source can be linked to diesel tailpipe and crankcase emissions from moving and idling trucks, and likely reflects both roadway emissions and emissions from loading operations nearby.

The influence of lagged variables appears more prominently in association with truck traffic. This feature probably is due to the more complex time-dependent relationship between truck emissions from vehicles arriving, waiting, loading or unloading, and then traveling on the roadways. It is important to note that the traffic variable in the model only reflects the proportional changes in truck traffic on the nearby multilane highway where monitoring was done. There are many other access streets and loading facilities near the site that were not monitored, but which experience truck traffic and also contribute to emissions nearby. The traffic

variable used here should be regarded more as a surrogate for local truck traffic, rather than a comprehensive measurement.

There is significant agreement between the variables identified in Table 4.2 and the factors identified from the hourly PMF results in Chapter 5. An evaluation of how the results in Table 4.2 agree with the hourly PMF is discussed further in Chapter 5.

A number of other hydrocarbon species were identified that show an association with both $PM_{2.5}$ and vehicle traffic in the area. This is consistent with other studies in the literature which show that a mixed set of hydrocarbon emissions are good predictors of the air pollution impacts linked to vehicles and other local sources. We note that these 'other hydrocarbon' features mostly appeared as a negative association with truck traffic, which implies that they have a *positive* association with passenger vehicles. To check for this association, these variables were entered in a model using passenger car traffic (car-fraction) as the dependent variable, and the expected positive relationship with car traffic was found. Therefore we can regard the Table 4.2 results as describing measured species which separate car and truck traffic; the variables with a positive association (upper panel) are identified with a shift toward more truck traffic, and the variables with a negative association (lower panel) may be associated with a shift toward more car traffic.

Finally, we note that although many hydrocarbon species were measured, the analysis shows that only a subset of species (~1/3) were needed to identify relatively strong associations with hourly $PM_{2.5}$, that explains almost 70% of the variance. However, we observed that lagged variables play a role in the association, which points out the important temporal changes and seasonal features of emissions in the area that impact the site. The data set in this analysis was selected to emphasize traffic-related impacts in keeping with the aims of the study, and mainly comes from the non-heating season. A more comprehensive analysis with the inclusion of data selected across all seasons may be warranted.

5. Results of Source Apportionment Modeling

In our source apportionment model using hourly data, we were able to distinguish seven source-related factors at the Duwamish industrial site. The detailed results of this analysis are presented in Appendix B.

Figure 5.1.1 shows the six derived source profiles. As shown, there is one profile representing the "other" sources of $PM_{2.5}$. There are also three distinct features that are related to motor vehicle emissions: "High Load Diesel", "Gasoline", and "Idling/Crankcase Diesel". In addition, there is a feature associated with combustion exhaust and fuel evaporative emissions we have chosen to name "Fueling / Port Operations". There are also two wood smoke features, one that has a higher gas to particle ratio and one that is opposite. Each of these PMF-derived features is briefly discussed below.

The correlation between model predictions for $PM_{2.5}$ and for benzene were high ($R^2 > 0.95$), although for $PM_{2.5}$ this was not surprising as the "Other $PM_{2.5}$" feature subsumed most of its variance.

5.1. Identifying Source-related Features

5.1.1. "High Load Diesel" Feature

The hourly contributions from the "High Load Diesel" feature are correlated with the hourly volume counts of large truck traffic on SR-99 during those hours when the wind is blowing from the direction of the roadway. The traffic measurements are discussed in Chapter 4. The correlation with Bin 4 (largest truck) volumes during these hours is shown in Figure 5.1.2. The daily average contribution from the "High Load Diesel" feature, as computed from the appropriate hourly values, is also correlated with the corresponding daily average 1-nitropyrene values on those days when both data sets overlapped as shown in Figure 5.1.3.

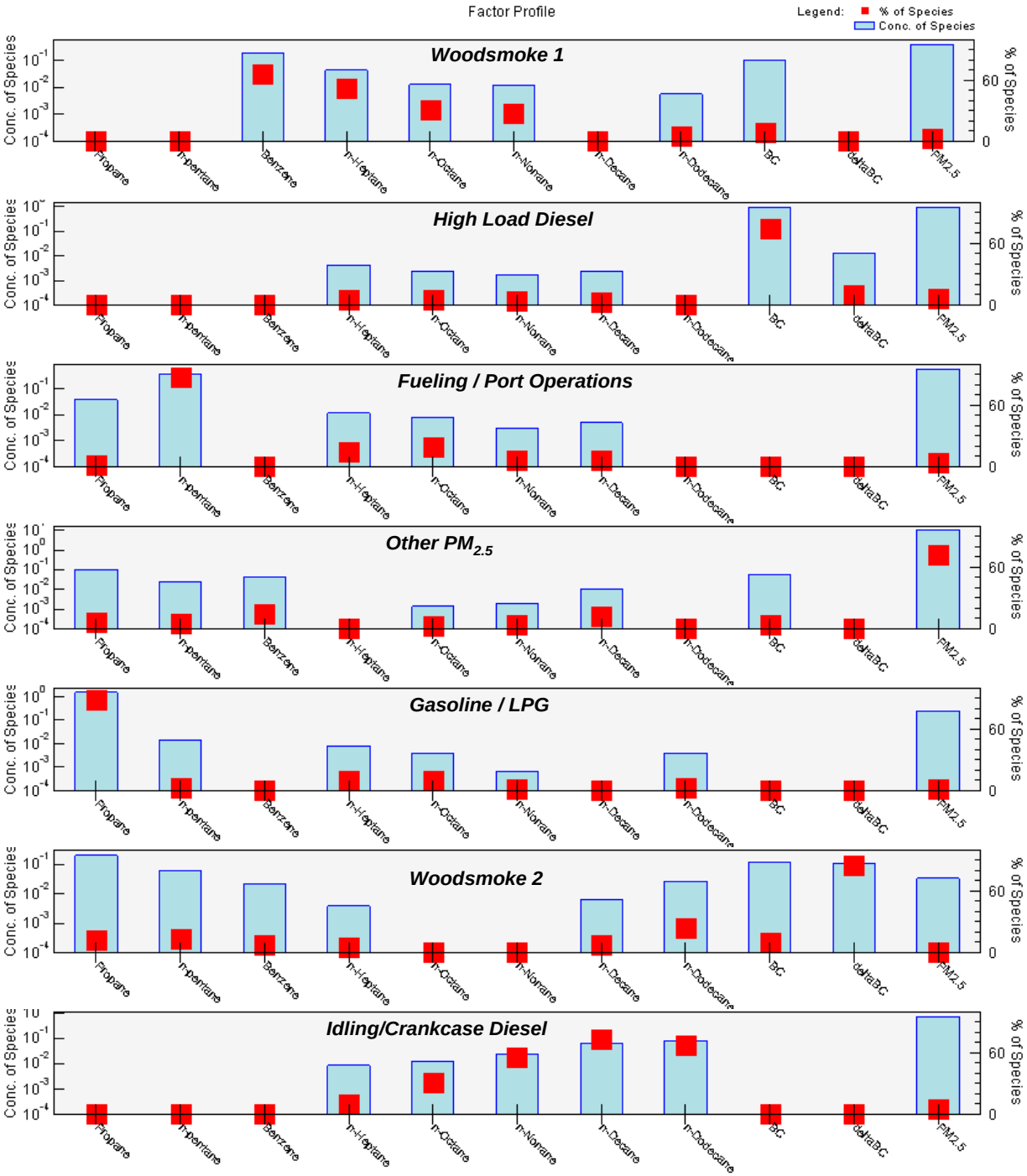

Figure 5.1.1: Source-related features at the Duwamish site derived from EPA PMF 3.0 based on hourly measurements of n-alkanes and selected fine particle metrics. The 1057 hourly measurements were collected over four different sampling periods in 2009: 1/28–2/6, 3/29–4/9, 5/6-5/26, and 7/30-8/11.

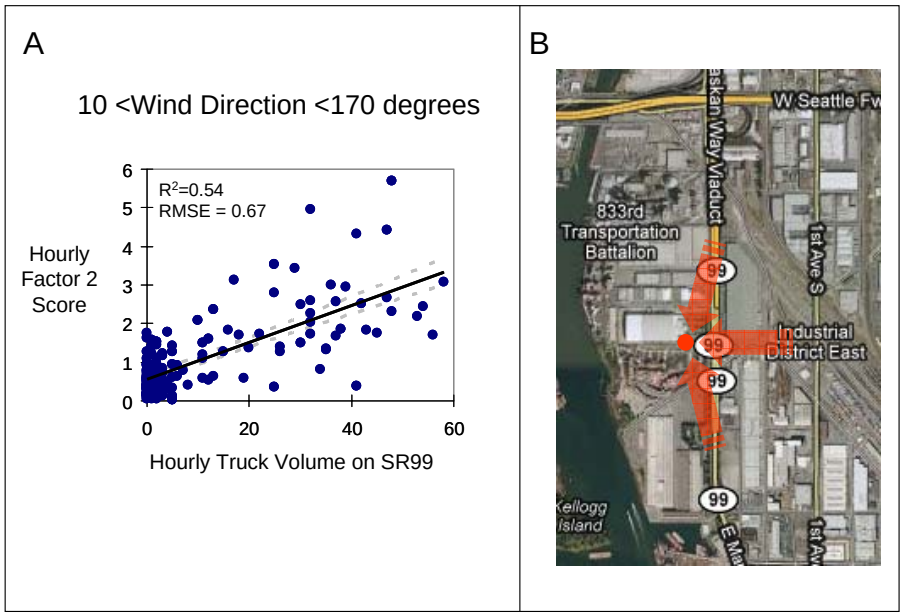

Figure 5.1.2: Scatter plot of the hourly average "High Load Diesel" factor score versus the hourly volume of large trucks on SR-99 (panel A) for periods when the wind was coming from that roadway (panel B). Details of the traffic counting methods are given in Chapter 2.

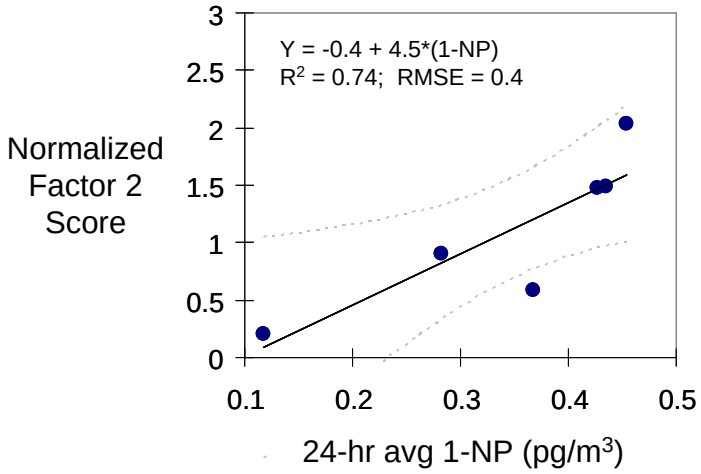

Figure 5.1.3: Scatter plot of the daily average "High Load Diesel" factor score versus the corresponding daily average 1-nitropyrene concentration from filter-based measurements (see Chapter 4). There were 6 days in 2009 when these two measurements overlapped (1/31, 2/6, 4/7, 5/13, 5/25 and 8/11).

5.1.2. "Fueling / Port Operations" Feature

The feature "Fueling/Port Operations" was named based upon three results. First, the conditional probability plot shown in Figure 5.1.4 implies that the hours with relatively high contributions from this feature (defined as twice the overall average of all hourly contributions from this

feature) occur when the wind comes from a relatively narrow set of wind directions. The port is upwind during these hours. Second, the feature is enriched in propane, pentane, heptane and octane, indicative of evaporative emissions from fuel transfer operations, also upwind of the site in this same direction. Third, the feature is associated with $PM_{2.5}$ and, more specifically, 1-nitropyrene. The latter association is shown in Figure 5.1.4 and indicates a combustion source or sources located in the same upwind direction.

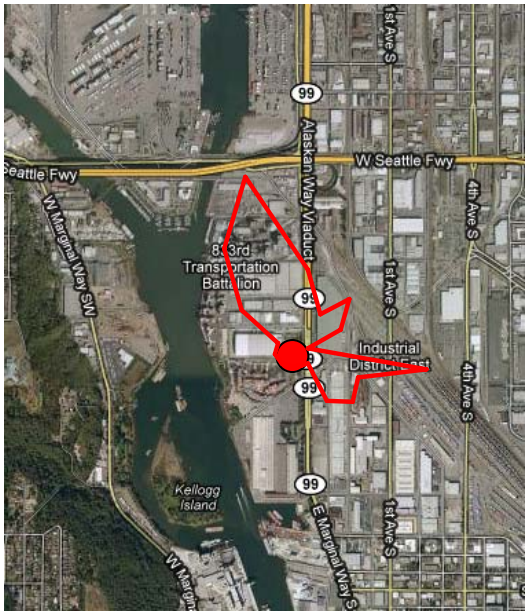

Figure 5.1.4: Conditional probability plot of the "Fueling/Port Operations" feature contributions. The lines connect points representing 20 degree wind sectors. The radial distance to each point from the central circle is proportional to the probability that the feature contribution is twice the overall period average when the wind comes from that sector. In this case, there is a high probability of large contributions to this feature when the wind comes from slightly west of due north.

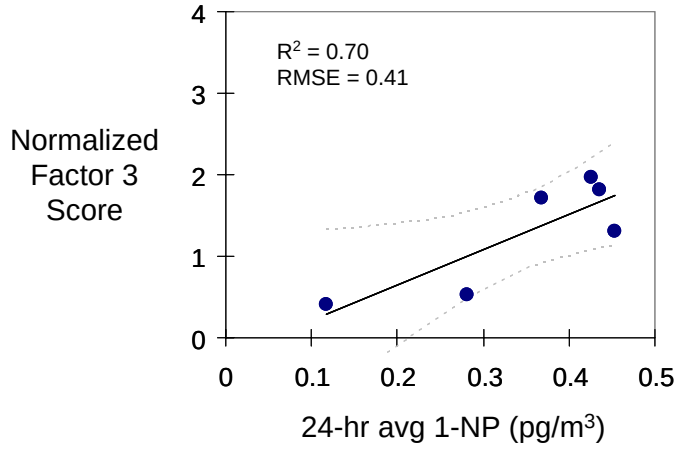

Figure 5.1.5: Scatter plot of the daily average "Fueling/Port Operations" factor score versus the corresponding daily average 1-nitropyrene concentration from filter-based measurements (see Chapter 6). There were 6 days in 2009 when these two measurements overlapped (1/31, 2/6, 4/7, 5/13, 5/25 and 8/11).

5.1.3. "Gasoline / LPG" Feature

The "Gasoline/LPG (Liquefied Petroleum Gas)" feature was identified based upon three results. First, the relative abundance of n-alkanes, with the exception of propane, are in reasonable agreement with those reported in the EPA speciated data base for light duty gasoline vehicles. This is shown in Figure 5.1.6. Second, the conditional probability plot indicates a strong contribution from south-easterly winds coming from both SR-99 and the surrounding residential/commercial areas of the Duwamish Valley. This is shown in Figure 5.1.7. Third, the fact that this feature is enriched in propane relative to light duty gasoline exhaust is indicative of a mixture of both light duty emissions and those from liquid propane vehicles, possibly those associated with warehousing operations to the southeast of the site.

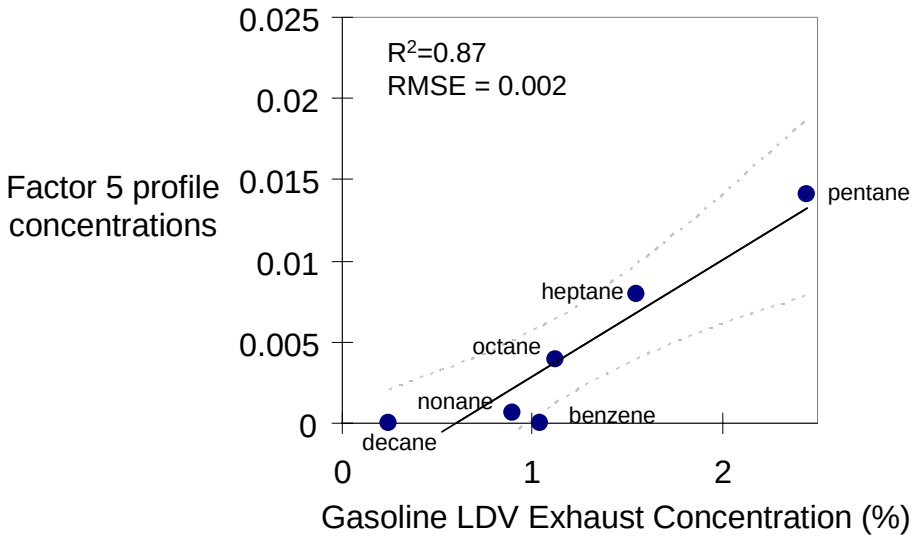

Figure 5.1.6: Scatter plot of the relative abundance of n-alkanes derived from the PMF profile versus those reported in the EPA Speciate database for light duty gasoline vehicles.

Figure 5.1.7: Conditional probability plot of the "Gasoline/LPG" feature contributions. The lines connect points representing 20 degree wind sectors. The radial distance to each point from the central circle is proportional to the probability that the feature contribution is twice the overall period average when the wind comes from that sector. In this case, there is a high probability of large contributions to this feature when the wind comes from the east/southeast.

5.1.4. "Idling/Crankcase Diesel" Feature

The "Idling/Crankcase Diesel" feature was identified based upon three results. First, the feature is selectively enriched in the larger n-alkanes and is the predominant source of both n-decane and n-dodecane in this data set. Second, although $PM_{2.5}$ is associated with this feature, there is very little black carbon. This soot-free, n-alkane-rich feature is indicative of exhaust at low engine loads associated with idle[44]. It is also potentially indicative of exhaust from crankcase blow-by due to heating of engine lubricating oils, given that this latter exhaust is rich in higher molecular weight n-alkanes[45]. Third and perhaps most importantly, the feature contributions are largest when the wind comes from the direction of the adjacent truck loading dock of the Washington Liquor Control warehouse as shown in Figure 5.1.8.

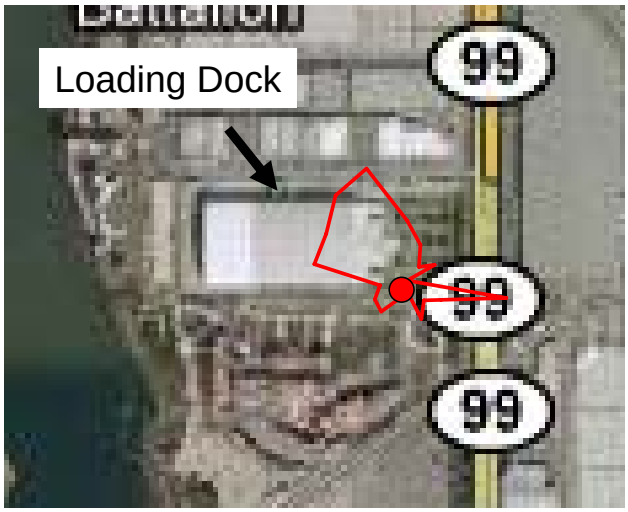

Figure 5.1.8: Conditional probability plot of the "Idling/Crankcase Diesel" feature contributions. The lines connect points representing 20 degree wind sectors. The radial distance to each point from the central circle is proportional to the probability that the feature contribution is twice the overall period average when the wind comes from that sector. In this case, there is a high probability of large contributions to this feature when the wind comes from the northwest, in line with the loading dock of the adjacent Washington State Liquor Control Board warehouse.

5.1.5. Wood Smoke Features

The two wood smoke features were identified by their association with daily average levoglucosan as shown in Figure 5.1.9. The "Wood Smoke 1" feature is enriched in vapor phase components relative to $PM_{2.5}$ and is a major contributor to benzene at this site. Specifically, it

contributed ~0.2 ppb benzene during the hours of hourly GC measurements, representing ~70% of all benzene sources during this period, even though the major contributions from this feature were mainly during the wintertime, less than 25% of all hours evaluated. This feature contributed 0.4 ug/m^3 of $PM_{2.5}$— only 3% of the overall average. In contrast, the "Wood Smoke 2" feature is relatively enriched in $PM_{2.5}$ relative to benzene, contributing 7% of the $PM_{2.5}$ and 18% of the benzene. It is associated with the hourly delta carbon values that have been shown in previous PSCAA studies to be classically associated with woodsmoke.[3]

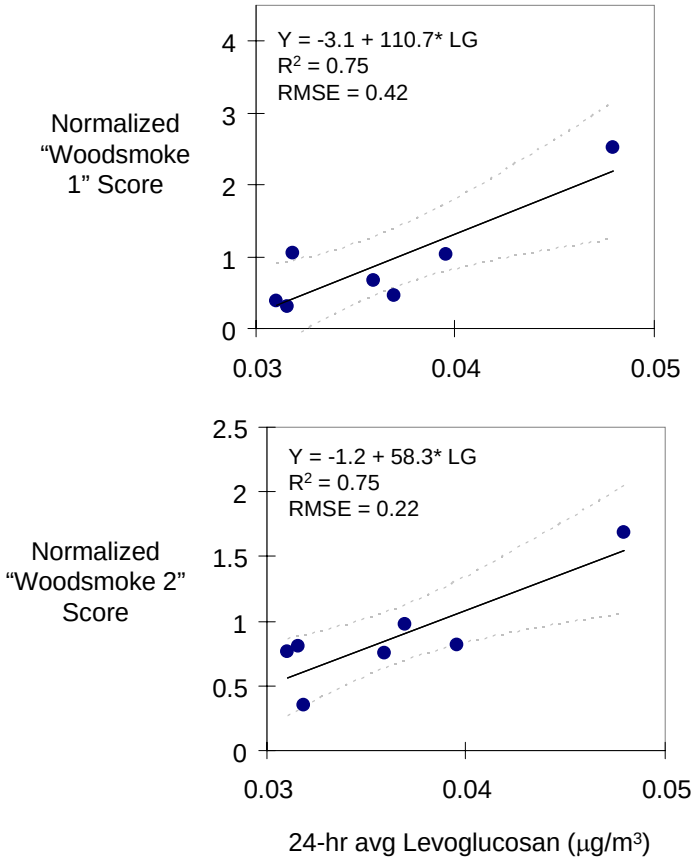

Figure 5.1.9: Scatter plots of daily average "Wood Smoke 1" and "Wood Smoke 2" factor scores versus 24-hour average levoglucosan values. There were only 7 days in 2009 when these two measurements overlapped (1/31, 4/1, 5/7, 5/13, 5/19, 5/25 and 7/30).

5.1.6 "Other $PM_{2.5}$" Feature

This feature is identified by its profile showing a relative high feature loading on $PM_{2.5}$ and relatively low loading on other species. As mentioned earlier, this feature is to be expected when combining the chosen VOC species with selected $PM_{2.5}$ metrics, given that the chosen VOCs are not necessarily good markers of all $PM_{2.5}$ sources. To examine this feature further, we did a

preliminary PMF analysis of the $PM_{2.5}$ speciation data at this site, as presented in the section 5.1.7 of this chapter. A comparison of the daily average contributions from the "Other $PM_{2.5}$" feature based on the hourly data and the sum of the contributions from the "Marine", "Secondary" and "Fuel Oil" features based on a PMF analysis of the $PM_{2.5}$ speciation data is shown in Figure 5.1.10. This is consistent with the general hypothesis that these latter sources of $PM_{2.5}$ are not well traced by the chosen VOCs.

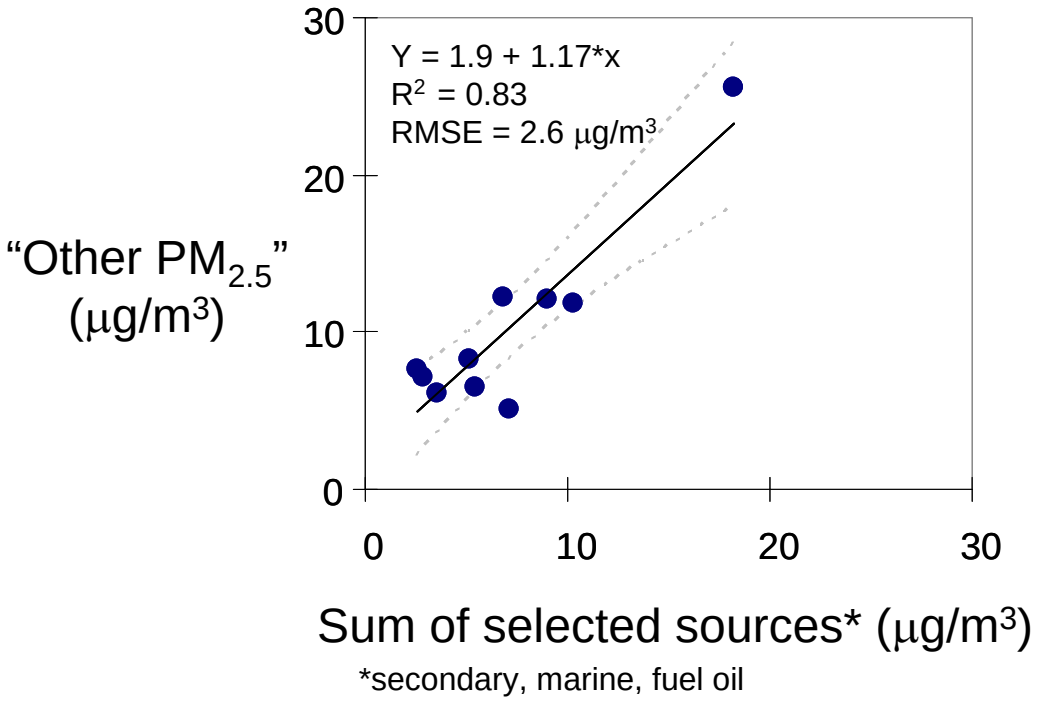

Figure 5.1.10: Scatter plot of the daily average "Other $PM_{2.5}$" contribution based upon the hourly measurements versus the sum of the daily average $PM_{2.5}$ contributions from the "Secondary", "Fuel Oil", and "Marine" PMF estimates based upon the one-in-six-day filter measurements. There were only 10 days of overlapping data during 2009 (1/31, 2/6, 4/1, 4/7, 5/7, 5/13, 5/19, 5/25, 7/30, and 8/11).

5.1.6. Comparison of Factors to Truck Traffic Multivariate Regressions in Chapter 4

As shown in the table below (repeated from Chapter 4), many of the compounds identified by the regression analysis, with truck traffic as a dependant variable, also shares relationships with the hourly PMF factors associated with diesel emissions. The factor described as a "high load diesel" feature has high loading on black carbon as found in the regression analysis in Chapter 4. Additionally, the factor described as a "fueling/port operations" feature ranks high in pentane and other light hydrocarbons (like trans-2-pentene). The "Gasoline/LPG" factor which is highly associated with propane and LPG from warehousing activities relates to the LAGS (propane)

features found in the regression analysis. As truck traffic on the roadway would not capture a "diesel crankcase" feature (which indicates diesel crankcase emissions likely from start and stop and maneuvering activities), the n-decane feature of this factor is negatively correlated in the regression analysis. The "wood smoke 2"feature, which shows a high loading on delta carbon, also shows a negative (inverse) association with truck traffic in this analysis. This could be due to the presence of wood smoke features in evening periods, when truck traffic is likely to be light in the neighboring warehouses and nearby roadways.

Table 4.2 (repeated from Chapter 4): Multivariate regression results for association between measurements and truck traffic. Truck traffic is modeled as the proportion of trucks (bins 2-4) in the total traffic. Values shown in the upper panel (green) have a positive association with truck traffic; values in the lower panel (rose) have a negative association with truck traffic. The independent variables within each panel are ranked in order of decreasing correlation with the truck traffic. Variables shown in bold type also were identified with factors in the PMF analysis of Hourly PM.

Dependent Variable: Truck Fraction R^2 adj. =.502	Unstandardized Coefficients	Std. Error	Standardized Coefficients		Sig.
	B		Beta	t	
(Constant)	.258	.013		19.663	.000
LAGS (Propane, 2)	.026	.004	.298	6.596	.000
Black Carbon	.017	.003	.221	5.205	.000
LAGS(Black Carbon, 2)	.015	.004	.190	4.268	.000
LAGS(Black Carbon, 1)	.011	.004	.143	2.606	.009
trans-2-Pentene	.012	.003	.126	3.781	.000
m-Diethylbenzene	.011	.004	.124	3.009	.003
LAGS (Propane, 1)	.010	.004	.110	2.320	.021
2-Methylhexane	.006	.004	.071	1.605	.109
LAGS (n-Butane, 2)	-.019	.003	-.292	-6.025	.000
Isobutane	-.014	.004	-.186	-3.815	.000
LAGS (n-Butane, 1)	-.012	.004	-.174	-3.169	.002
2,2,4-Trimethylpentane	-.012	.004	-.156	-2.941	.003
n-Decane	-.010	.003	-.137	-3.236	.001
2,3,4-Trimethylpentane	-.011	.003	-.128	-3.193	.001
UV Channel (Delta BC)	-.047	.010	-.126	-4.667	.000

This correspondence between the species identified in the traffic model and the PMF modeling results reinforces the factor identifications and descriptions. This also illustrates the complex set of emissions sources, both traffic and non-traffic related, that contribute to impacts at the site. Interestingly, the $PM_{2.5}$ regression model also identifies benzene as a significant factor associated with PM, which likely reflects the strong influence of wood smoke from nearby residences.

5.1.7. PMF Analysis of Daily Speciation Data

To further examine the "Other $PM_{2.5}$" feature, we conducted a PMF analysis of 61 days of $PM_{2.5}$ speciation data collected at this site between November 2008 and October 2009. The results of this analysis are included in Appendix B. Figure 5.1.11 shows the resulting source profiles and average contributions for a seven source PMF model.

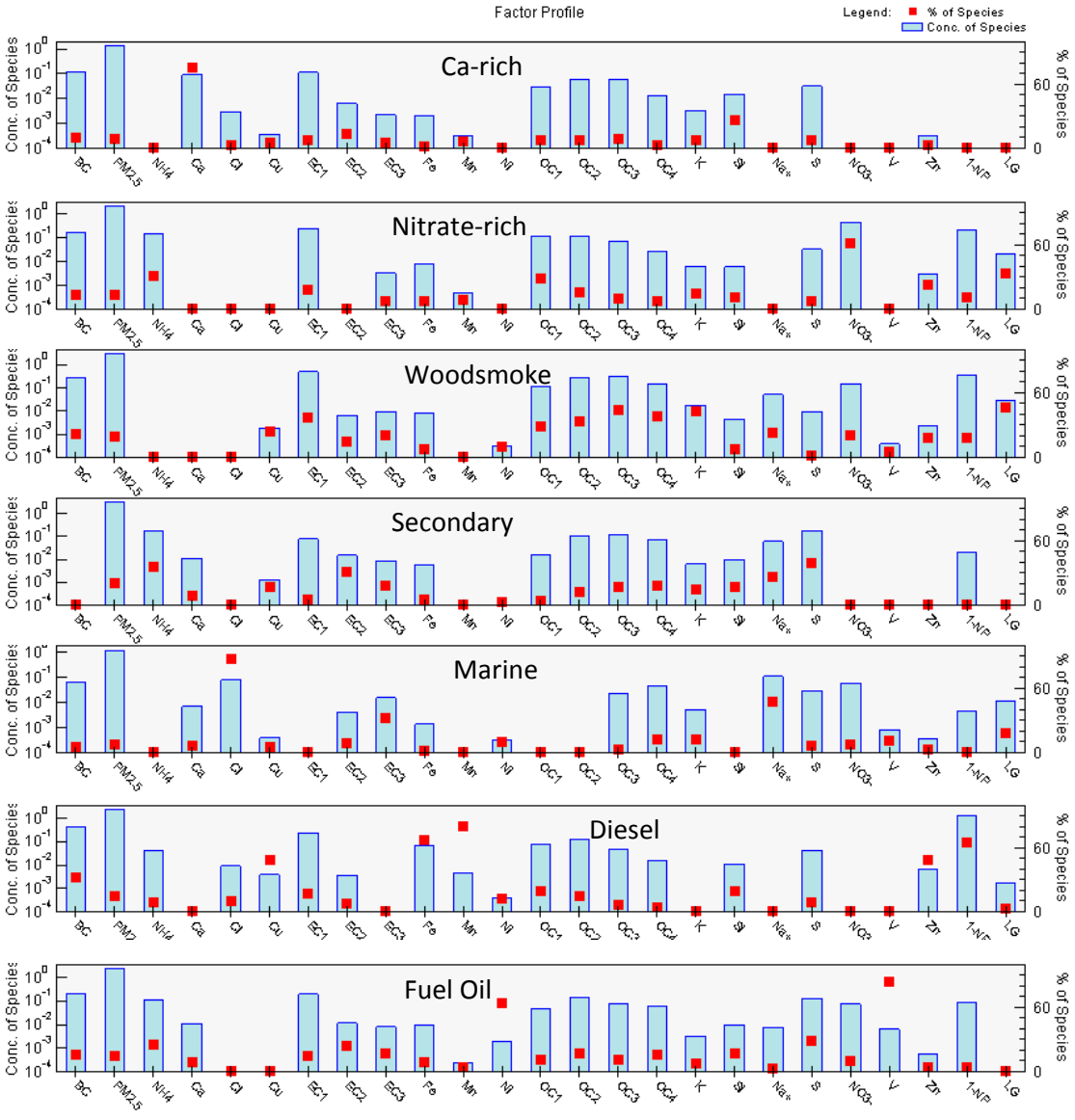

Figure 5.1.11: PMF features derived from 61 days of $PM_{2.5}$ speciation data collected every sixth day at the Duwamish site during the period between November, 2008 and October, 2009.

These results are to be considered preliminary because it is difficult to compare these results directly with the results of the PMF apportionment based upon the hourly data, given that there is very little overlap in the two data sets. It is also difficult to readily identify all possible source-related features influencing the daily $PM_{2.5}$ speciation data, given the relatively few $PM_{2.5}$ speciation measurements at this site.

5.2. Estimated Source Contributions to Benzene and $PM_{2.5}$

Tables 5.2.1 and 5.2.2 summarize the average PMF apportionment estimates at the Duwamish site based on all the available hourly and daily $PM_{2.5}$ speciation data, respectively. The median values and the corresponding 95^{th} percentiles estimated from 100 bootstrap runs are shown. Tables 5.2.3 and 5.2.4 show the results for only those ten days when the two data sets overlapped (1/31, 2/6, 4/1, 4/7, 5/7, 5/13, 5/19, 5/25, 7/30, and 8/11).

Table 5.2.1: Average PMF Feature Contributions Based on All Hourly Measurements

Analyte	Feature Contribution						
	Wood Smoke 1	High Load Diesel	Fueling / Port Operations	Other $PM_{2.5}$	Gasoline / LPG	Wood Smoke 2	Idling / Crankcase Diesel
$PM_{2.5}$ ($\mu g/m^3$)	0.2 (0 – 0.7)[1]	0.7 (0 – 1.4)	0.4 (0 – 0.8)	10.4 (10.1 – 10.6)	0.3 (0 – 1.0)	0.6 (0 – 1.2)	0.3 (0 – 1.2)
BC (μ g/m^3)	0.10 (0 – 0.35)	1.1 (0.4 – 1.9)	0.03 (0 – 0.12)	0.06 (0 – 0.22)	0.03 (0 – 0.14)	0.18 (0 – 0.62)	0.07 (0 – 0.38)
Benzene (ppbv)	0.26 (0.01 – 0.54)	0.004 (0 – 0.22)	0.02 (0 – 0.05)	0.05 (0.02 – 0.08)	0.005 (0 – 0.02)	0.07 (0 – 0.32)	0.02 (0 – 0.1)

[1]Median and 95% confidence interval based on 100 bootstrap runs

Table 5.2.2: Average PMF Feature Contributions Based on Daily $PM_{2.5}$ Speciation Data[1]

Analyte	Source-related PMF Feature Contribution						
	Ca-rich	Nitrate-rich	Wood Smoke	Secondary	Marine	Diesel	Fuel Oil
$PM_{2.5}$ (μ g/m^3)	1.3 (1.0 – 1.4)[2]	2.1 (1.6 – 2.4)	3.1 (2.3 – 3.6)	3.0 (2.8 – 3.2)	1.2 (1.1 – 1.3)	2.3 (1.8 – 2.9)	2.3 (1.9 – 2.7)
BC (μ g/m^3)	0.11 (0.02 – 0.21)	0.18 (0.09 – 0.36)	0.25 (0.09 – 0.44)	0.0 (0 – 0.09)	0.49 (0.01 – 0.10)	0.43 (0.19 – 0.69)	0.20 (0.04 – 0.42)

[1]Every 6th day 24-hr filter-based measurements between 11/08 and 10/09.
[2]Median and 95% confidence interval based on 100 bootstrap runs

Table 5.2.3: Average PMF Feature Contributions Based on Hourly Measurements for the 10 days when $PM_{2.5}$ Speciation Data were also available.

Analyte	Feature Contribution						
	Wood Smoke 1	High Load Diesel	Fueling / Port Operations	Other $PM_{2.5}$	Gasoline / LPG	Wood Smoke 2	Idling / Crankcase Diesel
$PM_{2.5}$ ($\mu g/m^3$)	0.2 (0.05)[2]	0.9 (0.6)	0.4 (0.3)	10.2 (6.0)	0.3 (0.2)	0.6 (0.3)	0.3 (0.3)
BC ($\mu g/m^3$)	0.10 (0.03)	1.4 (0.9)	0.03 (0.02)	0.06 (0.03)	0.03 (0.02)	0.16 (0.08)	0.07 (0.07)
Benzene (ppbv)	0.26 (0.07)	0.005 (0.003)	0.02 (0.15)	0.05 (0.029)	0.005 (0.004)	0.06 (0.03)	0.02 (0.02)

[1]1/31, 2/6, 4/1, 4/7, 5/7, 5/13, 5/19, 5/25, 7/30, and 8/11.
[2]standard error of the mean

Table 5.2.4: Average PMF Feature Contributions based on daily $PM_{2.5}$ speciation for those 10 days when hourly measurements were also available[1]

Analyte	Source-related PMF Feature Contribution						
	Ca-rich	Nitrate-rich	Wood Smoke	Secondary	Marine	Diesel	Fuel Oil
$PM_{2.5}$ (μ g/m^3)	1.6 (0.7)[2]	1.9 (0.6)	2.6 (0.7)	3.3 (0.9)	1.9 (1.0)	1.3 (0.7)	3.1 (0.9)
BC (μ g/m^3)	0.21 (0.08)	0.33 (0.05)	0.11 (0.04)	0.16 (0.04)	0.19 (0.10)	0.07 (0.04)	0.18 (0.05)

[1]1/31, 2/6, 4/1, 4/7, 5/7, 5/13, 5/19, 5/25, 7/30, and 8/11.
[2]standard error of the mean

6. Results of Measurement of Selected Nitro-polycyclic Aromatic Hydrocarbons (Nitro-PAHs) and Evaluation of 1-nitropyrene (1-NP) as a Marker for Diesel Exhaust

Nitro-PAHs (NPAHs) are a particularly important constituent of ambient PM, due to their carcinogenicity and mutagenicity[46] as well as their utility in source apportionment.[47] Distinct NPAHs are formed via different routes of production. For example, 1-nitropyrene (1-NP) has been proposed as a molecular marker for diesel particulate matter (DPM) since it is by far the most abundant NPAH in DPM while being much less abundant in PM derived from other sources.[1] Other NPAH isomers, such as 2-nitrofluoranthene (2-NFl) and 2-nitropyrene (2-NP) have been shown to be formed exclusively from atmospheric reactions, predominantly from gas-phase precursors.[48,49]

The concentration ratio of 2-NFl to 1-NP allows estimation of the contribution to ambient NPAH concentrations of atmospheric reaction formation routes as compared with direct emission from primary PM sources.[46,50] In addition, the ratio of the concentration of 2-NFl to 2-NP has been used to assess the relative contribution of two distinct production routes for 2-NFl.[51,52] For the reasons discussed above, measurements of ambient levels of NPAHs can yield valuable information about the atmospheric reaction conditions, sources of PM emissions, and processes contributing to NPAH formation for a particular geographical region.

One of the aims of this project was to evaluate the suitability of 1-NP as a marker for diesel exhaust $PM_{2.5}$ at the Seattle Duwamish air monitoring location. To address this aim, 1-NP concentrations were measured on partisol filters collected on 1 in 6 day cycle. A total of 42 filters were analyzed. Associations between 1-NP and other measured air toxics and surrogate variables were explored. Associations between 1-NP and estimated source contributions derived from PMF receptor modeling are also described.

The analytical method for 1-NP also permits measurement of the isomeric NPAHs 2-NFl and 2-NP with minimal extra effort. Therefore, concentrations of 2-NFl and 2-NP are also reported in this section, and their co-variability with other measured air toxics and surrogate variables is described.

6.1. Analysis of NPAHs

NPAH concentrations measured at the Seattle Duwamish site are summarized in Table 6.1.1 and Figure 6.1.1. Inspection of Figure 6.1.1 indicates that concentrations of all three NPAHs are somewhat correlated (i.e. all three compounds tend to have peak concentrations on the same days, and in general, NPAH concentrations are higher in winter compared to summer). Seasonal variation in NPAH concentrations are further examined in Table 6.1.2 and Figure 6.1.2.

Table 6.1.1: Summary statistics for NPAH concentrations (pg/m^3) at Seattle-Duwamish site November, 2008 – October 2009

NPAH	N	Minimum	Maximum	Median	Mean	Std. Error	Std. Deviation
2-NP	42	0.03	9.2	0.55	1.4	0.3	2.0
2-NFl	41	0.26	25	5.71	7.9	1.1	6.7
1-NP	42	0.12	49	1.58	4.6	1.5	9.5

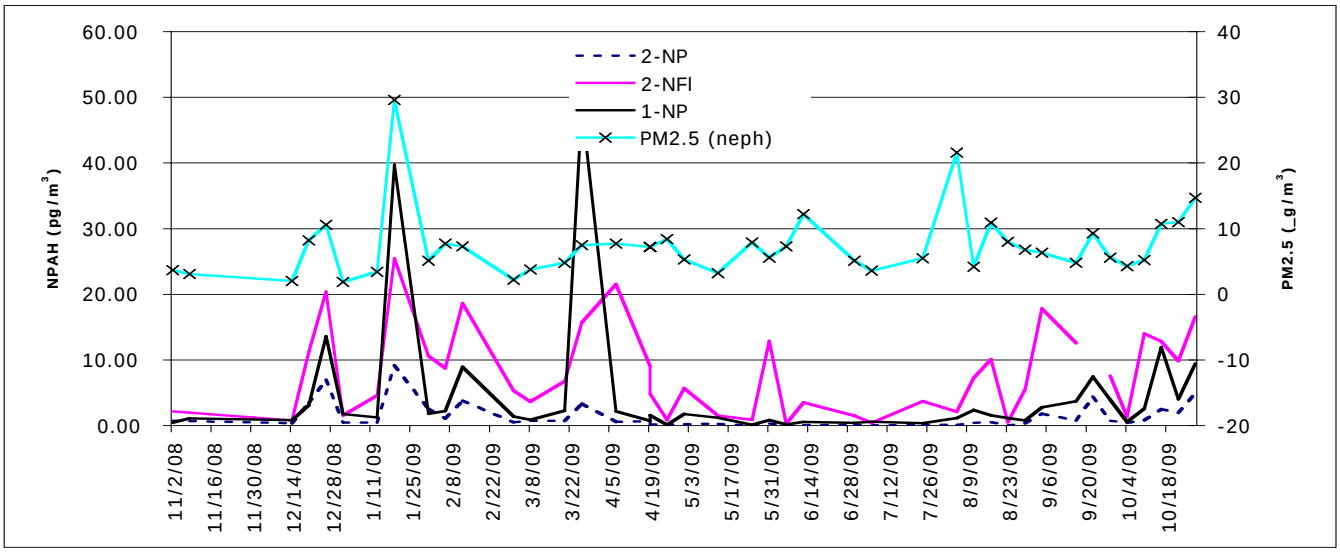

Figure 6.1.1: Temporal variation in $PM_{2.5}$ and NPAH concentrations at the Seattle Duwamish site.

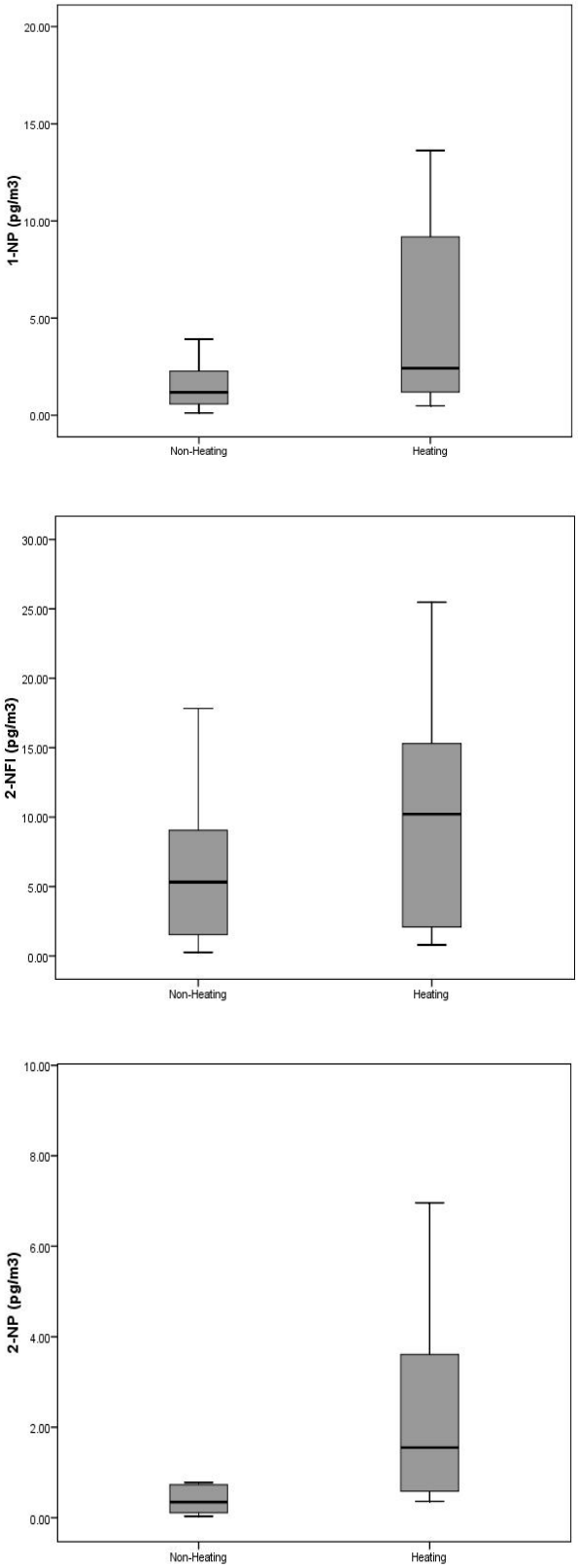

Figure 6.1.2: Seasonal variation in NPAH concentrations at the Seattle Duwamish site.

Table 6.1.2: Seasonal variation in NPAH concentrations (pg/m^3) at Seattle Duwamish site. p < 0.05 highlighted in boldface.

NPAH	Season	N	Median	Mean	Std. Deviation	Std. Error Mean	F (sig)*	p**
2-NP	Heating	16	1.6	2.5	2.6	0.65	**< 0.01**	**0.01**
	Non-heating	26	0.4	0.7	1.0	0.20		
2-NFl	Heating	16	10.2	10.1	7.7	1.9	0.19	0.10
	Non-heating	25	5.3	6.5	5.8	1.2		
1-NP	Heating	16	2.4	6.5	9.9	2.5	0.32	0.32
	Non-heating	26	1.2	3.4	9.3	1.8		

*Result of Levene's Test for Equality of Variances. F is significant only for 2-NP; thus can assume related variances for 1-NP and 2-NFl, but not for 2-NP.
**p-value for independent samples t-test comparing NPAH concentrations in heating vs. non-heating season.

As shown in Figure 6.1.2 and Table 6.1.2, concentrations of all three NPAHs are higher in the heating season (defined as October 1 to February 28), compared to the non-heating season. However, this difference is only statistically significant for 2-NP (for independent samples t-test, p = 0.01, Table 6.1.2). The observation of higher air contaminant levels in the heating season, compared to the non-heating season was also observed for $PM_{2.5}$ and many of the other air toxics in the Puget Sound area.[42] It is likely that this seasonal difference is driven primarily by increased atmospheric mixing (higher mixing heights) in summer compared to winter.

Previous studies have shown that concentrations of vehicle-derived air pollutants are typically higher on weekdays (when vehicle volumes are highest) compared to weekends. Therefore, we examined the difference between weekday and weekend concentrations of NPAHs (Table 6.1.3 and Figure 6.1.3). In addition, vehicle traffic counts for the period March-September 2009 were obtained from a series of in-road sensors placed in SR-99 adjacent to the Seattle Duwamish air monitoring site. The vehicle counts were binned into four categories based on vehicle length and number of axles. Bin 1 (1 and 2 axle vehicles) consisted of mainly of passenger cars. Bins 3 and 4 were combined into a single "heavy truck" variable. (See Chapter 2 for more details). It was assumed that most of the vehicles in the passenger car category were gasoline powered, whereas most of the vehicles in the heavy truck category were diesel powered. Weekday/weekend variation in vehicle counts by category is summarized in Figure 6.1.4 and Table 6.1.4.

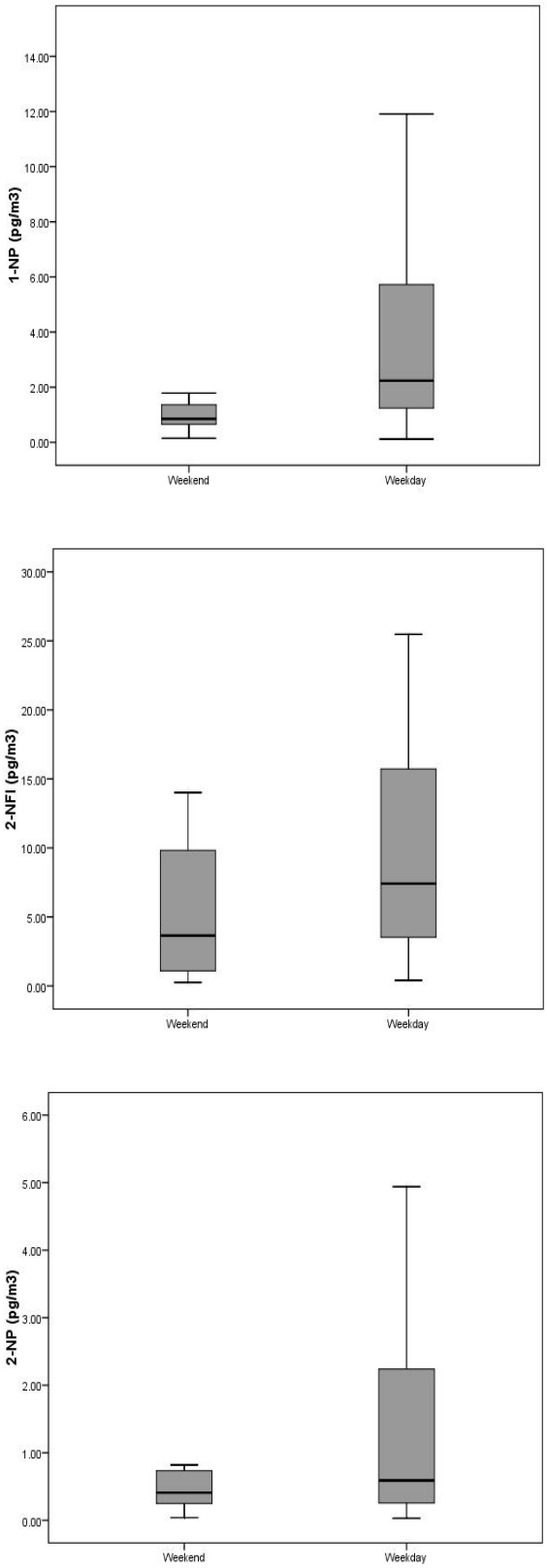

Figure 6.1.3: Weekday/weekend variation in NPAH concentrations at Seattle Duwamish.

Table 6.1.3: Weekday/weekend variation in NPAH concentrations (pg/m^3) at Seattle Duwamish site. p < 0.05 highlighted in boldface.

NPAH	Type of Day	N	Median	Mean	Std. Deviation	Std. Error Mean	F (sig)*	p**
2-NP	Weekday	27	0.59	1.7	2.3	0.45	**< 0.01**	0.07
	Weekend	15	0.41	0.77	0.95	0.25		
2-NFl	Weekday	26	7.4	9.3	7.3	1.4	0.09	0.07
	Weekend	15	3.7	5.3	4.9	1.3		
1-NP	Weekday	27	4.4	6.5	11.5	2.2	**0.01**	**0.02**
	Weekend	15	0.85	1.1	0.83	0.22		

*Result of Levene's Test for Equality of Variances. F is significant for both 1-NP and 2-NP; thus we can assume equal variances for 2-NFl, but not for 1-NP and 2-NP.
**p-value for independent samples t-test comparing NPAH concentrations on weekdays vs. weekends.

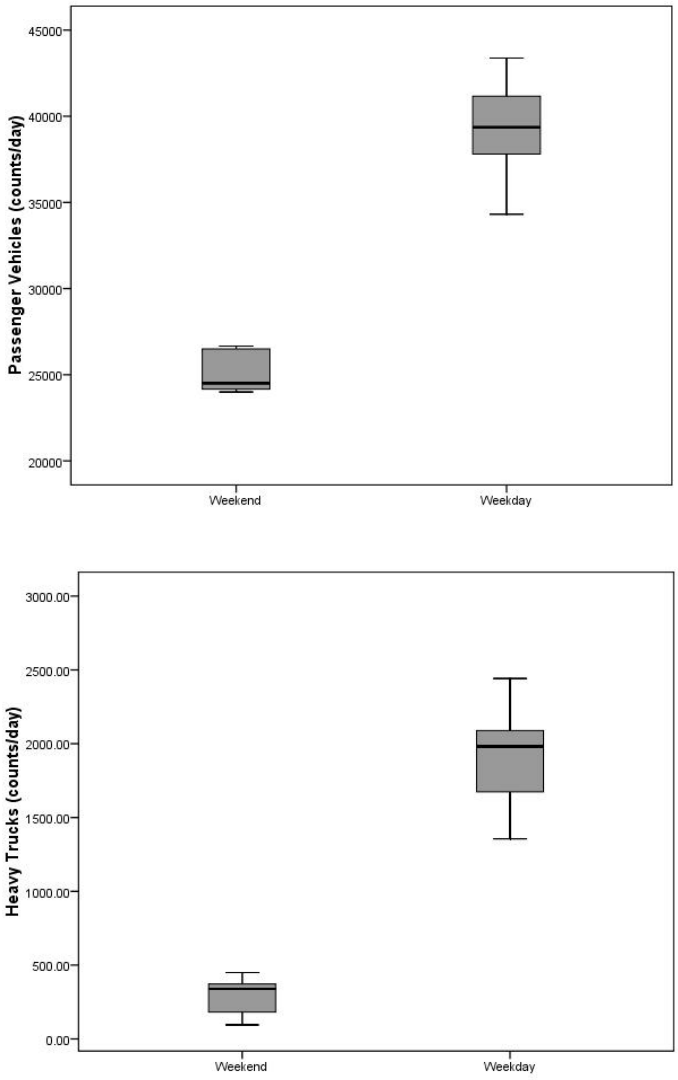

Figure 6.1.4: Weekday/weekend variation in traffic counts on highway 99, adjacent to Seattle Duwamish site.

Table 6.1.4: Weekday/weekend variation in traffic counts on highway 99, adjacent to Seattle-Duwamish site. P<0.05 highlighted in boldface.

NPAH	Type of Day	N	Median	Mean	Std. Deviation	Std. Error Mean	F (sig)*	p**
Passenger vehicles	Weekday	16	39358	38454	4872	1212	0.40	**< 0.01**
	Weekend	7	24510	24666	2296	868		
Heavy Trucks	Weekday	16	1982	1821	510	128	0.13	**< 0.01**
	Weekend	7	339	285	136	52		

*Result of Levene's Test for Equality of Variances. F is not significant for either passenger vehicles or trucks; therefore can assume equal variances for both variables.
**p-value for independent samples t-test comparing NPAH concentrations on weekdays vs. weekends.

Concentrations of all three NPAHs are higher on weekdays compared to weekends, however, this difference is only statistically significant for 1-NP (independent samples t-test, $p = 0.02$, Table 6.1.3). Vehicle counts for both passenger cars and for heavy trucks were also higher on weekdays compared to weekends, and these differences were statistically significant for both vehicle classes (independent samples t-test, $p < 0.01$ for both categories, Table 6.1.4). The weekday/weekend concentration ratio for 1-NP of approximately five is similar to the weekday/weekend ratio of truck counts (~six), and is much greater than the weekday/weekend ratio of passenger vehicle counts (~1.5). This is consistent with diesel exhaust being the major source of ambient 1-NP.

In contrast 2-NP and 2-NFl are not considered to be important components of primary emissions from gasoline or diesel exhaust – rather, they are derived from the photochemical transformation of gas phase precursors (pyrene and fluoranthene). However, since the gas phase precursors are themselves derived from vehicle exhaust (both gasoline and diesel),[53,54] it is not unexpected that levels of 2-NP and 2-NFl are also higher during the week (when total vehicle traffic is high) compared to weekends (when total vehicle traffic is low).

Two distinct pathways have been described for the atmospheric formation of 2-NFl and 2-NP: 1) the hydroxyl radical-initiated pathway ($OH^{\bullet}$), which yields both 2-NFl and 2-NP, and 2) the nitrogen (VI) oxide ($NO_3^{\bullet}$) initiated pathway, which yields primarily 2-NFl.[55] Studies by Arey, Zielinska, and colleagues concluded that ratios of 2-NFl/2-NP close to 10 indicated 2-NFl formation mostly via the hydroxyl-initiated pathway, while ratios closer to 100 indicated mostly - NO_3 initiated 2-NFl formation.[51] Because the $NO_3^{\bullet}$ radical (and associated NO_x species, NO_2 and N_2O_5) can play an important role in atmospheric chemistry,[51] particularly at night when these NO_x species exist at higher concentrations, the ratio of 2-NFl to 2-NP is of interest not only for

assessment of NPAH formation, but also because it provides insight into the overall atmospheric chemistry of a specific location or airshed. 2-NFl/2-NP ratios measured at the Seattle Duwamish site are shown in Table 6.1.5.

Table 6.1.5: Concentration ratio of 2-NFl to 2-NP. p < 0.05 highlighted in boldface.

2-NFl:2-NP	N	Median	Mean	Std. Error	F (sig)*	p**
All Data	41	9.5	12	1.7	-	-
Non-heating	25	16	17	2.2	**< 0.01**	**< 0.01**
Heating	16	3.3	5.0	0.9		
Weekend	15	5.8	11	2.8	0.93	0.48
Weekday	26	10	13	2.1		

*Result of Levene's Test for Equality of Variances. F is significant for heating vs. non heating but not for weekday/weekend comparison. Therefore, we can only assume equal variances for weekday/weekend comparison.
**p-value for independent samples t-test comparing NPAH concentration ratios heating vs. non-heating season and weekdays vs. weekends.

The average 2-NFl/2-NP ratio is 12. As noted above, this indicates a dominance of the hydroxyl radical-initiated pathway for the formation of these two compounds. Also shown in Table 6.1.5, the 2-NFl/2-NP ratio was not significantly different on weekdays compared to weekends. When the data are sorted by season, the 2-NFl/2-NP ratio is 3-fold higher in the non-heating season compared to the heating season. Both values are close to the benchmark value of 10 that is characteristic of the hydroxyl-radical formation mechanism. The higher 2-NFl/2-NP ratio in summer is consistent with the observation that concentrations of fluoranthene (the gas-phase precursor to 2-NFl) are 50% higher in summer vs. winter, where as levels of pyrene (precursor to 2-NP) do not change with season. Seasonal differences in the relative atmospheric lifetimes of 2-NFl and 2-NP would also result in seasonal differences in the 2-NFl/2-NP ratio.

The ratio of the concentrations of 2-NFl to 1-NP has also been employed to assess the relative influence of primary sources as opposed to atmospheric formation for ambient NPAH levels.[46,50,56] Some studies have implied that a 2-NFl/1-NP concentration ratio of 5 or greater has been reported as indicative of NPAH levels dominated by atmospheric reactions whereas a ratio less than 5 indicated a dominance of primary emissions.[46,50,56] Ratios of 2-NFl/1-NP are included in Table 6.1.6.

The average 2-NFl/1-NP ratio is 4.0. This ratio is rather close to the value of five that was taken to denote the crossover point between dominance of atmospheric formation compared to primary emissions. Therefore, it is concluded that both primary emissions and secondary aerosol are

important contributors to NPAH concentrations at the Seattle Duwamish site.

Table 6.1.6: Concentration ratio of 2-NFl to 1-NP. p < 0.05 highlighted in boldface.

2-NFl/1-NP	N	Median	Mean	Std. Error	F (sig)*	p**
All data	41	3.3	4.0	0.52	-	-
Non-heating	25	3.8	4.9	0.8	**< 0.01**	**0.02**
Heating	16	2.2	2.7	0.4		
Weekend	15	4.1	4.9	1.1	0.18	0.18
Weekday	26	3.0	3.5	0.5		

*Result of Levene's Test for Equality of Variances. F is significant for heating vs. non heating but not for the weekday/weekend comparison. Therefore, we can only assume equal variances for weekday/weekend comparison.
**p-value for independent samples t-test comparing NPAH concentration ratios heating vs. non-heating season and weekdays vs. weekends

The 2-NFl/1-NP ratio was somewhat lower on weekdays compared to weekends – consistent with lower contributions of primary vehicle emissions on weekends – although this difference was not statistically significant (p = 0.18, Table 6.1.6). The 2-NFl/1-NP ratio is also higher in summer compared to winter, and this difference is statistically significant. Although diesel (and hence 1-NP) emissions are not expected to vary seasonally, the rate of formation of 2-NFl is expected to be higher in summer compared to winter. This is because the photochemical processes leading to formation of 2-NFl will be more significant in summer when the flux of solar radiation is higher. In addition, concentrations of fluoranthene (the gas phase precursor to 2-NFl) are 50% higher in summer vs. winter.

6.2. Correlations of NPAHs with other air toxics

We explored associations between the NPAH concentrations, and concentrations of several other contaminants and indicator variables measured at the Duwamish site. These associations are summarized in Table 6.2.1. In both seasons, 1-NP is correlated with 1,3-butadiene, acetaldehyde, benzene, black carbon, elemental carbon, naphthalene, 2-NP and 2-NFl. In particular, many of these are variables that are typically associated with vehicle exhaust and diesel exhaust. 1-NP is also associated with truck traffic, but not passenger vehicles in the non-heating season (traffic data were not available for the heating season). 1-NP was correlated with delta carbon in the non heating season, but not the heating season (where delta carbon is expected to be dominated by wood smoke). 1-NP was correlated with $PM_{2.5}$ in the heating season, but not the non-heating season.

Table 6.2.1: Correlations (spearman rho) between NPAH and other species measured at the Seattle Duwamish site. p < 0.05 highlighted in boldface.

Measured Parameter	Non-Heating Season			Heating Season		
	2-NP (pg/m3)	2-NFl (pg/m3)	1-NP (pg/m3)	2-NP (pg/m3)	2-NFl (pg/m3)	1-NP (pg/m3)
1,3-Butadiene	**0.70****	**0.57****	**0.68****	**0.71****	**0.62***	**0.73****
Acetaldehyde	**0.51***	**0.78****	**0.43***	0.53	**0.62***	**0.62***
Acrolein	0.23	0.24	-0.01	0.23	0.17	0.10
Benzene	**0.75****	**0.76****	**0.69****	**0.69****	**0.63***	**0.70****
Black Carbon	**0.73****	**0.81****	**0.89****	**0.86****	**0.78****	**0.85****
Carbon Tetrachloride	0.16	0.14	0.36	-0.06	-0.10	-0.05
Chloroform	0.28	**0.42***	0.30	0.40	0.34	**0.54***
Elemental Carbon	**0.70****	**0.75****	**0.69****	**0.61***	0.51	**0.69****
Formaldehyde	0.13	**0.55****	-0.01	0.40	0.41	0.30
Levoglucosan	0.06	0.07	-0.13	0.54	0.27	0.44
Naphthalene	**0.72****	**0.86****	**0.64****	**0.67****	**0.74****	**0.75****
$PM_{2.5}$	0.16	0.37	0.12	**0.93****	**0.88****	**0.86****
Delta Carbon	0.10	0.00	**0.41***	-0.21	-0.21	-0.09
Passenger Vehicles	0.07	0.20	0.37	-	-	-
Heavy trucks	0.36	0.39	**0.62****	-	-	-
2-NP	-	**0.82****	**0.81****	-	**0.94****	**0.87****
2-NFl	**0.82****	-	**0.71****	**0.94****	-	**0.9****
1-NP	**0.81****	**0.71****	-	**0.87****	**0.90****	-

**Correlation is significant at the 0.01 level (2-tailed). *: Correlation is significant at the 0.05 level (2-tailed).

2-NP and 2-NFl were highly correlated with 1-NP in both seasons, and were correlated with many of the same traffic related chemicals that 1-NP was associated with (e.g. black carbon, elemental carbon, benzene, naphthalene). This observation is consistent with formation of 2-NP and 2-NFl from gas-phase precursors (pyrene and fluoranthene) that are abundant in emissions from both gasoline and diesel vehicles. However, 2-NP and 2-NFl were not specifically correlated with the passenger vehicle or truck variables.

We explored associations between the NPAH concentrations, and estimated source contributions derived from the PMF model that was based on the hourly non-methane hydrocarbon data from the GC-FID (Table 6.2.2). The hourly data had to first be composited to 24-hr averages for comparison with the NPAH data, and there were only 7 days of overlap between the two techniques.

As shown in Table 6.2.2, 1-NP shows a strong association with the "diesel tailpipe" source factor (#2) and a somewhat weaker association with the "Port/Fueling" factor (#3). It was not

significantly associated with any of the other source factors, including the crankcase feature (#7). This observation is in agreement with a study by Liu et al,[57] in which on-road emissions from diesel buses were measured. Separate samples were collected representing tailpipe emissions and crankcase emissions (collected from the vehicles' road-draft tubes). 1-NP was only found to be present in the tailpipe emissions. 2-NP and 2-NFl are both associated with the three sources: "Wood Smoke 1" (#1), "Port/Fueling" (#3), and "Gasoline/LPG" (#5). These associations are reasonable since all three are combustion sources and are likely to be a major source of the gas phase precursors pyrene and fluoranthene.

Table 6.2.2: Correlations (spearman) between NPAH concentrations and PMF-derived source contributions. $p < 0.05$ highlighted in boldface.

NPAH		Factor 1 "Wood Smoke 1"	Factor 2 "High Load Diesel"	Factor 3 "Port/Fueling"	Factor 4 "Other PM"	Factor 5 "Gasoline/LPG"	Factor 6 "Wood smoke 2"	Factor 7 "Crankcase"
2-NP	Spearman's rho	**0.847**	0.321	**0.821**	-0.5	**0.821**	0.5	0.464
	Sig. (2-tailed)	0.016	0.482	0.023	0.253	0.023	0.253	0.294
	N	7	7	7	7	7	7	7
2-NFl	Spearman's rho	**0.793**	0.429	**0.964**	-0.071	**0.857**	0.286	0.321
	Sig. (2-tailed)	0.033	0.337	0	0.879	0.014	0.535	0.482
	N	7	7	7	7	7	7	7
1-NP	Spearman's rho	0.414	**0.857**	0.714	-0.286	0.607	-0.036	-0.071
	Sig. (2-tailed)	0.355	0.014	0.071	0.535	0.148	0.939	0.879
	N	7	7	7	7	7	7	7

7. Results of Marine Emission Source Evaluation

7.1. Marine Emissions Background

Diesel particulate sources also include marine vessels that travel and moor in Puget Sound and the ports. The emissions from marine vessel traffic are a concern on the health of local populations in our area. To better understand maritime emissions, we studied a method for remotely monitoring local ship traffic and a method to assess potential ship emissions. We monitored ship traffic using routine transponder information, and monitored potential emissions using LIDAR (see Chapter 2 for more details on both techniques).

Among mobile sources, marine vessel emissions are perhaps the least understood in terms of their relative impact. The large ports in Seattle and Tacoma present concern for local populations, as marine emissions may contribute significantly to DPM exposures in areas such as the Duwamish River Valley. Various maritime activities have been found to contribute about 25% of the diesel particulate matter in our jurisdiction (Figure 7.1.1). These results are based on a series of assumptions about meteorological conditions, and the rate of emission from the vessels, among other variables.

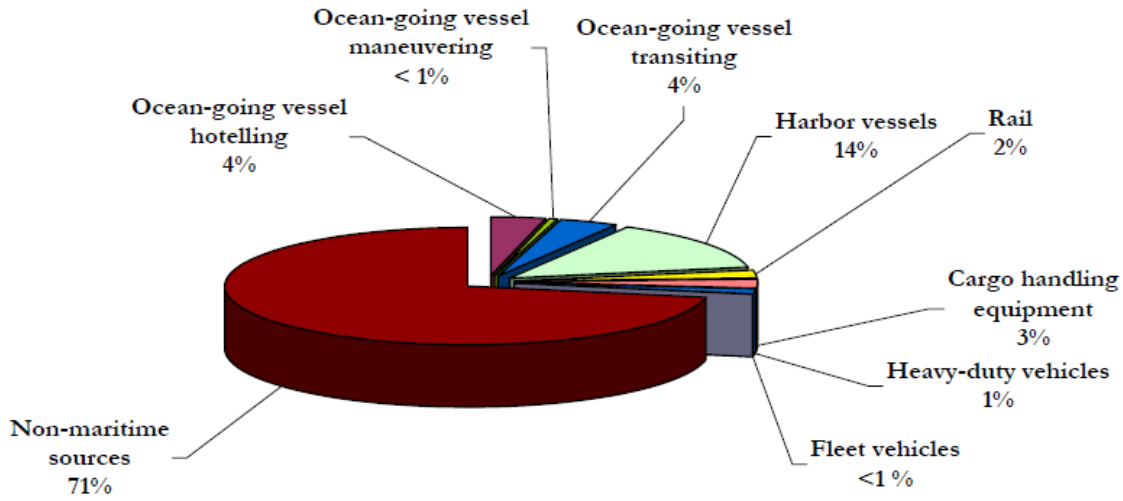

Figure 7.1.1 The above pie chart shows relative contributions of Maritime and Non-maritime DPM emissions in the PSCAA region (from the Puget Sound Emissions Inventory)[58]

7.2. Use of Automatic Identification System (AIS) in Modeling Emissions

7.2.1. AIS Overview

To better estimate diesel emissions from vessels, atmospheric dispersion modeling could be used with appropriate data inputs. However, there are many challenges to modeling a marine vessel's emission accurately. The DPM generation rate of the exhaust stack of a vessel varies according to the maximum continuous power rating (MCR) of the engine, the load placed on the engine (related to vessel speed), fuel type, and engine specific characteristics. The generation rate also depends on the emission factor (EF), or mass of pollutant produced per unit energy (g/kW•hr) invested in vessel operation.

In this study, remote monitoring of ship traffic was conducted by collecting data from Automatic Identification System radio transmissions from vessels operating in the Puget Sound. The Automatic Identification System (AIS) is a shipboard broadcast system operating in the VHF (very high frequency) radio band that provides a short range coastal tracking system for identifying and locating vessels. AIS transponders have a typical horizontal range of up to 75 km. AIS transponders are designed to automatically provide information about ship movements directly to other ships and to coastal authorities.

The International Maritime Organization (IMO) requires all ships over a certain size to carry AIS transponders (see Chapter 2 for more detail). AIS transponders are required to provide the ship's identity, type, position, course, speed, navigational status and other safety-related information automatically to appropriately equipped shore stations, other ships, and aircraft. A list of the associated AIS information available is provided in Table 7.2.1.

Table 7.2.1: AIS data provided by transponders

Data Broadcast Every 20 seconds	Data Broadcast Every 6 Minutes
Maritime Mobile Service Identity (MMSI) number	IMO ship identification number
Navigation status: "at anchor", "under way " etc.	Radio call sign
Rate of turn: right or left, 0 to 720 deg/minute	Vessel name
Speed over ground: 0 to 102 knots (0.1- resolution)	Type of ship/cargo
Position: Latitude/Longitude to 1/10000 minute	Dimensions of ship – to nearest meter
Course over ground: relative true north to 0.1 deg.	Location of GPS antenna on the vessel
True Heading: 0 to 359 degrees	Draught of ship – 0.1 meter to 25.5 meters
UTC time stamp to the nearest second	Destination – max 20 characters
	ETA at destination

The information from AIS broadcasts was logged over a period of 12 months by a remote computer and AIS receiver using an antenna located at our Seattle Queen Anne air monitoring site. A commercial software program automatically collected the signals and saved them as rows in a text file. A total of about 400,000 lines of vessel reports were logged, representing about 1600 unique vessels. Raw AIS signal logs were then post-processed using a custom computer program to produce summary files of vessel traffic in different areas representing a 4km by 4km grid of Puget Sound. This summary data was then imported into a GIS database and used to map vessel traffic in various regions and time periods.

In addition the above monitoring of general vessel traffic, the AIS system also provides much of the information needed to model emissions from a vessel. From the time dependant and independent information listed in Table 7.2.1, model inputs like engine loading (based on speed), engine types, and ship path can be extracted.

To assess the usefulness of the ship tracking data, a demonstration project was conducted to model the emissions from one cargo vessel that visited the Port of Seattle. In order to find an appropriate vessel for modeling, we arbitrarily chose three consecutive days (2/12/09-2/14/09), and then merged the three days into one file by importing them into SPSS. We removed extraneous information from the SPSS file by eliminating unnecessary columns (variables) and rows (e.g. incomplete/erroneous signals). The Maritime Mobile Service Identity (MMSI) number, speed, date and time, latitude, longitude, and status remained in the database as columns. We organized the data so that full vessel paths could be viewed as a series of chronological

signals, and the rows were then sorted first by time of signal and then by MMSI. The vessel movements in terms of latitude and longitude, along with the time stamp, vessel status (e.g. moored, underway, fishing, etc.), vessel speed (knots), MMSI, course, and heading were extracted from the database and used for more detailed modeling.

In the demonstration project, atmospheric dispersion modeling with CALPUFF was used to model the emissions from a specific vessel as it travels through the Puget Sound to Harbor Island, moors, and then travels back out. In addition to information from the AIS, additional information derived from the ship's registry and MMSI were used to derive emission factors for diesel particulate from the vessel. These data were combined with hourly meteorological data to estimate the concentration fields resulting from this vessel's activity. A summary of this detailed modeling is described here, and a more detailed report is provided in Appendix C.

7.2.2. AIS Remote Monitoring Methodology

The AIS data logged during the study was post-processed into summary files of vessel traffic in a set of 21 zones of 4km x 4km squares over Puget Sound from Vashon Island to Edmunds, WA. Vessel traffic in each zone was characterized by a set of descriptors, including vessel type, MMSI, speed, status and position. The track for moving vessels was described by a series of 'transit legs' representing the track crossing a contiguous period of time with a point of entry and exit in a zone, and while within a zone and the average speed and duration of time the vessel remained in the zone.

A database of vessel traffic was constructed with a computer program developed for this project. A program was written in the Python programming language to parse out each ship leg through a zone from the raw AIS data, calculating the average speed and time within the zone, and writing the information to a comprehensive database of ship movements over the entire study period. Each ship leg contained data about the time the ship entered and exited the zone, the average speed, number of signals sent by the ship during the leg, the class of the ship, and detailed information about the size (length, width, and depth) of the ship. These results were then aggregated by ship class and zone for approximately 1 year of data (January – December 2009), to produce the following results.

7.2.3. Marine Traffic Results

Figure 7.2.1 below illustrates the output contained in the summary files after post processing and importing into an appropriate database (SPSS) for about 1 year of data. The figure shows the number of ship legs logged in the 21 zones over the entire period of the study. Although most zones have moving traffic, a proportion of the zones have vessels that are moored and therefore contribute more to the total time rather than the number of legs, which largely depends on vessel movements.

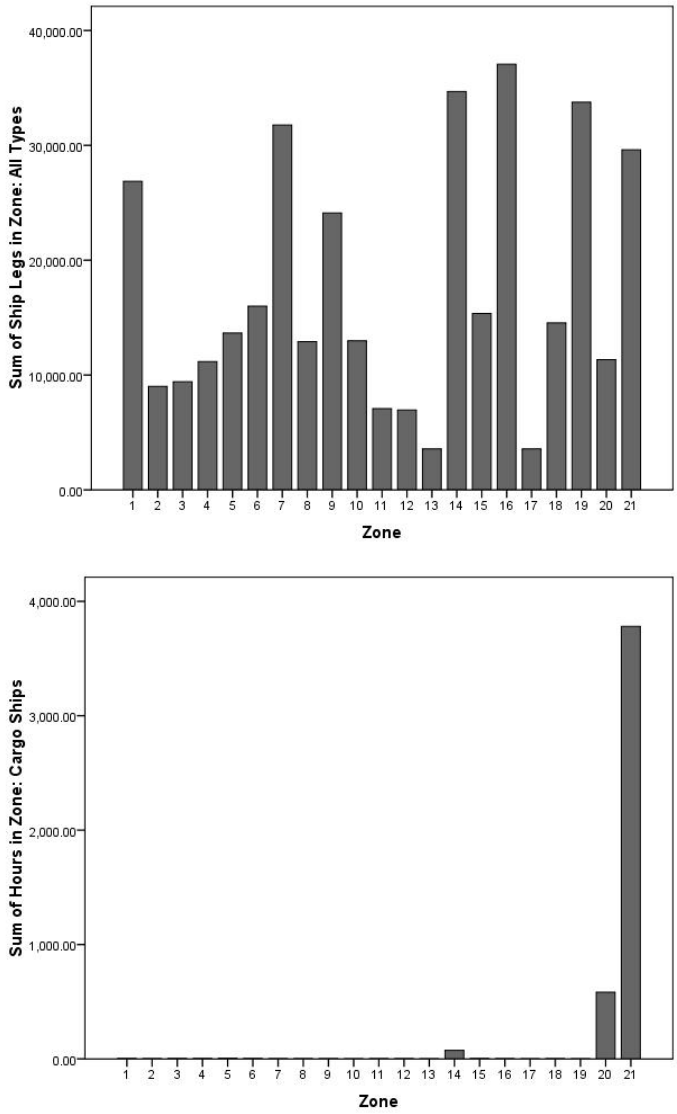

Figure 7.2.1: Top panel, Sum of Ship Legs in Zones for All Ship Types; Bottom panel, Sum of Hours in each Zone for Cargo Ships over 1 Year

In the AIS data, vessels are automatically assigned to one of 16 separate classes depending on their function, size, and registration. These vessel classes were subsequently grouped into large descriptive 'major classes' for summary presentation. Table 7.2.2 below shows summary data for three major classes of vessels that frequently were moving in the waterways. This table shows that the number of hours logged in each zone. Ferries and cargo ships contribute the majority of time across many zones, although tug boat movements also have an important contribution in some areas. In comparison, Table 7.2.3 shows data for the number of transit legs within a zone, which is an indication of the number of trips different vessels make traversing a zone. In this case, the ferries have a large influence, because of the frequent and routine movements across certain routes in Puget Sound. These two tables together relate to average emissions by vessels in each class, since it is the vessel speed which plays a major role in the amount of emissions.

Table 7.2.2: Sum of Hours in Zone by Ship Class: Moving Ships

Zone	Class		
	Cargo Ships	Ferry and Passenger Ships	Tugs
1	13.37	94.26	364.77
2	8.04	8.55	25.27
3	11.07	5.19	28.76
4	14.66	7.02	45.90
5	15.74	37.03	64.21
6	0.18	11.48	40.28
7	8.14	182.77	32.11
8	7.96	36.98	34.06
9	4.37	536.90	21.90
10	1.01	269.24	4574.22
11	6.82	8.75	293.65
12	3.96	2.20	29.43
13	0.93	1.70	14.37
14	78.31	3154.64	1874.00
15	1060.97	66.15	157.96
16	3.39	202.63	49.50
17	0.44	1.41	13.21
18	3.91	295.73	15.18
19	248.59	1923.85	12876.34
20	90.32	1199.52	556.86
21	10154.66	5313.99	7721.74

Table 7.2.3: Sum of Ship Legs in Zone by Ship Class: Moving Ships

Zone	Class		
	Cargo Ships	Ferry and Passenger Ships	Tugs
1	2925	18361	3511
2	2043	3572	2107
3	2872	1688	3159
4	2897	1767	4538
5	2905	2449	5844
6	2888	5281	5352
7	1647	23442	3226
8	1634	6219	3247
9	1124	19862	2119
10	798	8111	2610
11	1502	1150	2804
12	1484	874	2977
13	111	179	1813
14	93	1160	1872
15	1314	6036	4521
16	855	23705	5873
17	389	248	1901
18	915	11729	1601
19	23	783	1176
20	378	3300	2166
21	682	13061	8322

The following figures illustrate the data that can be extracted from the AIS data set and used to map vessel traffic across the region. Figure 7.2.2 presents a shaded map with information on the average speed of moving vessels within each zone across all vessel types over 1 year. The Washington State Ferry routes, noted on the map, again have a major contribution to traffic in the zones which they traverse. Figure 7.2.3 shows the same area, but now containing the total hours spent by moving ships in each zone. In this case, slow moving ship traffic near harbor areas, such as Elliot Bay and the ship channel/locks dominates the map. Figure 7.2.4 shows the total number of legs traveled in each zone by moving ships. This map again is dominated by traffic associated with the Washington State Ferries, because of the frequent trips over nearly fixed routes.

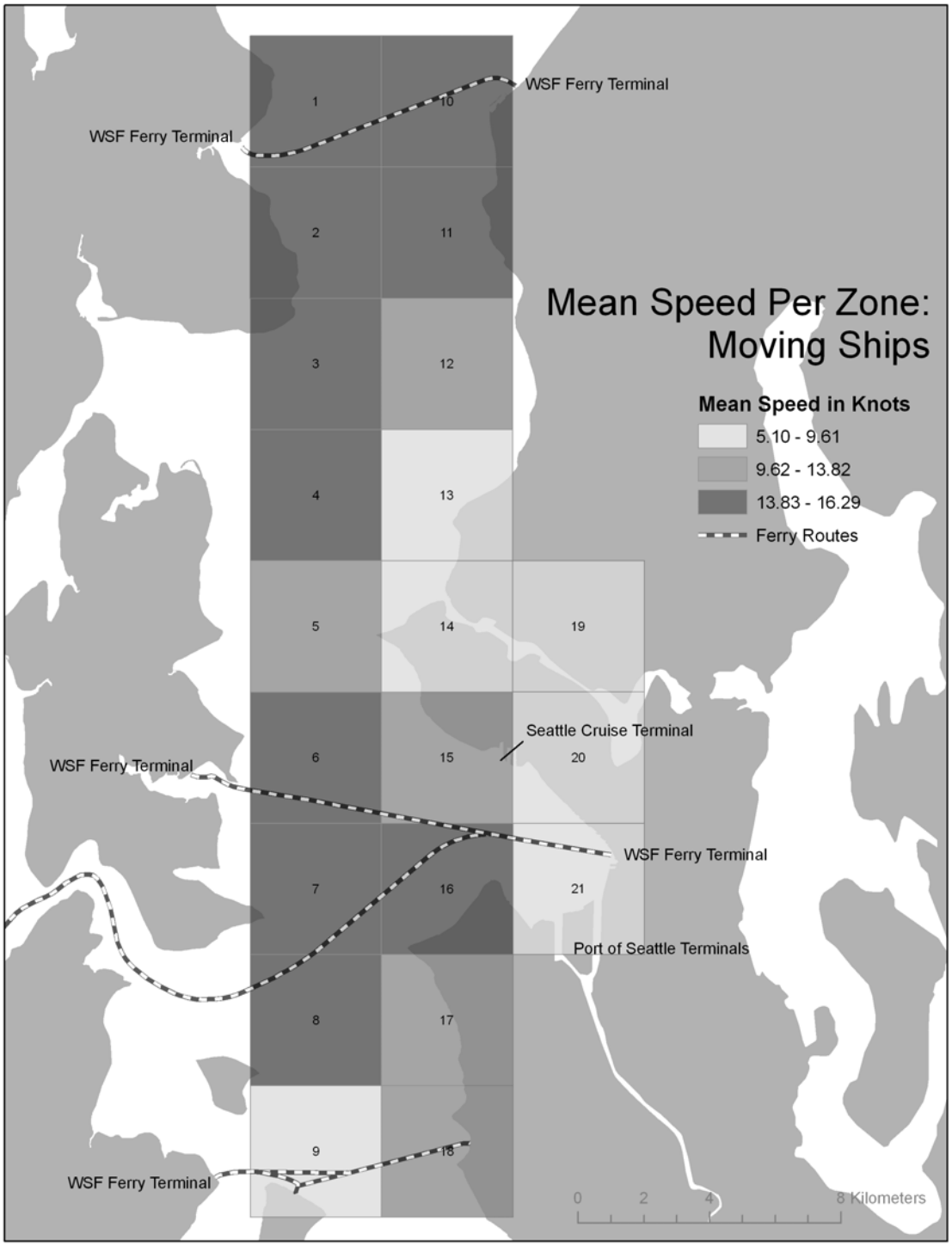

Figure 7.2.2: Mean Speed in Zones for Moving Ships (> 0.5 knots) over 1 Year (January – December 2009)

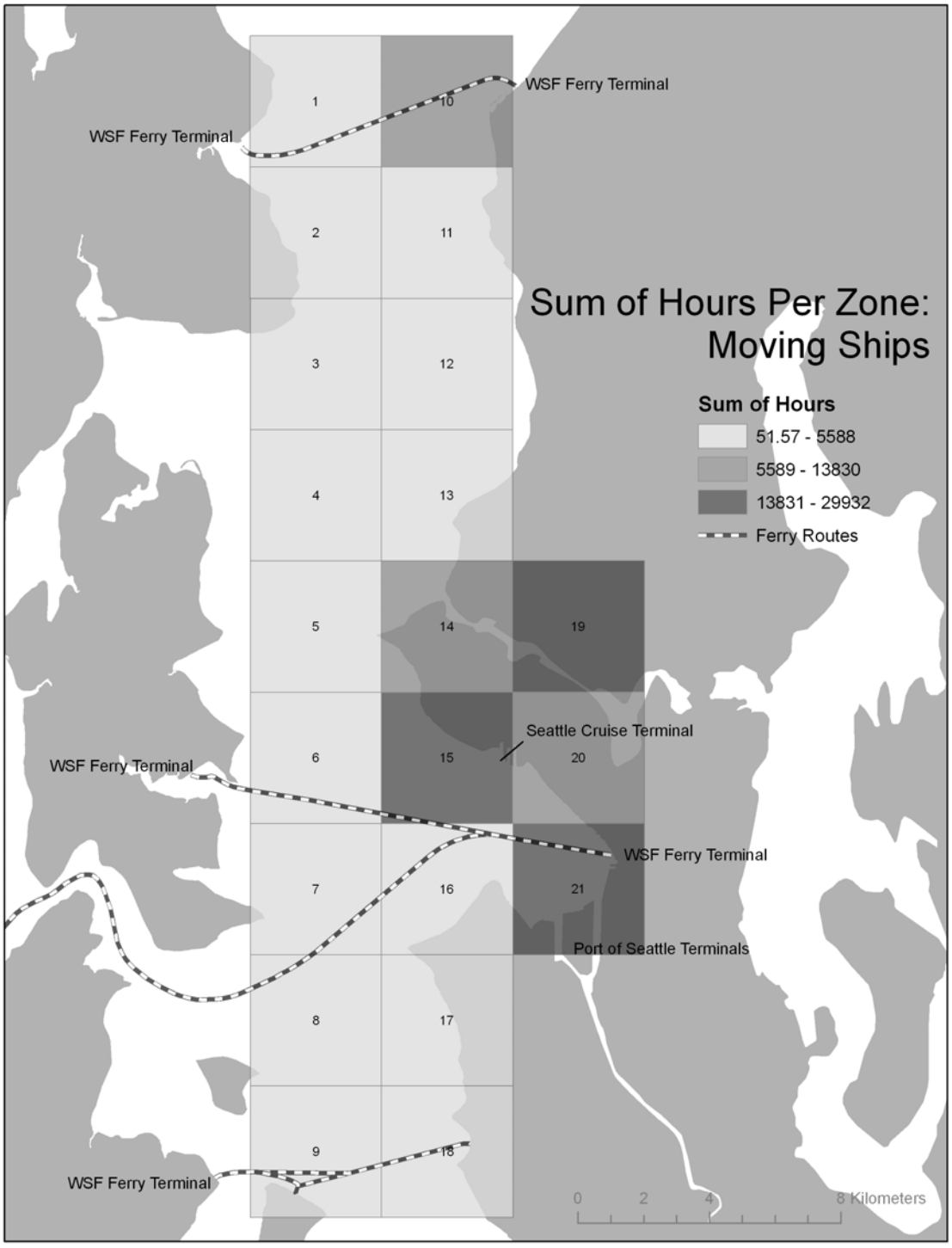

Figure 7.2.3: Sum of Hours per Zone for Moving Ships over 1 Year (January – December 2009)

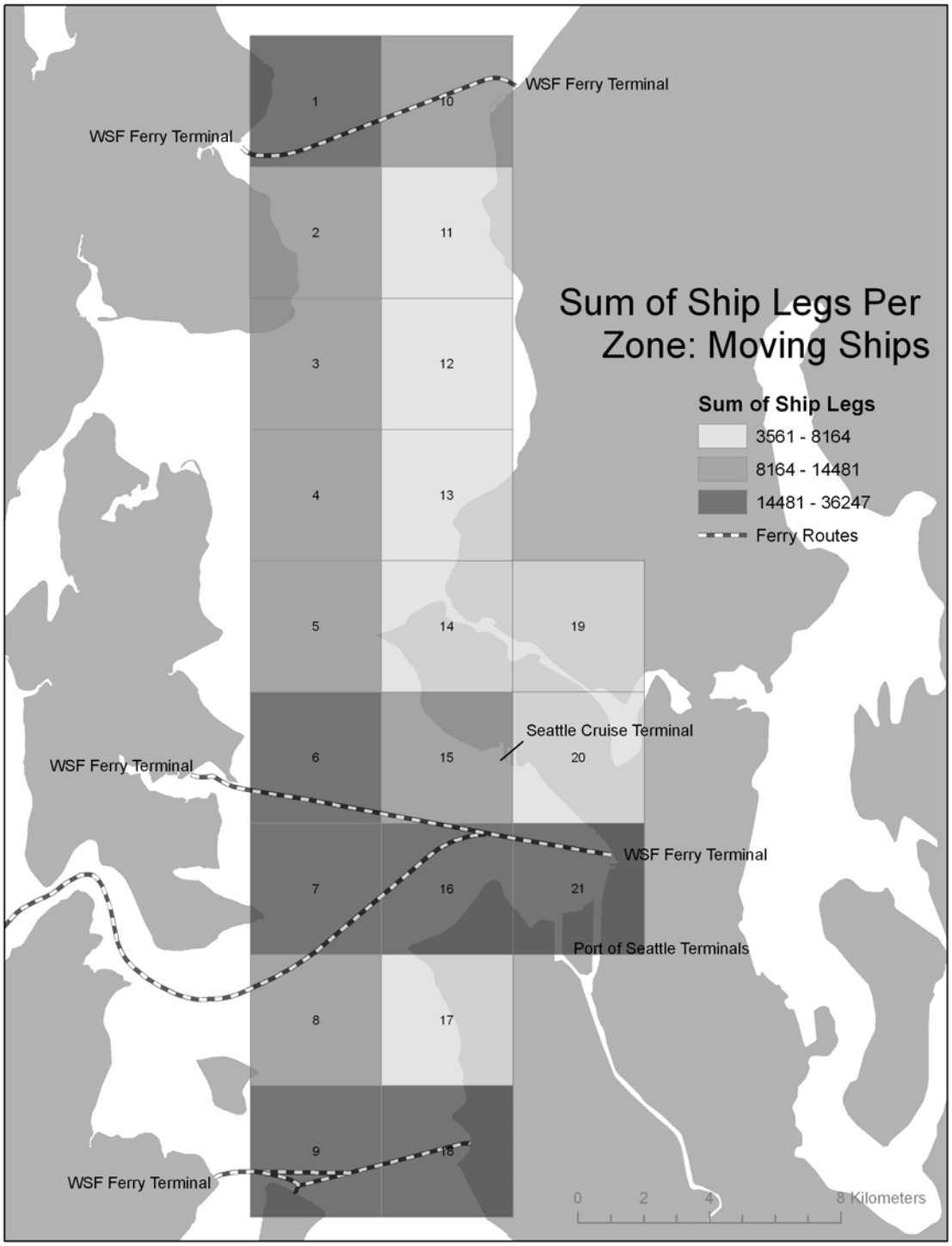

Figure 7.2.4: Sum of Ship Legs per Zone for Moving Ships over 1 Year (January – December 2009)

7.2.4. Demonstration project: modeling marine emissions

Given the positions of the vessels over time, modeling vessel traffic and emissions from vessels may be done using atmospheric dispersion modeling, although accurately modeling a marine vessel's emission is quite challenging. The DPM generation rate of the exhaust stack of a vessel varies according to the maximum continuous power rating (MCR) of the engine, the load placed on the engine, the fuel type being used by the vessel, and the emission factor (EF), which is the mass of pollutant produced per unit energy (g/kW•hr) invested in vessel operation.
The Puget Sound Emissions Inventory contains most of the necessary vessel specific information such as maximum speed (MS), maximum continuous rated engine power (MCRP) and an estimate of auxiliary engine power for large cargo vessels, which are a subset of the vessels that provided AIS signals. We therefore selected a large cargo vessel that was characterized in this inventory for more detailed modeling.

Figure 7.2.5: The vessel chosen for the demonstration project, shown with its identity concealed. Some vessel parameters are: draught-12.7 m, DWT-67660 tons, length- 270 m, width -40 m , MCR_p-46574 kW, MS-25 knots.

Additionally, we wanted a vessel to travel from the northern Puget Sound area, en route to the eastern side of Harbor Island in Seattle, moor there for some time, and then depart along a similar path back out of the modeling area. This shipping track was particularly desirable because it would be commonly encountered and ideal in terms of feasibility of measurement for ships in port by LIDAR. To ensure that the vessel track of choice involved mooring at Harbor Island, signals from outside the general Harbor Island area were temporarily filtered out of the dataset.

We then created a list of the remaining vessels and used the AIS marine traffic website to gather their length and width dimensions, deadweight tonnage (DWT), and vessel type (e.g. cargo, tug, etc.). The second largest vessel on the list was then chosen because it had an ideal shipping route (Figure 7.2.5). The shipping track used in this modeling demonstration is shown in Figure 7.2.6 below.

1. 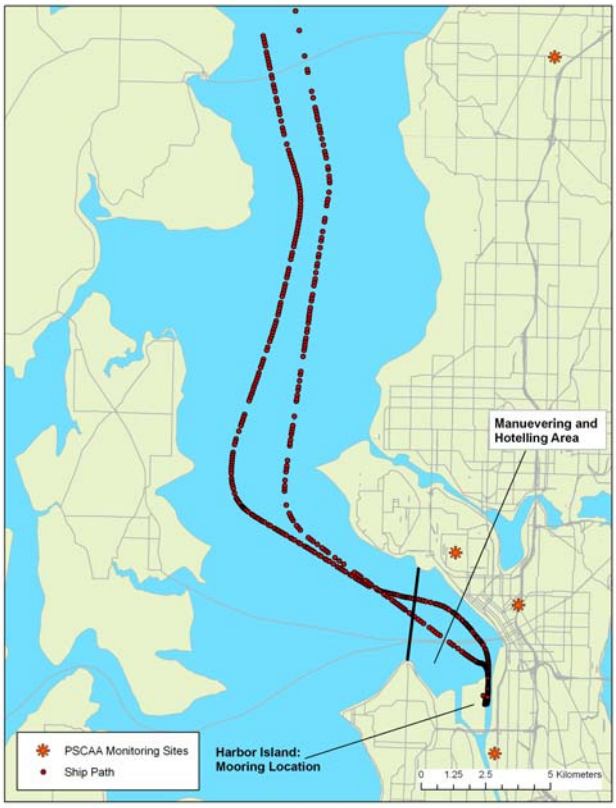

Figure 7.2.6: Map of the Puget Sound/Seattle area showing the track of the chosen vessel as derived from the AIS signals that were received. The vessel traveled along the track that is further west for the majority of the section where it is transiting into Harbor Island, and departed along the western route. The vessel was characterized as "maneuvering" when it was not hoteling, but was located east of the dark line drawn across Elliot Bay.

7.2.5. Approach to estimating emission factors

To model the emissions occurring between one signal and the next, a point source was created at the spatial midpoint between the coordinates given by consecutive AIS signals (Figure 7.2.7). The midpoint was determined for each pair of consecutive signals.

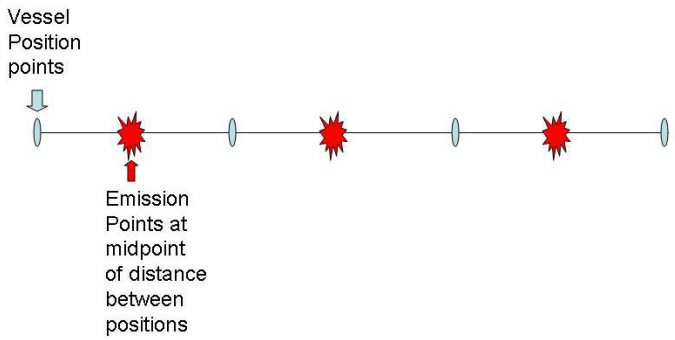

Figure 7.2.7: Maintaining the same times and positions given by AIS (light blue), a vessel's emission was represented by placing a source at the midpoint between two positions and having it emit during the period that the vessel passes between them.

The process used to estimate the emission rate (g/s) for each of these point sources is described below. The equation to obtain an emission rate (E), commonly used in larger scale emissions inventories such as the Puget Sound Maritime Air Emissions Inventory, is:

$$E = MCR_p \cdot LF \cdot A_h \cdot EF_{avg} \cdot FC$$

where MCR_p is the maximum continuous rated power of the vessel (kW), LF is the load factor or fraction of the engine's rated power that is used for operation, A_h is the time spent in a certain activity (e.g. hoteling, transit, maneuvering) usually given in hours, EF_{avg} is the average emission factor or mass of pollutant emitted per energy invested in operation (g/kW•hr), and FC is the fuel correction factor that adjusts emissions based on the type of fuel being used. The FC was not relevant to this study because the vessel that was ultimately chosen uses heavy fuel oil (HFO) with 2.5% sulfur, which has an FC of 1. A_h did not really apply in the usual sense either, as the quantity of interest was the instantaneous emission rate rather than tons emitted per year. However if this equation were used to estimate average emissions from multiple vessels over some time period, then A_h could be applied to account for these different activities.

For the load factor, the propeller law was used as was done previously in the Puget Sound Inventory:

$$LF = \left(\frac{S}{MS} \right)^3,$$

where S is the instantaneous vessel speed received from the AIS system, and MS is the maximum vessel speed. MCR_p and MS for the chosen vessel were both obtained from Appendix E of the Puget Sound Inventory, which contains these values for several ocean going vessels that commonly enter Puget Sound.[58]

In practice, the load factor is more accurate using some higher exponents than 3, such as 4.5 for large high-speed ships (some container vessels), 4.0 for some medium sized medium speed vessels (some roll-on roll-off cargos, reefers, and feeder container ships), and 3.5 for low speed ships (small feeder container ships, tankers, bulk carriers etc.).[60] For any given actual vessel speed, the load factor is a number between 0 and 1, so the cubic relationship gives higher load factors than those that result from higher exponents. To be conservative and over predict emission rates, the cubic relationship was used (as shown in the equation).

The choice of DPM emission factor, EF_{avg}, for both the main propulsion and auxiliary engines was 1.0 g/kW•hr. This estimate is used in the Puget Sound Marine Emissions Inventory and is also consistent with EPA's recommendations. EPA has cited values for ocean going vessels in the range of 0.98 to 1.11 g/kW•hr, and another study found an emission factor of 1.03 g/kW•hr after exhaust was cooled in a dilution system[59]. Also, it has the convenient property of being unity, which makes the scaling of the resulting concentration fields easier if one wants to use a different emission factor.

When these engines operate below 20% load, the emission factor increases because they run less efficiently. The value of EF_{avg} was adjusted for low loads using a table from the Puget Sound Emissions Inventory (Appendix C in the inventory) to get a power law equation that describes how the low load adjustment multipliers (LLAs) relate to the load factor. The following equation,

$$LLA = 0.1826 \cdot LF^{-0.9245}$$

is a good representation of the trend, except near the lowest and highest ends of the relevant load factor scale, which is from zero to 20% load in this case (Figure 7.2.8). To be consistent with the table of LLA multipliers in the Puget Sound Inventory, LLA should be equal to 1 when LF=0.20 and equal to 19.17 when $LF \leq 0.01$.[58] The load factors that result in LLAs of 1 and 19.17 are 0.1589 and 0.006514, respectively. The LLA values from LFs between 0.1589 and 0.20 are close

to 1, so when $0.01 < LF \leq 0.1589$, the equation was applied to adjust for low loads; when $LF \leq 0.01$, LLA was set to 19.17; when $LF > 0.1589$, LLA was set to 1.0.

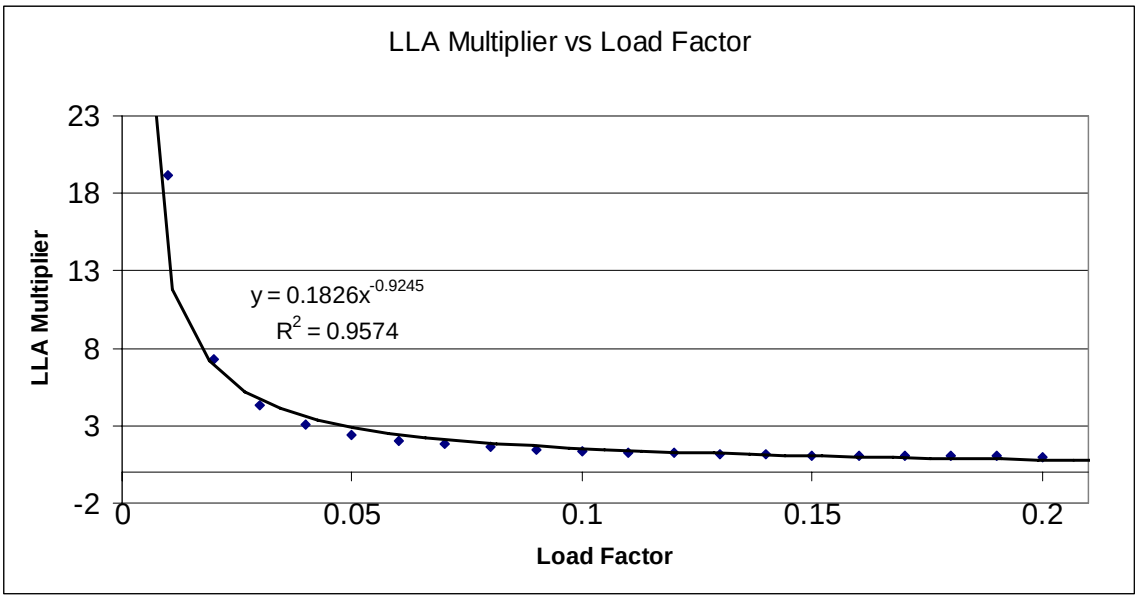

Figure 7.2.8: The power law equation shown was used to adjust for low loads when $0.01 < LF \leq 0.1589$. If $LF \leq 0.01$, LLA was set to 19.17 to be consistent with the Puget Sound Inventory. Near the high end of the curve, where $LF > 0.1589$, LLA was set to 1 (i.e. no adjustment at low load).

Certain weather conditions, hull fouling, acceleration, and other factors that alter the resistance to travel would also influence the true engine load factor. For our purposes, the load factor was adjusted for acceleration, as wave patterns and the extent of fouling were not available.

A "heavier" propeller relationship curve is applied when a vessel accelerates.[60] A vessel travelling at constant velocity would need less power than an accelerating vessel. Acceleration is an operational condition compared to traveling in very heavy seas with wave resistance.

In this project, load values were adjusted for acceleration based on established engine load tables.[60] An acceleration adjustment was introduced by adding 0.09 to the load factor during periods of clear acceleration from low speed to service speed.[60] This rather simple shift in load factor was chosen as the method of adjustment, even though other factors certainly may affect the load in significant ways. Small increases in vessel speed were not considered to be acceleration, and ultimately, only two periods of clear acceleration were adjusted. These periods both occurred after the vessel left the harbor and accelerated to service speed as it traveled north. When a vessel decelerates, the load factor is lower because the vessel's momentum decreases the required

engine power for a given velocity. However, for this study, the load was not adjusted for times when the vessel was decelerating.

For main propulsion engines, the LF was determined for each Universal Transverse Mercator (UTM) coordinate given by the AIS system using the vessel speed recorded at that location, including adjustment for low loads and acceleration. To determine the emission rate at the midpoint between two consecutive coordinates, the average emission rate of these two coordinates was calculated using the following equation:

$$E_{avg} = 0.5 \cdot MCR_p \cdot EF_{avg}\left[LLA_1\left[\left(\frac{S_1}{MS}\right)^3 + A_1\right] + LLA_2\left[\left(\frac{S_2}{MS}\right)^3 + A_2\right]\right],$$

where MCR_p is 46574 kW (propulsion engine power), MS is 25 knots, A_1 and A_2 were the LF adjustments for acceleration at each coordinate (either 0.09 or zero), and LLA_1 and LLA_2 were the low load adjustment multipliers determined by the acceleration-adjusted load factor obtained in the equation above. Note that averaging two values that are derived from a cubic relationship in this manner is not exact. Nevertheless, considering that the acceleration is not known on a continuous basis, and that the change in vessel speed between two consecutive signals is usually quite small, the simplified averaging method in the equation above was used in order to save computational time and simplify data preparation. The difference in results from using different averaging methods is minimal, especially compared to the impact of choosing different exponents in the load factor, but this averaging method does slightly overestimate the value of EF_{avg}. When the vessel was "moored", its propulsion engines are likely to be turned off while auxiliary engines run the necessary operation systems, so EF was set to zero during mooring periods. When the vessel was maneuvering, the load factor was set at 0.03. This value is also derived from the composite maneuvering load factors offered in the Puget Sound Inventory.[58]

The emission rate for the auxiliary engine at each coordinate was determined by using a table from the Puget Sound Inventory to determine appropriate load factors of this vessel type (Container-5000). Maneuvering requires the most demand at 49% load, followed by mooring at 16% load and transit at 13% load. Using the categories described earlier for activity type, the appropriate load factor (0.49, 0.16, or 0.13) was assigned for each AIS signal. Given the load factor, EF_{avg} (1.0 g/kW•hr), and auxiliary engine power rating (MCR_{pa}) of 11,360 kW, the average emission rate of the auxiliary engine was calculated for each midpoint between consecutive signals using the following equation:

$$E_{avg} = \frac{EF_{avg} \cdot MCR_{pa}\left(LF_1 + LF_2\right)}{2}$$

LLA multipliers and acceleration adjustments were not applied in this case, because the relationship between vessel speed and auxiliary engine load factors is qualitatively different. It is also important to note that the three possible LF values for auxiliary engines are averages across vessel types, as vessel-specific information on auxiliary engines is not widely available. To get the total emission rate of the vessel, the E_{avg} from the main propulsion and auxiliary engines were summed. This total E_{avg} was therefore used as the emission rate of each point source created from the midpoint between consecutive AIS signals.

The model was treated with each point emitting at this specific rate for the time period defined by the two signals used to calculate the spatial midpoint. After the time that the next AIS signal is reached, this source turns off and the source emitting at the next midpoint turns on. This process continues so that at any one time, exactly one source is emitting along the track of the vessel while the rest of the sources are inactive.

7.2.6. Emission Modeling Results

We used CALPUFF and post processing CALPOST to model the ship emissions from 1 ship coming into and out of the Port of Seattle. Overall, we found that emissions could be modeled, and this could be applied to multiple ships, although determining concentrations proved more difficult in application. We also found that meteorological conditions play a strong role in the dispersion of particulate matter from an individual ship's emissions and that nearby urban areas could potentially be affected by this modeled ship path in summer months.

The results for the modeling can be found in appendix C. The concentration fields shown in the appendix are modeled from one ship, and appear to much higher than prior peer-reviewed modeling studies using well-established methods.[2,61,62] Moreover, these published studies estimated *total* diesel emission estimates from all sources whereas our model is based only on *one* ship. At this time, we are still seeking to understand why the presented concentration fields appear so large. One area for further examination is the estimation of emission rates.

Overall, the AIS was shown to be particularly useful for passively collecting information on ship movements and activities, and with appropriate linkage to other data sources can be used to estimate emissions from ship traffic. The demonstration modeling project, showed that in principle it is possible to track a vessel both in transit and in port, and model the emissions during this time. This approach to monitoring ship traffic could provide an attractive and relatively low cost means of estimating marine emissions, but further examination and refinement of the modeled results is needed.

7.3. LIDAR Monitoring of Ships in Port

The LIDAR instrument was deployed on several field campaigns near the Port of Seattle, at Bush Point on Whidbey Island, and at Fort Flagler State Park, WA. The Port of Seattle could not provide any access to their property or facilities in support of this study. Consequently, it was necessary to place the LIDAR about 500 m away from the loading areas, across the shipping channel from Harbor Island at the Jack Perry Memorial Shoreline Public Access near Pier 36 at the end of South Massachusetts Street, Seattle, WA. An aerial photo of the location is shown below. This location was near ships during loading, but the view of the exhaust stacks was somewhat limited and blocked occasionally by equipment.

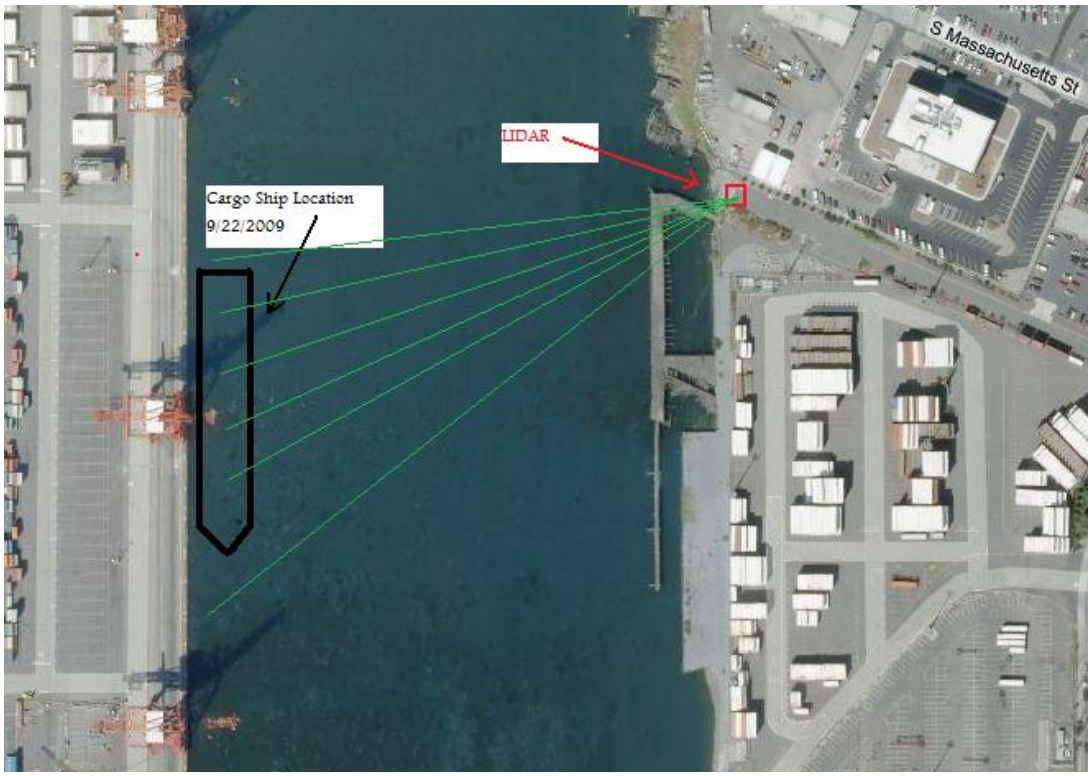

Figure 7.3.1: LIDAR monitoring placement across from Harbor Island, Port of Seattle

The ORCA Photonics LIDAR system was deployed at the public waterfront access on September 22, 2009. The location was at the east side of the entry of south Harbor Island of the Port of Seattle. A container ship was docked at T-18 during the observations. The LIDAR scanned vertically and horizontally across the entire solid angle surrounding the ship and was able to detect the plume of the auxiliary engine.

To visualize the data, the backscatter signal was normalized to the far-field background which was selected to represent ambient aerosol and molecular backscatter. A detector noise threshold also was applied so that backscatter intensity data below a minimum noise level (< 5 mV) was treated as zero for the purposes of clarity in data visualization. Additionally, the data for the initial 300 m was ignored in the data visualization step—again for clarity purposes. Figure 7.3.2(A) shows a polar plot (elevation = 3.00 m and azimuth = 6-15 degrees) of the backscatter intensity from LIDAR observations of the ship at the Port of Seattle terminal. It was deemed through visual inspection of each individual profile scan [Figure 7.3.2(B)] that eliminating this range of data in the plots causes no significant information loss if not presented in the final graphs. As noted in the plot, most of the signal occurs in the range of 500-600 m, which corresponds to the location of the ship exhaust stack.

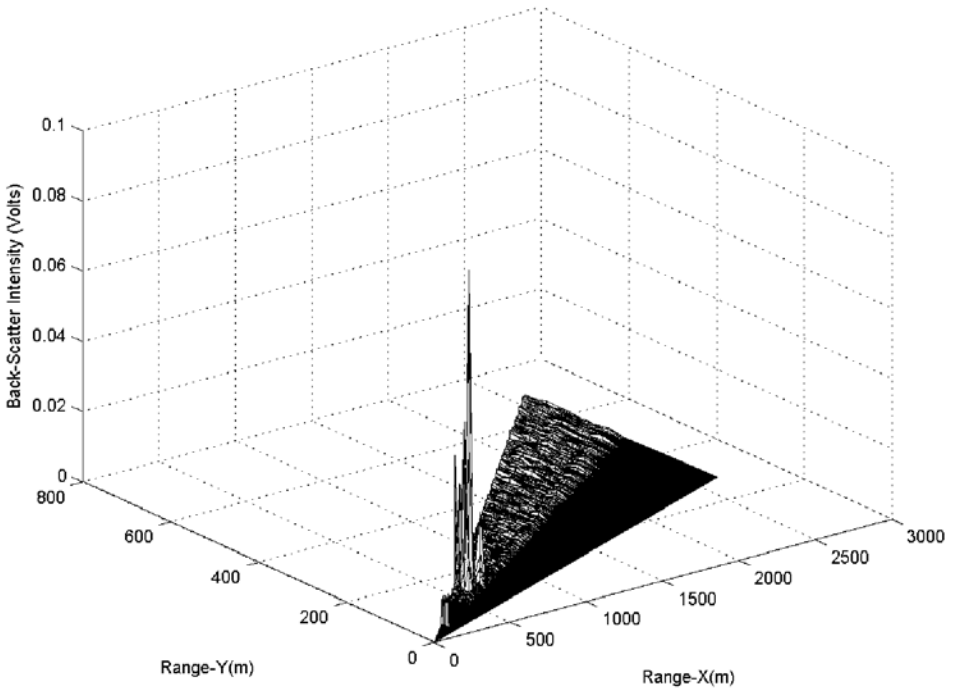

(A)

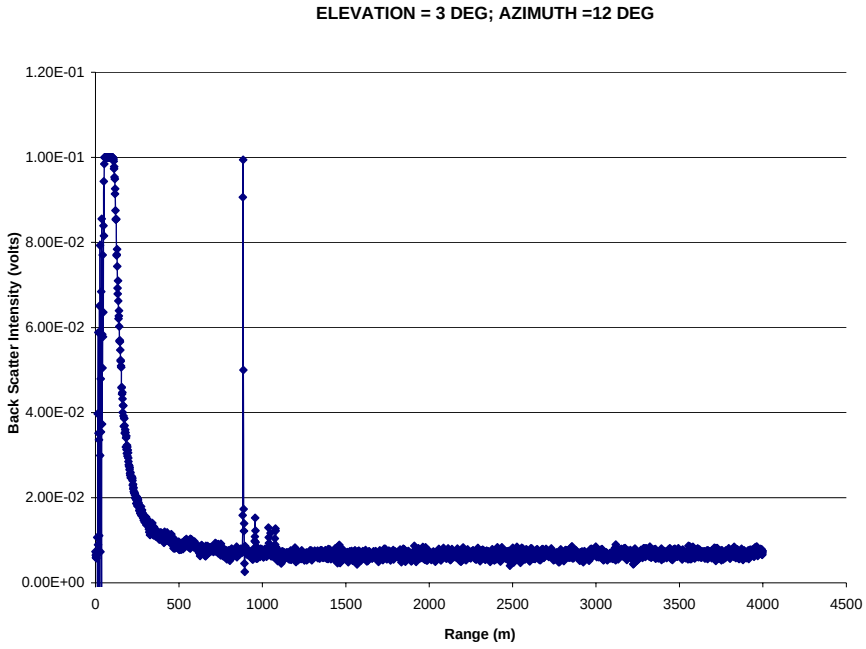

(B)

Figure 7.3.2: LIDAR scans of diesel exhaust emissions for a ship in port (auxiliary engines); (A) 3 dimensional polar plot of backscatter signal of the emissions from auxiliary stack; (B) Raw data from a LIDAR single profile scan of ship emissions.

Direct monitoring of ship emissions with LIDAR also was conducted, but successful data collection only was obtained for ships in port. Although many attempts were made to capture ships in transit, this was unsuccessful because of the rapid movements of the ships and the difficulty of deploying the portable LIDAR system in time to observe ships underway. The study showed that direct observations with LIDAR would require a much more intensive sampling effort, and would require a long-term field deployment of this equipment for monitoring. However, these results demonstrated that remote monitoring of marine traffic using LIDAR is feasible with existing technology.

8. Discussion and Conclusions

In this study, we evaluated a number of novel methods to estimate diesel emissions, gradients, and sources. This chapter summarizes our evaluation of these methods.

New source apportionment models using hourly $PM_{2.5}$, hydrocarbon, and aethalometer data were developed and applied to a diesel impacted site (Seattle Duwamish).

In this effort, we applied a Positive Matrix Factorization (PMF) model using hourly continuous data to distinguish 7 source related factors. The multiple source contributions to the site creates a complex set of factors related to both PM and hydrocarbons.

Using hourly hydrocarbon data, we characterized three distinct features related to motor vehicle emissions: "High Load Diesel", "Gasoline/LPG" and "Idling/Crankcase Diesel". In addition, we associated a factor with combustion exhaust and fuel evaporative emissions described as "Fueling/Port Operations". Highly time resolved hydrocarbon data demonstrated significant potential to successfully resolve different vehicle sources, such as gasoline, truck, and marine emissions elsewhere.

Two wood smoke features, one with higher gas concentrations, "Wood Smoke 1", and one with higher particle concentrations, "Wood Smoke 2", were identified. These factors show that the source contribution to PM at the site is due to many sources, and reflects a variety of factors other than the nearby highway and industrial activities. The "Wood Smoke 1" factor accounts for ~60% of the total benzene concentration. This factor complements our recent air toxics study which identified wood smoke impacted sites had the highest concentrations of benzene in the Puget Sound region.[42]

The PMF source factors account for more than 94% of the variability in PM, but a substantial portion of the PM is not highly associated with hydrocarbon traffic sources. This was not surprising as the "Other $PM_{2.5}$" feature included most of this variance.

A marker for diesel exhaust (1-nitropyrene) was successfully linked to both truck traffic and the hourly PMF results for "High Load Diesel".

This study is the first to measure nitro-polycyclic aromatic hydrocarbons (NPAHs) in ambient PM in the Seattle area. As described in the introduction, 1-nitropyrene has been proposed as a molecular marker for diesel particulate matter (DPM) since it is by far the most abundant NPAH in DPM, while being much less abundant in PM derived from other sources.[1]

The measurements reported herein support the use of 1-nitropyrene (1-NP) as a molecular marker for diesel particulate matter. 1-NP was readily measured in PM collected on readily available, post-weighed Teflon filters using standard $PM_{2.5}$ Federal Reference Method (FRM) sampling methods.

1-NP levels showed a strong association with heavy truck counts on SR-99, and the weekday to weekend ratio of 1-NP concentrations paralleled the weekday to weekend ratio of heavy truck counts. 1-NP was also strongly associated with other traffic derived air pollutants including 1,3-butadiene, acetaldehyde, benzene, black carbon, elemental carbon, and naphthalene. Additionally, 1-NP was associated with the "High Load Diesel" source feature from the hourly PMF results.

A multivariate analysis showed that VOC data can provide a source marker for vehicles and other sources. This analysis also demonstrated additional relationships to the hourly PMF analysis.

Based on multiple linear regression analysis, a subset of the VOC data was found to have statistically significant associations with hourly $PM_{2.5}$, truck traffic, and passenger vehicle traffic. The data generated by the real-time monitoring instruments consisted of 61 different variables observed on an hourly basis; more than 40 of these were VOC species retrieved from the auto GC after applying the automated alignment procedure developed for this study. A multivariate analysis showed that the VOC data can provide a source marker for vehicles and other sources, and this is associated with both truck (and car) traffic and $PM_{2.5}$ levels at the site.

The multivariate analysis identified many species that also appeared in the PMF analysis to apportion $PM_{2.5}$. This lends considerable weight to the reliability of the PMF analysis, which identified several vehicle-related sources for PM at the site. The data set selected for this analysis mainly comes from the non-heating season, which emphasized traffic-related impacts, in keeping with the aims of the study. A more comprehensive analysis with the inclusion of the 1 in 6 speciation data collected across all seasons may be warranted.

Remote monitoring of marine traffic to estimate diesel impacts is feasible with existing data sources and tools.

AIS logging was shown to be particularly useful for collecting information on ship movements and activities. With appropriate linkage to other data sources, passive AIS data collection can be used to estimate emissions from ship traffic and to classify ships by size and activities. The demonstration modeling project, showed that in principle it was possible to track a vessel both in transit and in port, and model the emissions during this entire time. This approach to monitoring ship traffic offers an attractive and relatively low cost means of estimating marine emissions, but further validation of the modeling results is needed.

This model was not intended to be used to estimate precise concentrations and was done for demonstration purposes. There are significant uncertainties in emissions based models, and the model was designed to find maximum concentrations. Therefore, only indirect observations about gradients and diffusion should be made as modeled concentrations were intended to be high and have large uncertainties.

Direct monitoring of ship emissions with LIDAR was conducted, and successful data collection was obtained for ships docked at the Port of Seattle from a significant distance. Although many attempts were made to capture ships in transit, this proved very difficult and was unsuccessful because of the rapid movements of the ships and the difficulty of deploying the portable LIDAR system in time to observe ships once notification was received that they were underway. The study showed that direct observations of ships in transit with LIDAR would require a much more intensive sampling effort, and would require a long-term field deployment of this equipment for monitoring.

A new method for processing Photochemical Assessment Monitoring Stations (PAMS) Ozone Precursor Analyzer data was developed.

An indirect benefit of this project was the introduction of a new process to align spectral data from the gas chromatographs used in the PAMS network. The procedure uses a software package (LineUp, InfoMetrix Inc) to align the chromatograms that typically drift with slight temperature and/or carrier gas pressure changes. These aligned files can then be batch processed, also in an automated manner, by the chromatography software package to identify and quantify VOCs present in the samples. This procedure dramatically reduced the amount of analyst time required to process the hourly GC data. Automation of the alignment process also has the advantage of removing potential for operator error or subjective operator identification of the analytes. This automated alignment procedure should prove especially useful to the EPA PAMS network operators, that use gas chromatography to measure 40+ VOCs on an hourly timescale.

The use of Open Path Fourier Transform Infrared Spectroscopy (OP-FTIR) for resolving gasoline and diesel emissions proved difficult.

The OP-FTIR had unanticipated equipment failures that contributed to reduced data collection during the study and only the May study period was selected for analysis. The instrument was able to measure ambient CO and CH_4 at the site, with 5 minute time resolution. After removing the methane features from the May dataset, the residual non-methane hydrocarbon feature was too small to provide reliable data for classifying gas and diesel vehicle signatures using a simple algorithm based on the C-H stretch spectrum.

Site access restrictions limited the beam path for the FTIR to only 71 meters, which was much shorter than desired (> 200 m). In addition, the beam path could only be located perpendicular to and some distance back from the roadway, rather than running across the highway or parallel to traffic. This configuration probably contributed to reduced roadway hydrocarbons in the beam, and coupled with the limited path length resulted in insufficient signal for the non-methane hydrocarbon analysis.

The study demonstrated that this method was not robust for measurements at ambient concentrations. The instrument could have had more optimal conditions, but it may still not prove successful at ambient concentrations.

A preliminary analysis combining hourly data with speciation data from 24 hour samples also offered very limited data.

A preliminary analysis also was conducted to combine the hourly data with the 1 in 6 speciation data from 24 hour samples, along with other markers such as levoglucosan. This analysis indicated that the "other PM" source had major factors related to OC rich, 1-nitropyrene rich fuel oil and secondary aerosol sources.

These data are limited because there is very little overlap (~10 days) in the two data sets. This makes it difficult to compare these results directly with the results of the PMF apportionment based on the hourly data. Also given the relatively sparse $PM_{2.5}$ speciation data at this site (~ 60 days) we cannot readily identify all possible source-related features influencing the daily $PM_{2.5}$ speciation data.

Processing of additional time periods for the hourly GC data to provide more overlap with the speciation data would strengthen the source apportionment of this other $PM_{2.5}$ data. The current results suggest there may be value in evaluating a source apportionment approach that combines both the multiple linear regression analysis and PMF. The multiple linear regression analysis would be used to pre-select variables for subsequent inclusion in the PMF model.

References

[1] Scheepers, PTJ, Velders, DD, Martens, MHJ, Noordhoek, J, Bos, RP. "Gas-chromatographic-mass spectrometric determination of nitro polycyclic aromatic hydrocarbons in airborne particulate matter from workplace atmospheres contaminated with diesel exhaust." *J Chromatogr A*, 1994, *677*, 107-121.
[2] Puget Sound Clean Air Agency, 2003. "Final Report – Puget Sound Air Toxics Evaluation". http://www.pscleanair.org/airq/basics/psate_final.pdf.
[3] Scheff, PA, Wadden, RA *Environmental Science & Technology*, 1993, 27, 617-625.
[4] Watson, JG, Chow, JC, Fujita, EM *Atmospheric Environment*, 2001, 35, 1567-1584.
[5] Abu-Allaban, M, Gertler, AW, Lowenthal, DH. *Atmospheric Environment*, 2002, 36, 5549-5557.
[6] Lai, CH, Chen, KS, Ho, YT, Peng, YP, Chou, YM. *Atmospheric Environment*, 2005, 39, 4543-4559.
[7] Srivastava, A. *Atmospheric Environment*, 2004, 38, 6829-6843.
[8] Srivastava, A. *Environmental Monitoring and Assessment*, 2005, 107, 363-373.
[9] Wohrnschimmel, H, Marquez, C, Mugica, V, Stahel, WA, Staehelin, J, Cardenas, B, Blanco, S. *Atmospheric Environment*, 2006, 40, 5125-5136.
[10] Gertler, AW, Fujita, EM, Pierson, WR, Wittorff, D N. *Atmospheric Environment*, 1996, 30, 2297-2305.
[11] Fujita, EM. *Science of the Total Environment*, 2001, 276, 171-184.
[12] Fujita, EM, Campbell, DE, Zielinska, B, Sagebiel, JC, Bowen, JL, Goliff, W S, Stockwell, W R, Lawson, DR. *Journal of the Air & Waste Management Association*, 2003, 53, 844-863.
[13] Latella, A, Stani, G, Cowbell, L, Duane, M, Janine, H, Astoria, C, Larsen, BR. *J Chromatogr A*, 2005, 29-39.
[14] Hellen, H, Hakola, H, Laurila, T. *Atmospheric Environment*, 2003, 37, 1413-1424.
[15] Jorquera, H, Rappengluck, B. *Atmospheric Environment*, 2004, 38, 4243-4263.
[16] Chan, CC, Nien, CK, Hwang, JS. *Atmospheric Environment*, 1996, 30, 25-33.
[17] Choi, YJ, Ehrman, SH. *Atmospheric Environment*, 2004, 38, 775-791.
[18] Choi, YJ, Calabrese, RV, Ehrman, SH, Dickerson, RR, Stehr, JW. *Journal of the Air & Waste Management Association*, 2006, 56, 169-178.
[19] Brown, SG, Frankel, A, Hafner, HR. *Atmospheric Environment*, 2007, 41, 227-237.
[20] Buzcu, B, Fraser, MP. *Atmospheric Environment*, 2006, 40, 2385-2400.
[21] Xie, YL, Berkowitz, CM. *Atmospheric Environment*, 2006, 40, 3070-3091.
[22] Guo, H, Wang, T, Simpson, IJ, Blake, DR, Yu, XM, Kwok, YH, Li, YS. *Atmospheric Environment*, 2004, 38, 4551-4560.
[23] Guo, H, So, K L, Simpson, I J, Barletta, B, Meinardi, S, Blake, D R. *Atmospheric Environment*, 2007, 41, 1456-1472.
[24] Kawashima, H, Minami, S, Hanai, Y, Fushimi, A. *Atmospheric Environment*, 2006, 40, 2301-2312.
[25] Seila, RL, Main, HH, Arriaga, JL, Martinez, G, Ramadan, A. *Science of the Total Environment*, 2001, 276, 153-169.
[26] US EPA. "Test Method 321 - Measurement of Gaseous Hydrogen Chloride Emissions at Portland Cement Kilns by Fourier Transform Infrared (FTIR) Spectroscopy", 1992. http://www.epa.gov/ttn/emc/promgate/m-321.pdf
[27] PerkinElmer Instruments. "VOC Ozone Precursor Analyzer User's Manual", 2001, Part number 0993-6563.
[28] US EPA. Publication EPA-454/B-93-051, 1994, http://www.epa.gov/ttnamti1/pams.html.
[29] Ishimaru, JM, Hallenbeck, ME. Technical Report WA-RD 466.2, WA Dept of Transportation. 1999.
[30] Wang, Y, Nihan, NL. "Can Single-Loop Detectors Do the Work of Dual-Loop Detectors?" *ASCE Journal of Transportation Engineering*, 2003, 129 (2), 169 - 176.
[31] Zhang, G, Wang, Y, Wei, H. "Artificial Neural Network Method for Length-Based Vehicle Classification Using Single-Loop Outputs", *Transportation Research Record*, 2006, 100-108.
[32] Cheevarunothai, P, Wang, Y, Nihan, NL. "Development of Advanced Loop Event Analyzer (ALEDA) for Investigations of Dual-Loop Detector Malfunctions". *12th World Congress on Intelligent Transportation Systems*, San Francisco, November 2005.
[33] Cheevarunothai, P, Wang, Y, Nihan, NL. *Transportation Research Record*, 2006, *1945*, 73-81.

[34] Cheevarunothai, P, Wang, Y, Nihan, NL. "Using Dual-Loop Event Data to Enhance the Accuracy of Truck Data." *Transport Research Record*, 2007, 131-137.
[35] Zhang, G, Avery, RP, Wang, Y. "A Video-based Vehicle Detection and Classification System for Real-time Traffic Data Collection Using Uncalibrated Video Cameras." *Transport. Research Record*. 2007, 138-147.
[36] Scheff, PA, Wadden, RA. *Environ Sci Technol*. 1993, 27, 617-625.
[37] Watson, JG, Chow, JC, Fujita, EM. *Atmos Environ* 2001, 35, 1567-1584.
[38] Allen, GA, Babich, P, Poirot, RL. "Evaluation of a New Approach for Real Time Assessment of Woodsmoke PM", Paper 16, presented at the Air & Waste Management Association Visibility Specialty Conference on Regional and Global Perspectives on Haze: Causes, Consequences and Controversies. Asheville, NC, October 25-29, 2004.
[39] http://www.infometrix.com/apps/19-0193_AlgorithmTN.pdf
[40] De Maesschalck, R, Jouan-Rimbaud, D, Massart, DL. "The Mahalanobis distance". *Chemometrics and Intelligent Laboratory Systems*. 2000, 50 (1), 1-18.
[41] http://www.infometrix.com/apps/32-0903_ProcGCAlignAB.pdf
[42] Puget Sound Clean Air Agency. "Tacoma and Seattle Area Air Toxics Evaluation", 2010. (for ANOVA methodology used here).
[43] Chatfield, C. "The analysis of Time Series: an introduction". Chapman Hall/CRC press, Boca Raton FL, 2004.
[44] Jobson, BT, Alexander, ML, Maupin, GD, Muntean, GG. *Int J Mass Spec*, 2005, 245, 78-89.
[45] Zielinska, B, Campbell, D., *Environ Sci Technol, 2008,* 42, 5661-5666.
[46] Hien, TT, Thanh, LT, Kameda, T, Takenaka, N, Bandow, H. "Nitro-polycyclic hydrocarbons and polycyclic hydrocarbons in particulate matter in an urban area of a tropical region: Ho Chi Minh City, Vietnam." *Atmos Environ*, 2007, *41*, 7715-7725.
[47] Cecinato, A, Marino, F, Di Filippo, P, Lepore, L, Possanzini, M. "Distribution of *n*-alkanes, polynuclear aromatic hydrocarbons and nitrated polynuclear hydrocarbons between the fine and coarse fractions of inhalable atmospheric particulates." *J of Chromatogr A*, 1999, *849*, 255-264.
[48] Arey, J, Zielinska, B, Atkinson, R, Winer, AM, Ramdahl, T, Pitts Jr, JN. "The Formation of Nitro-PAH from the Gas-Phase Reactions of Fluoranthene and Pyrene with the OH Radical in the Presence of NO_x", *Atmos Environ*, 1986, *20*, (12), 2339-2345.
[49] Sweetman, JA, Zielinska, B, Atkinson, R, Ramdahl, T, Winer, AM, Pitts Jr, JN. "A Possible Formation Pathway for the 2-Nitrofluoranthene Observed in Ambient Particulate Organic Matter", *Atmos Environ*, 1986, *20*, (1), 235-238.
[50] Ciccioli, P. "Formation and transport of 2-nitrofluoranthene and 2-nitropyrene of photochemical origin in the troposphere", *J Geophys Res.* 1996, *101*, 19567-19581.
[51] Arey, J, Zielinska, B, Atkinson, R, and Aschmann, SA. "Nitroarene Products from the Gas-Phase Reactions of Volatile Polycyclic Aromatic Hydrocarbons with the OH Radical and N_2O_5" *Int J of Chem Kinet.* 1989, *21*, 775-799.
[52] Feilberg, A, Poulsen, MWB, Nielsen, T, Skov, H "Occurrence and sources of particulate nitro-polycyclic aromatic hydrocarbons in ambient air in Denmark", *Atmos Environ*, 2001, *35*, 353-366.
[53] Schauer, JJ, Kleeman, MJ, Cass, GR, and Simoneit, BR. "Measurement of emissions from air pollution sources. 5. C1-C32 organic compounds from gasoline-powered motor vehicles". *Environ Sci Technol.* 2002, 36 (6), 1169-80.
[54] Schauer, JJ, Kleeman, MJ, Cass, GR, and Simoneit, BR. "Measurement of Emissions from Air Pollution Sources. 2. C1 through C30 Organic Compounds from Medium Duty Diesel Trucks". *Environ Sci Technol,* 1999, 33 (10), 1578–1587.
[55] Atkinson, R, Arey, J, Zielinska, B, Aschmann, SA. "Kinetics and Nitro-Products of the Gas-Phase OH and NO_3 Radical-Initiated Reactions of Napthalene-d_8, Fluoranthene-d_{10}, and Pyrene", *Int J Chem Kinet*, 1990, 22, 999-1014.
[56] Albinet, A, Leoz-Garziandia, E, Budzinski, H, Villenave, E, Jaffrezo, J-L. "Nitrated and oxygenated derivatives of polycyclic aromatic hydrocarbons in the ambient air of two French alpine valleys Part I: Concentrations, sources and gas/particle partitioning", *Atmos Environ,* 2008, *42*, 43-54
[57] Zielinska B, Campbell D, Lawson DR, Ireson RG, Weaver CS, Hesterberg TW, Larson T, Davey M, and Liu LJ. "Detailed characterization and profiles of crankcase and diesel particulate matter exhaust emissions using speciated organics", *Environ Sci Technol.* 2008, 42 (15), 5661-5666.

[58] Puget Sound Maritime Forum, Starcrest Consulting Group. "Puget Sound maritime air emissions inventory", 2007, http://www.pscleanair.org/programs/dieselsolutions/diesel_downloads/Puget%20Sound%20Maritime%20Air%20Emissions%20Inventory.pdf.

[59] Moldanova, J, Fridell, E, Popovicheva, O, Demirdjian, B, Tishkova, V, Faccinetto, A, Focsa, A. "Characterization of particulate matter and gaseous emissions from a large ship diesel engine", *Atmospheric Environment*. 2009, 43 (16), 2632.

[60] MAN B & W Diesel A/S. 1996. "Basic principles of ship propulsion". Copenhagen: MAN B&W Diesel.

[61] Kim E, Hopke, PK, Larson, TV, Maykut, NN, Lewtas, J. "Factor Analysis of Seattle Fine Particles. *Aerosol Sci Technol*. 2004. 38 (7): 724-738.

[62] Kim, E, Hopke, P. "Source characterization of ambient fine particles at multiple sites in the Seattle area", *Atmospheric Environment*, 2008. 42: 6047-6056.

Appendix A: Geometric Means and Geometric Standard Deviations (GSD) by Month at Seattle Duwamish for Each Analyzed Species

		Month				
Species (Concentration Units)	**Measure**	**March**	**April**	**May**	**July**	**August**
Propane (ppbv)	Geometric Mean	1.42	1.84	.79	.73	.52
	GSD	1.48	2.09	1.99	1.98	1.93
	Total N	8	60	473	46	238
Propylene (ppbv)	Geometric Mean	.26	.31	.24	.29	.20
	GSD	1.37	1.65	1.78	1.60	1.67
	Total N	8	60	473	46	238
Isobutane (ppbv)	Geometric Mean	.28	.52	.14	.12	.09
	GSD	1.48	2.81	1.94	2.89	2.39
	Total N	8	60	473	46	238
n-Butane (ppbv)	Geometric Mean	.55	1.20	.41	.50	.36
	GSD	1.73	3.40	2.26	3.71	2.74
	Total N	8	60	473	46	238
t-2-Butene (ppbv)	Geometric Mean	.04	.04	.03	.04	.03
	GSD	.	1.56	1.51	1.85	1.76
	Total N	8	60	473	46	238
1-Butene (ppbv)	Geometric Mean	.06	.07	.05	.11	.12
	GSD	1.29	1.47	1.46	1.30	1.27
	Total N	8	60	473	46	238
c-2-Butene (ppbv)	Geometric Mean	.04	.05	.03	.04	.03
	GSD	1.28	1.59	1.46	1.78	1.75
	Total N	8	60	473	46	238
Isopentane (ppbv)	Geometric Mean	.25	.69	.42	.22	.14
	GSD	1.88	3.30	2.67	5.57	4.58
	Total N	8	60	473	46	238
n-Pentane (ppbv)	Geometric Mean	.14	.31	.19	.37	.23
	GSD	1.64	2.81	2.34	2.90	2.49
	Total N	8	60	473	46	238
t-2-Pentene (ppbv)	Geometric Mean	.03	.04	.02	.05	.03
	GSD	.	1.65	1.66	2.66	2.54
	Total N	8	60	473	46	238
1-Pentene (ppbv)	Geometric Mean	.04	.05	.03	.03	.02
	GSD	.	1.56	1.66	2.16	2.07
	Total N	8	60	473	46	238
c-2-Pentene (ppbv)	Geometric Mean	.03	.04	.02	.04	.03
	GSD	1.14	1.33	1.66	2.84	2.36
	Total N	8	60	473	46	238
2,2-Dimethylbutane (ppbv)	Geometric Mean	.05	.05	.03	.11	.07
	GSD	1.10	1.80	1.77	2.81	2.47
	Total N	8	60	473	46	238
Isoprene (ppbv)	Geometric Mean	.14	.09	.03	.06	.04
	GSD	1.17	1.66	1.44	2.04	2.04
	Total N	8	60	473	46	238
Methylcyclopentane (ppbv)	Geometric Mean	.05	.09	.17	.10	.06
	GSD	1.60	1.81	1.00	2.22	2.25
	Total N	8	60	473	46	238
Benzene (ppbv)	Geometric Mean	.19	.24	.16	.21	.19
	GSD	1.41	1.61	1.61	1.75	1.57
	Total N	8	60	473	46	238

		Month				
Species (Concentration Units)	**Measure**	**March**	**April**	**May**	**July**	**August**
Cyclohexane (ppbv)	Geometric Mean	.05	.06	.04	.10	.04
	GSD	1.47	1.66	2.03	2.28	2.36
	Total N	8	60	473	46	238
2-Methylhexane (ppbv)	Geometric Mean	.06	.08	.04	.07	.04
	GSD	3.17	1.72	1.99	1.89	2.26
	Total N	8	60	473	46	238
3-Methylhexane (ppbv)	Geometric Mean	.08	.10	.07	.10	.07
	GSD	3.05	1.89	1.93	1.69	1.79
	Total N	8	60	473	46	238
2,4-Dimethylpentane (ppbv)	Geometric Mean	.09	.06	.07	.04	.03
	GSD	1.62	1.40	1.00	2.06	2.13
	Total N	8	60	473	46	238
2,3-Dimethylpentane (ppbv)	Geometric Mean	.06	.08	.05	.05	.03
	GSD	2.24	1.62	1.91	1.89	2.05
	Total N	8	60	473	46	238
2,2,4-Trimethylpentane (ppbv)	Geometric Mean	.06	.08	.05	.05	.03
	GSD	1.83	1.74	2.18	2.28	2.27
	Total N	8	60	473	46	238
n-Heptane (ppbv)	Geometric Mean	.05	.07	.05	.05	.04
	GSD	1.84	2.06	2.00	2.33	2.19
	Total N	8	60	473	46	238
Methylcyclohexane (ppbv)	Geometric Mean	.03	.06	.08	.06	.04
	GSD	2.02	1.87	2.22	2.36	2.03
	Total N	8	60	473	46	238
2,3,4-Trimethylpentane (ppbv)	Geometric Mean	.03	.03	.02	.02	.01
	GSD	1.21	1.52	2.11	1.73	2.01
	Total N	8	60	473	46	238
Toluene (ppbv)	Geometric Mean	.26	.44	.35	.35	.24
	GSD	2.04	2.17	2.02	1.96	1.93
	Total N	8	60	473	46	238
2-Methylheptane (ppbv)	Geometric Mean	.02	.03	.01	.02	.01
	GSD	1.97	1.53	1.92	2.43	2.37
	Total N	8	60	473	46	238
3-Methylheptane (ppbv)	Geometric Mean	.03	.03	.02	.06	.03
	GSD	1.19	1.76	1.89	1.40	1.73
	Total N	8	60	473	46	238
n-Octane (ppbv)	Geometric Mean	.04	.04	.02	.04	.02
	GSD	1.63	2.07	2.10	2.57	2.24
	Total N	8	60	473	46	238
Ethylbenzene (ppbv)	Geometric Mean	.04	.06	.07	.06	.04
	GSD	1.87	2.23	2.14	1.96	1.85
	Total N	8	60	473	46	238
m,p-Xylene (ppbv)	Geometric Mean	.13	.22	.26	.20	.13
	GSD	2.19	2.39	2.28	1.96	2.09
	Total N	8	60	473	46	238
Styrene (ppbv)	Geometric Mean	.06	.07	.08	.11	.04
	GSD	1.31	1.71	2.12	2.36	1.90
	Total N	8	60	473	46	238
o-Xylene (ppbv)	Geometric Mean	.05	.09	.12	.08	.05
	GSD	2.01	2.30	2.22	1.83	1.97
	Total N	8	60	473	46	238

		Month				
Species (Concentration Units)	**Measure**	**March**	**April**	**May**	**July**	**August**
n-Nonane (ppbv)	Geometric Mean	.02	.03	.03	.04	.02
	GSD	1.46	2.05	2.19	2.48	2.13
	Total N	8	60	473	46	238
Isopropylbenzene (ppbv)	Geometric Mean	.03	.03	.02	.01	.01
	GSD	1.18	1.74	1.75	2.11	1.72
	Total N	8	60	473	46	238
n-Propylbenzene (ppbv)	Geometric Mean	.02	.03	.04	.01	.00
	GSD	1.22	1.97	2.69	1.74	2.09
	Total N	8	60	473	46	238
1,3,5-Trimethylbenzene (ppbv)	Geometric Mean	.03	.04	.05	.04	.03
	GSD	1.32	1.82	2.09	2.25	2.14
	Total N	8	60	473	46	238
o-Ethyltoluene (ppbv)	Geometric Mean	.02	.03	.03	.02	.01
	GSD	1.29	1.97	1.91	1.86	2.00
	Total N	8	60	473	46	238
1,2,4-Trimethylbenzene (ppbv)	Geometric Mean	.07	.13	.13	.07	.05
	GSD	2.09	2.27	2.26	1.81	1.92
	Total N	8	60	473	46	238
1,2,3-Trimethylbenzene (ppbv)	Geometric Mean	.04	.07	.09	.08	.04
	GSD	1.55	2.16	2.12	1.59	1.91
	Total N	8	60	473	46	238
m-Diethylbenzene (ppbv)	Geometric Mean	.03	.04	.04	.03	.02
	GSD	1.64	1.53	1.99	1.66	1.79
	Total N	8	60	473	46	238
p-Diethylbenzene (ppbv)	Geometric Mean	.04	.04	.04	.04	.02
	GSD	1.23	1.85	2.00	1.83	1.91
	Total N	8	60	473	46	238
n-Decane (ppbv)	Geometric Mean	.03	.05	.07	.07	.03
	GSD	1.36	2.05	2.40	2.28	1.96
	Total N	8	60	473	46	238
n-Undecane (ppbv)	Geometric Mean	.02	.05	.11	.07	.04
	GSD	1.66	1.94	1.00	2.01	2.15
	Total N	8	60	473	46	238
n-Dodecane (ppbv)	Geometric Mean	.05	.11	.13	.08	.03
	GSD	1.79	2.10	2.58	2.60	2.41
	Total N	8	60	473	46	238
PM2.5 TEOM-FDMS (µg/m3)	Geometric Mean	9.49	11.60	11.18	19.99	16.54
	GSD	1.26	1.40	1.38	1.58	1.42
	Total N	8	60	473	46	238
UV Channel (µg/m3)	Geometric Mean	.47	.82	.62	1.03	.77
	GSD	3.27	2.06	2.18	3.05	2.25
	Total N	8	60	473	46	238
Black Carbon Channel (µg/m3)	Geometric Mean	.47	.83	.64	1.15	.85
	GSD	3.39	2.13	2.20	3.08	2.23
	Total N	8	60	473	46	238

Appendix B: Results of PMF Source Apportionment Analyses

Part I: PMF Model Results for Hourly Data

Factor 1: Woodsmoke 1

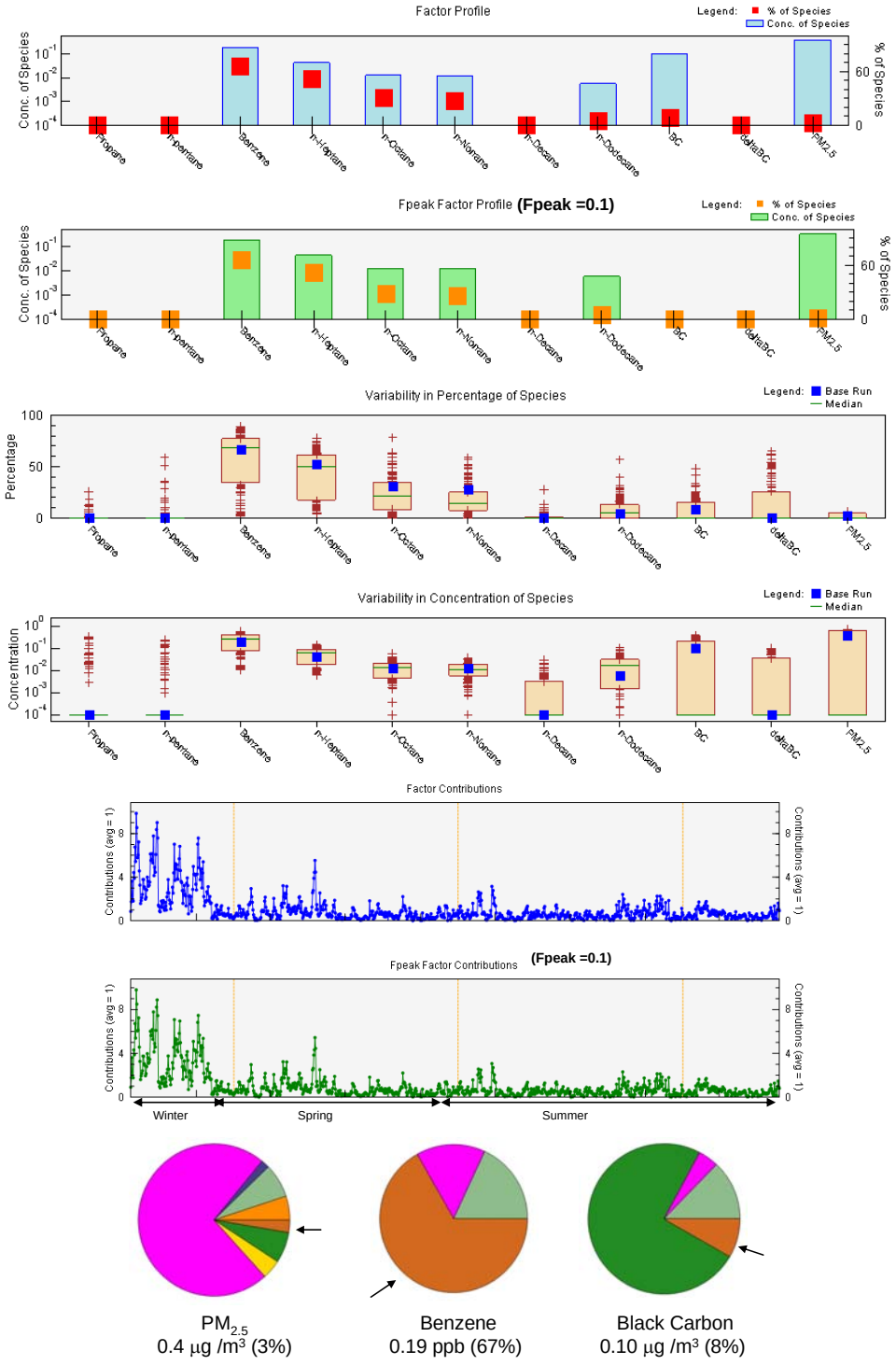

$PM_{2.5}$
0.4 µg /m³ (3%)

Benzene
0.19 ppb (67%)

Black Carbon
0.10 µg /m³ (8%)

Factor 2: Diesel Tailpipe

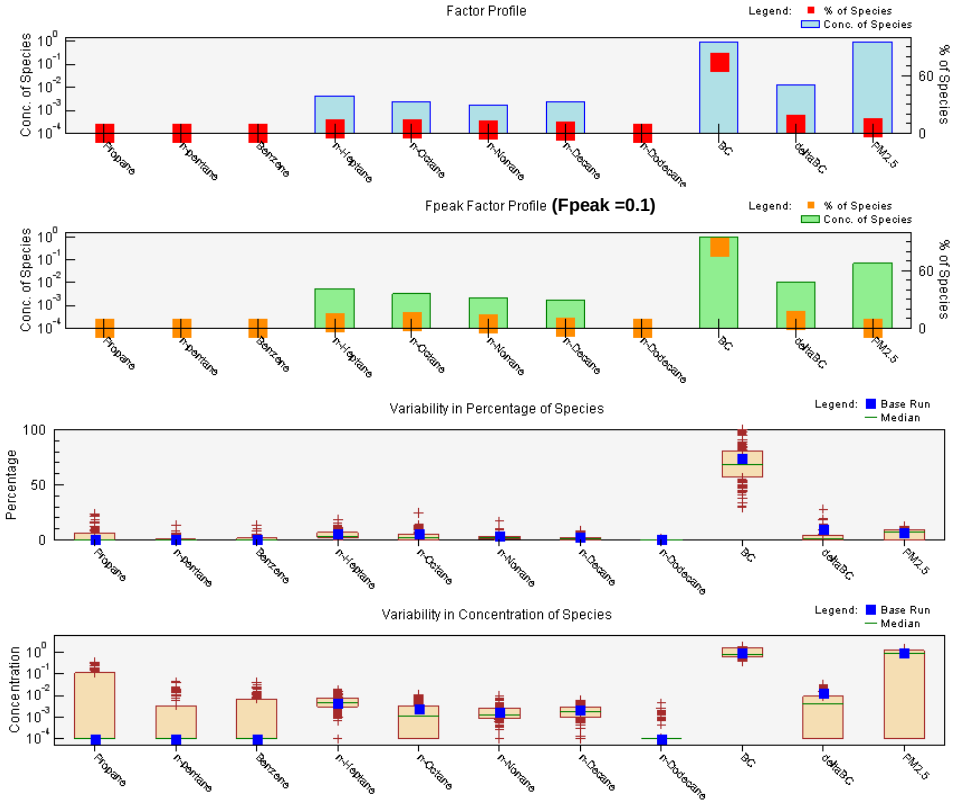

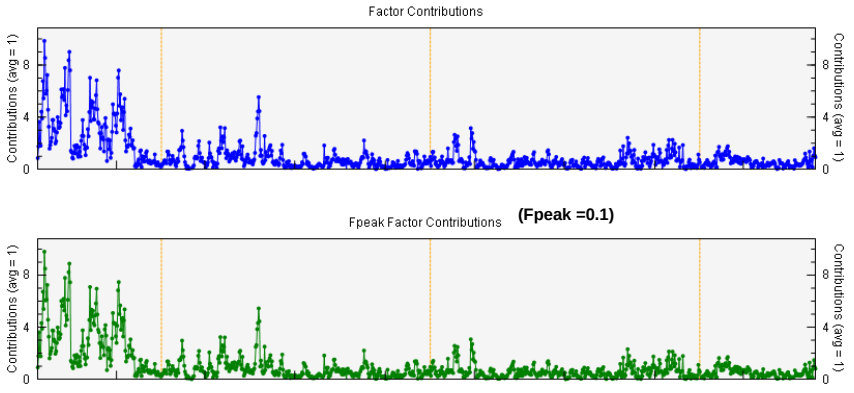

$PM_{2.5}$
0.4 μg /m³ (3%)

Benzene
0.19 ppb (67%)

Black Carbon
0.10 μg /m³ (8%)

Factor 3: Fueling / Port Operations

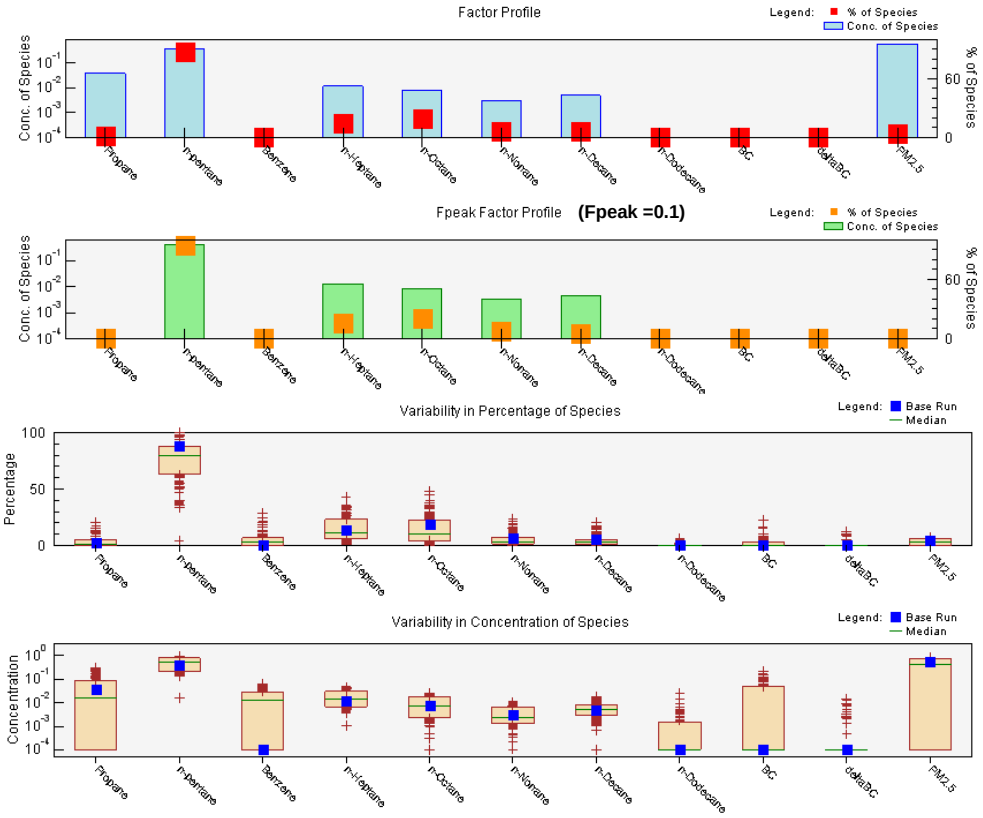

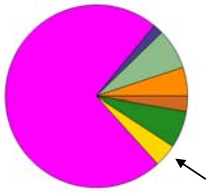

$PM_{2.5}$
0.6 µg /m^3 (4%)

Factor 4: Other $PM_{2.5}$

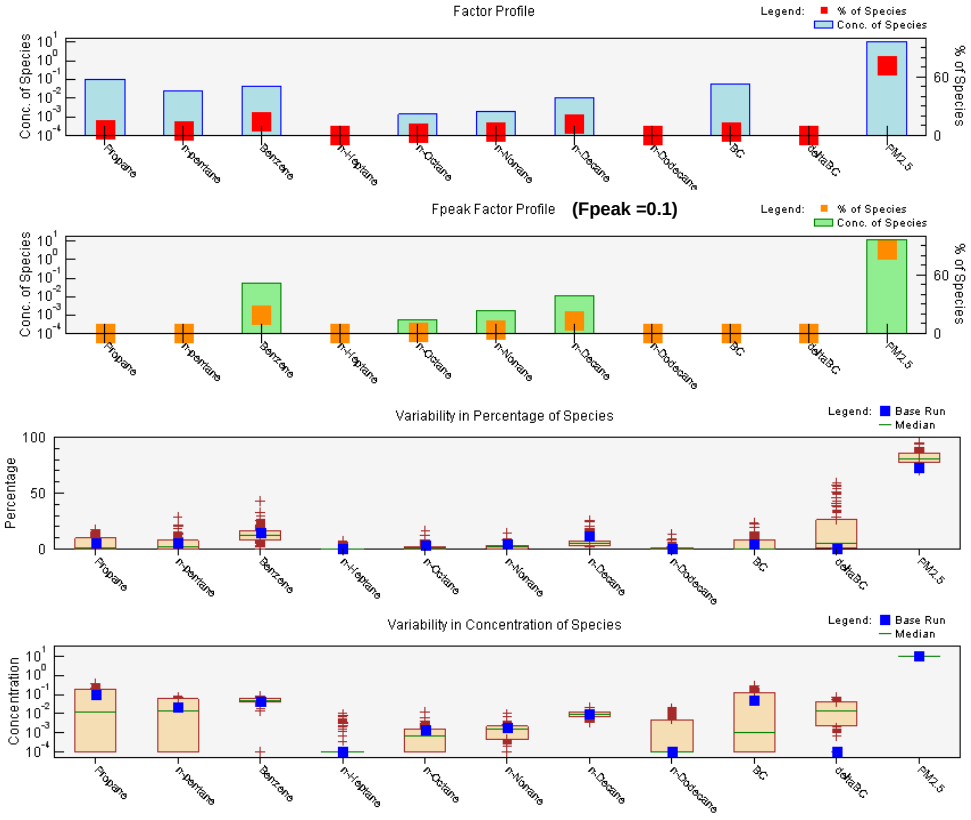

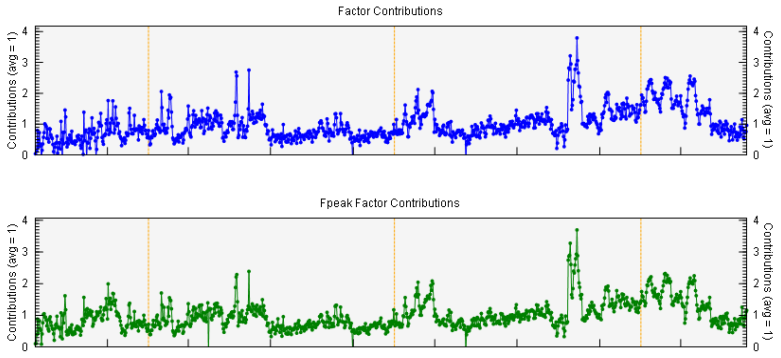

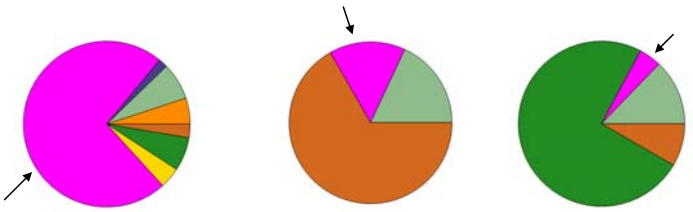

$PM_{2.5}$
10.4 μg /m^3 (73%)

Benzene
0.04 ppb (15%)

Black Carbon
0.05 μg /m^3 (4%)

Factor 5: Gasoline / LPG

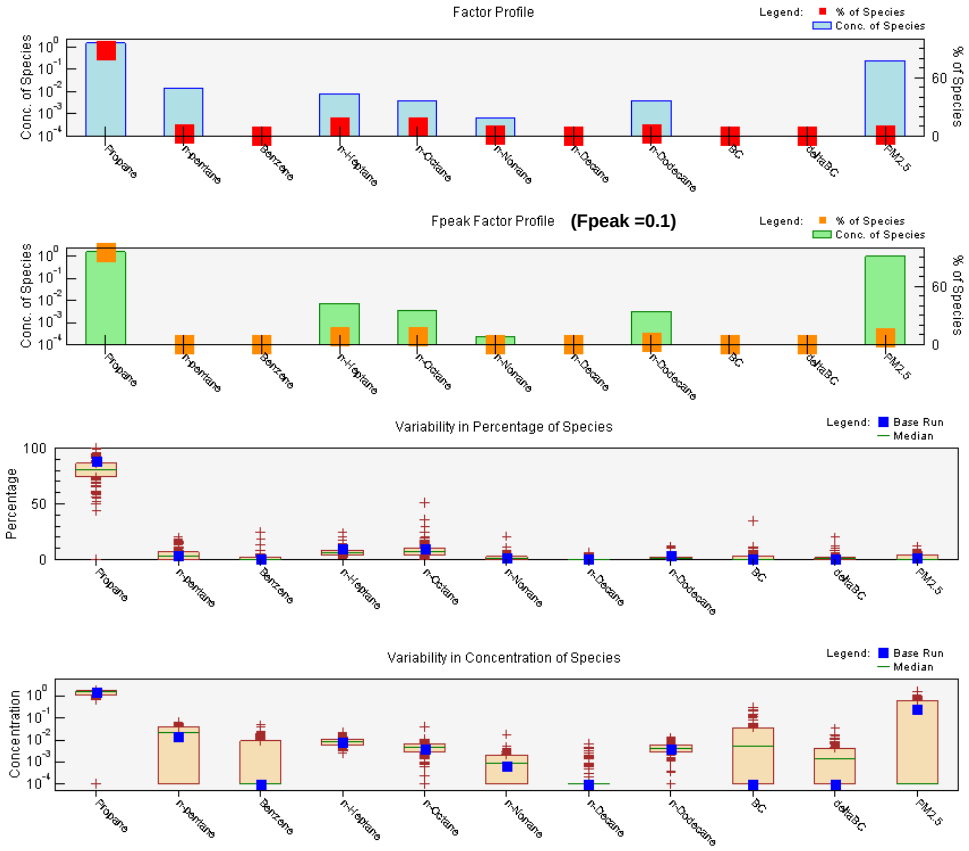

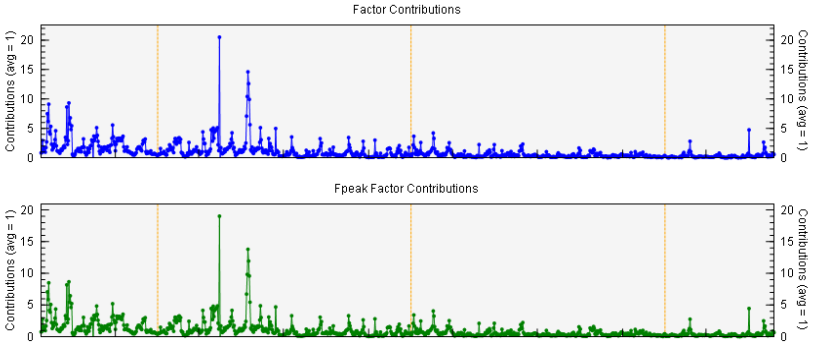

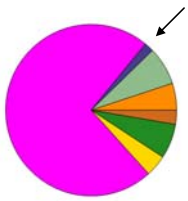

$PM_{2.5}$
0.25 μg /m³ (2%)

Factor 6: Woodsmoke 2

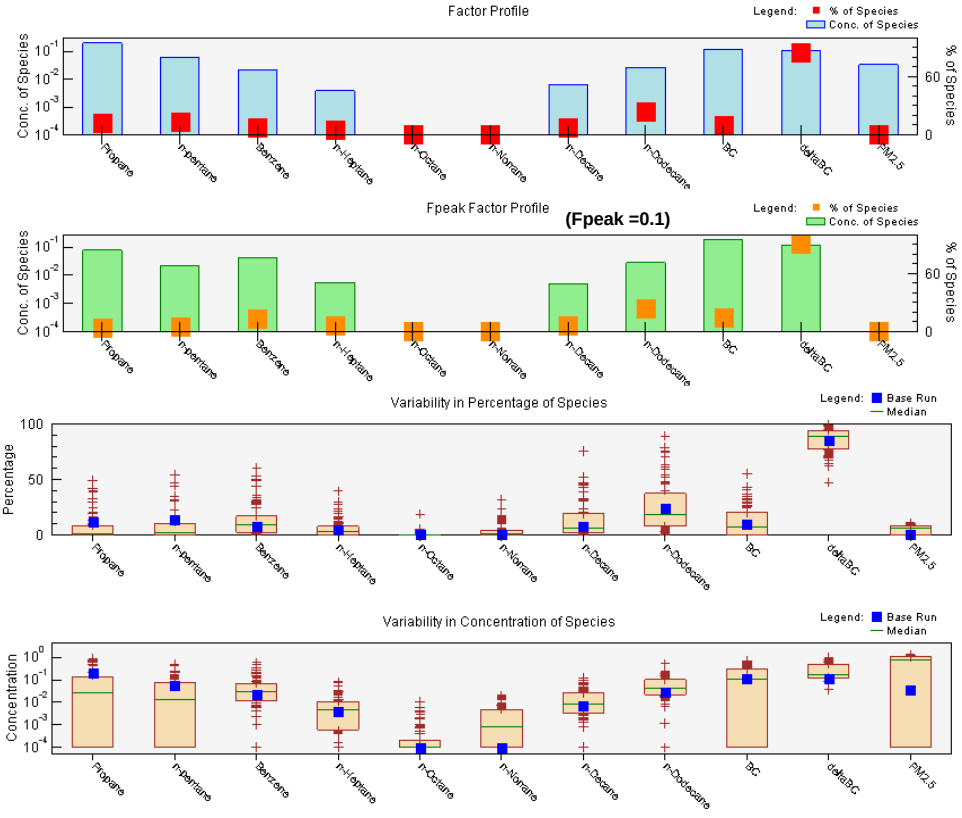

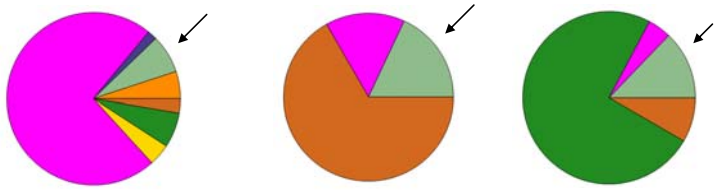

$PM_{2.5}$
1.0 μg /m³ (7%)

Benzene
0.05 ppb (18%)

Black Carbon
0.16 μg /m³ (13%)

Factor 7: Diesel Crankcase

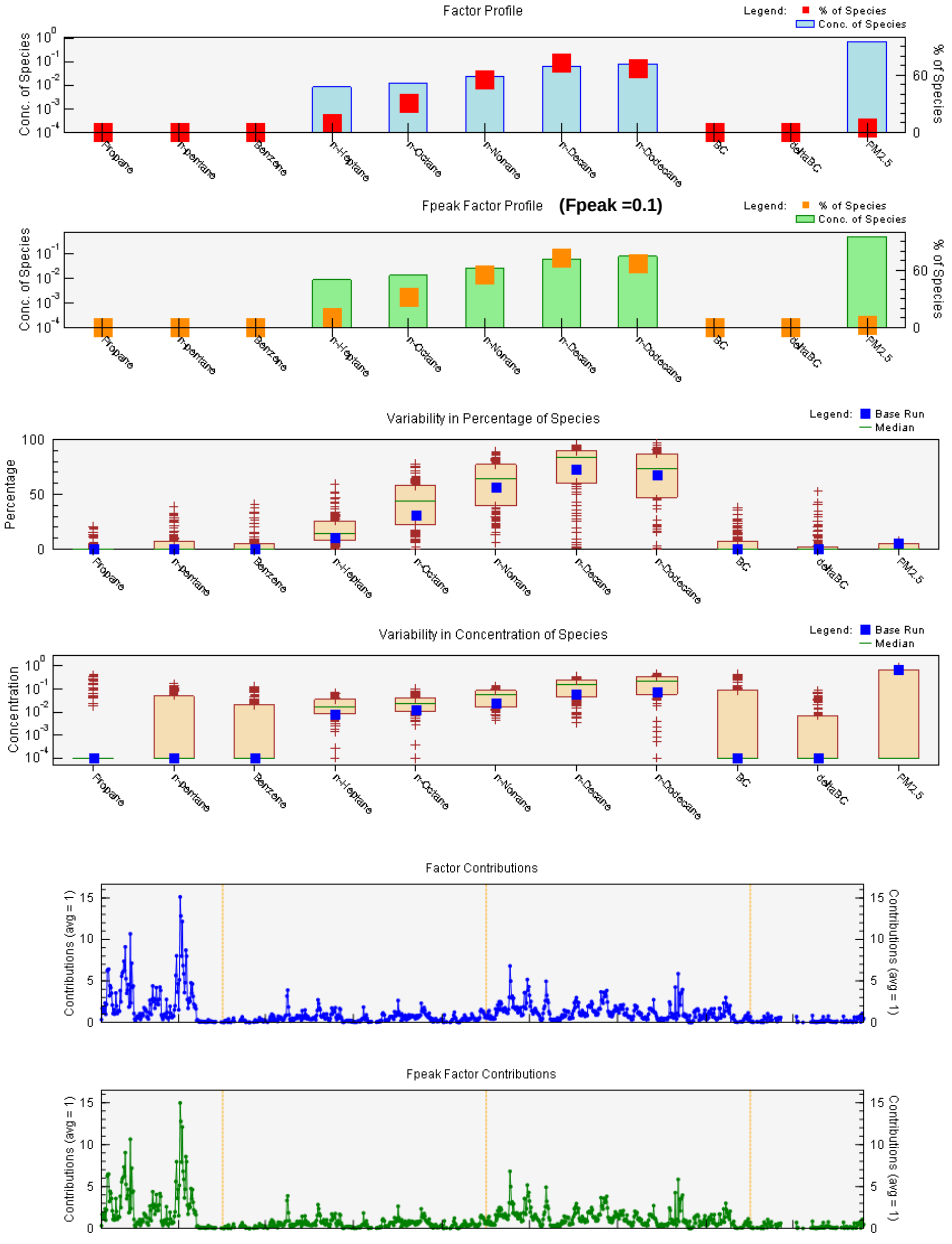

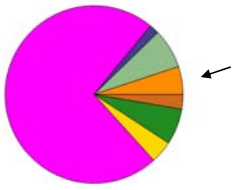

$PM_{2.5}$
0.7 µg /m^3 (5%)

Part II: PMF Model Results for Daily Speciation Data

PMF Derived Factor Profiles for Base Case Run

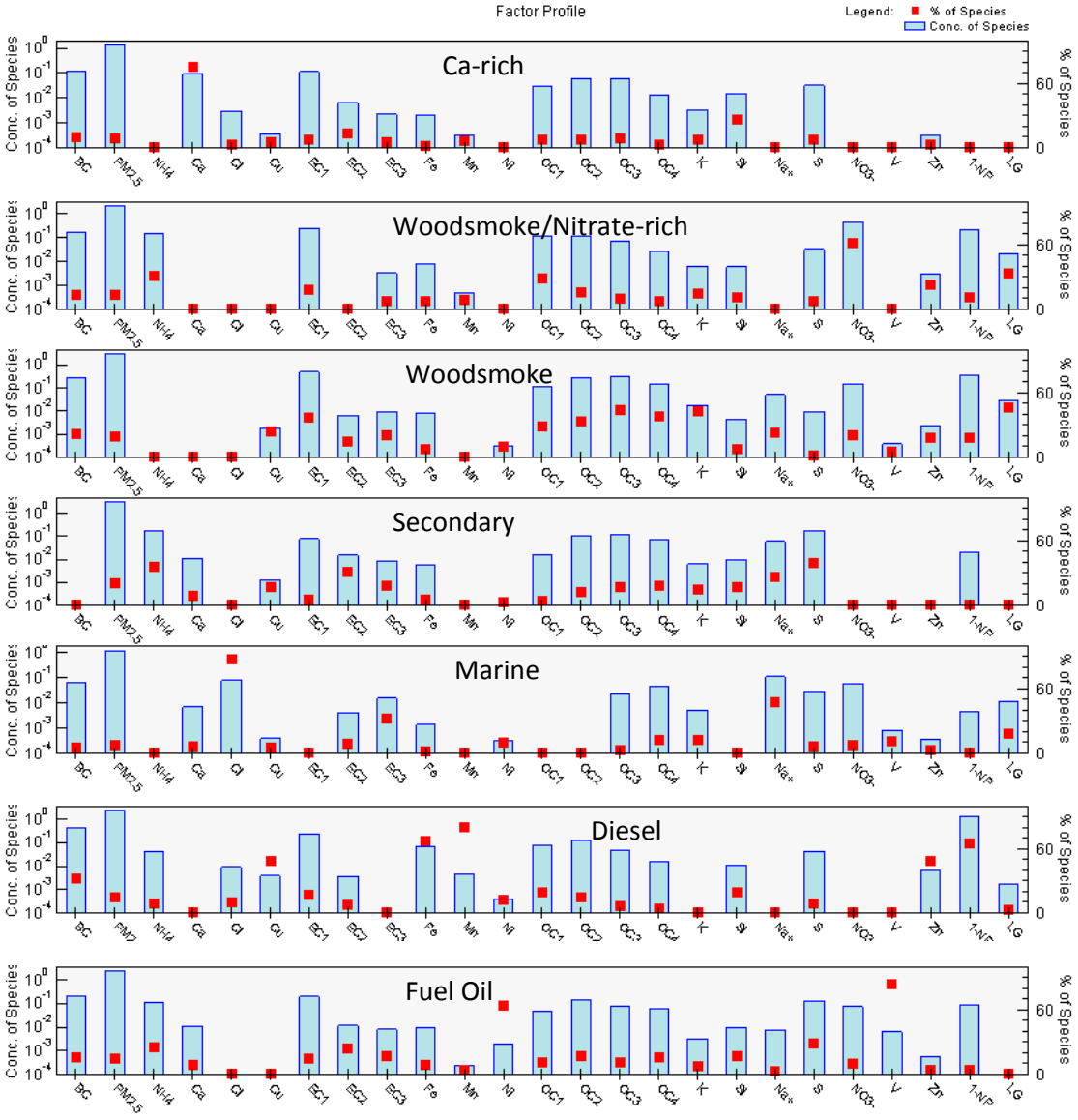

PMF Derived Factor Profiles for 100 Bootstrapped Runs (expressed as overall average contributions by species and factor)

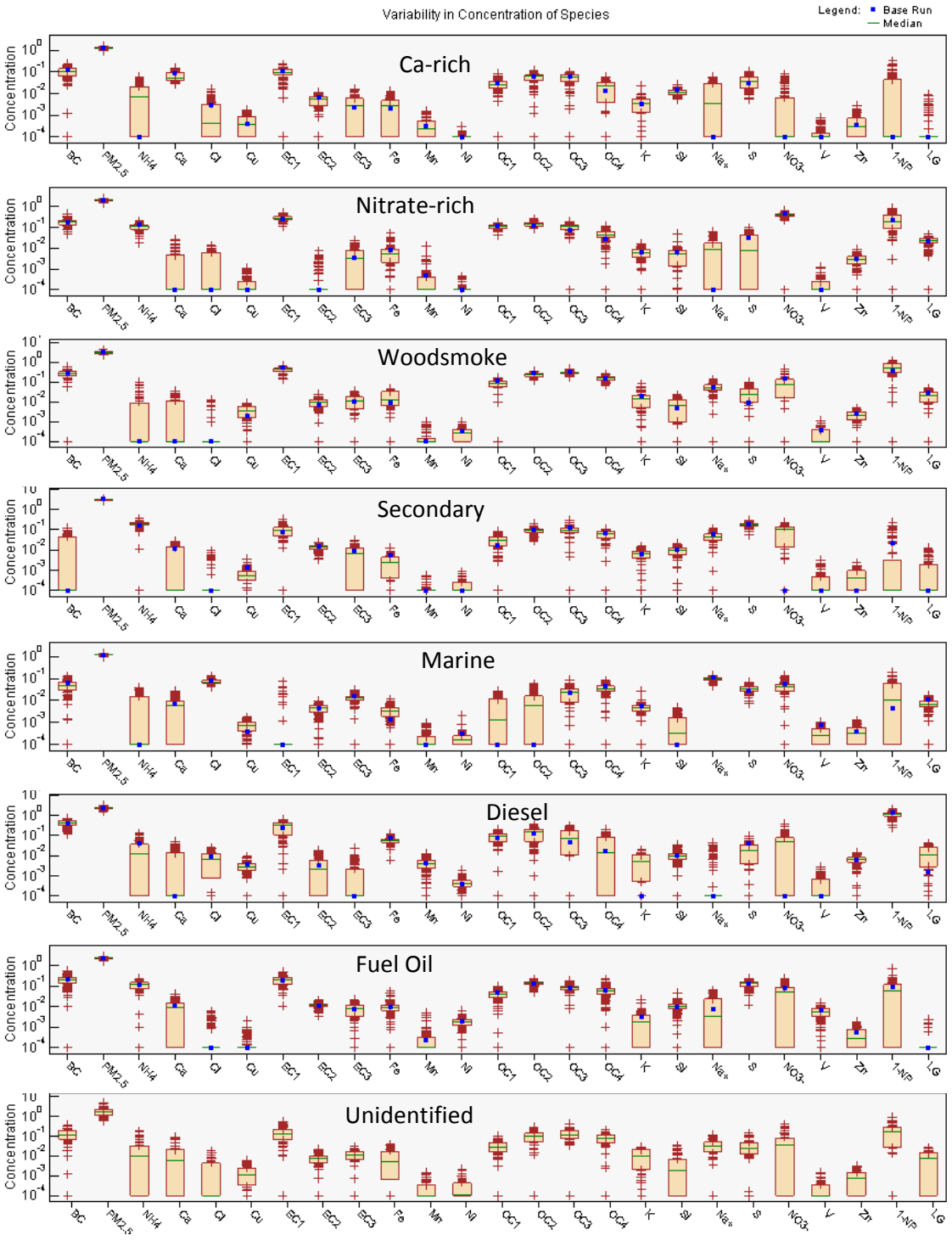

PMF Derived Factor Profiles for 100 Bootstrapped Runs (expressed as overall average percentage of species by species and factor)

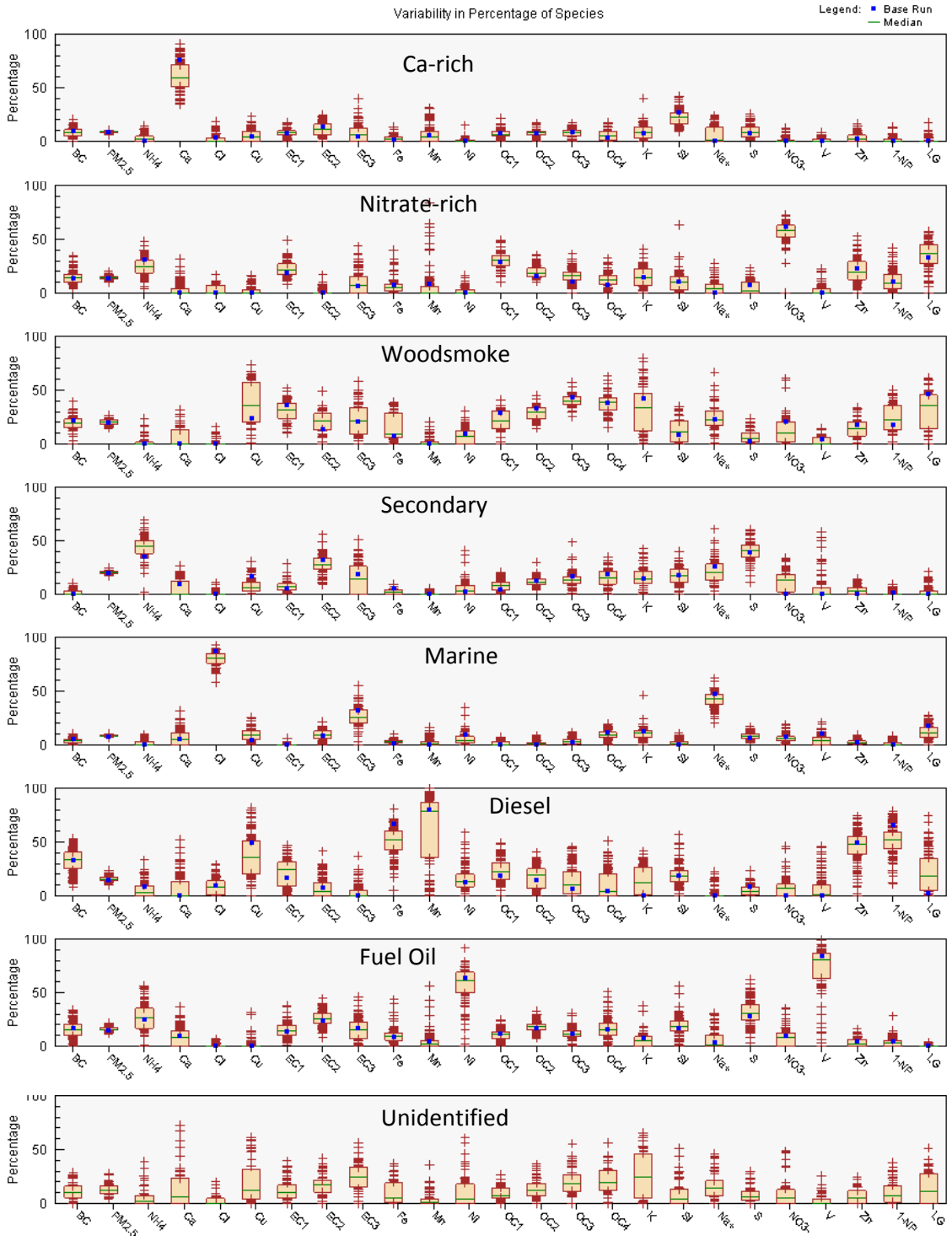

(Continued)

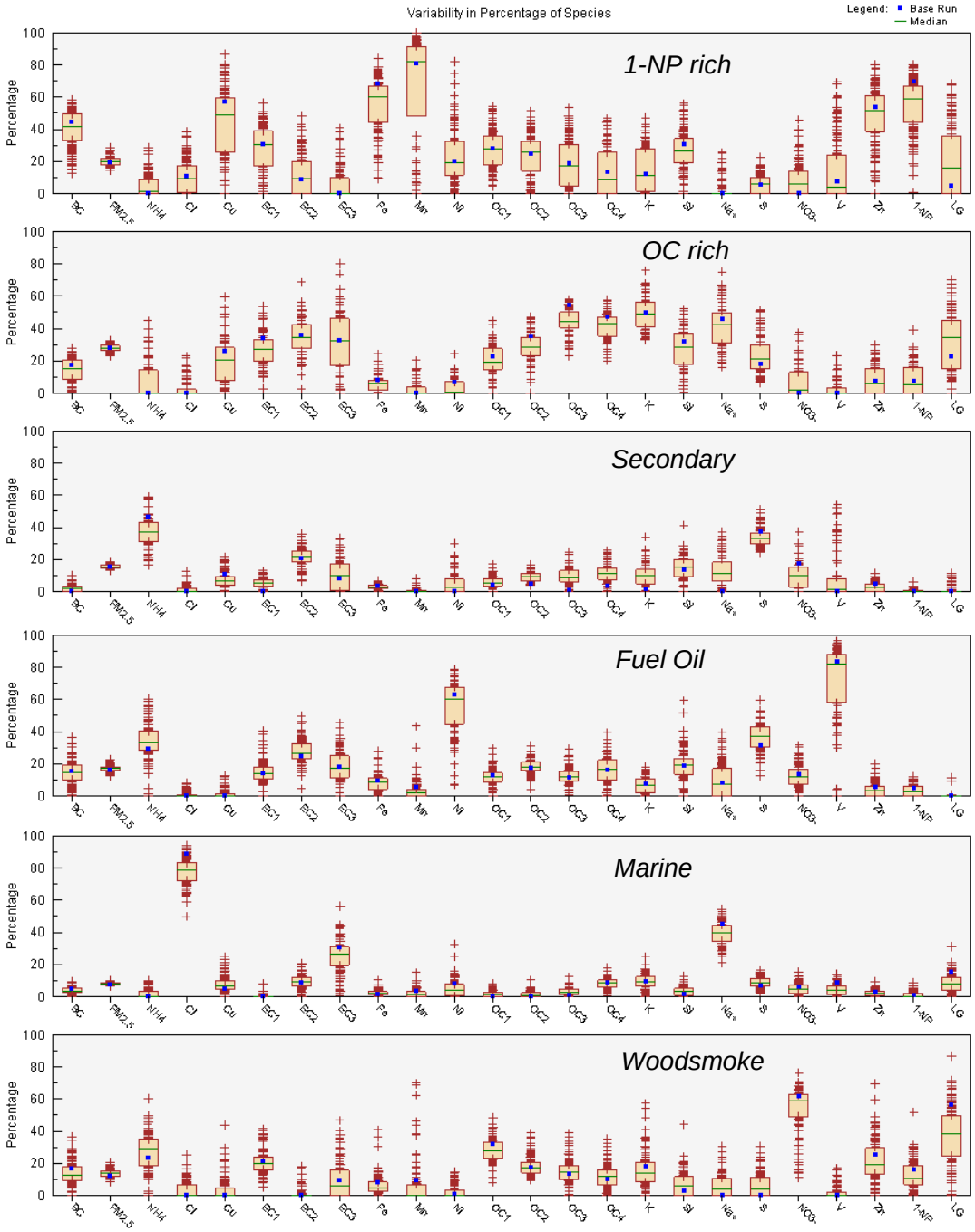
Variability in Percentage of Species
Legend: Base Run
Median
1-NP rich
OC rich
Secondary
Fuel Oil
Marine
Woodsmoke
Percentage
0
20
40
60
80
100
OC
PM2.5
NH4
Cl
Cu
EC1
EC2
EC3
Fe
Mn
Ni
OC1
OC2
OC3
OC4
K
Si
Na+
S
NO3-
V
Zn
1-NP
LG

Average PMF Feature Contributions by Selected Species

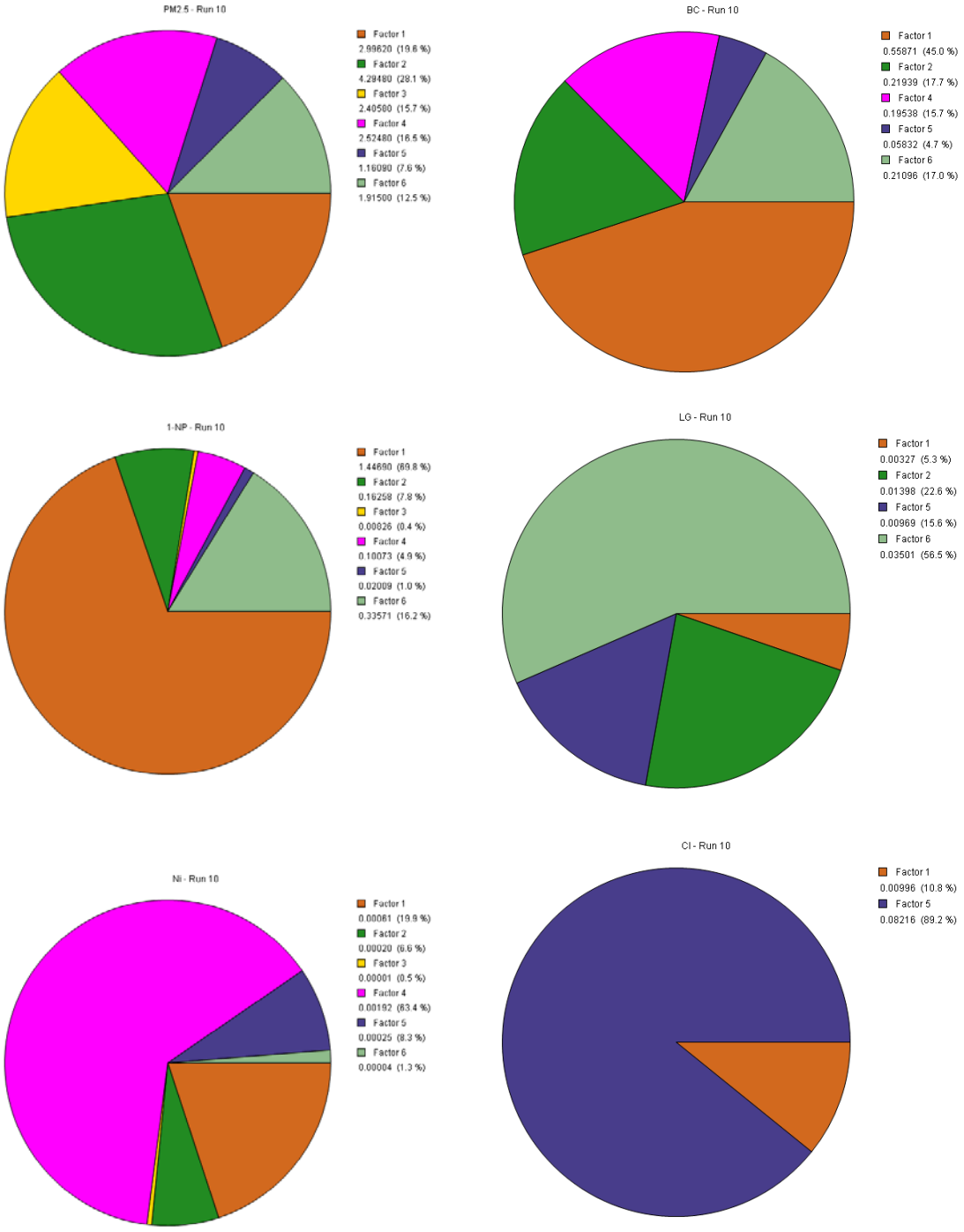

Average PMF Feature Contributions by Selected Species

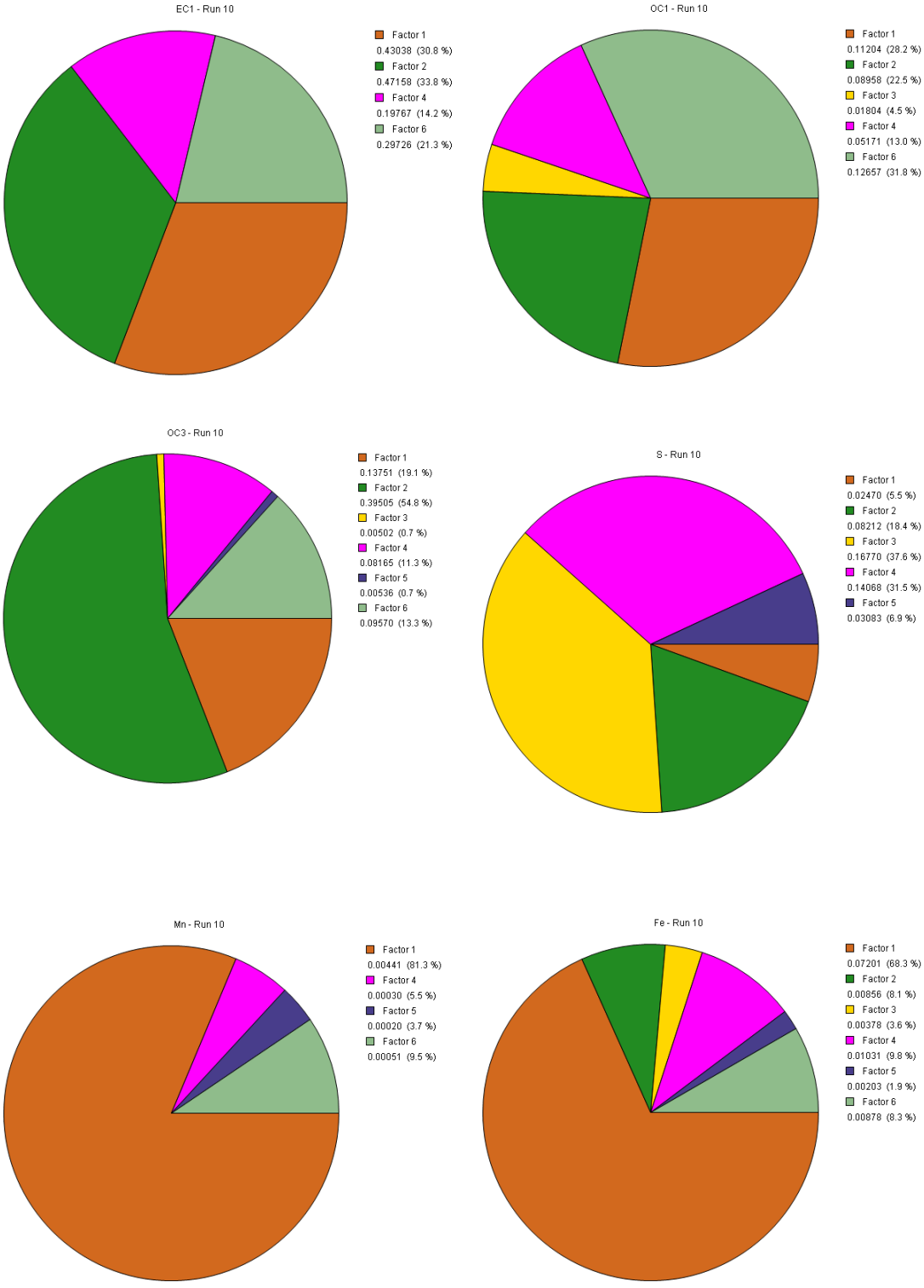

Predicted versus measured species concentrations by sample

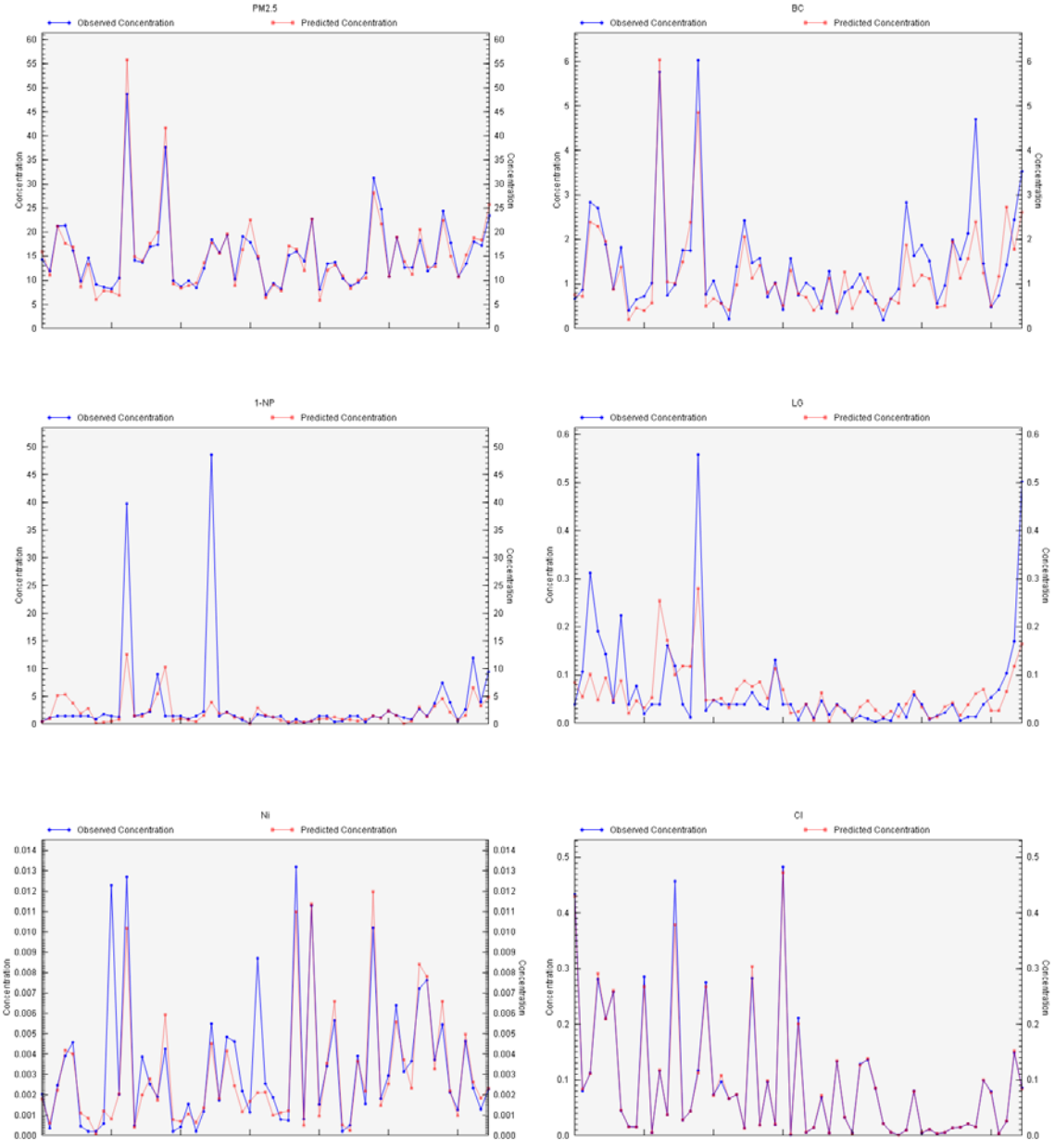

Appendix C: Modeling Marine Particulate Matter Emissions using AIS

(the report is shown on the following pages)

Appendix C: Modeling Marine Particulate Matter Emissions using AIS

Modeling the Fate of Diesel Particulate Matter Emissions from a Selected Marine Vessel Using CALPUFF View

by

Jake Braden

University of Washington, Department of Environmental and Occupational Health Sciences

May 24, 2009

Abstract

The EPA has recently funded a project proposed by the Puget Sound Clean Air Agency (PSCAA) to develop improved methods of source apportionment of air toxics. The project, entitled "Evaluation of Methods for Air Toxics Source Apportionment Using Real-Time Continuous Monitoring Instruments", is motivated by a growing need to improve characterization of air toxics emission sources within the current air monitoring system in Puget Sound. A risk evaluation performed in 2003 by PSCAA found diesel particulate matter (DPM) to be responsible for as much as 75-80% of total cancer risk due to air toxics. Due to the proclivity of DPM to cause cancer relative to other air toxics, it is given the utmost priority for monitoring and control. DPM sources arise from a wide range of transportation modes, such as by railroad, many types of heavy equipment, vehicles on the highway, and marine vessels that travel through the Puget Sound and moor at one of the many ports. As the extent to which marine vessel activities impact local populations is the least understood among these source types, the objective of this project was to develop a method for modeling marine emissions. In this study, atmospheric dispersion modeling with CALPUFF was used to model the emissions from a specific vessel as it travels in and out of the Puget Sound to Harbor Island. Signals derived from the Automated Identification System (AIS) that carry information about the vessel's identification, speed, position, and status were used to establish a series of point sources along the vessel's track, modeling the vessel as a mobile point source. The concentration fields resulting from this vessel's activity were modeled for four meteorological conditions, with one example for each season.

Introduction

As a result of the federal Clean Air Act Amendments of 1990, 189 hazardous air pollutants (HAPs) have been identified and prioritized for control by the U.S. EPA, including toxic metals and volatile organic compounds (VOCs). The National-scale Air Toxics Assessment (NATA) has also established estimates of human health risks in terms of both cancer and non-cancer outcomes associated with exposure to ambient concentrations of these species. Among these HAPs is diesel engine exhaust, or more specifically, diesel particulate matter (DPM), which has been hypothesized to be both a risk factor for lung cancer, an exacerbating factor for those who have certain allergies or asthmatic symptoms as well as being an irritant of the eyes, throat, and bronchial passages (Wu et al., 2007).

The potential carcinogenicity of DPM has been a topic of much scientific discourse, with individuals on both side of the issue making valid arguments. DPM is listed by the International Agency for Research on Cancer (IARC) to be a probable carcinogen, considering the evidence in favor of its carcinogenicity to be sufficiently demonstrated by animal studies, but limited in

application to human studies. Animal studies on the toxicology of TDE in laboratory rats, mice, and hamsters typically involved exposing them to concentrations that are orders of magnitude higher than what would occur in the environment or occupational settings for humans. Because of this unrealistic experimental setup, the applicability of the results to humans is reduced even though DPM was found to be carcinogenic (Hesterberg TW et al., 2006).

Another example of experimental methodologies interfering with making applicable conclusions is when toxicological studies involve the use of adsorbed organic materials in DPM as their risk factor of interest. In these studies, one controversial issue is that strong non-aqueous solvents like dichloromethane are often used to extract the known mutagens in DPM (e.g. PAHs). This reduces the applicability of the research to humans because the organic solvents do not represent the biological environment of the lung; the argument is therefore that the compounds present in the intact particles have limited bioavailability, and extracting them chemically renders the study less applicable. There is also some evidence from other animal studies that tumor formation was an affect that is nonspecific to DPM; similar results are obtained when high doses of particles composed of substitution compounds such as titanium dioxide, talc, and carbon black are used. Thus, a lung overload mechanism of induction of tumor formation can be hypothesized, and this prevents the specific attribution of risk to DPM itself (Hesterberg TW et al., 2006).

The literature on the topic of DPM related health effects is extensive, but as exemplified above, providing definitive evidence of carcinogenicity in humans is a great challenge. It is generally believed by leading regulatory agencies such as EPA and California EPA that DPM toxicity is complex and probably involves factors related to the physical characteristics of the fine particles (i.e. their small size and large surface area), a possible synergistic relationship between diesel particles and the toxicity of the polycyclic aromatic hydrocarbons (PAHs) that are found in DPM, and DNA damage linked to the presence of reactive oxygen species resulting from exposure to both DPM-related organics and the particles to which they adsorb.

In summary, the mechanistic details of carcinogenesis related to DPM exposure are not fully understood, but this has not prevented agencies from taking action to reduce exposure to DPM. In the Puget Sound area, the Puget Sound Clean Air Agency (PSCAA) has performed its own risk assessment of local air toxics and their relative potential to adversely affect health. They have concluded that mobile pollution sources like vehicles and marine vessels account for 85-95% of cancer risk from air toxics exposure, with stationary sources accounting for the small remainder of the risk. In this relatively recent assessment, DPM was estimated to account for approximately 70-85% of the cancer risk from air toxics in the Puget Sound area (Figure 1). It is thus receiving high priority in terms of air toxics reduction (Keill and Maykut, 2003).

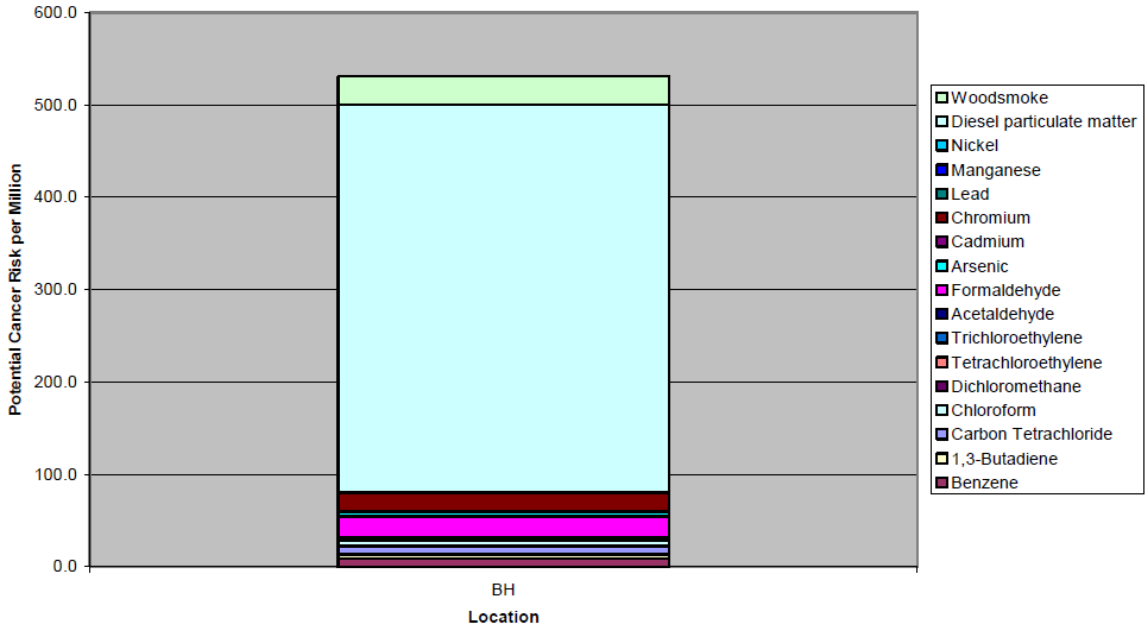

Figure 1. The entire bar represents 100% of the potential risk of cancer due to ambient air pollution, with colored sections of the bar denoting the contribution of individual air toxics. The large blue bar in the middle represents the portion of the total risk due to DPM (70-85% of total risk). This pertains to Beacon Hill and is derived from ambient air monitoring data and carcinogenicity studies (Keill and Maykut, 2003).

DPM is unlike many other of the air toxics in the sense that it is not a specific chemical, but rather a mixture of elemental carbon (30-90%), organic carbon (7-49%), metals and other elements (1-5%), sulfates and nitrates (1-4%), along with small quantities of other compounds. It sources include heavy equipment, passenger vehicles, locomotives, marine vessels, and other less significant sources (Wichmann, 2007). In order to prioritize the control of these different sources, it is essential to know their relative contribution to the total DPM concentrations in different areas. The measurement of black carbon (BC) with aetholometers has been used in the past to estimate DPM concentrations, but this method has the limitation that it cannot distinguish between BC from wood smoke and traffic exhaust when both sources are present in the same environment (Wu et al., 2007).

Receptor modeling results from using monitoring instruments at specific sites (e.g. Beacon Hill) in Seattle have commonly been used to estimate DPM exposures, but in addition to the difficulty of distinguishing DPM from wood smoke, more significant challenges arise when trying to discern whether measured aerosol particles are from gasoline or diesel engine exhaust. Researchers have used positive matrix factorization (PMF) algorithms to analyze different data sets and sampling periods, comparing results in order to evaluate the ability of these receptor

models in resolving the contributions from gasoline and diesel engines, but the PMF models were shown to be inadequate for the task (Table 1). Results from these models depend on the specific algorithm used, sample period, and type of speciation data (IMPROVE or STN). Suggested explanations for this inadequacy include low time resolution of the measurements of aerosols, a lack of specific organic chemical markers of DPM and gasoline derived particles, and the similarity between particles from diesel engines operating at low loads and particles from gasoline engines.

PMF Algorithm	**PMF-2**	**ME-2**	**Extended ME-2 w/size and mass**	**Mass Constrained ME-2**	**PMF-2**		**Constrained ME-2 w/bootstrap**	
Speciation Data Set	IMPROVE	IMPROVE	IMPROVE	STN	IMPROVE	STN	IMPROVE	STN
Period	96-1999	96-2000	2000-2003	2000-2004	2000-2004		2000-2003	
"Gasoline"	0.4	0.8	0.6	0.3	0.9	2.5	0.2 [0.9, 0.1]	0.2 [1.2, 0.1]
"Diesel"	1.6	1.9	1.4	0.7	0.2	0.2	0.9 [1.1, 0.4]	1.8 [2.6, 0.1]
Residual Oil	0.9	0.2	0.7	0.4	0.6	0.4	0.5 [0.7, 0.4]	0.6 [0.8, 0.4]

Table 1: Various DPM Concentration Estimates at Beacon Hill (µg/m^3). The above algorithms were used in different studies and gave qualitatively different results, suggesting that the current understanding of gasoline and diesel exhaust portions of particulate matter measurements needs improvement. This table was acquired from the original proposal from PSCAA to EPA (Himes and Gilroy, 2007).References for each column from left to right are (Maykut NN et al., 2003), (Kim et al., 2004), (Larson et al., 2006), (Wu et al., 2007), (Kim and Hopke, 2008),(Larson, 2006).

In order to resolve these issues and build confidence in DPM exposure estimates that better characterize its spatial and temporal distribution in the environment, the PSCAA has applied for and received support from the EPA to conduct a multifaceted research project to improve the estimation of local exposure to DPM in the Puget Sound. The following goals were outlined at the time of the PSCAA proposal to the EPA:

1) Develop improved methods for resolving the relative contributions from diesel and gasoline combustion sources to total air toxics.

2) Evaluate LIDAR (light radar) technology for use in directly monitoring DPM emission from maritime vessels.
3) Evaluate the use of 1-nitropyrene (1-NP) as a specific chemical marker of DPM.
4) Develop a continuous monitoring method for ambient gas phase hydrocarbons at sites where monitoring already exists using GC-FID and OP-FTIR analytical methods.
5) Utilize Positive Matrix Factorization (PMF) and UNMIX as analytical tools to develop a source apportionment model that utilizes data from continuous monitoring for aerosols and gas phase hydrocarbons, ultimately quantifying the relative contributions of different emission sources to concentrations of DPM at monitoring sites.
6) Validate the source apportionment model with real data.

Among mobile sources, marine vessel emissions are the least understood in terms of their relative impact. The large ports operated in Seattle and Tacoma present some concern for local populations, as marine emissions of DPM may contribute significantly to DPM exposures in areas such as the Duwamish River Valley. In terms of a proportion of total DPM emissions, various maritime activities have been found to contribute approximately 24% in the region for which PSCAA has jurisdiction (Figure 2).

One goal of the PSCAA project was to use LIDAR technology to make direct observations of the emissions' plume of selected vessels, following each of the plumes back to landfall. Coming at the problem from another angle, the project was also intent on modeling the vessel traffic with global positioning system (GPS) data gathered from the ships. Given the positions of the vessels over time, modeling vessel traffic and emissions from vessels may be done using atmospheric dispersion modeling, although modeling a marine vessel's emission accurately is quite a challenge. The DPM generation rate of the exhaust stack of a vessel varies according to the maximum continuous power rating (MCR) of the engine, the load placed on the engine, the fuel type being used by the vessel, and the emission factor (EF), which is the mass of pollutant produced per unit energy (g kW^{-1} hr^{-1}) invested in vessel operation.

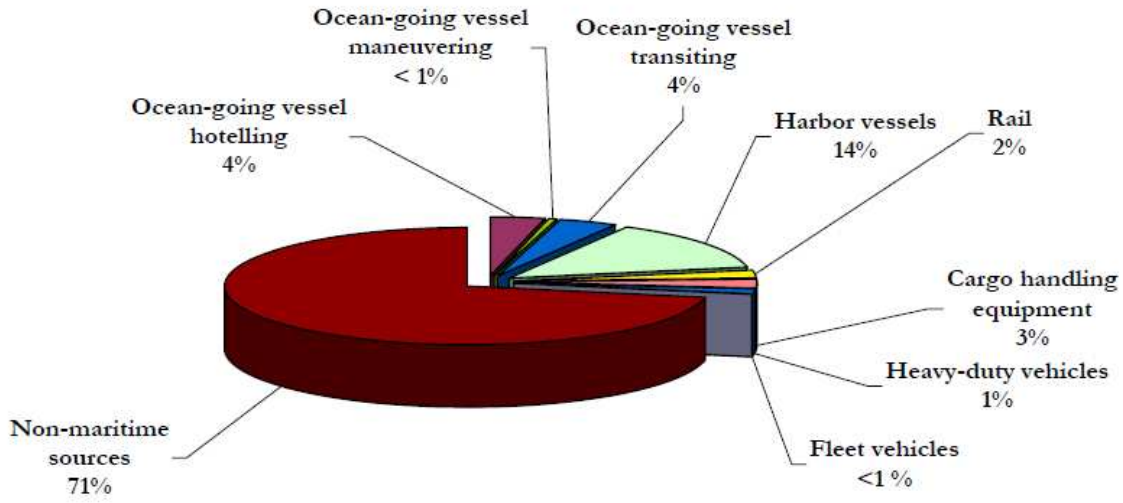

Figure 2. The above pie chart shows relative contributions of Maritime and Non-maritime DPM emissions in the PSCAA region (see Figure 3) in 2005 (Aldrete et al., 2007).

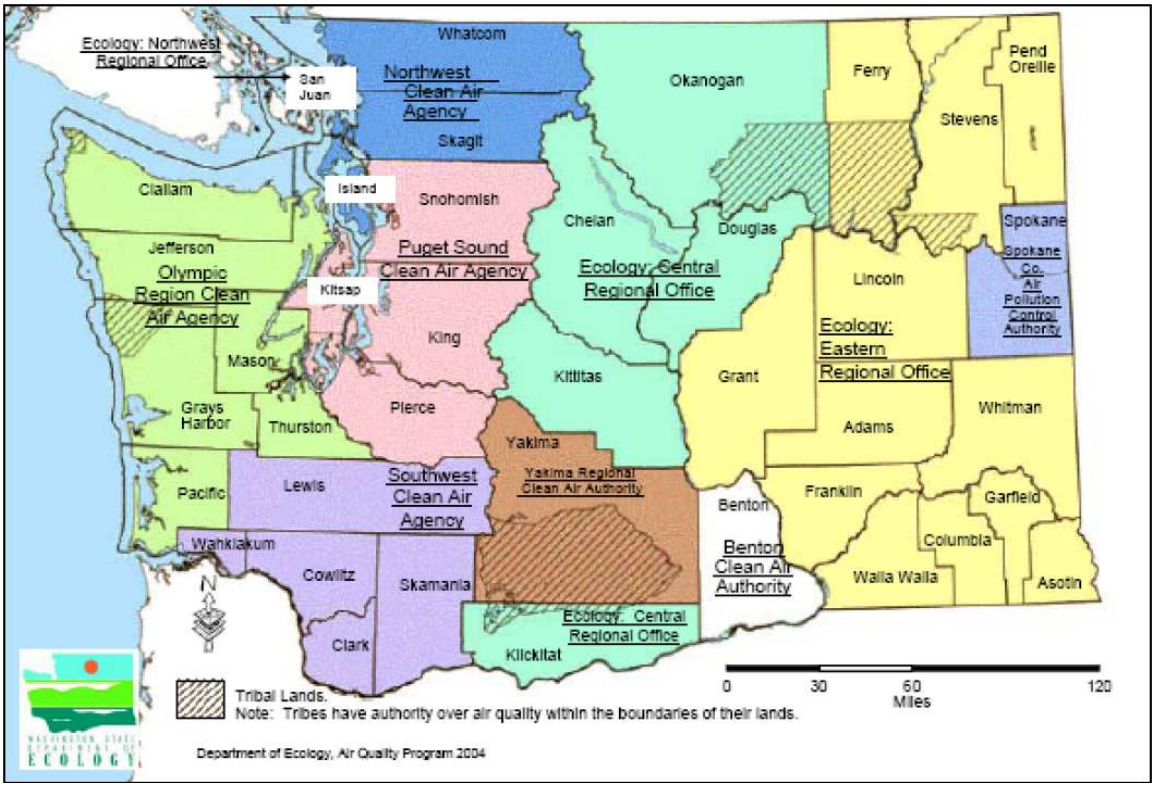

Figure 3. The jurisdiction of PSCAA is in King, Snohomish, Kitsap, and Pierce counties, which is shown above in the pink region (Aldrete et al., 2007).

In this study, an approach was developed for using the atmospheric dispersion model CALPUFF (Version 6), and a user interface CALPUFF View (Version 2.3) purchased from Lakes Environmental Software in order to model the fate of DPM from a selected marine vessel. CALPUFF is a complex and comprehensive, multilayer, multi-species, non-steady state Lagrangian puff dispersion model. Unlike steady-state models, CALPUFF can simulate the effects of spatially and temporally variable meteorological conditions on the fate of pollutants. The formulation of this Lagrangian model is better suited for individual sources and groups of sources than the formulation of a grid-based Eulerian model. CALPUFF estimates the effects of wet and dry scavenging, chemical transformation, and advective transport of pollutant species, including particulate matter, over distance scales from meters to hundreds of kilometers. It is considered to be suitable for modeling near field effects under various meteorological conditions such as stagnation, fumigation, temperature inversion, recirculation, light and calm winds, and transport over water and coastal regions. It also has algorithms for computing the subgrid effects of terrain impingement, and is the EPA preferred model for long range pollutant transport. It also calculates near source effects of building downwash, partial plume penetration, and transitional plume rise.

The three main components of the CALPUFF modeling system are CALMET, CALPUFF, and postprocessing programs that handle the output of the previous two components (CALPOST). CALMET is a 3-dimensional meteorological model that produces fields of wind (speed and directional components), temperature, mixing height, and atmospheric turbulence, along with several other fields. The CALMET model can use either observational data from surface stations and radiosonde measurements of upper air conditions, modeled data such as that from the MM5 community model NCEP/NCAR Reanalysis Data set, or a combination of modeled data and observations to create these fields, which are also adjusted to account for the effects of terrain in the geographical modeling area. A complete description of the technical approach and capabilities of these models is available in the user's guides for CALPUFF (Scire, Strimaitis, and Yamartino 2000) and CALMET (United States 1995).

Finally, as is critical for this present research, CALPUFF can accommodate arbitrarily varying emissions from point, area, line, and volume sources by utilizing special input files. In this study, a marine vessel was represented as a series of point sources placed along the vessel's track. Based on whether a vessel is in a particular location, each source was either actively emitting at a rate estimated using its speed and other variables, or inactive (emitting zero mass/time). The instantaneous position of each point source was given by signals sent out from the vessel through an Automated Identification System (AIS).

A similar approach was taken when the EPA conducted a screening study used a set of point sources along different coasts to represent vessel traffic and model the fate of sulfur oxides from vessels (EPA, 2008). However, in their approach, point sources were spaced approximately 25 km apart along shipping routes near major coastlines, emitting continuously for the modeling period. The spatial distribution was chosen based on known vessel traffic patterns and estimations of the ship density along those shipping lanes. For the current study, one vessel was modeled rather than an entire shipping lane of vessels, so it was important to represent both the physical location of the vessel and its emission rate at that position as variables that change over time. The scope of our study was also different than the EPA study in that rather than seeking to characterize the emissions from all vessels in a shipping lane, the specific aim here was to create and refine an appropriate method of modeling one vessel in a manner that can be easily replicated by future researchers. With this one vessel modeled in CALPUFF, the meteorological conditions that act on the ship's emissions' plume were varied to gain an understanding of how common Seattle weather patterns influence the fate of these emissions, thus informing policy makers and industrial stakeholders as to possible intervention strategies.

The meteorological data fields that were ultimately used were derived from MM5 modeled data for the year 2008, purchased from Lakes Environmental, which was used as an input for CALMET. MM5 is a prognostic meso-scale meteorological model developed by Pennsylvania State University and the U.S. National Center for Atmospheric Research. It uses objective analyses of global weather reports to produce a gridded meteorological field which takes into account the energy and momentum equations of the atmosphere. These weather reports are from global models maintained by the National Center for Environmental Protection (NCEP) and other agencies such as the United Kingdom Meteorological Office (UKMO), and are available in 2.5 degrees by 2.5 degrees spatial resolution and 6-hour time resolution. MM5 uses a nested grid approach to create a file containing hourly values of several meteorological variables, incorporating estimates of terrain surface boundary conditions by using land use information with 1 km grid cells. Lakes Environmental used the 2008 weather reports as inputs for the MM5 model in order to generate output ready for further processing.

The MM5 output was then processed by CALPUFF's MM5 processor CALMM5 to produce a formatted text file at 4 km grid resolution that contains the following variables:

- Pressure (mb)
- Elevation (m)
- Temperature (K)
- Wind direction (deg)

- Horizontal and vertical wind speed (m/s)
- Relative humidity (%)
- Mixing ratios of vapor, cloud water, rain water, ice water, snow, and graupel (g/kg)

In our case, the meteorological fields described by these text files produced by CALMM5 had 4 km grid resolution and 18 vertical levels for a 50 km^2 square area centered at Harbor Island. This meteorological data was provided on a disk from Lake's Environmental. We then input the data into the CALMET model, which produced the final meteorological field in a binary data file called CALMET.DAT based on the user-defined settings outlined below. One can alter the grid spacing at this point in CALPUFF View, although reducing the grid size does not necessarily produce a better wind field. Our final meteorological grid was set to have 1 km grid cells, so it contained a total of 2500 (50 by 50) grid cells to cover the modeling area. This setting could be altered in CALPUFF depending on one's preferences; one can have up to 210 grid cells in the X and Y direction (i.e. East or North); this is the limiting factor of meteorological grid size. One can alter spatial resolution of this grid, but the grid spacing must be at least 10 m. These choices all affect the size of the meteorological file CALMET.DAT, which needs to be less than 2 gigabytes, and the computational time required to complete the CALMET model run. For all models, the refined analysis option was chosen rather than the screening analysis option.

CALMET User Defined Settings

Many projects were ultimately developed, but in general, the following CALMET settings were used to generate the CALMET.DAT file. They are discussed below in the order that they appear in the CALMET wizard. Many of the alterations to CALMET settings mentioned below were made because it was a requirement of using the MM5 data.

CALMET-Run Information

The run period always was defined such that if the entire vessel path was entered starting near the beginning of the run period, enough time passed that concentrations of particulate matter at all receptors were at zero by the end of the run period (typically 5 days). The run option to "compute all data fields required by CALGRID or CALPUFF" was selected. The MM4/MM5/M3D option was selected for all three weather categories, and the checkbox for precipitation also was checked.

Grid Settings

The meteorological grid was automatically produced for each project when the center of the modeling area was selected with its latitude at 47.5898 N and its longitude at 122.3512 W. From this center, the modeling area was originally defined as a 50 km^2 square. As stated above, the final meteorological grid had 1 km grid spacing, and the default grid cell heights were used almost exclusively for each CALPUFF project in this study. The geological data files and computational grid also were derived from this same designated area.

Modules/Stations, Mixing Height Parameters, Overwater Surface Fluxes, Relative Humidity, and Temperature Parameters

For these windows, the default settings were used. On the temperature parameters window, the option to "Use MM5 data for surface and Upper Air Data (NOOBS=0, 1, 2)" was selected.

Wind Field Options

The "Use Prognostic Wind Fields" checkbox was selected, along with the option to use MM5 as the initial guess field. The MM5 files purchased from Lakes Environmental also were specified in this window. For the Surface Wind Vertical Extrapolation section, the "Ignore Layer 1 of Upper Air Stations" checkbox was checked and the "Do Not Extrapolate" option was selected.

Wind Field-Initial Guess

For this window, everything was kept as default except that the bias for vertical layer 1 was set to -1; this was mandatory, given that MM5 data was being used.

Wind Field-Step 1

This window was kept as default except that the option to compute kinematic effects was checked, and the radius of influence of terrain features was set to 50 km.

Wind Field-Step 2

For this window, under the wind field interpolation section, the maximum radius of influence over land surface, over land aloft, and over water were set to 100 km, 200 km, and 1 km, respectively, as these were the values used in the refined analysis tutorial. The relative

weighting of the Step 1 Field versus observations were set to 20 km for the surface layer and 100 km for layers aloft. The remaining options were left as their defaults.

CALMET Output Options

This window remained in default settings except the Cloud Data Options box was checked as required if using MM5, and the option to generate cloud cover from prognostic RH was selected.

CALPUFF User-Defined Settings

The run period and the time step for each CALPUFF project were chosen based on the needs of the particular project. The regulatory option to check selections against guidance for long range transport was selected. In the species and deposition window, The 5-species MESOPUFF chemistry model was selected and 'PM10' was added to the species list. Using the tab for deposition, all the checkboxes for each species were unchecked except for 'PM10', as this was the only species of interest for this project. Species deposition settings, such as the geometric mass mean diameter (D_p) and geometric standard deviation (σ_g) values in the "Dry (Particle)" window, were adjusted to be as representative as possible of DPM.

The size distribution of particles emitted from heavy duty diesel engines is lognormal and tri-modal, with the nuclei, accumulation, and coarse modes typically present. It is rather difficult, however, to identify an appropriate value for D_p and σ_g. The nuclei mode (0.005-0.05 μm diameter) has about 90% of the number of particles but less than 20% of the total mass emitted. The accumulation mode (0.05-1 μm diameter) is most of the mass emitted (~60-75%) but much fewer particles, and the course mode (>1 μm) accounts about 5-20% of the mass emitted (See Table 6 from Desantes et al., 2005) (Figure 4). The particle size distribution from a heavy duty diesel engine in one study, which was operating at 75% load, to have a count median diameter (CMD) of approximately 50 nm with σ_g =2. One of the Hatch-Choate equations,

$$MMD = CMD \exp(3 \ln^2 \sigma_g),$$

where MMD is the mass median diameter of the particle distribution, allows for the conversion from the CMD to the MMD, which for a lognormal distribution is approximately the same value as D_p (Ramachandran 2005). When viewing Figure 4, it is clear that the distribution is not perfectly lognormal because there is more than one mode in the mass weighted curve, so this mathematical transformation may not produce as accurate of a result as desired. In any case,

using this equation, a CMD of 50 nm and σ_g of 2 gives an MMD of 281 nm. A D_p 0.281μm and σ_g of 2 were therefore specified in the species deposition window of CALPUFF. These values are nearly identical to the default settings (Dp=0.48 μm, σ_g =2) that are specified for 'PM10'. With these settings established for CALPUFF and CALMET, PTEMARB.DAT text files were then constructed to complete all the necessary CALPUFF inputs.

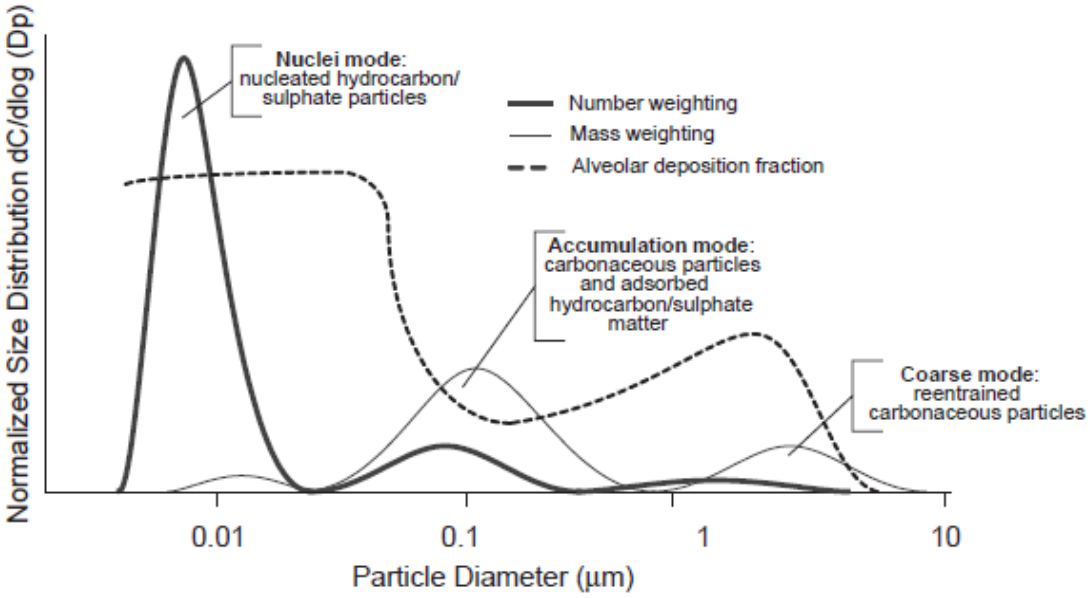

Figure 4. The above figure from Desantes et al. shows qualitatively how particles of different sizes are typically distributed for a large diesel engine, both in terms of mass and number (2005). Looking at the mass weighting, it is clear that the geometric mass mean diameter D_p that was calculated above does not perfectly match this figure. This is because the equation used to obtain D_p assumes a perfectly lognormal distribution, which is not the case on this graph; three modes are present. Attempting to place the D_p of 0.281 μm on the particle diameter axis, and considering the effect that the coarse mode would have on D_p, this value seems reasonably accurate.

For the Chemical Transformation and Meteorological/Landuse windows in the CAPLUFF sequential tool, the default settings were used, which included using the MESOPUFF II Scheme as the chemical transformation method. For the Plume Rise Options, the transitional plume rise, stacktip downwash, vertical wind shear above stack top, and partial plume penetration option boxes were checked. Inversion strength for partial plume penetration was set to be computed from temperature gradients. The remaining settings in this Plume Rise window, along with the settings in the Dispersion and Complex Terrain Effects windows were left at their defaults. Finally, in the CALPUFF Output Options window, the only list file output options that

were selected were the concentration, wet flux and dry flux of PM10. All other settings were left as their defaults except that under the Binary Files and Debug tab, the option to create a file for relative humidity was foregone.

With regard to the CALMET and CALPUFF settings, more investigation into the implications of using each feature in CALPUFF may be needed when more specific scientific questions are explored in the future, but for the purpose of this research project, these settings seemed appropriate. Each CALPUFF project created had these same settings, with alterations being made to the time period of interest, the time step used in CALPUFF (either 60 seconds, 5 minutes or 15 minutes), and the specific PTEMARB.DAT text files chosen as point source inputs.

Information Management

As required for the representation of a string of arbitrarily emitting point sources, a text file called PTEMARB.DAT, whose general format is outlined in documents produced by Earth Tech (Earth Tech, 2006), was manually constructed through a series of data processing steps. An example of the format is shown below (Figure 5). The general structure is such that at the top of the text file, a series of header records informs the model of the overall time period of interest, pollutant species to be modeled, and geographical area. Then, the time-invariant properties of each source are defined, such as the source identifier and location in UTM coordinates, exhaust stack height, stack diameter and stack base elevation, along with a building downwash flag, vertical momentum flux factor, and user defined flag (e.g. fuel code). Then, for user-defined emission periods that must lie within the overall period of interest, the previously specified sources are assigned their time-variant emission parameters such as the exit temperature (K), exit velocity (m/s), initial sigma-y and sigma-z values (m), and emission rate (g/s).

The only pollutant species modeled for these projects was 'PM10'. When entered into the text file this way, the model is informed to use the properties associated with the pollutant called PM10 in the species library of CALPUFF; the model also uses the estimated D_p and σ_g specified above. The UTM zone 10 and Pacific time zone UTC-0800 were designated in the header records of all projects. The time period of interest was altered according to meteorological conditions that were to be tested in each CALPUFF project. The text file requires a molecular weight for each pollutant species modeled, but because we were only interested in particulate matter, any value placed there would not really make sense. Stating the molecular weight as 50 g/mole was therefore an arbitrary decision, but it should be noted that placing any value in this data field yields the same modeling results (50 billion g/mole, for example, has no effect). One could use the molecular weight of carbon, as the DPM is mostly composed of carbon, but it

seems that this value is simply not relevant for the calculations that take place within CALPUFF for determining the fate of 'PM10'.

The following process was used to gather the necessary data requirements for the time-invariant and time-variant portions of the text file. First, AIS signals obtained from an antenna located on top of Queene Anne hill provided the information needed to describe the vessels' tracks. These signals are sent out from all vessels over 299 gross tons. The approximate position of vessels in terms of latitude and longitude, along with the time of the signal, vessel status (e.g. moored, underway, fishing, etc.), vessel speed (knots), Maritime Mobile Service Identities (MMSI), course, and heading were included in each AIS signal. A software program automatically collected the signals for a full day then saved them as rows in a text file. Second, in order to find an appropriate vessel for modeling, we arbitrarily chose three consecutive days (2/12/09-2/14/09), and then merged the three days into a single data file by importing them into SPSS Version 16.0. We removed extraneous information from the SPSS file by eliminating unnecessary columns (variables) and rows (e.g. garbage signals). The MMSI, speed, date and time, latitude, longitude, and status remained in the database as columns. To organize the data so that full vessel paths could be viewed as a series of chronological signals, the rows were then sorted first by time of signal and then by MMSI.

The Puget Sound Emissions Inventory contains the necessary vessel specific information such as maximum speed (MS), maximum continuous rated engine power (MCR_p) and an estimate of auxiliary engine power for a subset of the vessels that provided AIS signals in our SPSS file. We therefore preferred a large cargo vessel that was characterized in this inventory. Additionally, we wanted a vessel that traveled from the northern Puget Sound area en route to the eastern side of Harbor Island, moored there for some time, and then departed along a similar path back out of the modeling area. This shipping track was particularly desirable because in future studies in which model validation with LIDAR measurements may take place, this track would be commonly encountered and ideal in terms of feasibility of measurement. To ensure that the vessel track of choice involved mooring at Harbor Island, signals from outside the general Harbor Island area were temporarily filtered out of the dataset. We then created a list of the remaining vessels and used the AIS marine traffic website to gather their length and width dimensions, deadweight tonnage (DWT), and vessel type (e.g. cargo, tug, etc.). The second largest vessel on the list was chosen because it had an ideal shipping route (Figure 6).

```
PTEMARB.DAT     2.1          Comments, times with seconds, time zone, coord info
1
Test Example
UTM
10N
NAS-C   02-21-2003
KM
UTC-0800
2008  272   0  0000  2008  276  0 0000
6   1
'PM10'
50
'9#####10000'   539.87053   5295.45627   40   1.9   0   0   1   0
'9#####10001'   539.90136   5295.32317   40   1.9   0   0   1   0
'9#####10002'   539.93228   5295.19278   40   1.9   0   0   1   0
'9#####10003'   539.97350   5295.01329   40   1.9   0   0   1   0
'9#####10004'   540.01595   5294.82924   40   1.9   0   0   1   0
'9#####10005'   540.04870   5294.69604   40   1.9   0   0   1   0
2008   272   00   0000      2008   276   00   0000
'9#####10000'   537   24.6   1   1   478
'9#####10001'     0      0   0   0     0
'9#####10002'     0      0   0   0     0
'9#####10003'     0      0   0   0     0
'9#####10004'     0      0   0   0     0
'9#####10005'     0      0   0   0     0
```

Figure 5. The above example PTEMARB.DAT file contains the necessary information for representing a vessel track as a series of point sources. Beginning at the first line in bold, the time period of interest is defined for the text file, following by the number of sources and pollutant species (100 and 1), then the species identifier. The next line is typically molecular weight (50 g/mol shown here is irrelevant because it is particulate matter), followed by a series of sources and the time invariant parameters. Then the sub-period for which the time variant parameters shown below it are true is defined, followed by the parameters themselves. In this example, there are six sources at different locations, and for the entire time period of interest, the first source identified is emitting 478 g/s of particulate matter while the other sources are not emitting.

Figure 6. The vessel chosen for this project is shown with its identity concealed. Some vessel parameters are: draught-12.7 m, DWT-67660 tons, length- 270 m, width -40 m (AIS website), MCR_p-46574 kW, MS-25 knots.

The itinerary found for this vessel was used to extract the full set of this particular vessel's chronological AIS signals from the SPSS files. The signals were imported into Microsoft Excel, where the spatial boundaries of the modeling area in CALPUFF were used to eliminate out of range signals (see Table 2 for example of data at this stage). A Visual Basic routine was used to remove letter characters from the cells in the latitude, longitude, and speed columns so that they could be read as numerical values. Latitudes and longitudes were then converted to Universal Transverse Mercator (UTM) coordinates (units of km) by using a spreadsheet calculator that is available online. The validity of this calculator was tested by comparing some of the coordinates from its output with some of the results from an analogous coordinate converter tool that came with CALUFF. This latter tool works well for conversion of a small number of latitudes and longitudes, but was not preferred simply because only one coordinate at a time could be converted. Fortunately, the difference in resulting UTM coordinates of the two tools was very small for the values of the easting ($\sim 10^{-5}$ m) and northing (~0.15m), so the online tool was assumed to be an acceptable method of transforming large numbers of latitudes and longitudes.

MMSI	Status	Speed	Lat	Long	Date_Time
#####	under way	13.9kt	47.445667N	122.407667W	090129 113703
#####	under way	14.0kt	47.445833N	122.407833W	090129 113659
#####	under way	14.1kt	47.446167N	122.408000W	090129 113655
#####	under way	14.2kt	47.446333N	122.408000W	090129 113651
#####	under way	14.2kt	47.446667N	122.408167W	090129 113647
#####	under way	14.2kt	47.447167N	122.408333W	090129 113639

Table 2. After importation of a set of signals from the entire track of our chosen vessel within the Puget Sound, the starting format of the data was at the stage shown above. A series of alterations were then performed to reformat the data so that PTEMARB.DAT files could be constructed. The spaces in the column labeled 'Date_Time' are formatted as YYMMDD HHMMSS where Y=year, M=month, D=day of the month, H=hour (0-23), M=minute (0-59), S=second (0-59).

Dates as seen in Table 1 were reformatted by creating separate cells in each row for the four digit year (2008), Julian day of the year (0-366), hour (0-23), and second (0-3599).

Vessel activities were categorized as either hotelling (status column says "moored"), in transit (status column says "underway"), or maneuvering, as these categories effect the method of determining emission rates for main propulsion and auxiliary engine emissions. Any signals that were not registered as "moored", but that were received from locations south of the UTM northing 5274.915 km and east of the UTM easting 546.158 km (UTM zone 10) were categorized as maneuvering (see Figure 12). This is where tug boats have probably begun to assist the larger vessels in their landing (personal communication with Coast Guard official).

Table 1 contains all of the variables and information needed to construct a PTEMARB.DAT text file except for the exhaust parameters. Stack height was estimated to be about 40 m by using the height of the cargo containers as a measurement unit (standard height~ 2.6m) and measuring the number of container heights required to reach from sea level to the top of the stack. A stack diameter of 1.9 m, an exit velocity of 24.6 m/s and an exit temperature of 537 K were used. These values seemed reasonable as they were used in the EPA study mentioned before (EPA, 2008), and the latter two values were similar to those found in another study as well (Moldanova et al., 2009). Initial sigma-y and sigma-z values for the sources were set to 1 m, which is the CALPUFF default value for point sources created in the CALPUFF sequential tool. These two parameters provide CALPUFF with an estimate of the initial horizontal and vertical dispersion, respectively, of the plume as a result of emission.

Gridded receptors were placed over the full modeling area. A nesting factor of 1 was used, which produces a single receptor in the center of each meteorological grid cell. This means that all 2,500 grid cells contained one receptor at ground level (default elevation of receptors is 0

m). With every data input requirement obtained except for the emission rates of each point source along the vessel track, a method was developed estimate these rates that was based on common approaches found in larger scale emissions inventories.

Approach to estimating emission factors

To model the emissions occurring between one signal and the next, a point source was created at the spatial midpoint between the coordinates given by consecutive AIS signals (Figure 7). The midpoint was determined for each pair of consecutive signals and recorded in a new column in Excel. The process used to estimate the emission rate (g/s) for each of these point sources is discussed below.

The equation commonly used in larger scale emissions inventories, such as the Puget Sound Maritime Air Emissions Inventory, to obtain an emission rate E (g/hr, often converted to tons/yr) is

$$E = MCR_p \cdot LF \cdot A_h \cdot EF_{avg} \cdot FC \qquad (1),$$

where MCR_p is the maximum continuous rated power of the vessel (kW), LF is the load factor or fraction of the engine's rated power that is used for operation, A_h is the time spent in a certain activity (e.g. hotelling, transit, maneuvering) usually given in hours, EF_{avg} is the average emission factor or mass of pollutant emitted per energy invested in operation ($g \cdot kW^{-1}hr^{-1}$), and FC is the fuel correction factor that adjusts emissions based on the type of fuel being used. An FC of 1 was used in this study because the vessel that was ultimately chosen uses heavy fuel oil (HFO) with 2.5% sulfur, which has an FC of 1. It is also possible, however, that within our area of interest , the vessel must legally switch to a fuel with less sulfur content. If it is later determined that a different FC was appropriate, resulting concentration fields could be adjusted with a scalar in CALPOST; this is due to the fact that the emission rate is linearly dependent on FC, which should also be constant throughout the vessel's track in this area. A_h did not really apply in the usual sense, as the quantity of interest was the instantaneous emission rate rather than tons emitted per year. For the load factor, the propeller law was used as was done previously in the Puget Sound Inventory;

$$LF = \left(\frac{S}{MS} \right)^3 \qquad (2),$$

where S is the instantaneous vessel speed received from the AIS system, and MS is the maximum vessel speed. MCR_p and MS for the chosen vessel were both obtained from Appendix E of the Puget Sound Inventory, which contains these values for several ocean going vessels that common

enter the Puget Sound. The propeller law states that the "necessary power delivered to the propeller is proportional to the rate of revolution to the power of 3." (Aldrete et al., 2007).

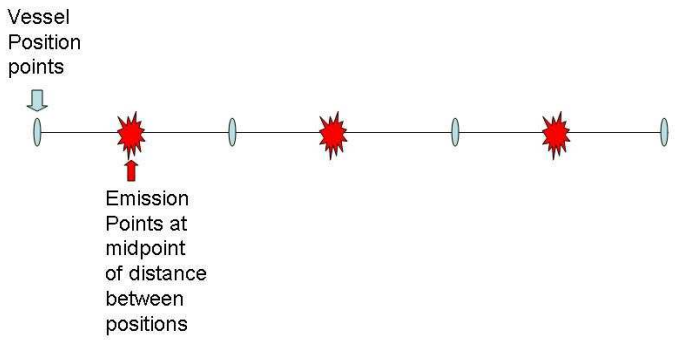

Figure 7. Maintaining the same times and positions given by AIS (light blue), a vessel's emission was represented by placing a source at the midpoint between two positions and having it emit during the period that the vessel passes between them.

In practice, it has been found that some higher exponents should be placed on the right side of equation 2, such as 4.5 for large high-speed ships (some container vessels), 4.0 for some medium sized medium speed vessels (some RoRo's, reefers, and feeder container ships), and 3.5 for low speed ships (small feeder container ships, tankers, bulk carriers etc.) (MAN B & W Diesel A/S. 1996). For any given actual vessel speed, the LF from equation 2 is a number between 0 and 1, so the cubic relationship gives higher load factors than those that result from higher exponents; higher load factors then tend to overestimate the emission rate for any given vessel speed. In the interest of being conservative, the cubic relationship was chosen.

The choice of DPM emission factor, EF_{avg}, for both the main propulsion and auxiliary engines was 1.0 $g \cdot kW^{-1}hr^{-1}$. As stated in the Puget Sound inventory, this estimate is reasonable because it is consistent with the EPA's recommendations; EPA has cited values for ocean going vessels in the range of 0.98 to 1.11 $g \cdot kW^{-1}hr^{-1}$, and another study found an emission factor of 1.03 $g \cdot kW^{-1}hr^{-1}$ after exhaust was cooled in a dilution system (Moldanova et al., 2009). Also, it has the convenient property of being unity, which makes the scaling of the resulting concentration fields easier if one wants to use a different emission factor.

When these engines operate below 20% load, the emission factor increases because they run less efficiently. The value of EF_{avg} was adjusted for low loads using a table from the Puget Sound Emissions Inventory (see Table 3.19 in the inventory) to get a power law equation that describes how the low load adjustment multipliers (LLAs) relate to the load factor. The following equation,

$$LLA = 0.1826 \cdot LF^{-0.9245} \qquad (3),$$

is a good representation of the trend except near the lowest and highest ends of the relevant load factor scale, which is from zero to 20% load in this case (Figure 8). To be consistent with the table of LLA multipliers in the Puget Sound Inventory, LLA should be equal to 1 when LF=0.20 and equal to 19.17 when $LF \leq 0.01$ (Aldrete et al., 2007). The load factors that result in LLAs of 1 and 19.17 are 0.1589 and 0.006514, respectively. The LLA values from LFs between 0.1589 and 0.20 are close to 1, so when $0.01 < LF \leq 0.1589$, the equation was applied to adjust for low loads; when $LF \leq 0.01$, LLA was set to 19.17; when LF>0.1589, LLA was set to 1.0.

It is important to note that certain weather conditions, fouling, acceleration, and other factors that alter the resistance to travel would also influence the true engine load factor. For our purposes, the LF was adjusted for acceleration, as information on wave patterns and the extent of fouling was not available. Using Figure 18 from Chapter 3 of "Basic Principles of Ship Propulsion" (See Figure 9 below), it is clear that a "heavier" propeller relationship curve should

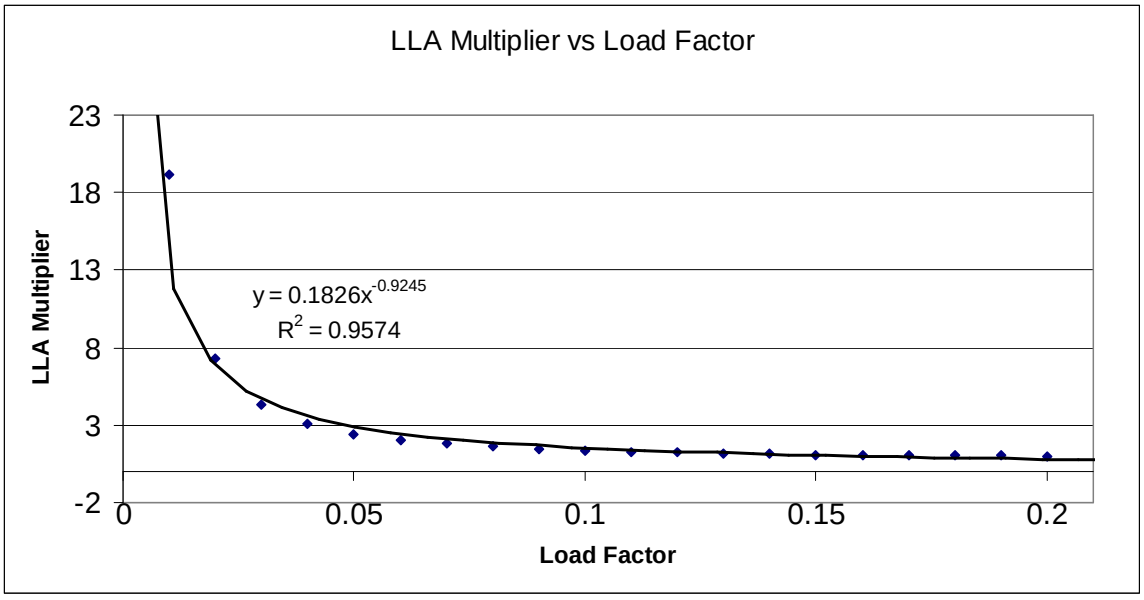

Figure 8. The power law equation shown was used to adjust for low loads when $0.01 < LF \leq 0.1589$. If $LF \leq 0.01$, LLA was set to 19.17 to be consistent with the Puget Sound Inventory. Near the high end of the curve, where LF>0.1589, LLA was set to 1 (i.e. no adjustment for low load).

be applied when a vessel accelerates. There would be significant difference in the power required from an engine propelling a vessel traveling at a constant velocity V at time t and the power required if accelerating through the same instantaneous condition. Acceleration is an operational condition compared to traveling in very heavy seas with wave resistance. The rate of acceleration also is critical, and operators presumably accelerate at a rate that balances the needs of quick travel and keeping the load on the engine reasonable.

In this project, LF values were adjusted for acceleration based on the load diagram shown in Figure 9. Line 2, representing conditions that resemble acceleration, is shifted to the left (heavier) of line 6, which represents light weather and clean hull (no fouling) conditions, by an amount that increases with increasing engine speed (note the logarithmic scale). For a given engine speed near the high end of the engine speed scale (let's use 95% engine speed for this example), the corresponding engine shaft power percentage on lines 2 and 6 are about 85% and 76%, respectively. For a given engine speed near the low end of the engine speed scale (let's use 80% engine speed for this example), the corresponding engine shaft power percentage on lines 2 and 6 are about 52% and 44%, respectively (MAN B & W Diesel A/S. 1996). Adding 0.09 to the LF during periods of clear acceleration from low speed to service speed was thus the chosen method of adjustment, even though other factors certainly affect the LF in significant ways. Small increases in vessel speed were not considered acceleration, and ultimately, only two periods of clear acceleration were adjusted for. These periods both occurred after the vessel left the harbor and accelerated to service speed as it traveled north. When a vessel decelerates, the LF could be even lower than line 6 in the load diagram because the vessel's momentum decreases the required engine power for a given velocity. For this study, the LF was not adjusted for times when the vessel was decelerating.

For main propulsion engines, the LF was determined for each UTM coordinate given by the AIS system using the vessel speed recorded at that location, including adjustment for low loads and acceleration. To determine the emission rate at the midpoint between two consecutive coordinates, the average emission rate of these two coordinates was calculated using the following equation;

$$E_{avg} = 0.5 \cdot MCR_p \cdot EF_{avg} \left[LLA_1 \left[\left(\frac{S_1}{MS} \right)^3 + A_1 \right] + LLA_2 \left[\left(\frac{S_2}{MS} \right)^3 + A_2 \right] \right] \quad (4),$$

where MCR_p is 46574 kW (propulsion engine power), MS is 25 knots, A_1 and A_2 were the LF adjustments for acceleration at each coordinate (either 0.09 or zero), and LLA_1 and LLA_2 were the low load adjustment multipliers determined by the acceleration-adjusted load factor obtained from equation 3.

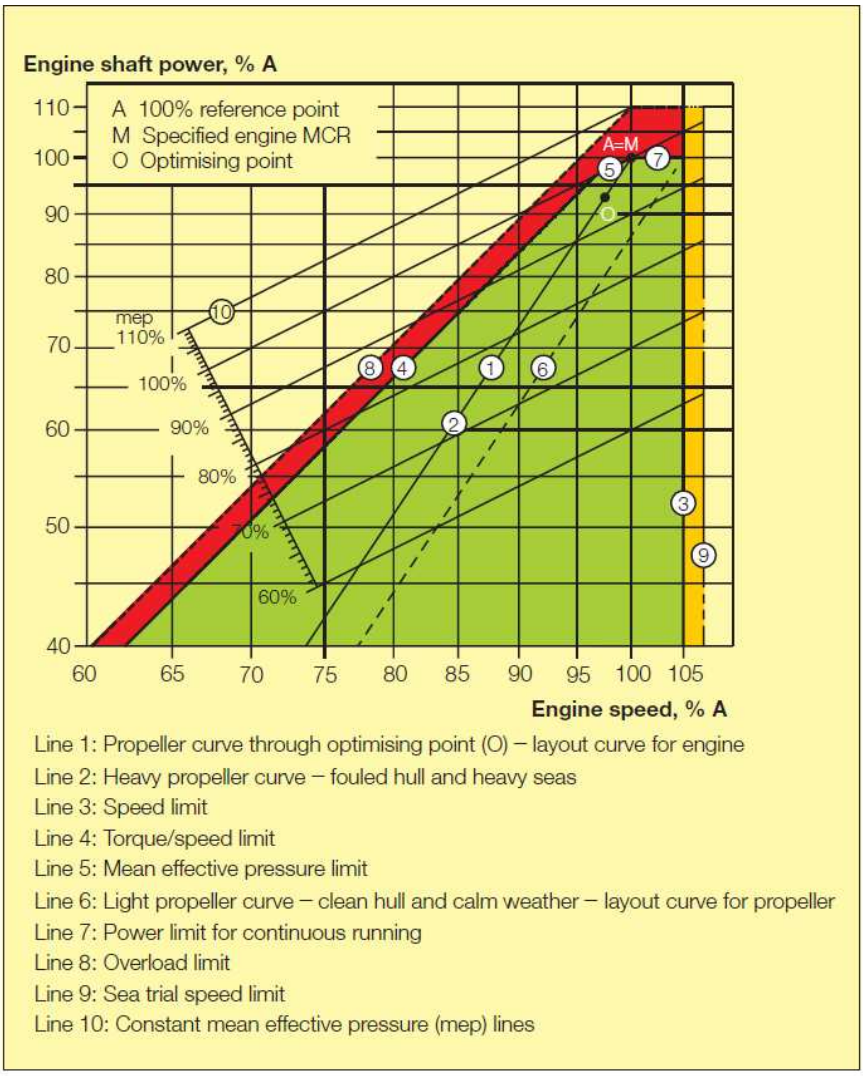

Fig. 18: Engine load diagram

Figure 9. Figure 18 from "Basic Principles of Ship Propulsion" is shown (MAN B & W Diesel A/S. 1996).This figure shows the relationship between the engine shaft power requirement and engine speed for different conditions. Acceleration as an operational condition has been compared to Line 2 on the graph, a vessel operating with fouled hull and under heavy seas.

Note that averaging two values that are derived from a cubic relationship in this manner is not exact. For example, if LLA_1 and LLA_2 were both 1 and A_1 and A_2 were both 0, as is often the case, equation 4 reduces to

$$E_{avg} = MCR_p \cdot EF_{avg}\left[\frac{LF_1 + LF_2}{2}\right] \qquad (5).$$

The exact value of the term inside the brackets of equation 5, LF_{avg}, assuming constant acceleration, would be given by the average value function;

$$LF_{avg} = \left(\frac{1}{MS}\right)^3\left(\frac{1}{S_2 - S_1}\right)\int_{S_1}^{S_2} S^3 dS \qquad (6).$$

Considering that the acceleration is not known on a continuous basis, and that the change in vessel speed between two consecutive signals is usually quite small, the simplified averaging method in equation 4 was used in order to save computational time and simplify data preparation. The difference in results from using different averaging methods is minimal, especially compared to the impact of choosing different exponents in equation 2, but this averaging method does slightly overestimate the value of EF_{avg}. When the vessel was "moored", its propulsion engines are likely to be turned off while auxiliary engines run the necessary operation systems, so the emission factor was set to zero during mooring periods. When the vessel was maneuvering, the LF was set 0.03. This value is also derived from the composite maneuvering load factors offered in the Puget Sound Inventory (Aldrete et al., 2007)(see Table 3.20).

The emission rate for the auxiliary engine at each coordinate was determined by using a table from the Puget Sound Inventory to determine appropriate load factors of this vessel type (Container-5000) (See Table 3.24). Maneuvering requires the most demand at 49% load, followed by mooring at 16% load and transit at 13% load (Aldrete et al., 2007). Using the categorizations described earlier for activity type, the appropriate load factor (0.49, 0.16, or 0.13) was assigned for each AIS signal in a new column in Excel. Given the LF, EF_{avg} (1.0 $g \cdot kW^{-1}hr^{-1}$), and auxiliary engine power rating (MCR_{pa}) of 11,360 kW, the average emission rate of the auxiliary engine was calculated for each midpoint between consecutive signals using the following equation;

$$E_{avg} = \frac{EF_{avg} \cdot MCR_{pa}\left(LF_1 + LF_2\right)}{2} \qquad (7).$$

LLA multipliers and acceleration adjustments were not applied in this case, because the relationship between vessel speed and auxiliary engine load factors is qualitatively different. It is also important to note that the three possible LF values for auxiliary engines are averages across

vessel types, as vessel-specific information on auxiliary engines is not generally available. To get the total emission rate of the vessel, the E_{avg} from the main propulsion and auxiliary engines were summed. This total E_{avg} was therefore used as the emission rate of each point source created at the midpoint between consecutive AIS signals, each emitting at this specific rate for the time period that passes between the two signals. Once the time of the second signal is reached, this source turns off and the source emitting at the next midpoint turns on. This process continues such that at a given time, exactly one source is emitting along the track of the vessel while the rest of the sources are inactive.

In terms of information management, these calculations required the creation of several new columns in excel, but only a portion of the resulting columns were needed to construct the PTEMARB.DAT text file. An intermediate worksheet was then created to store the relevant data in a format that was more readily converted into the PTEMARB.DAT text file format (see Table 3 for an abbreviated example). This format was then saved as a tab delimited text file, and a simple computer program was written (i.e. a Perl Script) to reformat the data so it could be readily input into CALPUFF.

Since the signals for the mooring period were all basically from the same location, this period was condensed in terms of the number of signals. The final complete vessel track contained 529 point sources. Because the version of CALPUFF that was used only accepts 100 sources at a time in a text file, additional programming scripts were written to cut the full vessel

9#####10000	539.87053	5295.45627	40	1.9	0	0	1	0					
9#####10001	539.90136	5295.32317	40	1.9	0	0	1	0					
9#####10002	539.93228	5295.19278	40	1.9	0	0	1	0					
9#####10003	539.97350	5295.01329	40	1.9	0	0	1	0					
9#####10004	540.01595	5294.82924	40	1.9	0	0	1	0					
9#####10005	540.04870	5294.69604	40	1.9	0	0	1	0					
2008	114	16	737	2008	114	16	749	9#####10000	537	24.6	1	1	478
2008	114	16	749	2008	114	16	761	9#####10001	537	24.6	1	1	478
2008	114	16	761	2008	114	16	773	9#####10002	537	24.6	1	1	478
2008	114	16	773	2008	114	16	796	9#####10003	537	24.6	1	1	478
2008	114	16	796	2008	114	16	809	9#####10004	537	24.6	1	1	478
2008	114	16	809	2008	114	16	821	9#####10005	537	24.6	1	1	478

Table 3. This format contains all the relevant information needed to construct a PTEMARB.DAT text file but is not in the correct format. This format is useful in that one can easily alter emission rates, dates, or other variables to suit the needs of a CALPUFF project. The top 6 rows are the time-invariant records as shown in Table 1. Starting from the far left cell on the seventh row from the top, 14 cells must be filled in. The first four cells are the 4-digit year, Julian day (0-366), hour (0-23), and second (0-3599) of the start time for emission of the source identified in the 9th cell from the left. The next four cells give the end time for the emission of this source. After the source identifier in the 9th cell, the 10th cell is the exit temperature (K), followed by the exit velocity (m/s), initial sigma-y (m), initial sigma-z (m), and emission rate (g/s).

track into 6 pieces and construct a PTEMARB.DAT text file for each piece. Separate model runs with identical CALPUFF run periods were performed for each of the text files to complete the vessel path. Each CALPUFF run produces three important binary output files: CONC.DAT, WFLX.DAT, and DFLX.DAT. These files contain time-weighted average values of the concentration, wet deposition fluxes, and dry deposition fluxes at each gridded receptor chosen in the CALPUFF run, for each time step. The 6 sets of these three binary output files were then summed together using the postprocessor CALSUM.exe to get one final set of three binary files that characterized the entire vessel path (See Procedure A in appendix B for more details).

We also wanted to observe the effects of specific sections of the vessel track independently. The original vessel track with 529 point sources was therefore split into three portions: transit en route to Harbor Island, mooring, and transit out of the Puget Sound. This was done to observe how mooring activity may affect the areas nearby Harbor Island. During the mooring period for this vessel, the auxiliary engines were set to be running at a constant load of 16% for the duration of the vessel's stay. This assumption may not be realistic, but information about engine activity while the vessel is moored was not available.

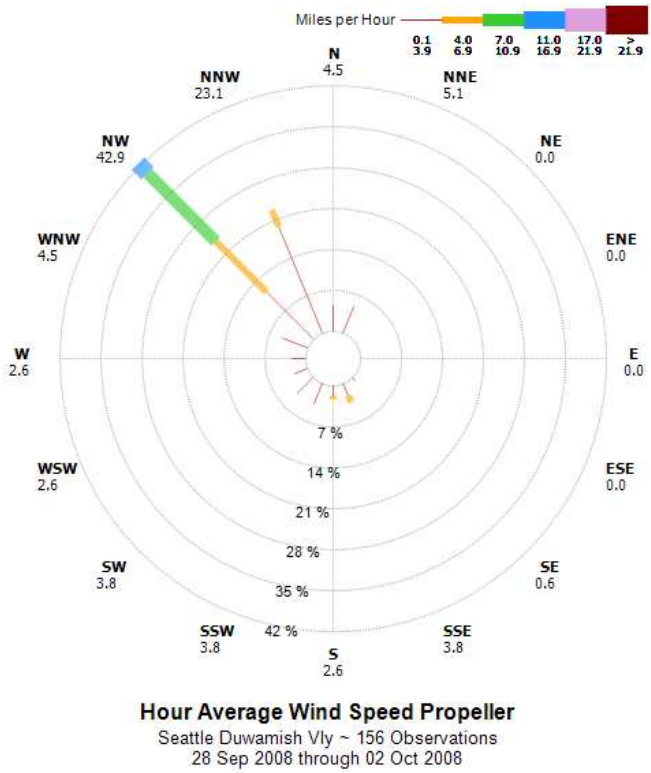

Figure 10. The above wind rose indicates the percentage of the time that wind was blowing *from* the direction indicated (PSCAA website). The time period shown was used in the CALPUFF model, with the vessel entering the modeling area from the north at about 4:00 pm on the first day, September 28, 2008, and leaving the modeling area by 1:00 am on September 30, 2008.

The first modeling period was initially selected by using available wind rose plots from the PSCAA website to identify times when vessel emissions would likely impact areas of interest. The surface station used to generate the wind rose plot shown in Figure 10 is located in the Duwamish River Valley near sea level. The intent of basing the choice of meteorological modeling period of this first CALPUFF project on the above wind rose was to see if the wind directions and speeds that it indicated related closely to the fate of the emissions' plume. It was later determined that the wind rose did not provide a good prediction of the fate of these emissions, however, so modeling periods for subsequent projects were chosen using a different strategy. The wind rose shown here was derived from measurements near sea level in the Duwamish River Valley. Plume rise phenomena carry the emitted material to higher elevations, where it is often the case that winds are blowing in a different direction than those indicate by surface stations. It is these higher wind layers that often determine the direction that the plume takes, although plume rise is a complex phenomenon depending on several factors. It is difficult to find upper air observations that are informative to this end, however, so we simply chose to observe the fate of emissions from a continuously emitting point source at Harbor Island, visually inspecting how the meteorological conditions that were present at each CALMET time step influence the concentration fields over time.

Several new CALPUFF projects were created with this point source in order to span the entire year of 2008. Its emission rate was set at 30 g/s, reflecting the previously estimated emission rate during moorage at Harbor Island. The reason for creating more than one project for this purpose was to keep the size of each CALMET.DAT files reasonably small. This set of projects provided a means to examine the feasibility of using observations of each wind field layer and how it emits influences the fate of the emissions' plume in different seasons. This type of observation was then used to choose the subsequent meteorological periods into which we placed the vessel's track.

Because the first modeling period chosen served as an example for the autumn season, three additional time periods were chosen as examples of winter, spring, and summer. For each seasonal example, 6 CALPUFF projects were completed for a total of 24 projects. These subprojects included, for each season:

- The full vessel track modeled using a 1-minute CALPUFF time step
- The mooring period with a 15-minute time step
- Transit en route to Harbor Island using a 1-minute time step
- Transit en route to Harbor Island using a 5-minute time step

- Transit out of the Puget Sound using a 1-minute time step
- Transit out of the Puget Sound using a 5-minute time step.

Some additional analyses also were done to examine the possible effects of changing some of the model parameters. For example, although building downwash was not modeled for any of the above 24 projects, this factor needed to be tested when the wind is blowing the emissions' plume down the length of the vessel. From looking at the photographs of this vessel, if the ship is fully loaded, it functions as a rectangular building with a length of about 250 m, width of 36 m, and height of 29 m (11 m lower than the stack height). Because the containers aboard these vessels were standard sized with a height of 2.6 m, the height of the containers could be used to estimate ship height. In order to gain insight into the possible effects of building downwash, a building was drawn into the model in a way that places the position of the stack and ship orientation as illustrated in figure 11. The Building Profile Input Program (BPIP) was run in CALPUFF View to obtain the necessary inputs for the plume rise model enhancements method, also called PRIME, and the CALPUFF model was run both with and without this feature in order to observe the difference in model outputs.

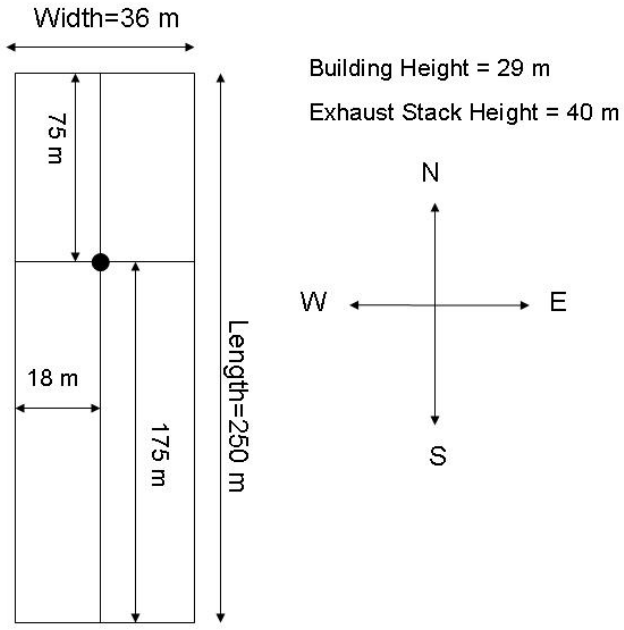

Figure 11. The dimensions of the vessel and stack position (black circle) that were used to run BPIP and model building downwash are shown. The meteorological conditions chosen were such that winds near the stack height were blowing from due north for about 4 hours. The wind speed was 1.3-6.2 m/s near the point source for this time period, with wind speeds closer to the low end of this range for the 30 m wind layer, and closer to the high end of this range at the 60 m wind layer.

It should be noted that as our modeling technique involved using a series of stationary point sources to represent the motion of a vessel. This method does not account for the fact that an effective wind field is felt by the stack as a result of the vessel's velocity. In reality, this effective wind field would be summed with the natural meteorological wind field, and the final wind field would undoubtedly be different from the natural wind field alone. The difference could easily be qualitative as well, so the limitations of this building downwash test should be considered in the interpretation of the results.

The effect of using varying exit temperatures was also examined for mooring activity, using the meteorological conditions that were present during a portion of the summer and winter CALPUFF projects. For each of these seasons, the normal exit temperature of 537 K was used in addition to lower temperatures of 480 K, 420 K, 360 K, and 300 K. The resulting concentration fields may be compared in the results section.

For each of the figures that are contained in the following results section, a CALPOST run period was selected in a manner that results in a meaningful concentration field. For example, for the CALPUFF model runs that served to characterize the full vessel path, the CALPOST run period (e.g. July 1, hour 16, to July 3, hour 2) was chosen because the vessel enters the modeling area shortly after this start time and leaves the modeling area shortly before this end time. In this way, times when the vessel is not emitting pollutants into the modeling area were minimally represented in the time weighted average. The averages should therefore be interpreted with this in mind.

Results

The positions of the point sources are shown on the following page, with the area that defines vessel activity as either maneuvering or hotelling (Figure 12). Descriptive statistics of the spatial density of the point sources ultimately used in this model are shown in Table 4. The pictorial results of a selected subset of the models that were run are presented in the appendix. Time-weighted averages for the transit-in and transit-out sections of each vessel route are not shown because a problem with the CALPOST software currently prevents the establishment of CALPOST run periods less than 2 hours in duration. When this programming issue is resolved by the creators of CALPUFF, shorter averaging periods may be used to obtain a manageable number of figures to represent the transit of vessels, which will in turn reduce the number of figures needed in future publications.

Section of Vessel Track (n=number of signals)	Max (m)	Average (m)	SD (m)
Transit In (n=202)	560	130	69
Maneuvering In (n=90)	189	63	41
Mooring (n=373)	287	19	35
Maneuvering Out (n=107)	440	46	63
Transit Out (n=126)	1011	206	156

Table 4. The distance (m) between the positions given by consecutive AIS signals indicate that these point sources are spaced reasonably close together, especially compared to the meteorological grid resolution of 1km. The number of signals shown here exceeds the number of sources in the final model because the number of sources for the mooring period was reduced to down to a single source emitting at Harbor Island.

Rather than discuss the precise meaning of each of the 39 figures (see Table 5), it is more parsimonious to explain them in groups. Figures S1, A1, W1, and SP1 are examples of the concentration fields resulting from a CALPUFF run period that encompasses the entire vessel path in one continuous model run. These fields were computed using the smallest practical time step of 1 minute. The concentration fields computed using a smaller time step are basically identical, so the 1-minute time step was clearly adequate to integrate all of the small emission periods given in the PTEMARB.DAT text file. The mooring periods are described with two figures for each season to get the average concentrations and highest ranking concentrations (Figures S2, S3, A1, A2, W2, W3, SP2, and SP3). For one of the 24 CALPUFF projects that was created, the transit out of the Puget Sound starting at Harbor Island during the summer (5-minute time step), a time series is provided to illustrate how the emissions from a vessel can be visualized using the "Selected Days" tab in CALPOST along with the option for "Daily Averaging" (Figures S4-S16). This transit period spanned a two hour meteorological period, so the color-coded mixing heights and wind fields are shown (wind field layer at 240 m) for each hour during this transiting period (Figures SMH-1 and SMH-2). The results of the building downwash test are given in Figures S17 and S18. Figures S19-S23 and W4-W8 provide a visualization of the effect of decreasing the exit temperature of the exhaust in the summer and winter seasons, respectively. To aid in the interpretation of the figures, Appendix C contains figures describing some of the meteorological conditions present during each seasonal model run.

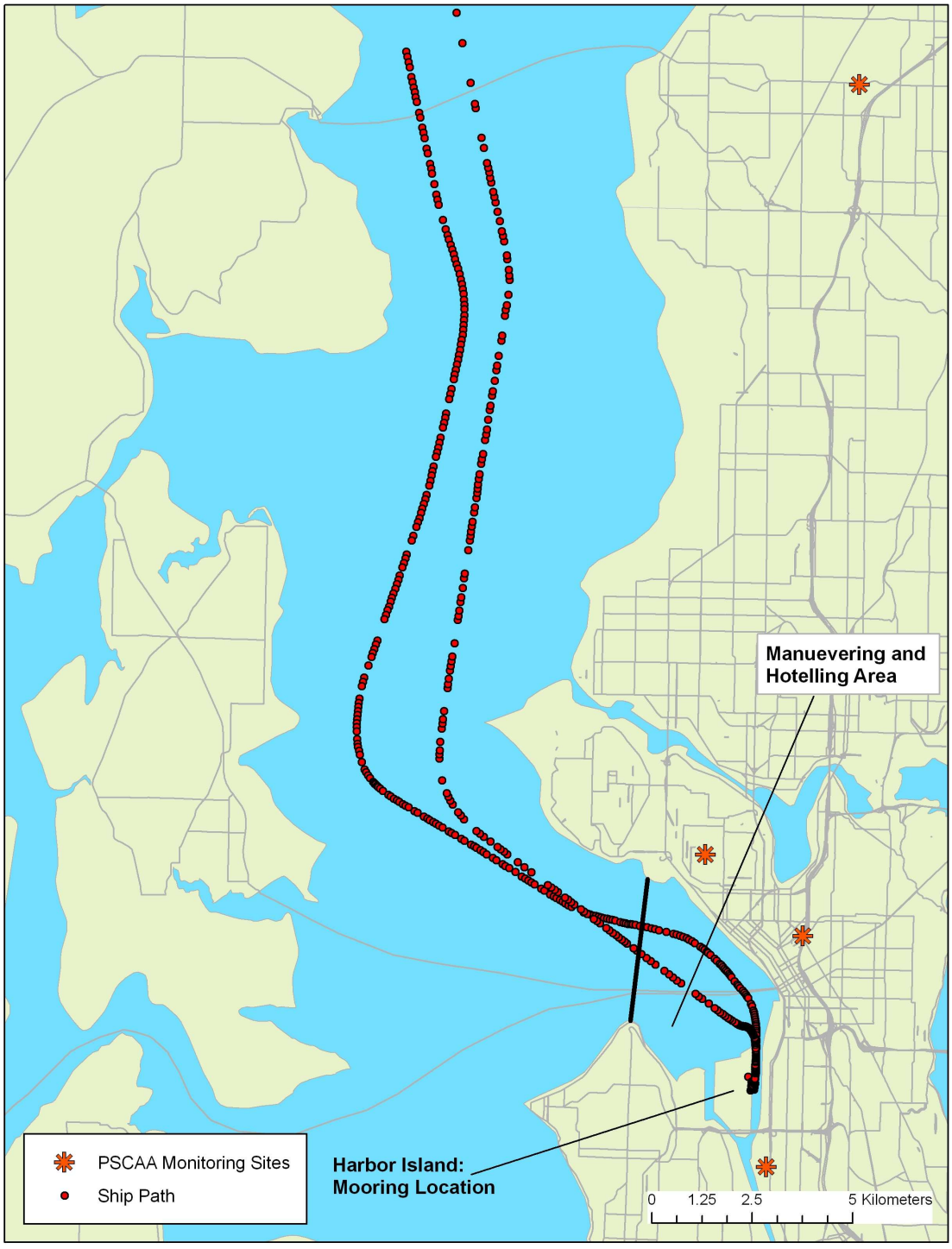

Figure 12. The above map of the Seattle area shows the track of the chosen vessel as derived from the AIS signals that were received. The vessel traveled along the track that is further west for the majority of the section where it is transiting into Harbor Island, and departed along the western route. The vessel was characterized as "maneuvering" when it was not hotelling, but was located east of the dark line drawn across Elliot Bay.

Figure ID	Season	Section of Vessel Track	CALPUFF Time Step	Information given by each Field
S1	Summer	Complete	1 minute	Avg Conc. Over CALPOST run period
S2	Summer	Mooring	15 minutes	Avg Conc. Over CALPOST run period
S3	Summer	Mooring	15 minutes	Highest Ranking 15 minute Conc.
SMH-1	Summer	Transit Out Hour 1	N/A	Mixing Height for hour 1
SMH-2	Summer	Transit Out Hour 2	N/A	Mixing Height for hour 2
S4	Summer	Transit Out Time Series*	5 minutes	**Avg Conc. of 5 previous minutes, 00:20-00:25
S5	Summer	Transit Out Time Series	5 minutes	Avg Conc. of 5 previous minutes, 00:25-00:30
S6	Summer	Transit Out Time Series	5 minutes	Avg Conc. of 5 previous minutes, 00:30-00:35
S7	Summer	Transit Out Time Series	5 minutes	Avg Conc. of 5 previous minutes,00:35-00:40
S8	Summer	Transit Out Time Series	5 minutes	Avg Conc. of 5 previous minutes, 00:40-00:45
S9	Summer	Transit Out Time Series	5 minutes	Avg Conc. of 5 previous minutes, 00:45-00:50
S10	Summer	Transit Out Time Series	5 minutes	Avg Conc. of 5 previous minutes, 00:50-00:55
S11	Summer	Transit Out Time Series	5 minutes	Avg Conc. of 5 previous minutes, 0:55-01:00
S12	Summer	Transit Out Time Series	5 minutes	Avg Conc. of 5 previous minutes, 01:00-01:05
S13	Summer	Transit Out Time Series	5 minutes	Avg Conc. of 5 previous minutes. 01:05-01:10
S14	Summer	Transit Out Time Series	5 minutes	Avg Conc. of 5 previous minutes, 01:10-01:15
S15	Summer	Transit Out Time Series	5 minutes	Avg Conc. of 5 previous minutes,01:15-01:20
S16	Summer	Transit Out Time Series	5 minutes	Avg Conc. of 5 previous minutes, 01:20-01:25
S17	Summer	With Downwash	5 minutes	Avg Conc. Over CALPOST run period
S18	Summer	Without Downwash	5 minutes	Avg Conc. Over CALPOST run period
S19	Summer	Mooring-Exit T (537 K)	5 minutes	Avg Conc. Over CALPOST run period
S20	Summer	Mooring-Exit T (480 K)	5 minutes	Avg Conc. Over CALPOST run period
S21	Summer	Mooring-Exit T (420 K)	5 minutes	Avg Conc. Over CALPOST run period
S22	Summer	Mooring-Exit T (360 K)	5 minutes	Avg Conc. Over CALPOST run period
S23	Summer	Mooring-Exit T (300 K)	5 minutes	Avg Conc. Over CALPOST run period
A1	Autumn	Complete	1 minute	Avg Conc. Over CALPOST run period
A2	Autumn	Mooring	15 minutes	Avg Conc. Over CALPOST run period
A3	Autumn	Mooring	15 minutes	Highest Ranking 15 minute Conc.
W1	Winter	Complete	1 minute	Avg Conc. Over CALPOST run period
W2	Winter	Mooring	15 minutes	Avg Conc. Over CALPOST run period
W3	Winter	Mooring	15 minutes	Highest Ranking 15 minute Conc.
W4	Winter	Mooring-Exit T (537 K)	5 minutes	Avg Conc. Over CALPOST run period
W5	Winter	Mooring-Exit T (480 K)	5 minutes	Avg Conc. Over CALPOST run period
W6	Winter	Mooring-Exit T (420 K)	5 minutes	Avg Conc. Over CALPOST run period
W7	Winter	Mooring-Exit T (360 K)	5 minutes	Avg Conc. Over CALPOST run period
W8	Winter	Mooring-Exit T (300 K)	5 minutes	Avg Conc. Over CALPOST run period
SP1	Spring	Complete	1 minute	Avg Conc. Over CALPOST run period
SP2	Spring	Mooring	15 minutes	Avg Conc. Over CALPOST run period
SP3	Spring	Mooring	15 minutes	Highest Ranking 15 minute Conc.

Table 5. The figures named in the left column are presented on the following pages. They are sorted by season and type. The concentrations (ug/m^3) in each figure one of a few types: the highest ranked concentration obtained for a given receptor (located at ground level at center of each meteorological grid cell) across all time steps in the CALUPFF run, the average concentration across all time steps in the CALPOST run period, or the average concentration at each time step as is shown for the time series. The latter average is computed by the model from the results of *sampling* time steps, which occur more frequently than the *CALPUFF* time step chosen in CALPUFF. The scales on the axes of each figure are given in meters. *The time series was on July 3, 2008.**Each time period is shown as the "beginning hour:minute-end hour:minute" in military time

Discussion

In viewing the figures, it is important to understand their basic limitations and applicability. The vessel track is accurately represented as a series of point sources in so far as this method is a good approximation of a continuously moving point source. As the distance between consecutive point sources increases for any reason, such as when the vessel increases speed while holding the frequency of AIS signals constant, the representativeness of the model decreases for simple mathematical reasons. Additional sources could be added to fill in gaps that are larger than desired, but this step was not performed because the distances seemed adequate considering the meteorological grid resolution in CALMET (1 km grid cells). In the future, a program could be written to add sources where distances exceed a certain threshold value.

One basic limitation of the figures listed in table 4 is that they are derived from only one vessel in an area where hundreds of vessels are active emitting DPM every day. It is therefore more useful to view these figures as demonstrations of the types of outputs that one can obtain from CALPUFF View rather than definitive answers to scientific questions. This does not mean that one cannot be confident in the results in terms of what they represent, but the emission rates used in this model do need to be validated in the future. The method used to obtain these emission rates needs to be refined, as the relationship between vessel speed and load factors is probably much more complicated than was assumed for this project. The vessel-specific characteristics, such as hull shape, extent of fouling, whether or not a vessel is loaded, and many other factors that influence the amount of air, residual, and frictional resistance to travel should be considered in future studies if feasible (MAN B & W Diesel A/S. 1996). Obtaining accurate load factors is probably the most challenging task involved in estimating emission rates.

In this project, the maneuvering activity was approached in a highly simplified manner that was based on the method used in the Puget Sound Inventory and some advice from a Coast Guard official for establishing a general area in which vessels usually receive assistance from tug boats. More research will be required to determine the appropriate load factors for the transition between transit and docking, and vice versa, including the extent to which tug boats are powering the movement of the larger vessel. Propulsion engines are still definitely under power, but the load factor relationship that was applied to transiting periods breaks down completely when tug boats are assisting. There is also the emission of the tug boats themselves to consider, but that is essentially the point where one is moving towards answering more comprehensive scientific questions about the emissions from all vessels in the area. The Puget Sound inventory addresses the emissions of tug boats as well, but because their speed is also not indicative of their load factors, an entirely different approach to estimating their emission rates would be required as

well. One would at least need to know the specific ways that tugs boats approach, attach, and detach from these vessels in order to obtain vessel tracks such as the one constructed for this research project. One could then model each of the ships involved in a large vessel's arrival or departure with separate PTEMARB.DAT text files and then sum the resulting concentration fields from each ship together.

The figures resulting from sensitivity tests of exit temperature (S19-S23, W4-W8) and building downwash (S17-18) provide insight into how accurate these quantities should be prior to entering them into the model. The exit temperature plays an important role in plume rise, so clearly this variable should be chosen with care, although the difference in concentration field does not appear to be as significant as expected until quite low temperatures are reached. The best way to deal with this type of issue is to have an accurate estimate of the true exit temperature of the vessels being modeled. Perhaps agencies that perform source testing would be a good resource for this information in the future.

The difference in the appearance of the concentration fields that were obtained by including or excluding the modeling of building downwash were minimal at longer distances from the source but notable near the source (Figures S17 and S18). Building downwash occurs when the aerodynamic turbulence caused by buildings in close proximity to an elevated point source causes a portion of the pollutants emitted to mix in a downward fashion, which ultimately causes higher concentrations closer to the ground. The E.P.A. considers building downwash to be an important consideration when the distance from the stack tip to the nearest part of the building is less than or equal to 5 times the lesser of the projected building width or building height. The figures indicate that when using the plume rise model enhancements method (PRIME) as the method of modeling downwash, ground level concentrations are increased near the source under these meteorological conditions. Although the EPA still recommends the use of the Industrial Source Complex and SCREEN3 models for receptors in the far wake and near wake, respectively, these models have inherent weaknesses that the PRIME method improves on. A comprehensive comparison of these models can be found elsewhere (Schulman LL et al., 2000). In the future, when the overall approach of modeling vessels is being refined, including building downwash in the model runs is therefore advisable. The modeling time does not appear to be significantly increased by adding this feature to a CALUFF model run.

Looking at the other figures, such as those representing full vessel tracks and mooring periods, the most useful comparisons are within each season, which is the reason the figures are sorted this way. For example, one can see when looking at one season at a time, the variability in concentration at each receptor could be quite high when comparing the highest ranking

concentrations with the run period averages. In many cases, the highest ranking concentrations are approximately an order of magnitude higher than the period averages. Looking across seasons, the meteorological conditions are obviously leading to quite different distributions of particulate matter resulting from the same vessel track. A sophisticated model was not required to show that this would be the case, but it helped illustrate the challenges involved in solving another problem, which is finding the meteorological conditions that lead to pollution spreading to certain areas of interest. It is possible that the simplest way to approach the problem is by first narrowing the time period of interest to a season or month of the year, then finding a set of hours where their geographical area of interest is affected and examining the associated meteorological conditions. The set of CALPUFF projects that were created to view the fate of emissions from mooring activity during all parts of the year are particularly informative for this purpose.

It is often difficult to determine which wind layers are dominating the transport of the pollutant by viewing various CALPOST and CALMET outputs, especially when all the relevant wind field layers are blowing in the same direction. For this, one needs a better understanding of the plume rise algorithms that are functioning behind the scenes in CALPUFF. To describe how these algorithms work in the depth necessary for completeness would be a laborious task and is beyond the scope of this paper. It is worth mentioning that in the CALPUFF model, the general approach for a point source is to apply the Brigg's equations of plume rise due to buoyancy and momentum as described in the CALPUFF user's guide (see page 80) (Scire, Strimaitis, and Yamartino 2000). These deterministic relationships might prove useful in terms of calculating, for each ambient temperature, an expected plume rise at various downwind distances for different wind speeds (at stack height), exhaust exit velocities and exit temperatures. This may not be practical, but it is important to establish some systematic method of determining which wind layers are the most influential in pollutant transport during each season or category of meteorological conditions. Perhaps the method already exists, and needs only to be found in the vast literature on atmospheric dispersion.

In principle, the greater the temperature difference between an emissions' plume and the ambient environment, the higher the plume will rise in the atmosphere. The mixing height and adiabatic lapse rate are also important variables to consider for estimating plume rise. One can view hourly maps of mixing heights (e.g. Figures SMH-1 and SMH-2) and temperatures at each elevation in the CALMET meteorological grid if desired. These items along with several other meteorological variables can also be printed out in table form for each hour using the postprocessor PRTMET.exe (Earth Tech, 2006). In any case, it is clear that wind roses produced from surface stations do not typically provide adequate information for predicting

whether a plume will affect specific areas. Time resolved upper air wind fields are needed for this purpose. In the absence of MM5 modeled data for the time period of interest, however, alternative approaches will be needed to visualize these wind fields.

Conclusion

In the future, several practical issues with completing this type of modeling project would need to be addressed. There are several steps required to construct the PTEMARB.DAT text tile starting from AIS signals, and these are described in the methods section of this report. Many opportunities exist for automation of these steps with simple computer programs. First, the management of information that occurs prior to running a model could be refined so that more vessels could be chosen in less time. The data reduction steps that occur between receiving AIS signals from all over the Puget Sound and obtaining chronological signals from specific vessels could be further programmed. Essentially, one must remove signals coming from outside the area of interest, variables (i.e. columns) other than those contained in Table 2, and signals associated with vessels that one is not intending to model.

The data transformations and calculations to obtain information needed to complete the text file required for CALPUFF were done in Excel for this project, but it would be more efficient to set up an equivalent routine in a more sophisticated programming environment such as MATLAB. Altering the meteorology is rather laborious at this stage, but a competent programmer could make this process much easier by enabling the manipulation of dates within completed PTEMARB.DAT text files. The current method, which is less preferable, is outlined in Procedure B of Appendix B at the end of this report.

Once the text files needed to run CALPUFF are completed, additional information management steps are required in order to complete vessel tracks that are represented by more than 100 point sources. This process in outlined in Procedure A (Appendix B), and also presents some opportunities for programming. First, before more vessel modeling projects are done, the version of CALPUFF that accepts 200 sources rather than 100 should be downloaded from the TRC website and entered in the executables folder of CALPUFF View. Secondly, the repetitive process of summing together CALPUFF output files would take much less time if some of copying, pasting, creating of new folders, renaming binary output files et cetera, were programmed to occur automatically after each CALPUFF run.

In summary, the estimation of emission rates may require some refinement by competent individuals in the field of ship propulsion. Automation of many of the steps required to model a complete vessel track will enable future researchers to complete several vessel tracks in a short period of time, which will diversify the types of scientific questions that can be addressed using

this method. The resulting concentration fields can be exported as shape files or other file types that can be further analyzed with GIS or statistical software. Associations could then be drawn between the distribution of DPM concentrations and the distribution of populations of interest, leading to a better understanding of human exposures to DPM. Upon future validation with LIDAR measurements and subsequent adjustment of emission rates, this modeling approach will contribute to the production of useful scientific data; this will then inform health officials, policy makers and others as to the potential health impacts resulting from marine vessel activity.

References

Aldrete, Guiselle, Bruce Anderson, Joyce Kristiansson, Joseph Ray, and Sam Wells. 2007. *Puget sound maritime air emissions inventory.*

Desantes, J. M., V. Bermudez, J. M. Garcia, and E. Fuentes. 2005. Effects of current engine strategies on the exhaust aerosol particle size distribution from a heavy-duty diesel engine. *Journal of Aerosol Science*. 36, (10): 1251-76.

Earth Tech, Inc. 2006. *Development of the next generation air quality models for outer continental shelf (OCS) applications, final report: Volume 3 calpuff user's guide.* , http://www.src.com/calpuff/download/MMS_Files/MMS2006_Volume3_CALPUFF_Postprocessors.pdf (accessed March 1, 2009).

EPA. United states. environmental protection agency. office of transportation and air quality. assessment and standards division.; atmospheric & environmental research,inc. modeling sulfur oxides (SOx) emissions transport from ships at sea. in U.S. Environmental Protection Agency, Office of Transportation and Air Quality [database online]. [Washington, D.C.], 2008.

Hesterberg TW, Bunn WB 3rd, Chase GR, Valberg PA, Slavin TJ, Lapin CA, and Hart GA. 2006. A critical assessment of studies on the carcinogenic potential of diesel exhaust. *Critical Reviews in Toxicology* 36, (9): 727-76.

Himes, Katerine, and Mike Gilroy. 2007. *Evaluation of methods for air toxics source apportionment using real-time continuous monitoring instrument*s. Research Proposal ed.

Keill, Leslie, and Naydene Maykut. 2003. *Final report: Puget sound air toxics evaluation.* , http://www.pscleanair.org/airq/basics/psate_final.pdf (accessed January 10, 2009).

Kim, E., and P. K. Hopke. 2008. Source characterization of ambient fine particles at multiple sites in the seattle area. *Atmospheric Environmen*t 42, (24): 6047-56.

Kim, E., P. K. Hopke, T. V. Larson, N. N. Maykut, and J. Lewtas. 2004. Factor analysis of seattle fine particles. *AEROSOL SCIENCE AND TECHNOLOG*Y 38, (7): 724-38.

Larson, Timothy. 2006. *Estimates of $PM_{2.5}$ source contributions in seattle, WA: A comparison of receptor model predictions using both IMPROVE and enhanced STN data sets" prepared for EPA national environmental research labs contract # U2C619 QT-RT-04001775, october 2005.*

Larson, T. V., D. S. Covert, E. Kim, R. Elleman, A. B. Schreuder, and T. Lumley. 2006. Combining size distribution and chemical species measurements into a multivariate receptor model of PM2~.~5~ (DOI 10.1029/2005JD006285). *Journal of Geophysical Research*. 111, (D10): D10S09.

MAN B & W Diesel A/S. 1996. *Basic principles of ship propulsio*n. Copenhagen: MAN B&W Diesel.

Maykut NN, Lewtas J, Kim E, and Larson TV. 2003. Source apportionment of PM2.5 at an urban IMPROVE site in seattle, washington. *Environmental Science & Technology* 37, (22): 5135-42.

Moldanova, Jana, Erik Fridell, Olga Popovicheva, Benjamin Demirdjian, Victoria Tishkova, Alessandro Faccinetto, and Cristian Focsa. 2009. Characterisation of particulate matter and gaseous emissions from a large ship diesel engine. *Atmospheric Environment*. 43, (16): 2632.

Ramachandran, Gurumurthy. 2005. *Occupational exposure assessment for air contaminants*. Boca Raton: Taylor & Francis.

Schulman LL, Strimaitis DG, and Scire JS. 2000. Development and evaluation of the PRIME plume rise and building downwash model. *Journal of the Air & Waste Management Association (1995)* 50, (3): 378-90.

Scire, J. S., D. G. Strimaitis, and R. J. Yamartino. 2000. *A User's guide for the CALPUFF dispersion model (version 5.0)*Earth Teach, Inc.

United States. 1995. *Environmental protection agency. emissions, monitoring,and analysis division. A user's guide for the CALMET meteorological mode*l. Research Triangle Park, NC: U.S. Environmental Protection Agency, Emissions, Monitoring and Analysis Division.

Wichmann, H. E. 2007. Diesel exhaust particles. *Inhalation Toxicolog*y 19, : 241-4.

Wu, Chang-fu, Timothy V. Larson, Szu-ying Wu, John Williamson, Hal H. Westberg, and L-J Sally Liu. 2007. Source apportionment of PM2.5 and selected hazardous air pollutants in seattle. *The Science of the Total Environment*. 386, (1): 42.

Appendix B

Procedure A

1) With PTEMARB.DAT text files completely prepared for input into CALPUFF, and CALMET already having been run, use the option for external source file to retrieve the first PTEMARB.DAT file. In the external source file window, make sure that the number of point sources in the file (presumably 100 sources as this is the current limit) matches the number shown in the field on the right next to "No. of Point Sources in File."
2) Run the CALPUFF model, and exit out of any windows that appear. In the current project's folder, copy the three binary output files Conc.dat, wflx.dat, and dflx.dat into a new folder where results from all runs will later be summed together using the postprocessor calsum.exe.
3) Repeat steps 1 and 2 for PTEMARB.DAT text file until you have the three binary output files from all your runs inside the new folder under new names; each time you copy the three files into the new folder, rename them as conc00n.dat, wflx00n.dat, dflx00n.dat where n is the number of times you have copied the three files into this folder. For this first time, the names will thus be conc001.dat, wflx001.dat, anddflx001.dat. This will ease the process of summing them together later.
4) In order to sum all these files together, the summation must be done separately for each type of file (Conc.dat, dflx.dat, and wflx.dat) (Earth Tech, 2006). Once the final set of three files resulting from the summation is available, copy them into the same folder as the project file that is being worked on (e.g. projectname.cpv), and make sure that the three old binary files that may be present in that same folder are removed. This way, you can run CALPOST and it will read in the summed files rather than any old files. In order for CALPOST to read them, they must be named conc.dat, dflx.dat, and wflx.dat.
5) Run CALPOST with the settings that are appropriate for your scientific question. To get a picture of the output down to the level of the CALPUFF time step, i.e. 1 minute concentration averages when a 1 minute time step was used in CALPUFF, go to the selected days tab of the CALPOST user interface, select days that you want these averages for, and use the daily averaging period option to select the pollutant species. This creates many files, so make sure and limit the time period to what you need.

Changing the Weather Conditions for a Vessel Track

Altering the weather conditions to which an emissions plume is exposed requires that a project contain the associated weather conditions (i.e. the time period modeled in CALMET), so one may have to create a new project depending on whether that is true. Currently, the more time consuming task is changing the emissions period, and hence the days or hours listed in the PTEMARB.DAT text files so that they fit the meteorology in a desired manner. The process takes longer than it could because many numbers must be changed, and the current method is to open the excel file that was used to generate the text file and alter the days and hours in their respective columns. Then the same procedure to produce a text file must be repeated. The general process is currently given in the following steps:

1) Determine the desired weather period and ideal start time for the emission period in terms of the Julian day of the year (0-366) and hour (0-23).
2) Alter the dates and/or times in the columns of the excel worksheets that contain the vessel tracks in the format exemplified in Table 3 of this report.
3) Complete procedure B.

Procedure B

1) Save the Excel Worksheet in the format shown in Table 3 of this report as a tab delimited text file in at least two locations on the computer, one of which should be the same location batch files used in the next steps.
2) Using the Start menu, go to “Run…” and type "cmd" on the line and press enter. Use the command line to open the directory where the saved tab delimited text file and the software that alters are both located.
3) On the command line, type shred.bat, hit the space key, and enter the name of the tab delimited text file that you saved in that directory in step 1. This batch file, shred.bat, will then cut the text file into smaller text files. They must be shredded in this way because the model will only accept 100 sources at a time. A different version of CALPUFF from TRC will accept 200 sources, so at some point this new model should be downloaded from the TRC website. That would mean the shred.bat file would need to be changed to accommodate 200 rather than 100 sources.
4) Now that the shred.bat file has produced a number of text files in the directory, drag each one of them, one at a time, onto the batch file prepdat.bat, which should also be in the same directory. This takes the shredded files and formats each one of them to be ready for input into CALPUFF. In each file produced however, at the top of the file, the start

date and end date of the emission file must be adjusted to make sure they are where they should be. In adjusting these items, you must then adjust the start time and end time in the time variant portion of the text file so that these times match the times at the top of the file. Otherwise, the file will not run successfully. Save these files somewhere in the CALPUFF project folder under a descriptive name.

5) Use these files to complete Procedure A.

Appendix A: Figures Illustrating Selected Results of Concentration Fields

Figure ID	CALPOST Run Period Begins	CALPOST Run Period Ends
S1	July 1, hour 16	July 3, hour 2

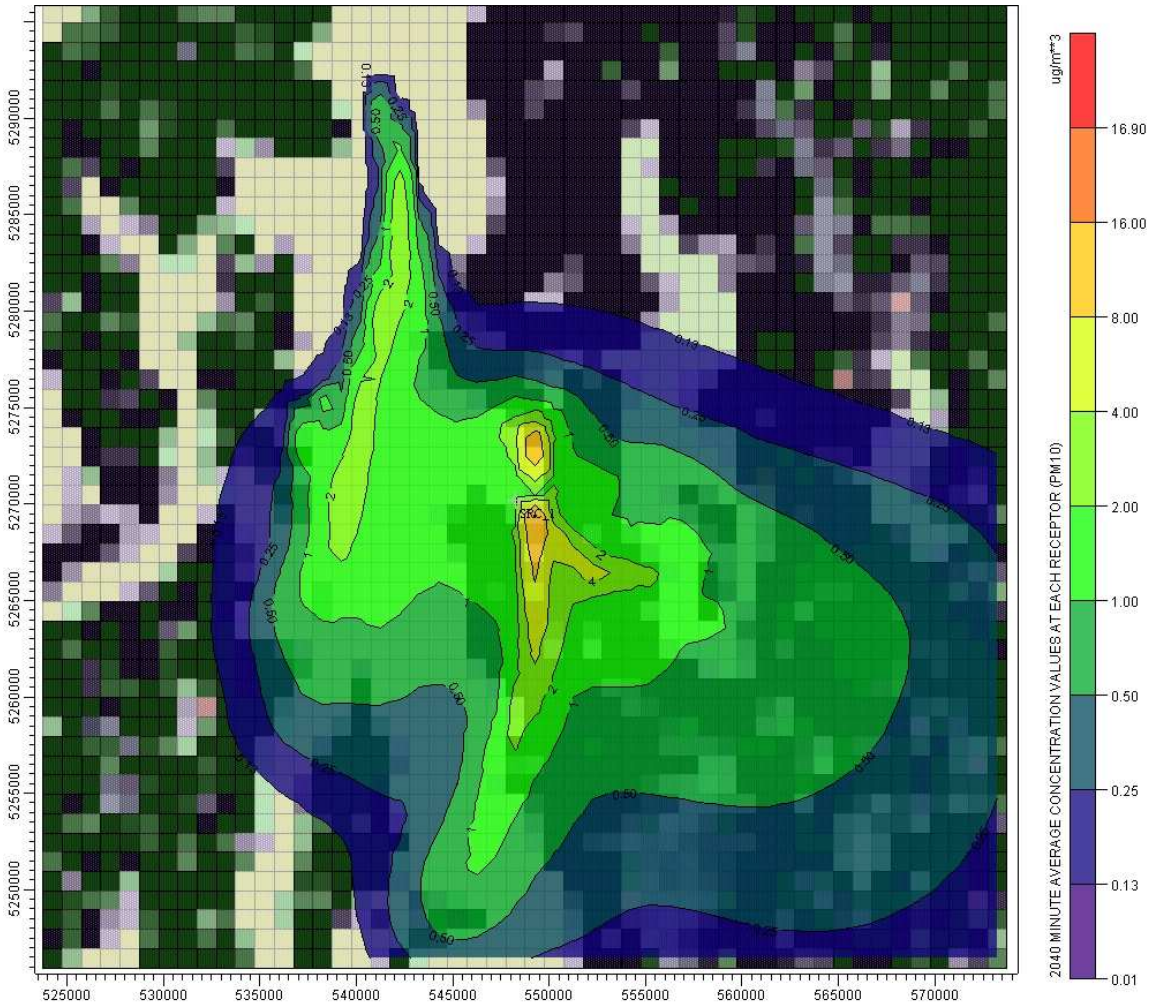

Figure ID	CALPOST Run Period Begins	CALPOST Run Period Ends
S2	July 1, hour 18	July 3, hour 0

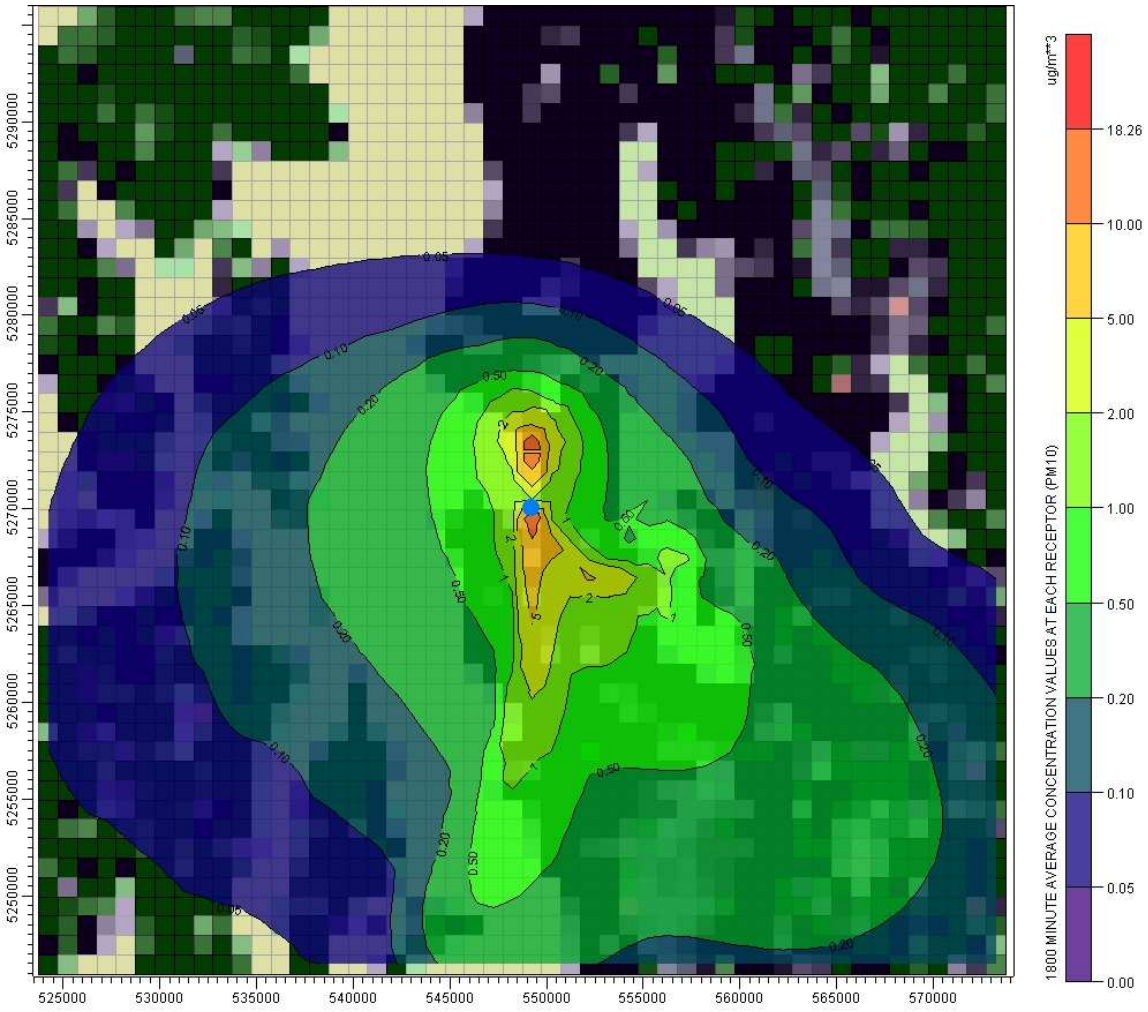

Figure ID	CALPOST Run Period Begins	CALPOST Run Period Ends
S3	July 1, hour 18	July 3, hour 0

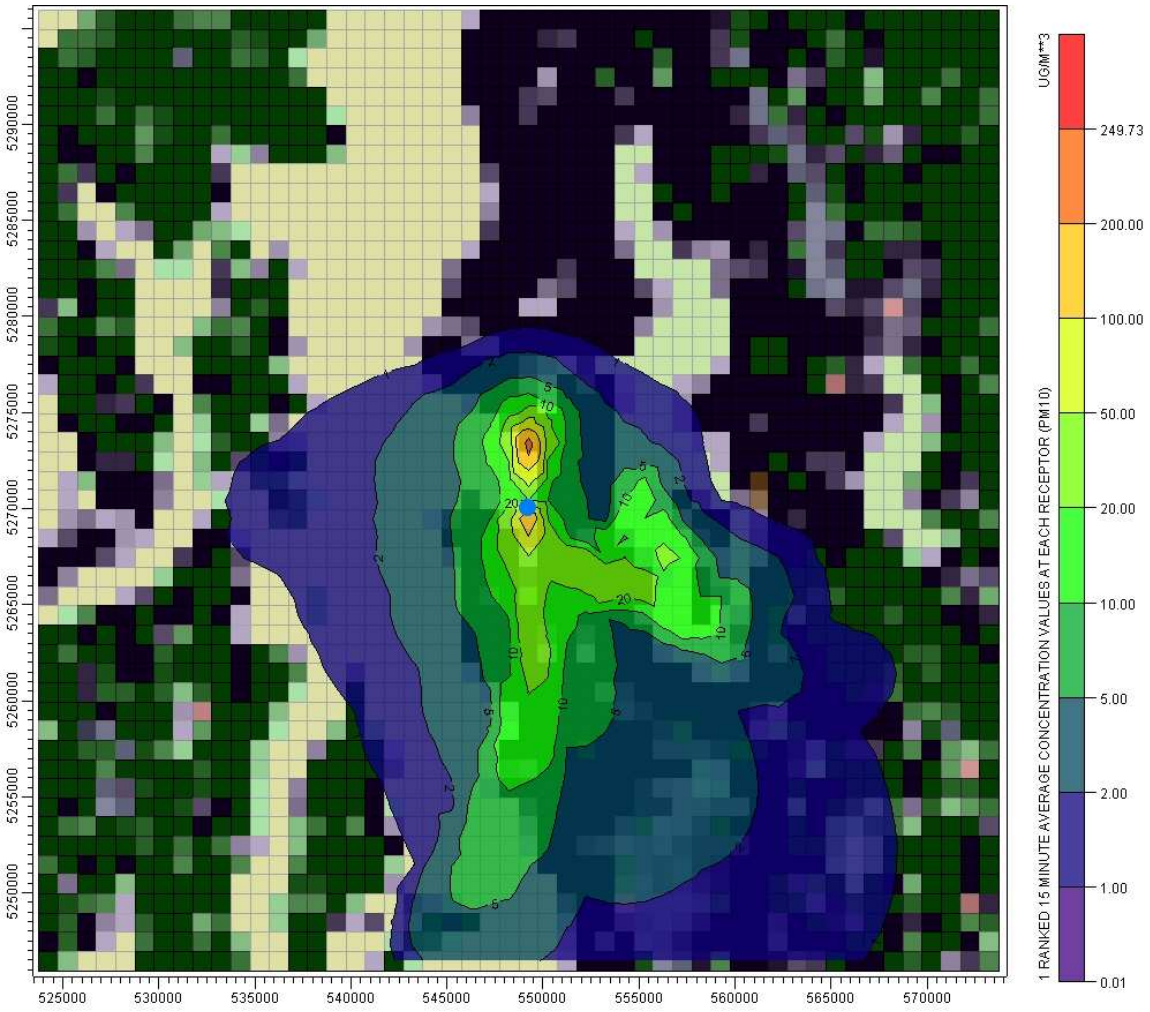

Figure ID	CALPOST Run Period Begins	CALPOST Run Period Ends
SMH-1	July,3 hour 0	

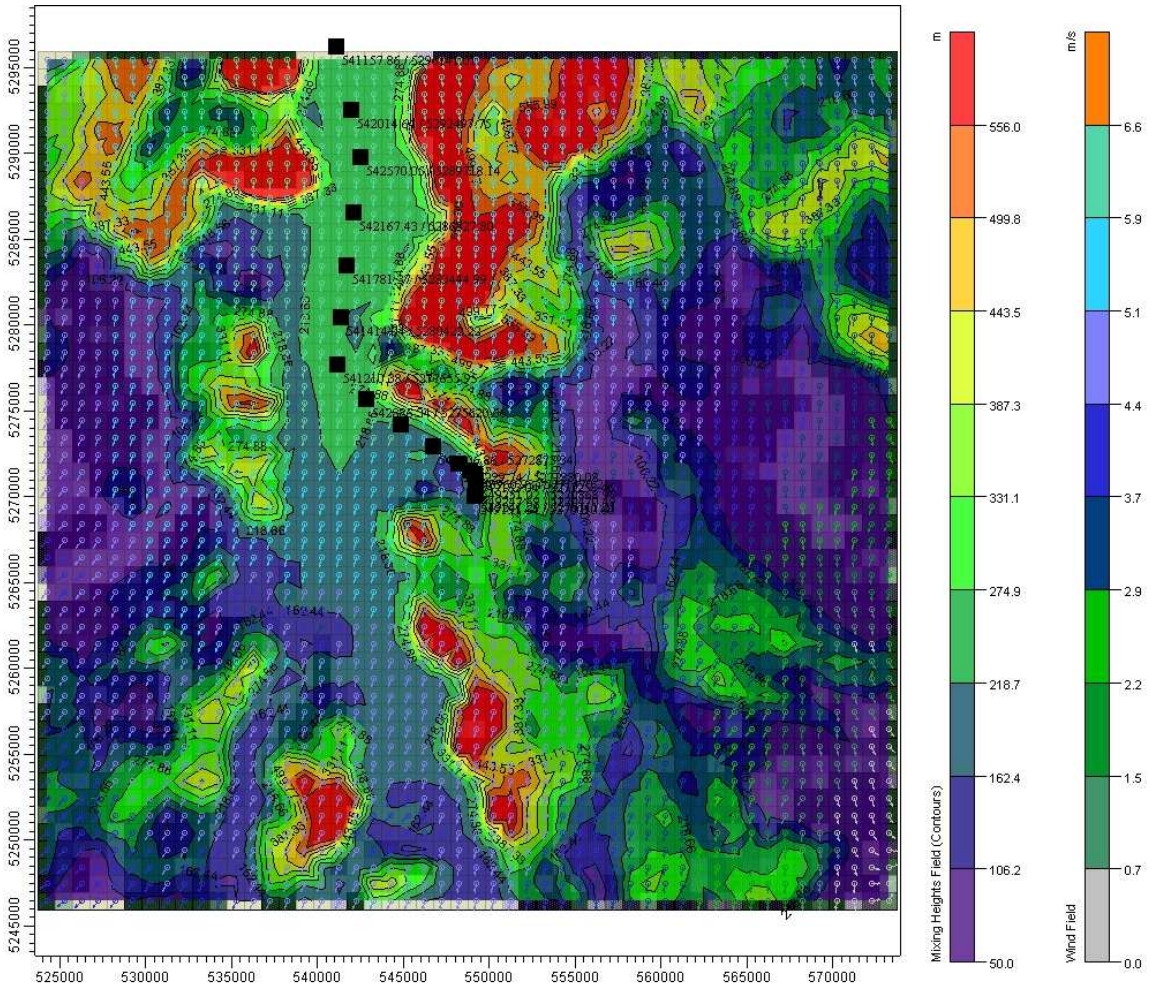

Figure ID	CALPOST Run Period Begins	CALPOST Run Period Ends
SMH-2	July 3, hour 1	

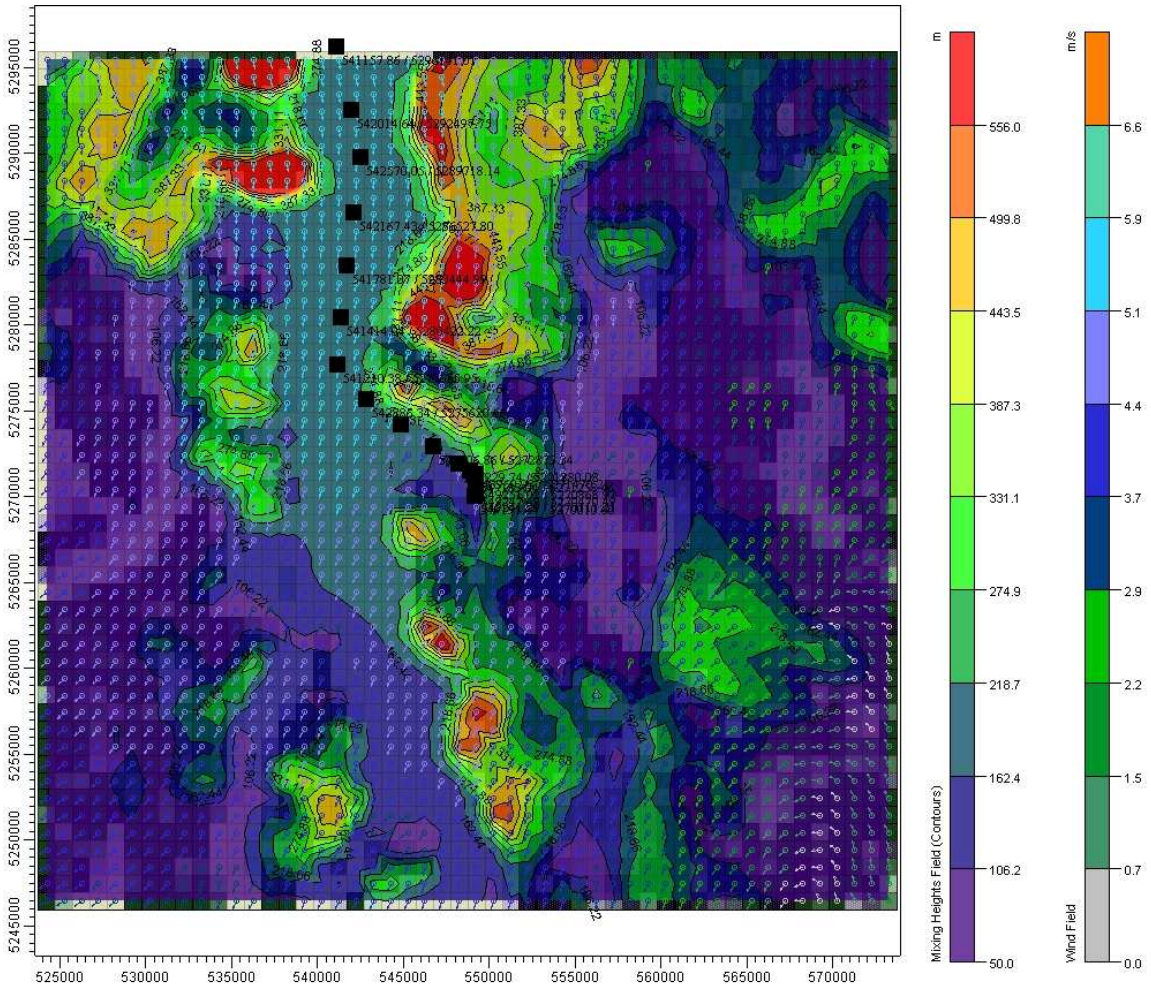

Figure ID	CALPOST Run Period Begins	CALPOST Run Period Ends
S4	July 1, hour 16	July 3, hour 2

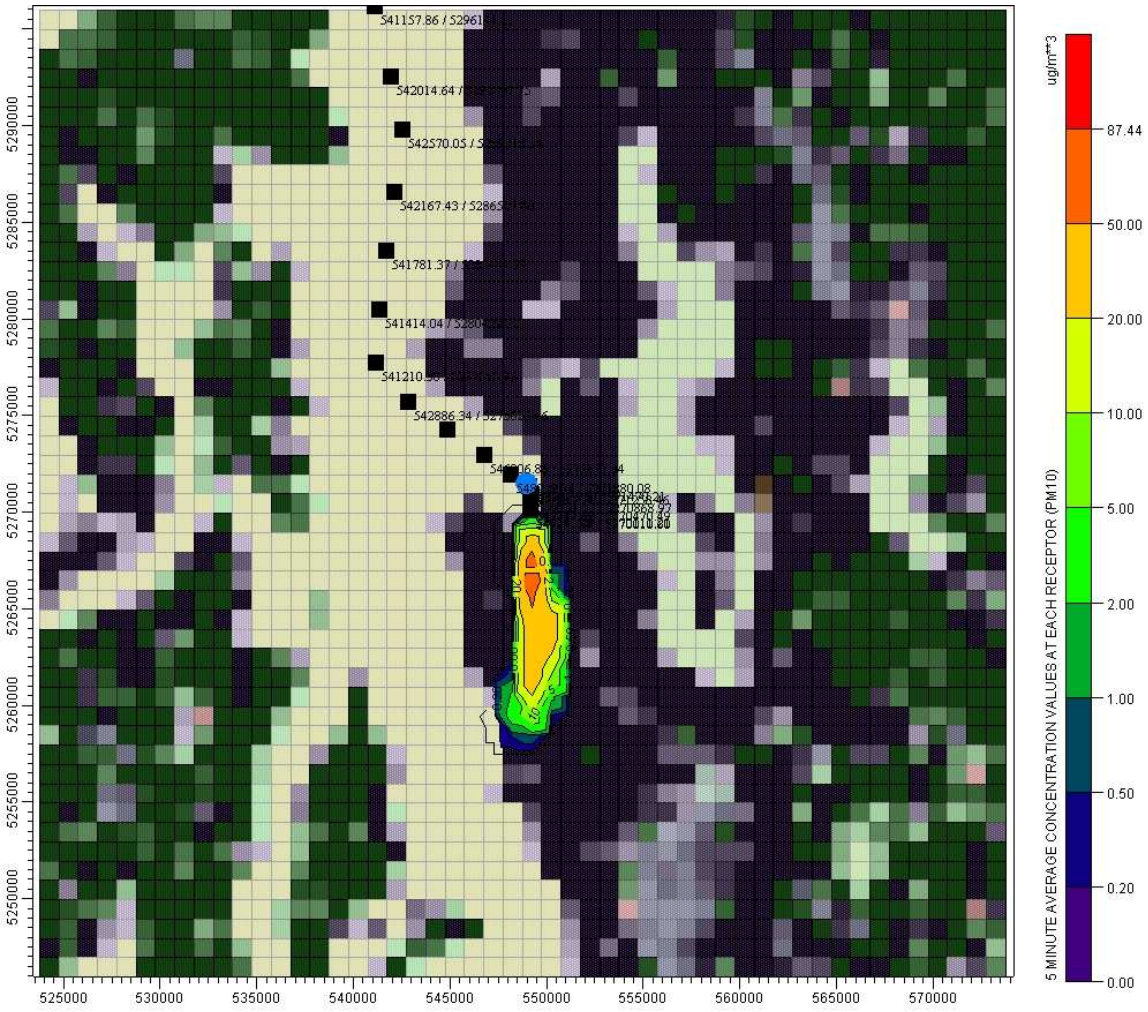

Figure ID	CALPOST Run Period Begins	CALPOST Run Period Ends
S5	July 1, hour 16	July 3, hour 2

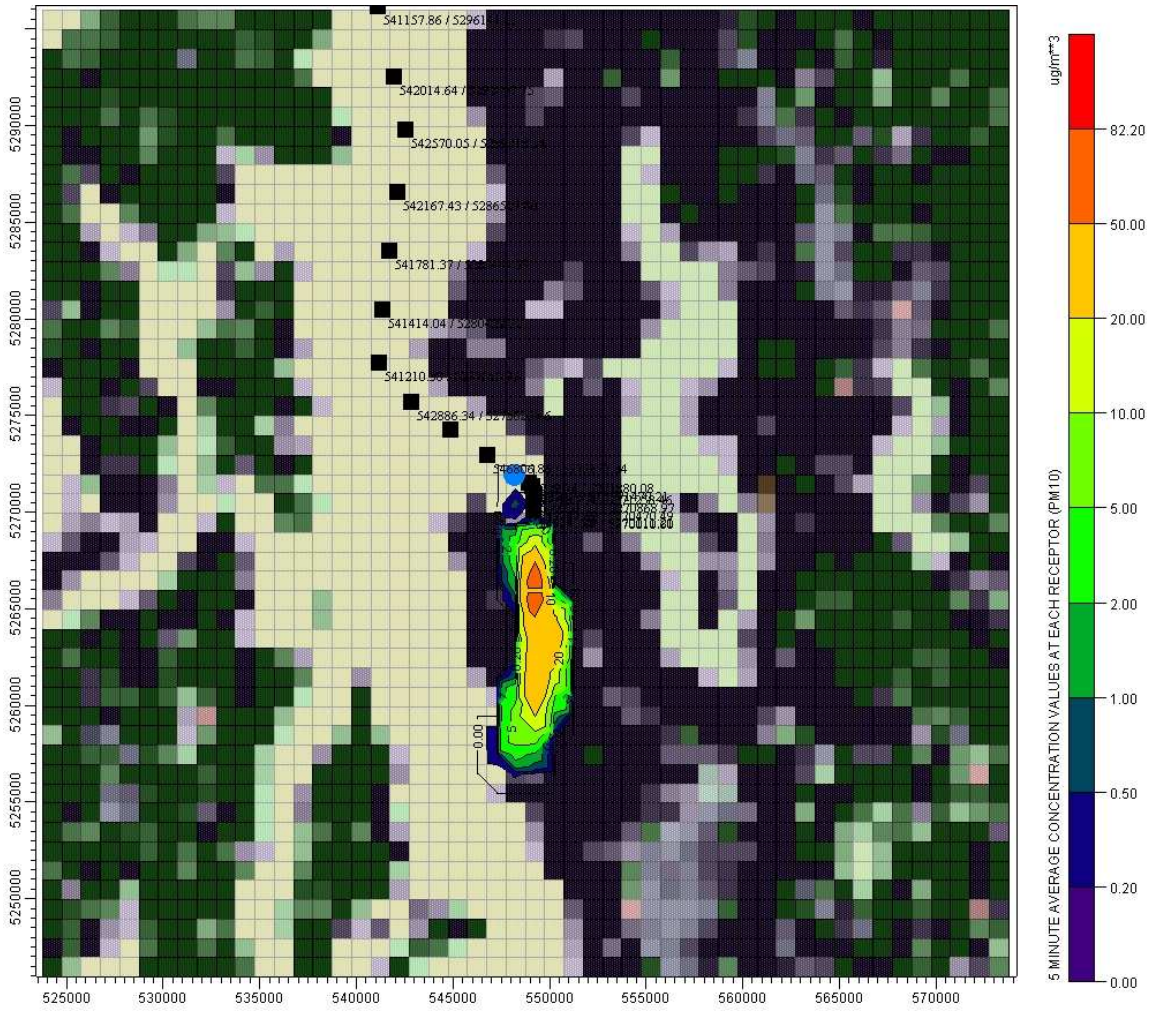

Figure ID	CALPOST Run Period Begins	CALPOST Run Period Ends
S6	July 1, hour 16	July 3, hour 2

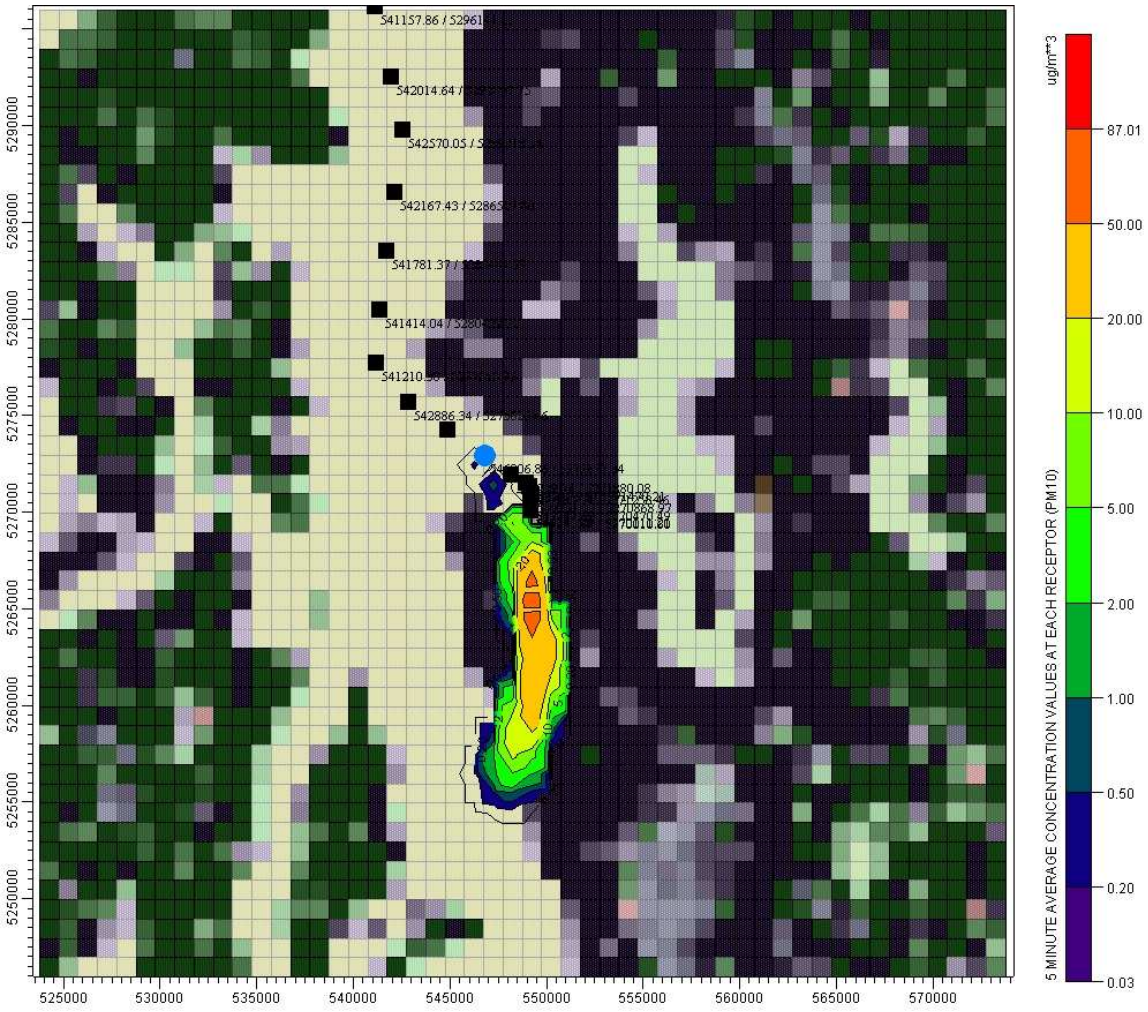

Figure ID	CALPOST Run Period Begins	CALPOST Run Period Ends
S7	July 1, hour 16	July 3, hour 2

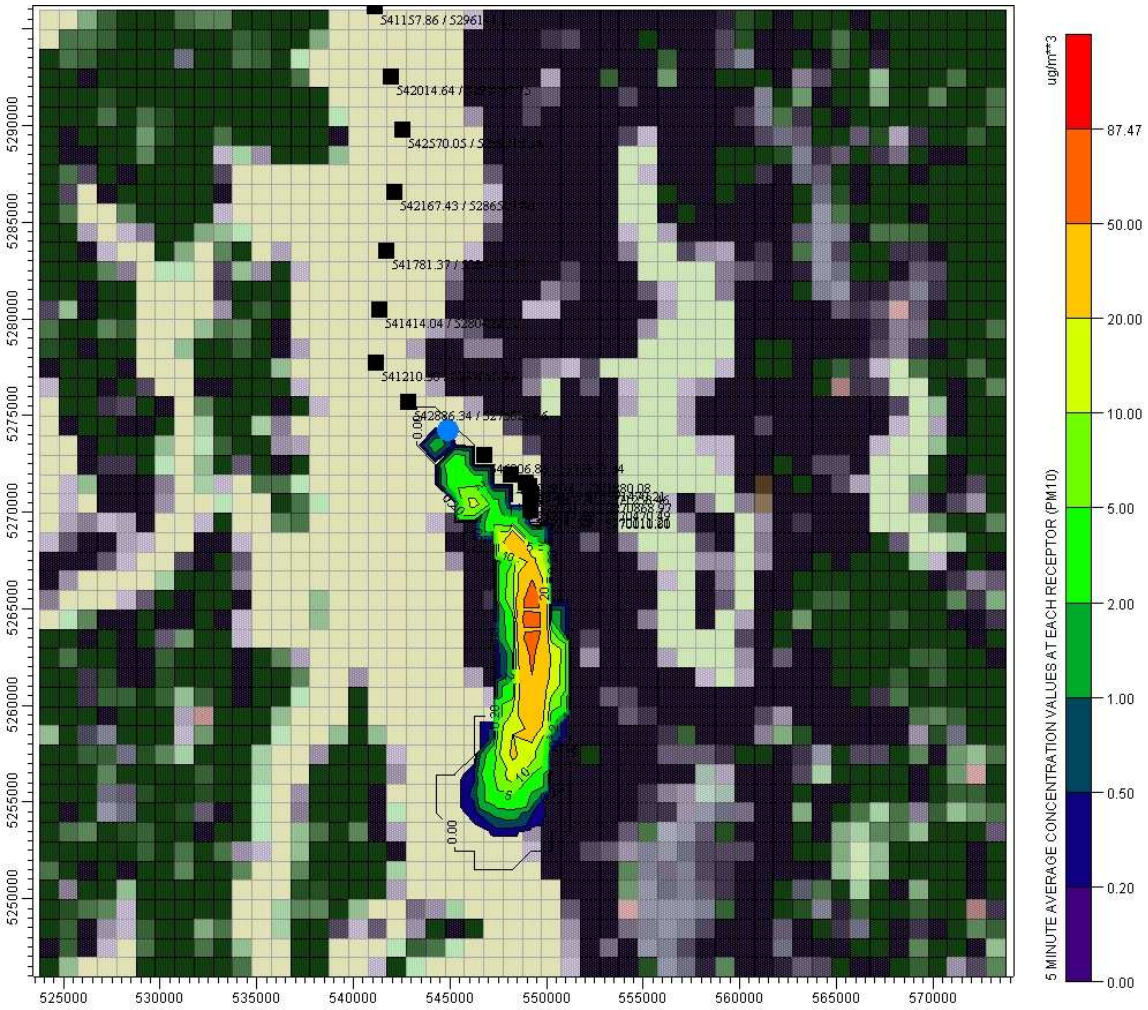

Figure ID	CALPOST Run Period Begins	CALPOST Run Period Ends
S8	July 1, hour 16	July 3, hour 2

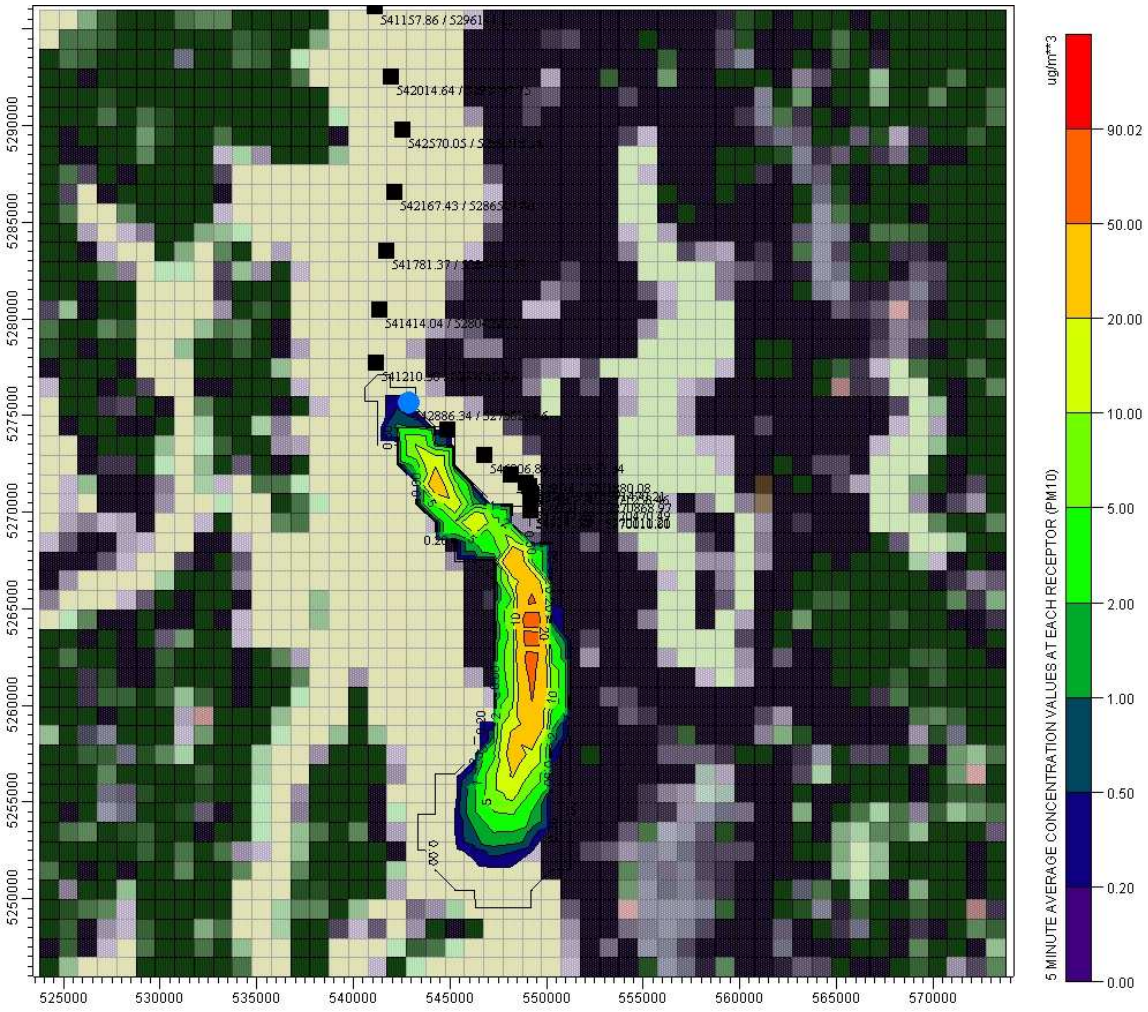

Figure ID	CALPOST Run Period Begins	CALPOST Run Period Ends
S9	July 1, hour 16	July 3, hour 2

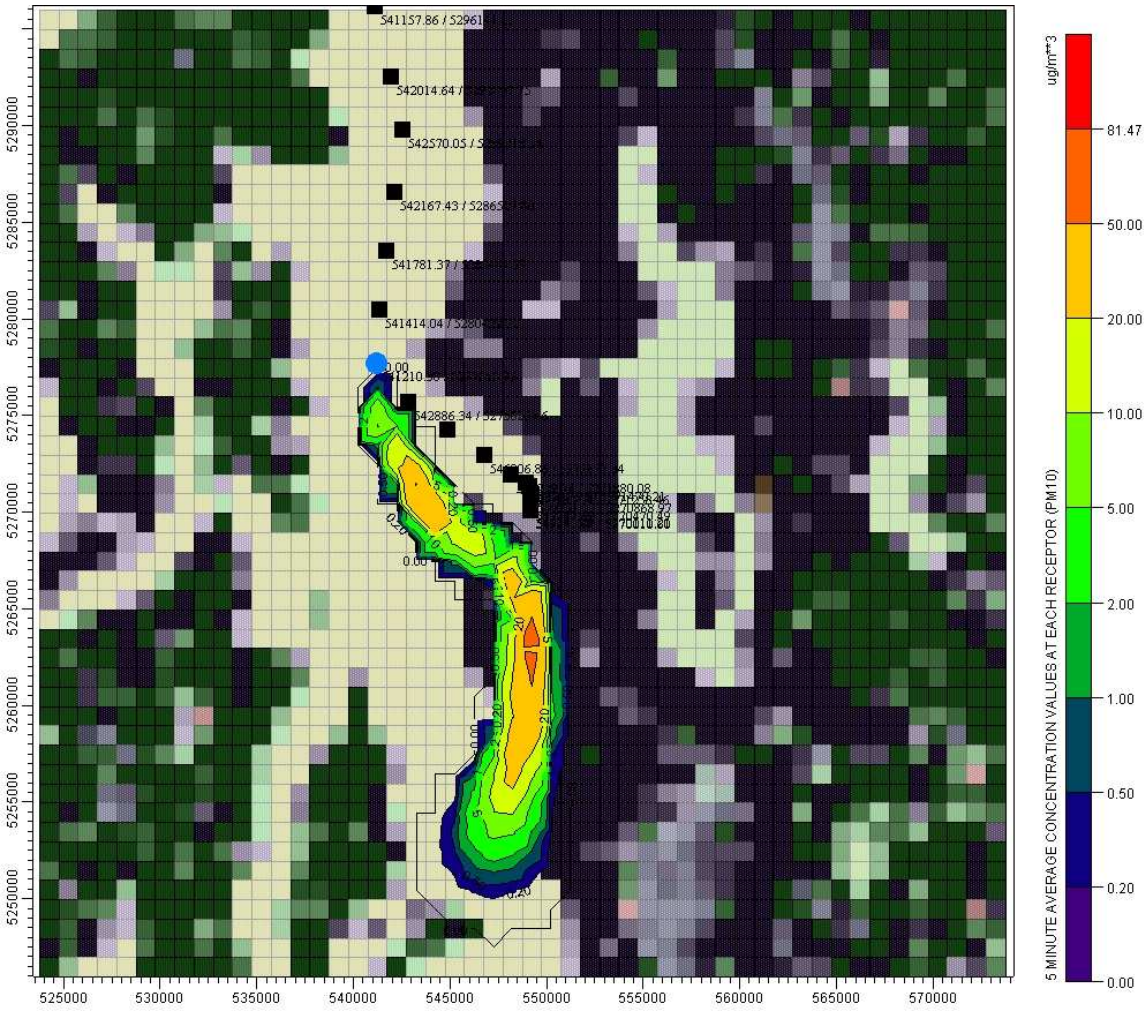

Figure ID	CALPOST Run Period Begins	CALPOST Run Period Ends
S10	July 1, hour 16	July 3, hour 2

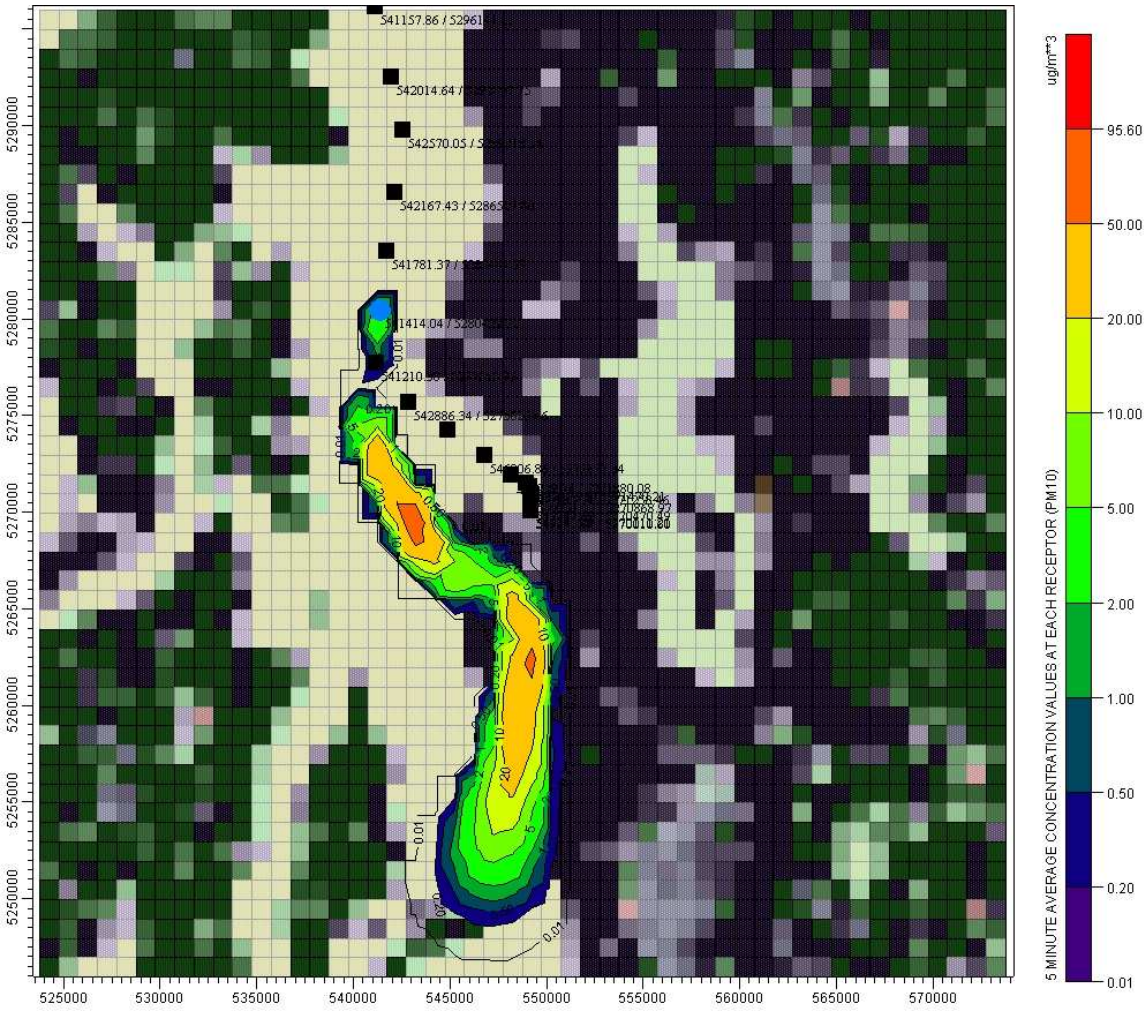

Figure ID	CALPOST Run Period Begins	CALPOST Run Period Ends
S11	July 1, hour 16	July 3, hour 2

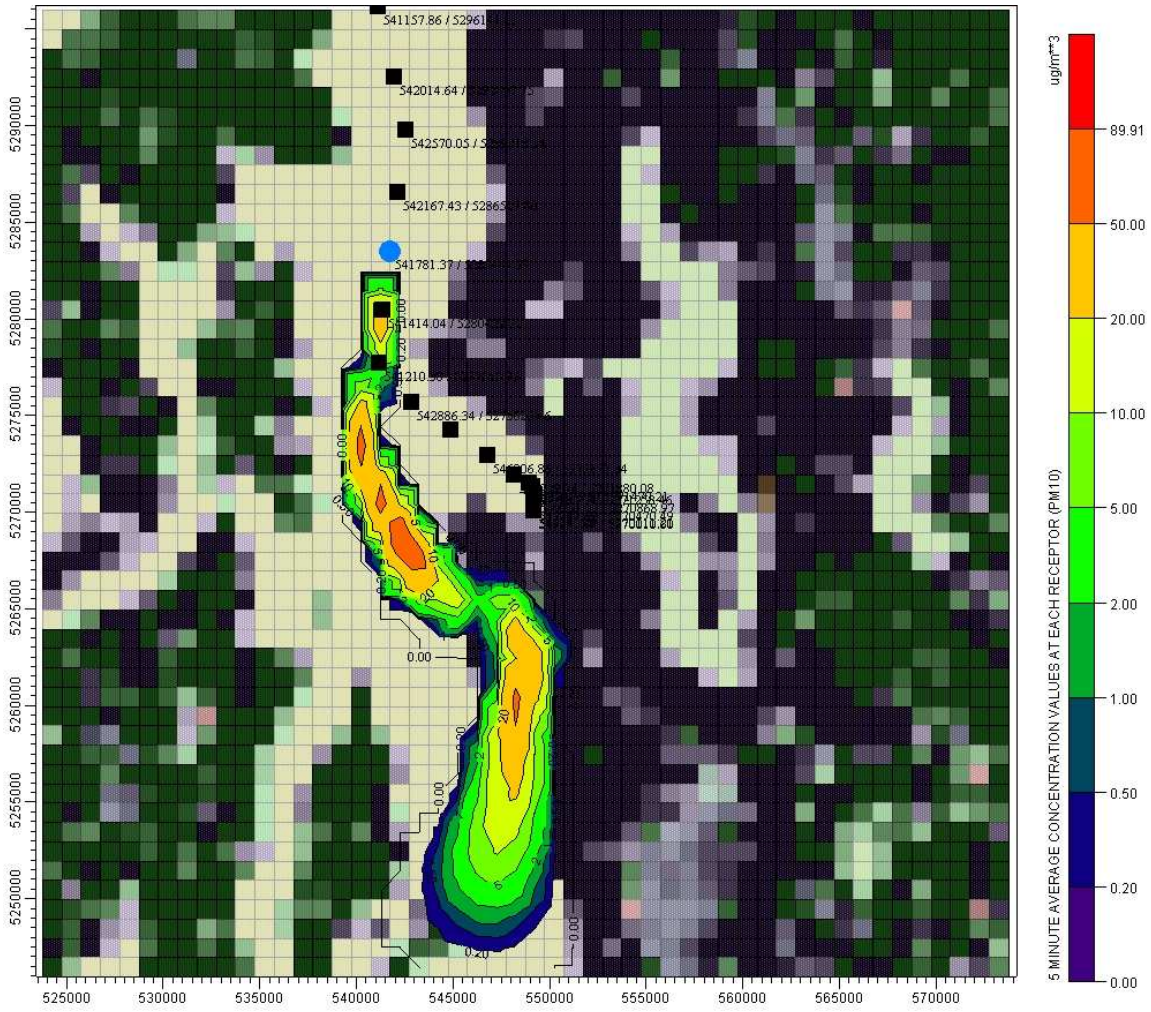

Figure ID	CALPOST Run Period Begins	CALPOST Run Period Ends
S12	July 1, hour 16	July 3, hour 2

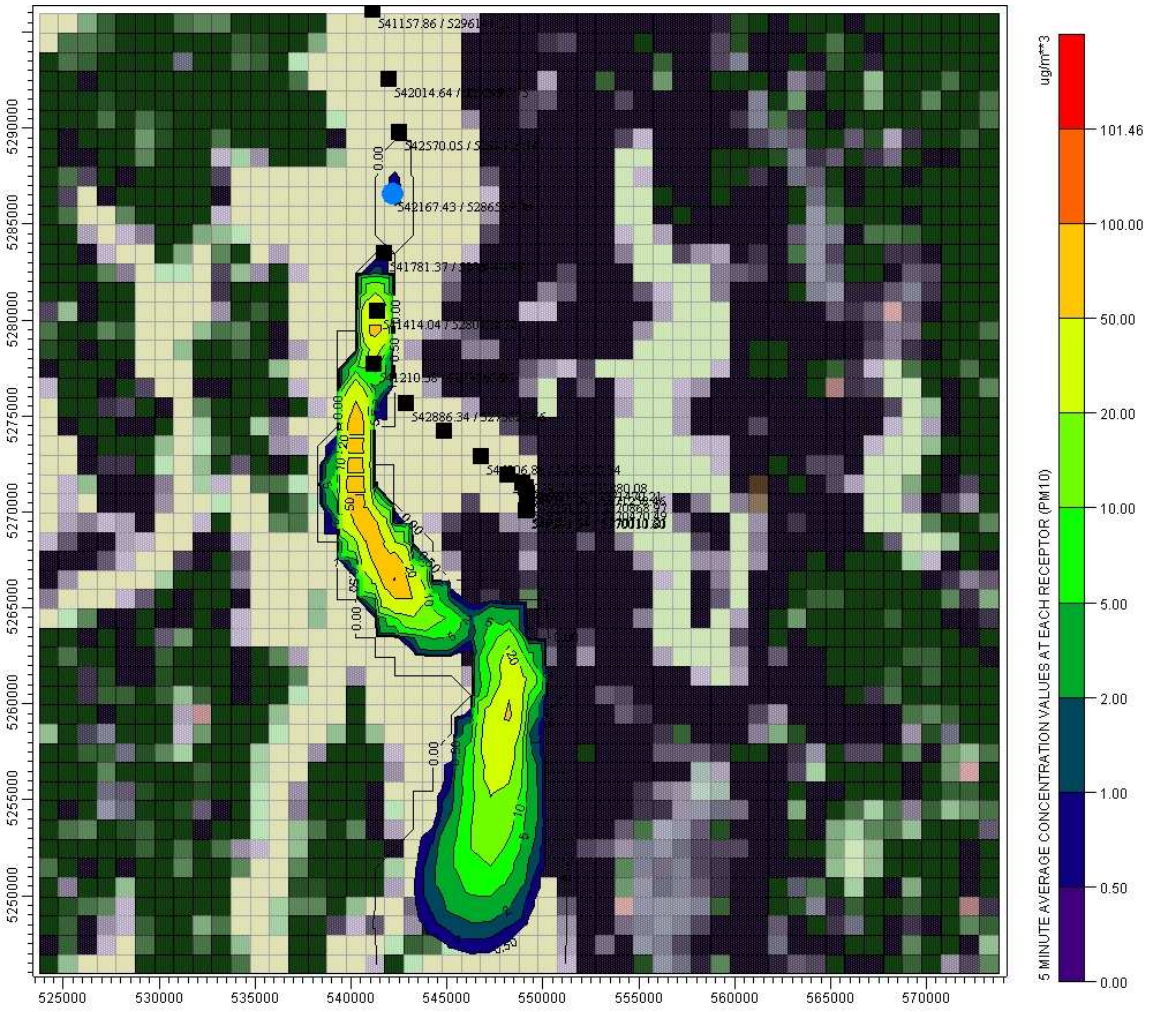

Figure ID	CALPOST Run Period Begins	CALPOST Run Period Ends
S13	July 1, hour 16	July 3, hour 2

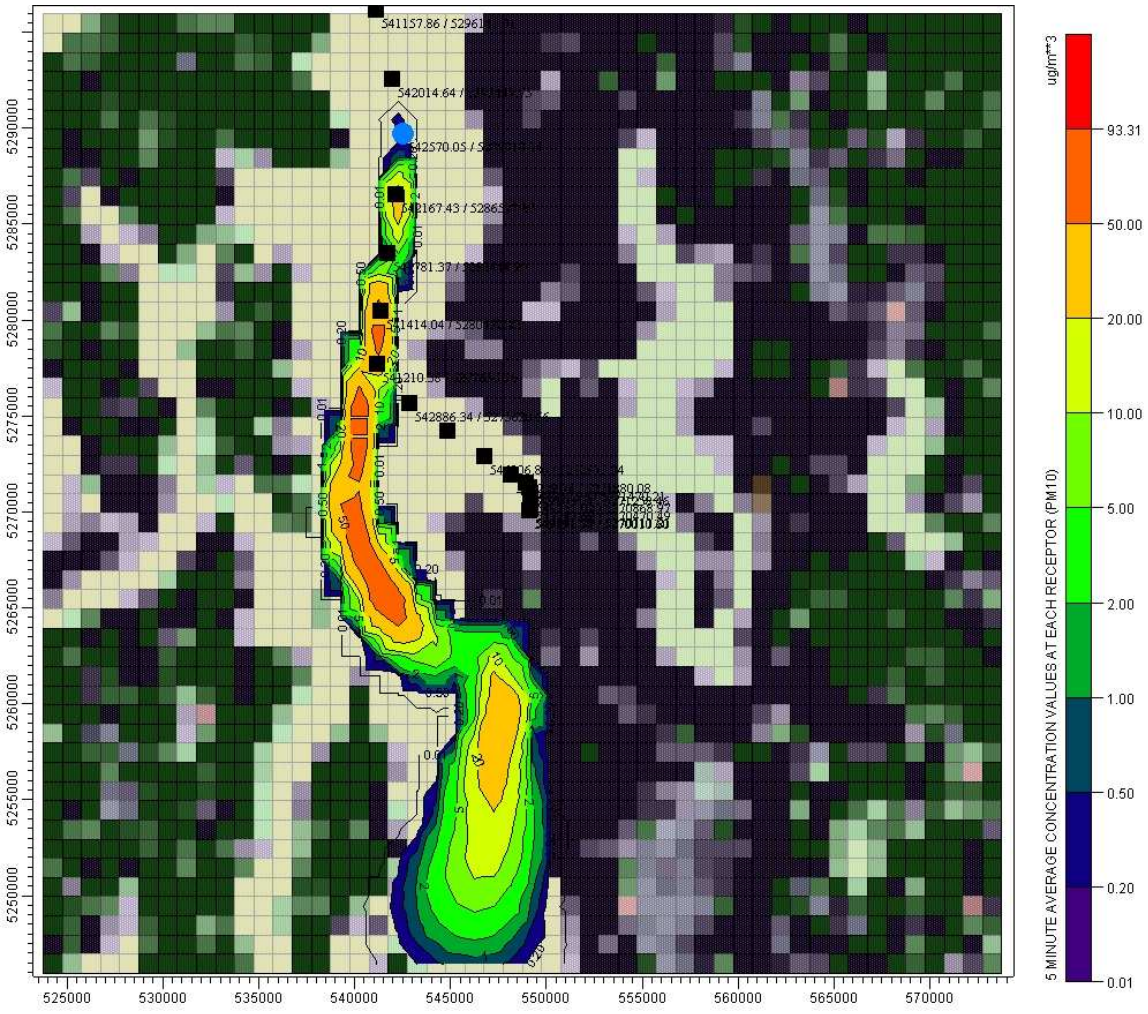

Figure ID	CALPOST Run Period Begins	CALPOST Run Period Ends
S14	July 1, hour 16	July 3, hour 2

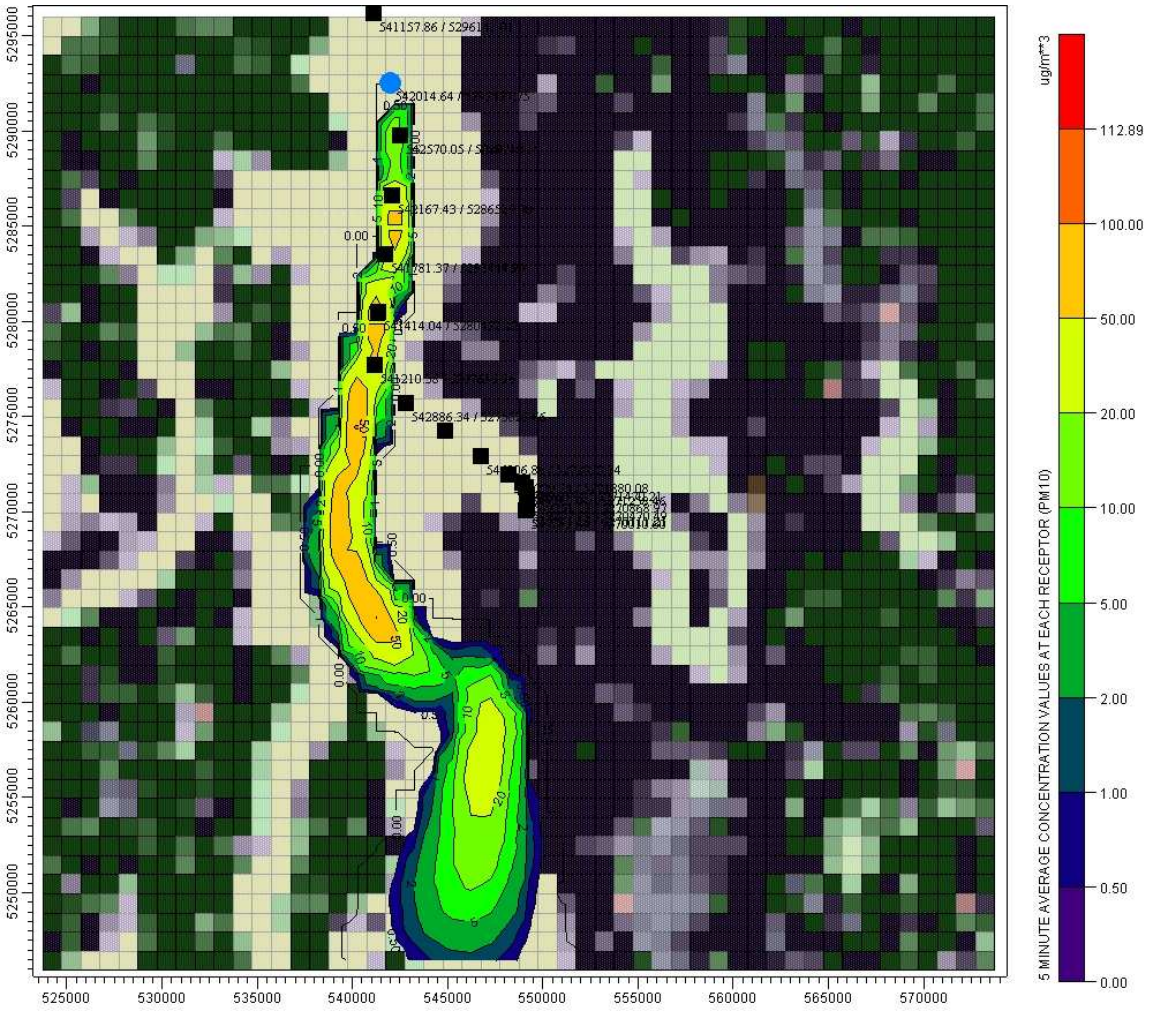

Figure ID	CALPOST Run Period Begins	CALPOST Run Period Ends
S15	July 1, hour 16	July 3, hour 2

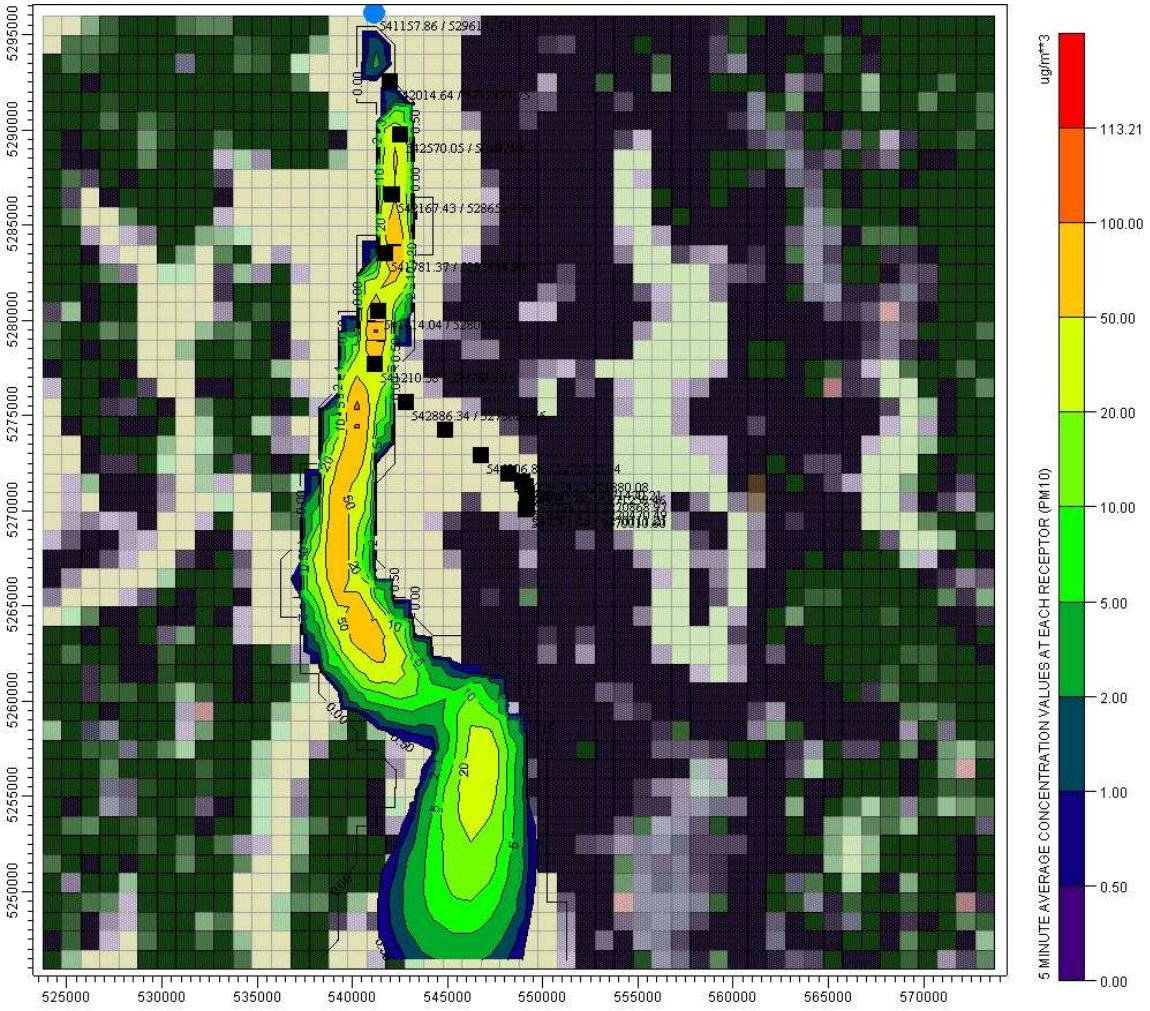

Figure ID	CALPOST Run Period Begins	CALPOST Run Period Ends
S16	July 1, hour 16	July 3, hour 2

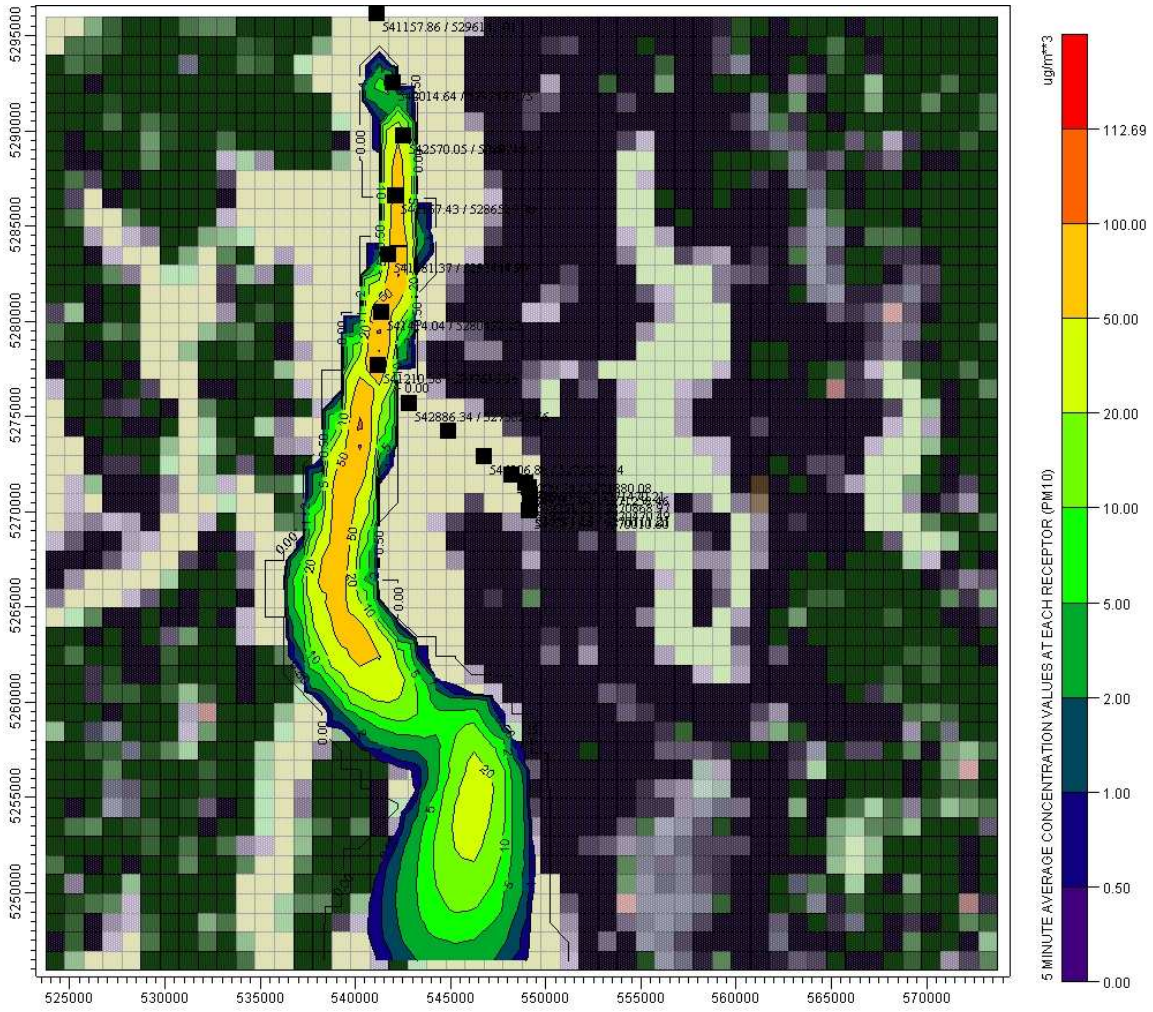

Figure ID	CALPOST Run Period Begins	CALPOST Run Period Ends
S17	July 3, hr 16	July 3, hr 20

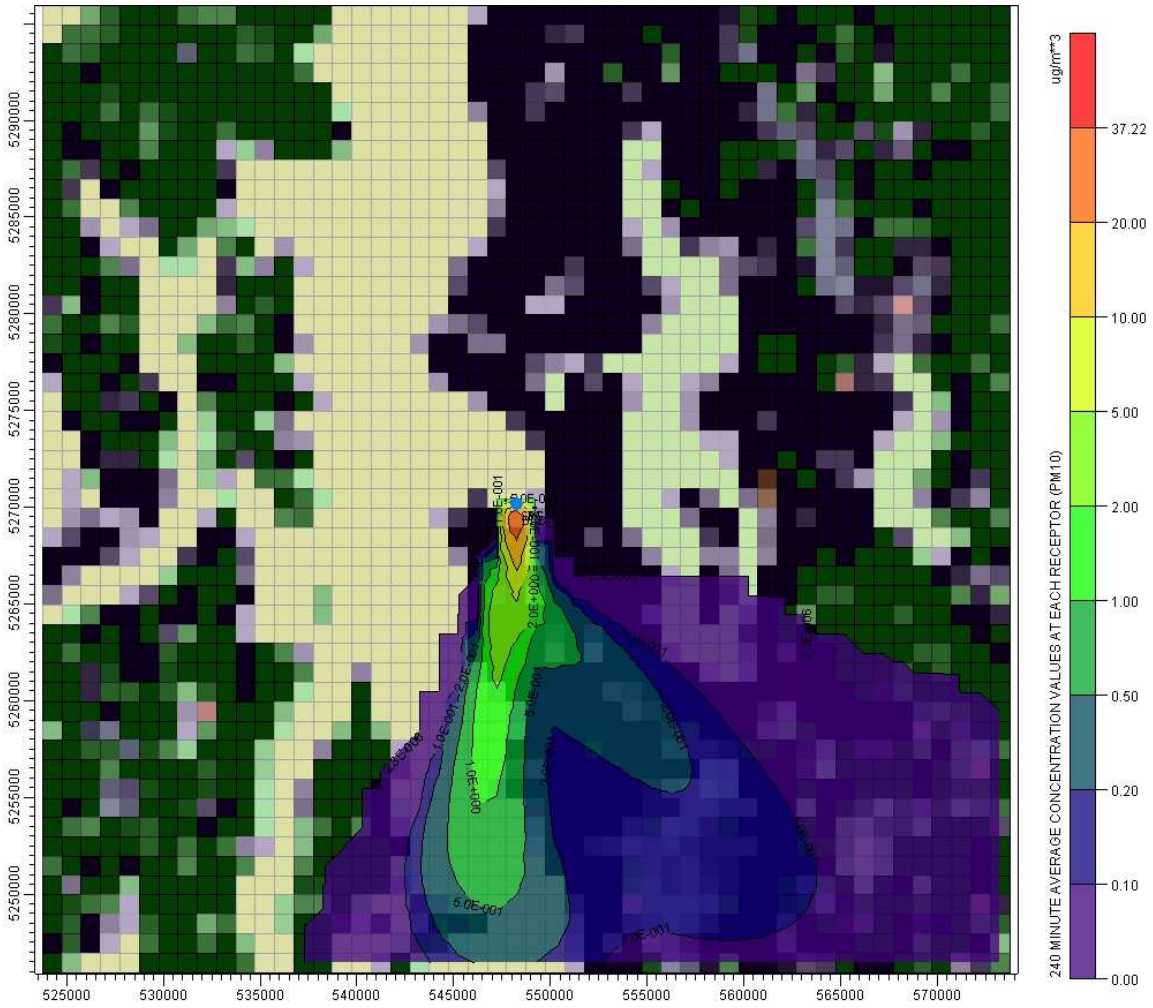

Figure ID	CALPOST Run Period Begins	CALPOST Run Period Ends
S18	July 3, hr 16	July 3, hr 20

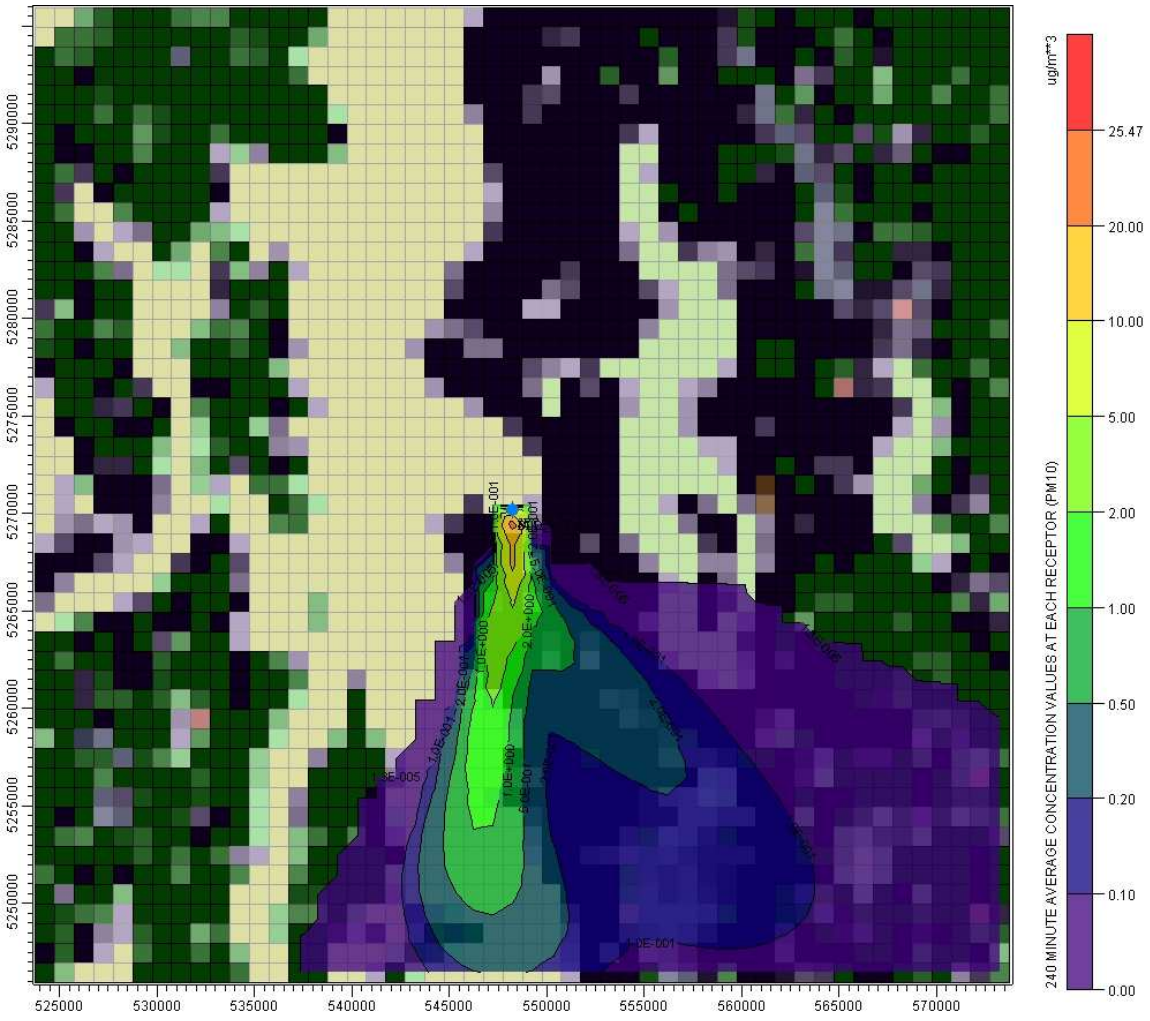

Figure ID	CALPOST Run Period Begins	CALPOST Run Period Ends
S19	July 3, hr 16	July 3, hr 20

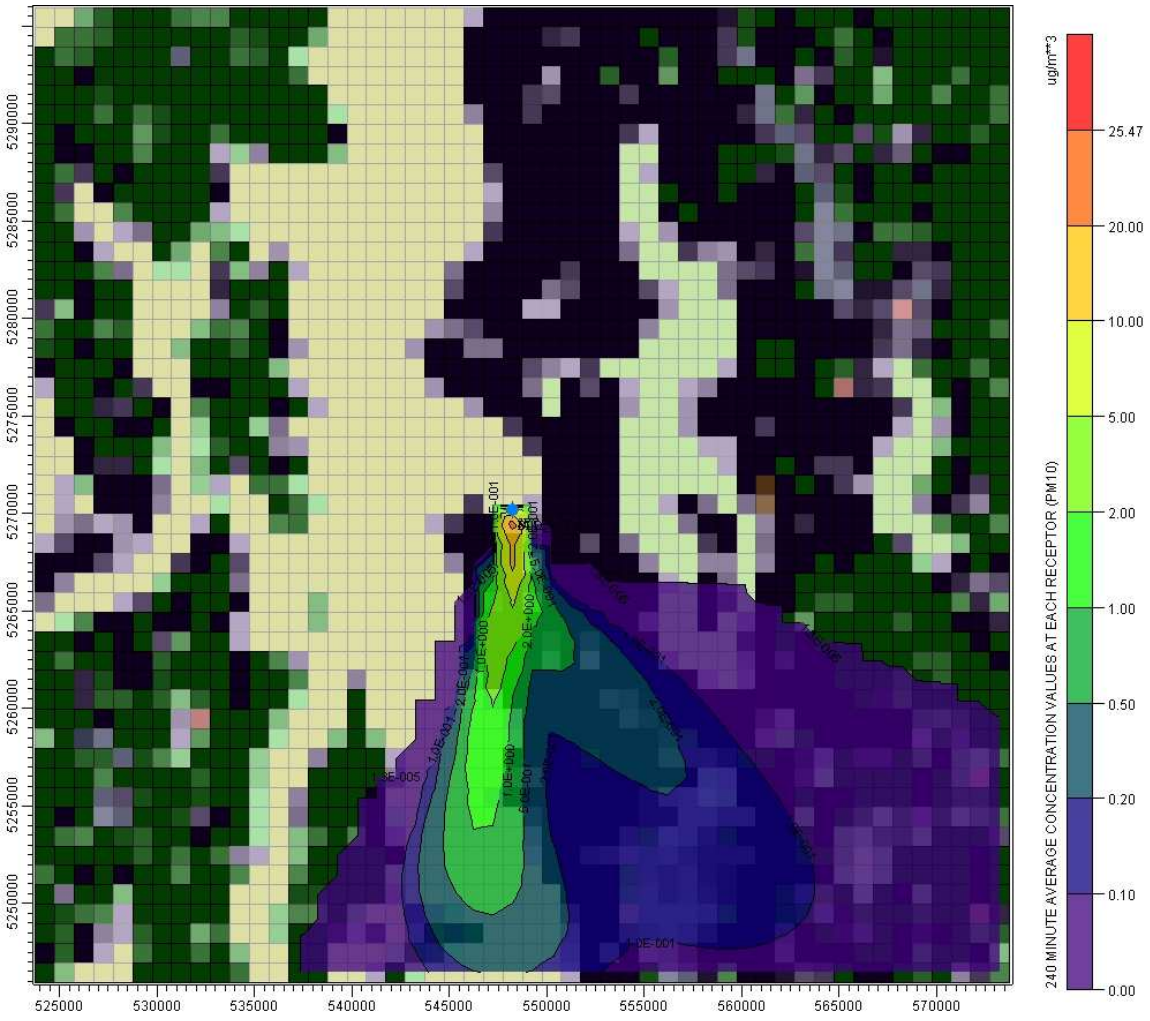

Figure ID	CALPOST Run Period Begins	CALPOST Run Period Ends
S20	July 3, hr 16	July 3, hr 20

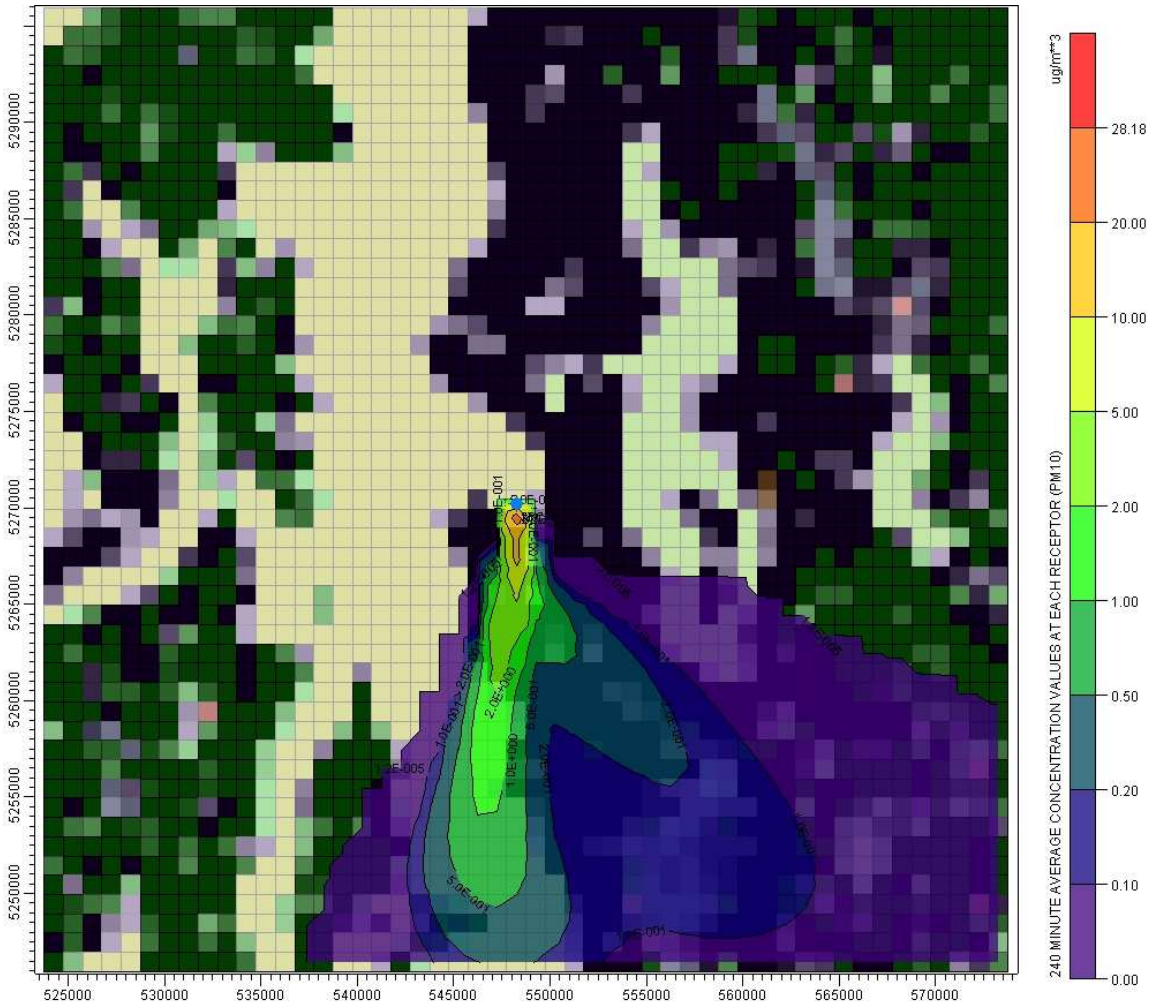

Figure ID	CALPOST Run Period Begins	CALPOST Run Period Ends
S21	July 3, hr 16	July 3, hr 20

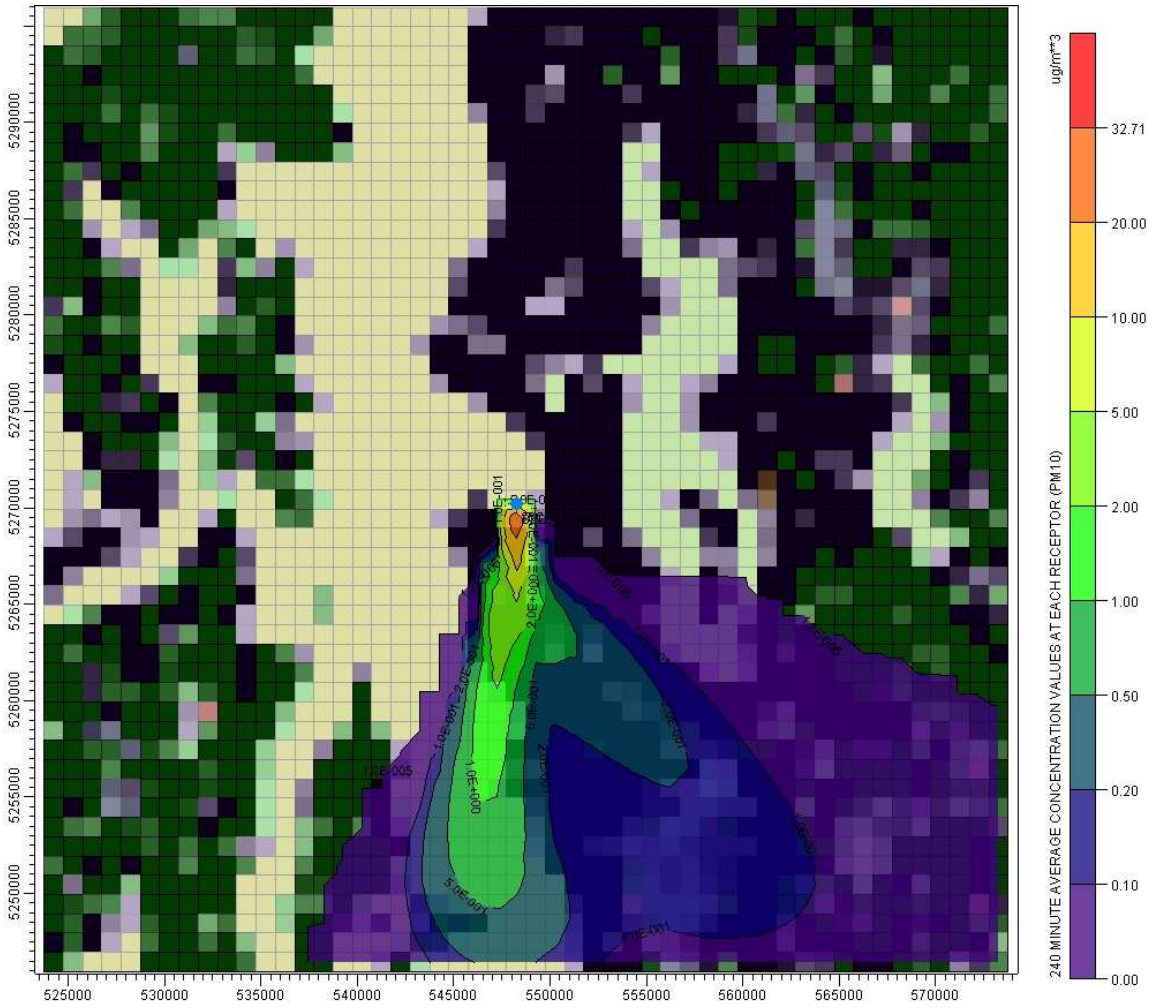

Figure ID	CALPOST Run Period Begins	CALPOST Run Period Ends
S22	July 3, hr 16	July 3, hr 20

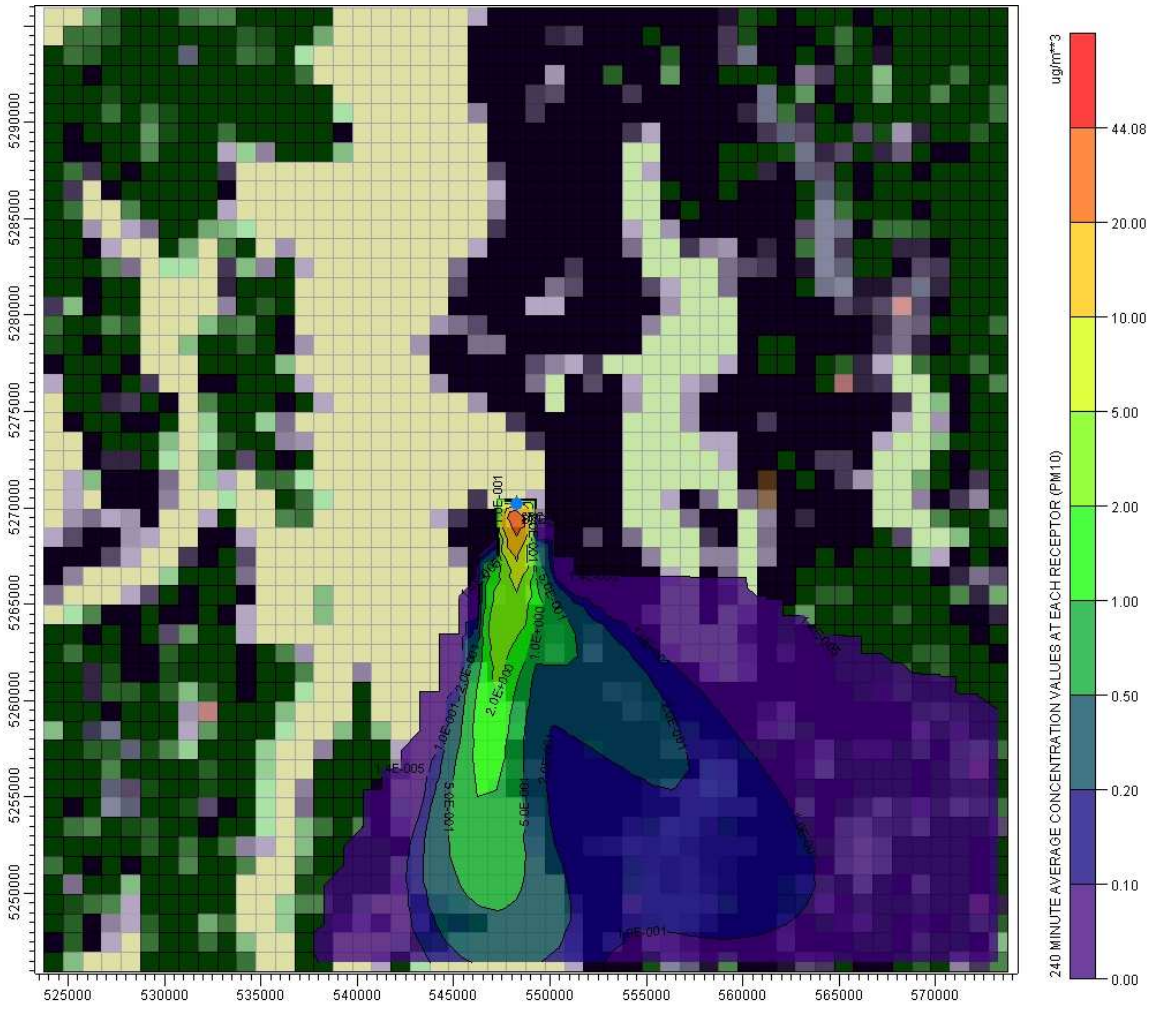

Figure ID	CALPOST Run Period Begins	CALPOST Run Period Ends
S23	July 3, hr 16	July 3, hr 20

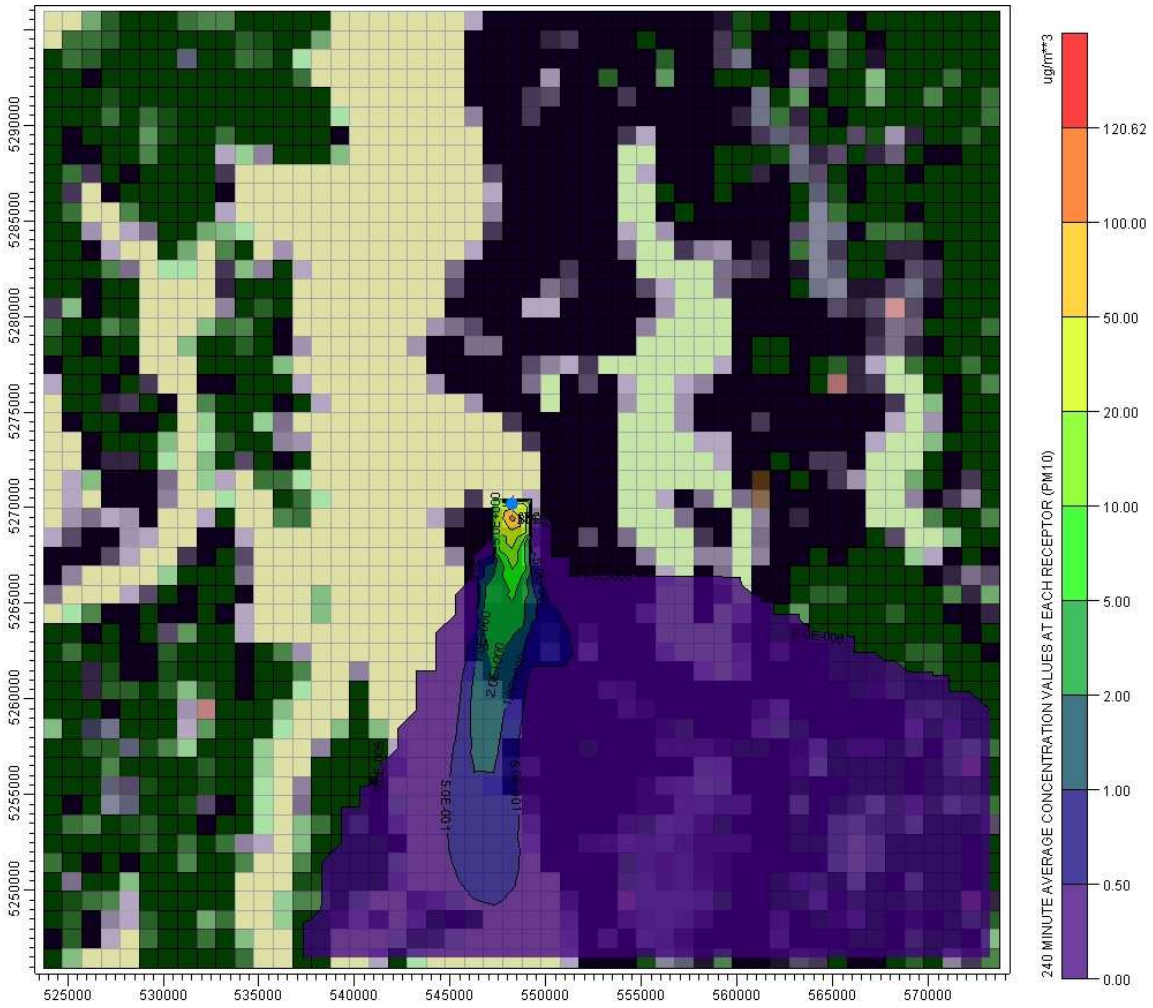

Figure ID	CALPOST Run Period Begins	CALPOST Run Period Ends
A1	Sep 28, hour 16	Sep 30, hour 2

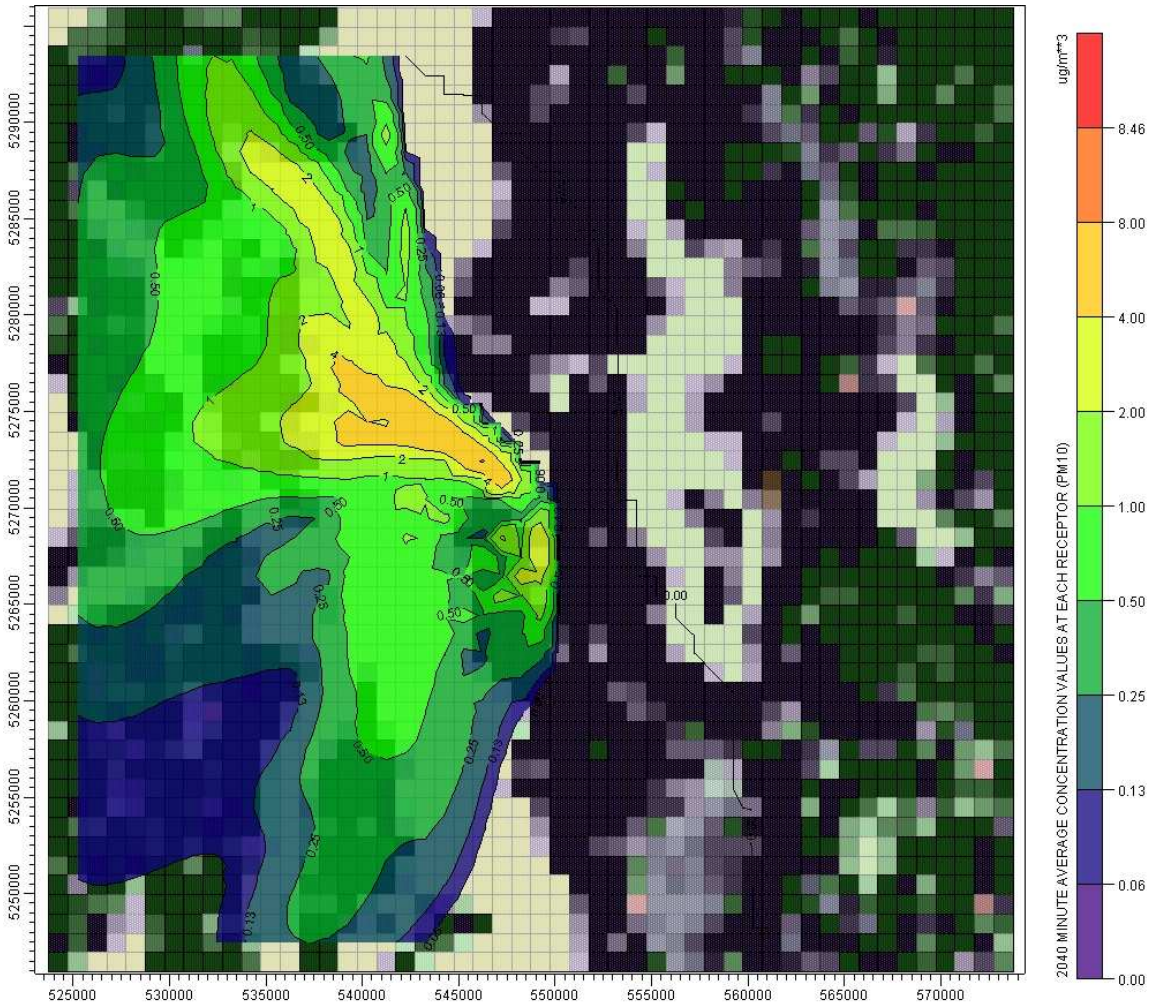

Figure ID	CALPOST Run Period Begins	CALPOST Run Period Ends
A2	Sep 28, hour 18	Sep 30, hour 0

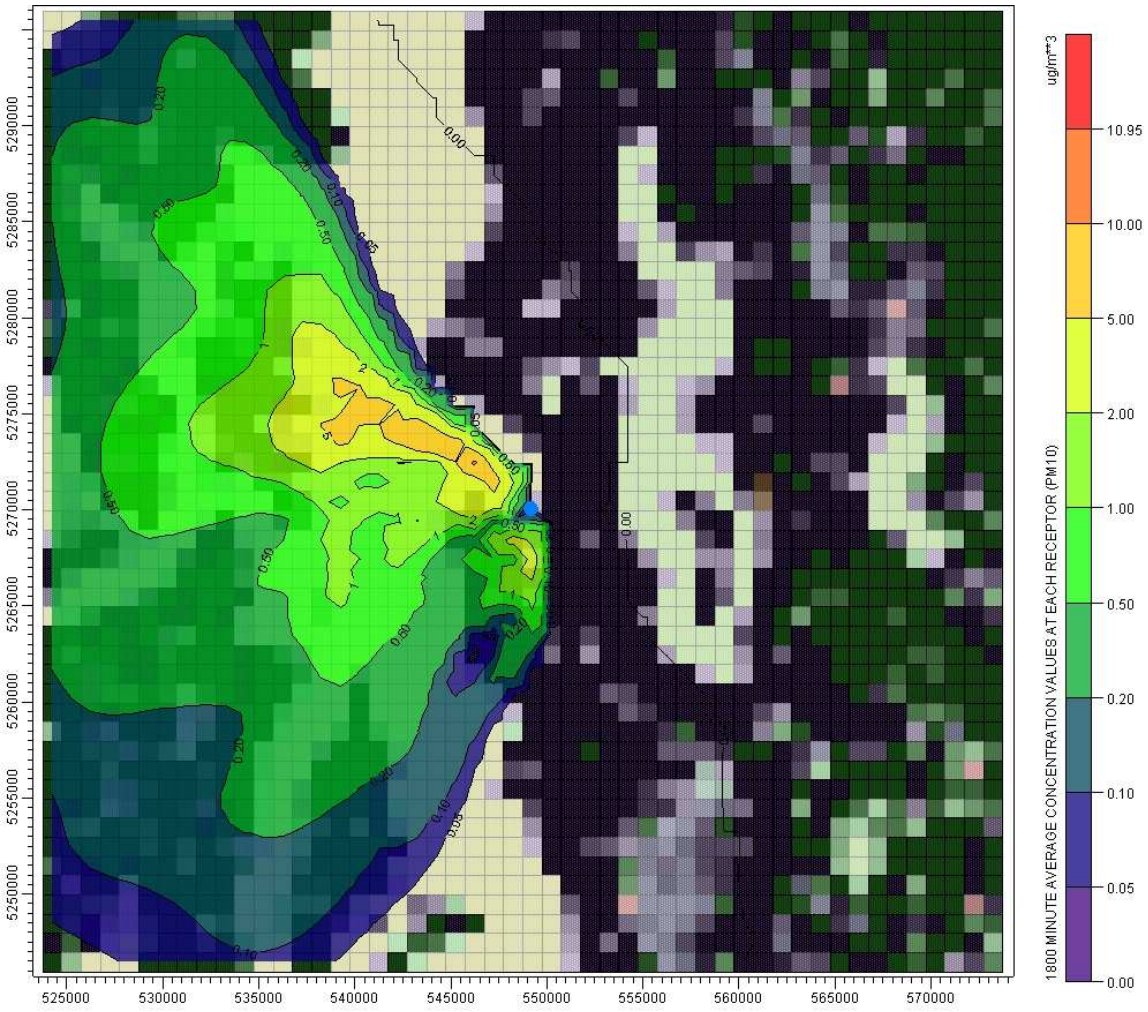

Figure ID	CALPOST Run Period Begins	CALPOST Run Period Ends
A3	Sep 28, hour 18	Sep 30, hour 0

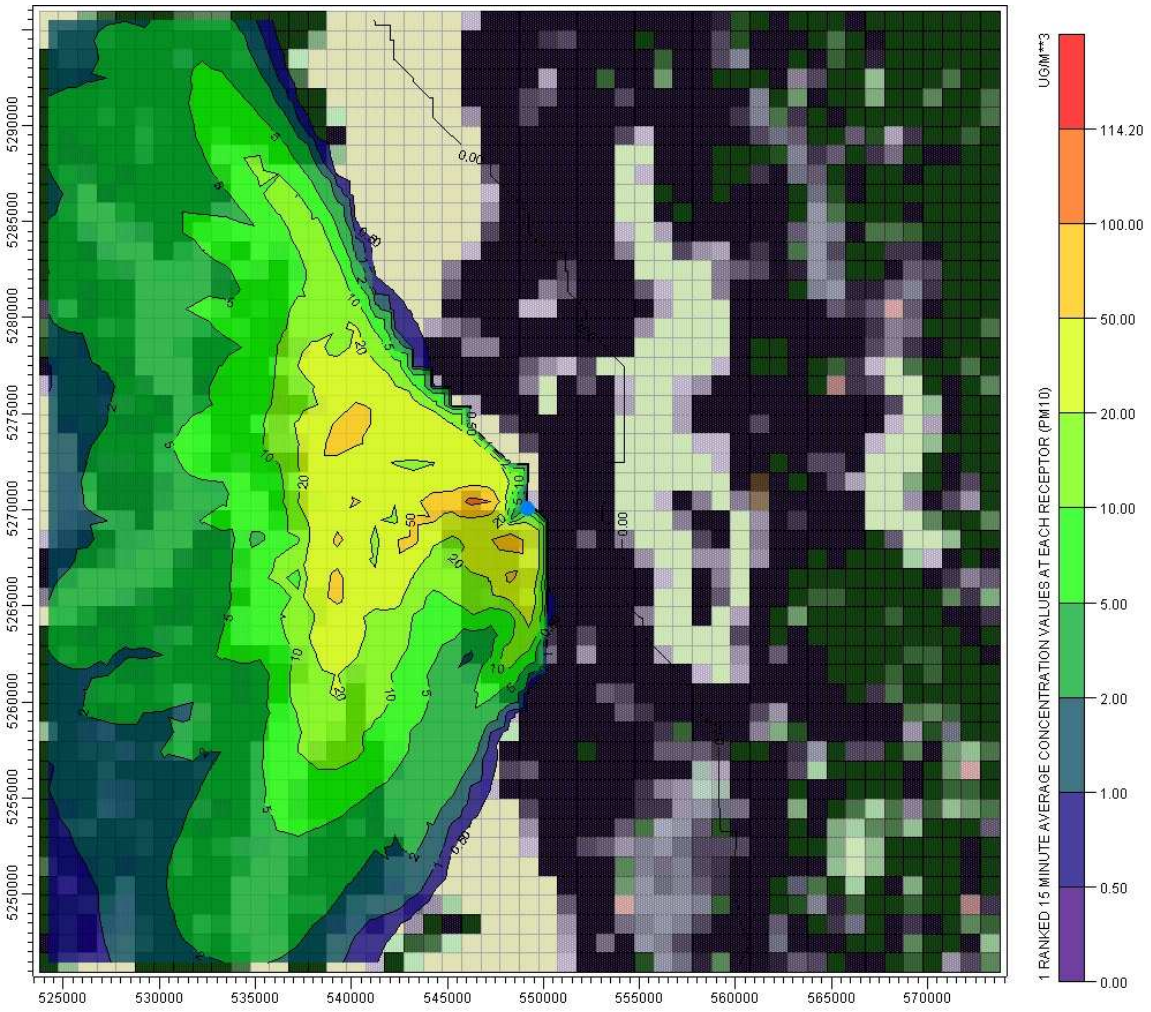

Figure ID	CALPOST Run Period Begins	CALPOST Run Period Ends
W1	Jan 16, hour 17	Jan 18, hour 2

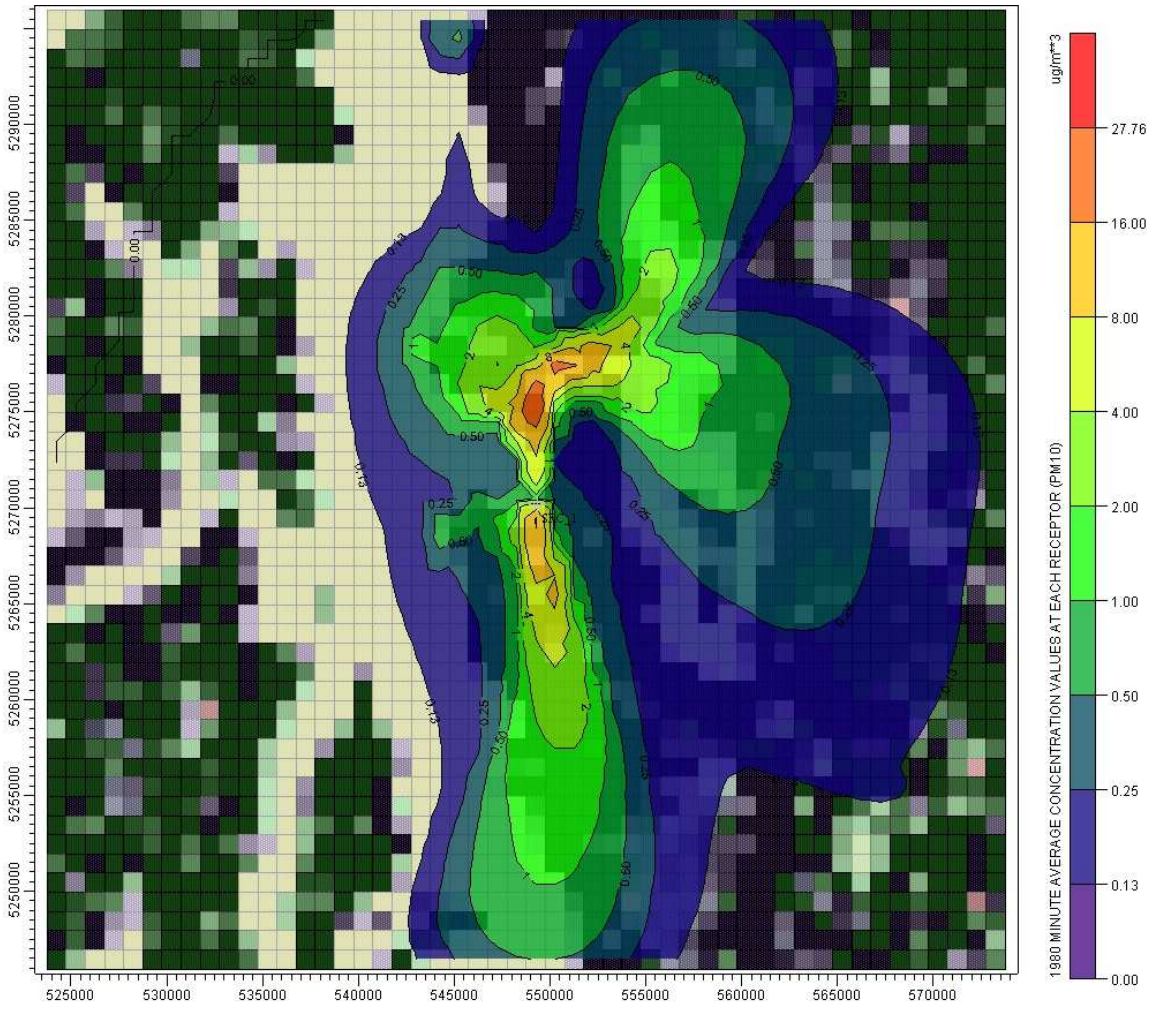

Figure ID	CALPOST Run Period Begins	CALPOST Run Period Ends
W2	Jan 16, hour 19	Jan 18, hour 0

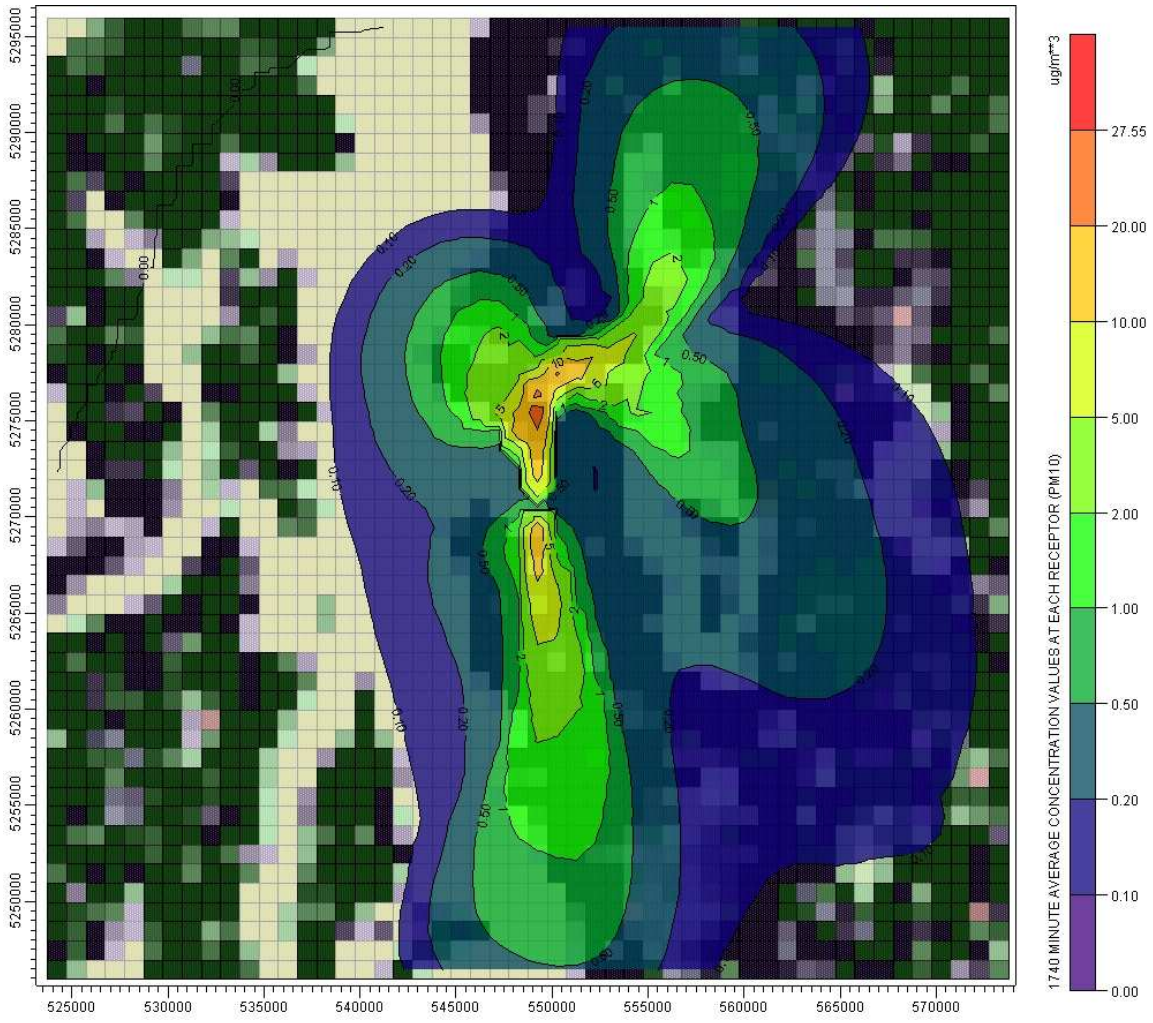

Figure ID	CALPOST Run Period Begins	CALPOST Run Period Ends
W3	Jan 16, hour 19	Jan 18, hour 0

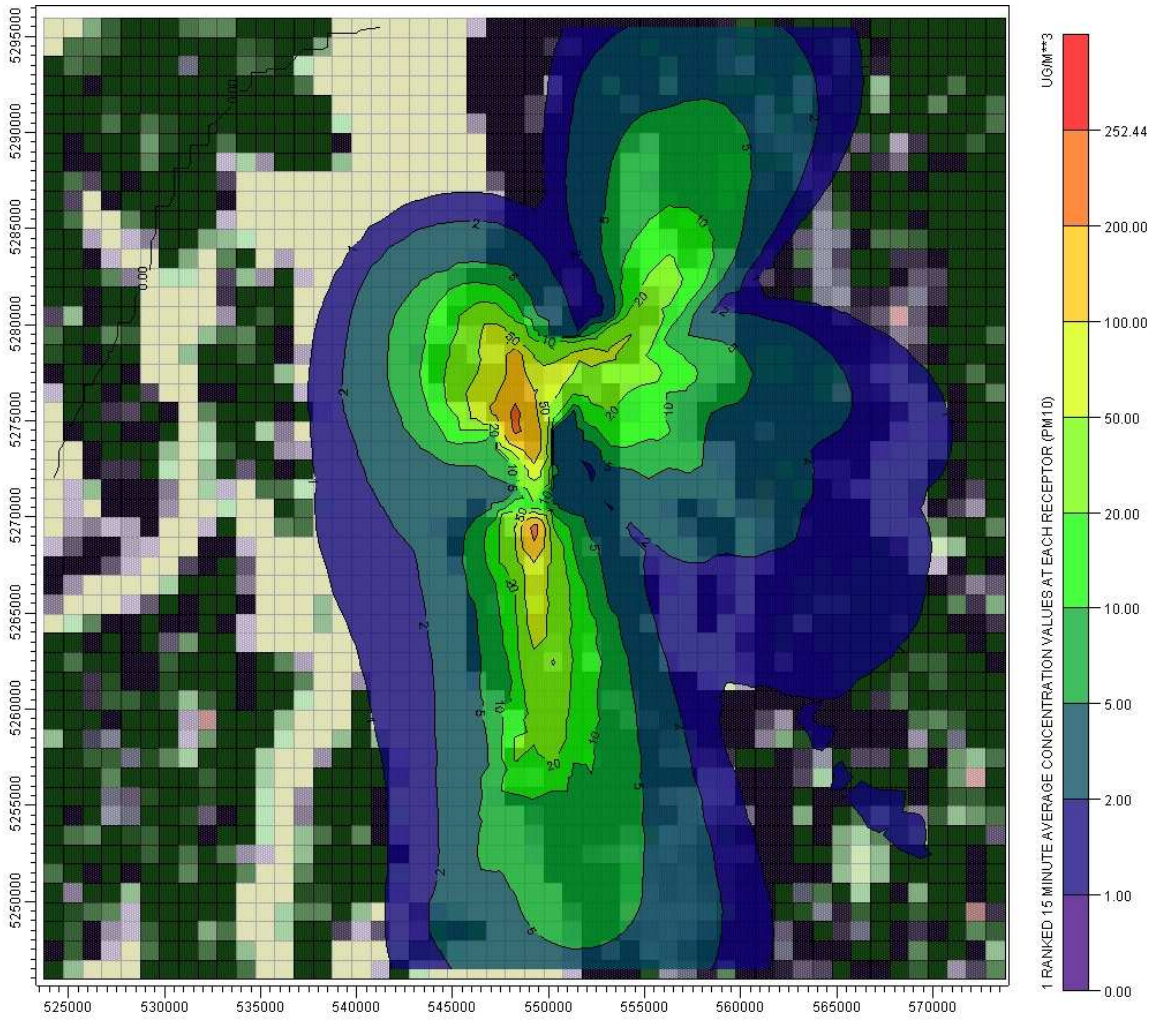

Figure ID	CALPOST Run Period Begins	CALPOST Run Period Ends
W4	Jan 16, hour 12	Jan 16, hour 16

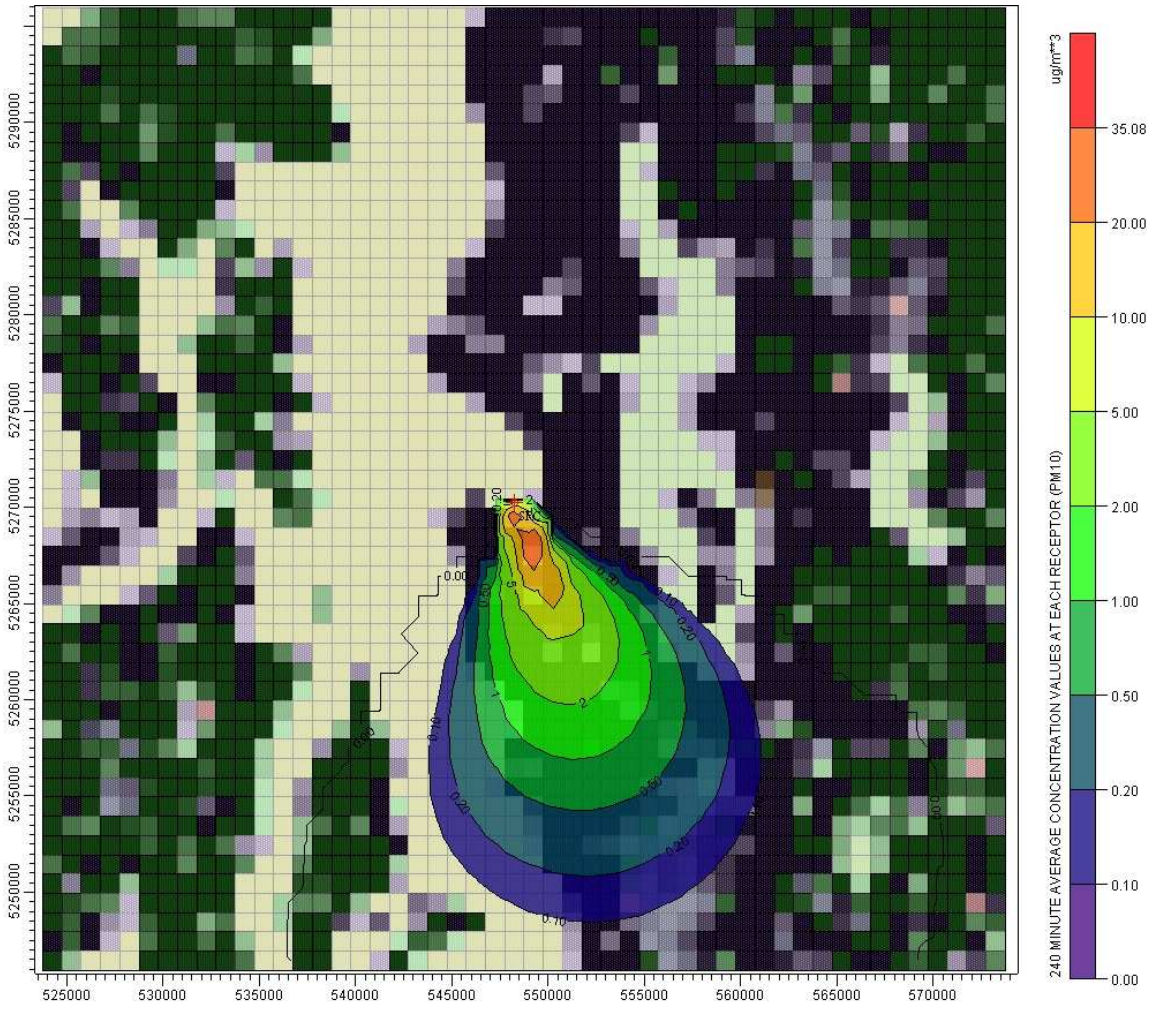

Figure ID	CALPOST Run Period Begins	CALPOST Run Period Ends
W5	Jan 16, hour 12	Jan 16, hour 16

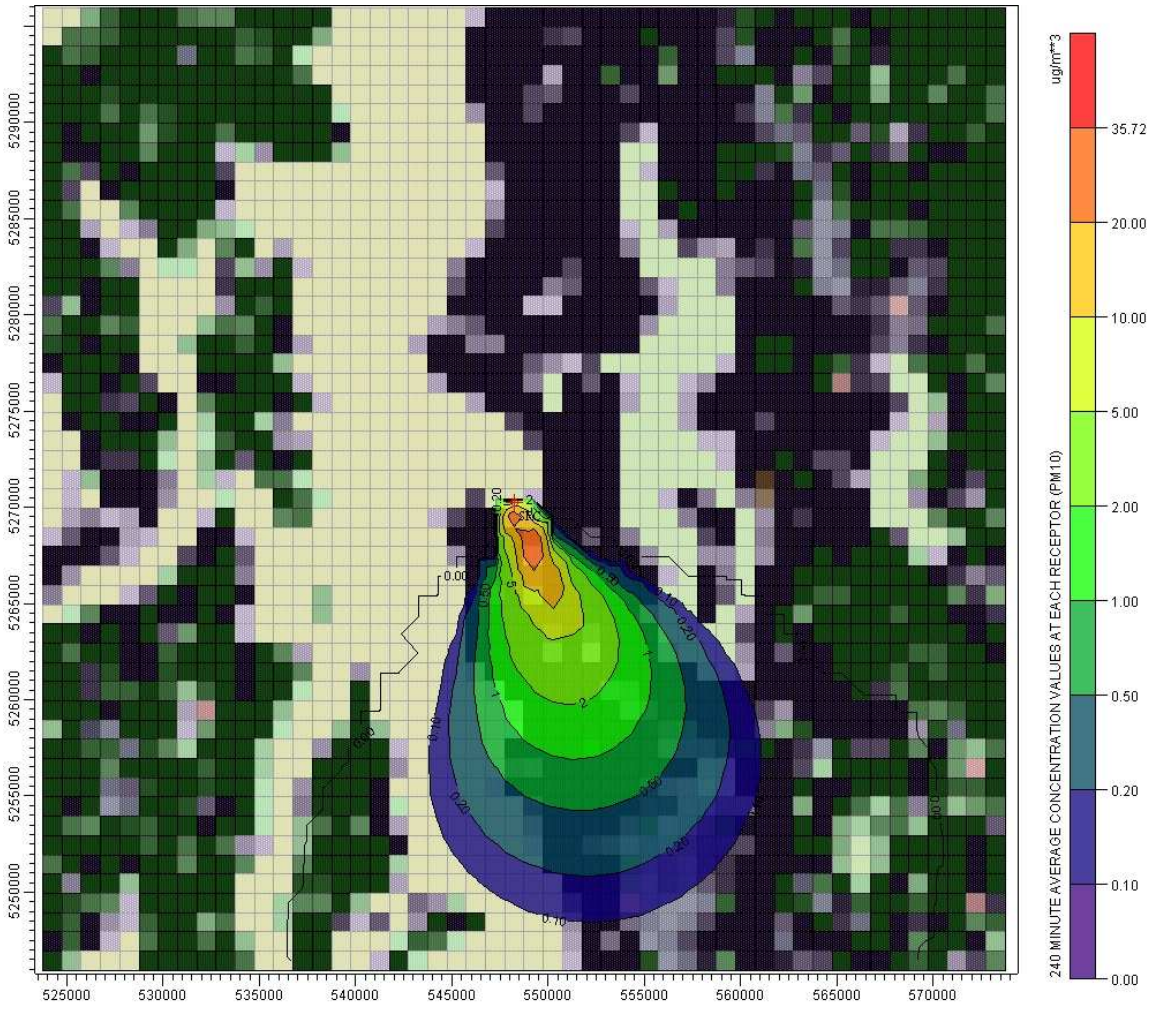

Figure ID	CALPOST Run Period Begins	CALPOST Run Period Ends
W6	Jan 16, hour 12	Jan 16, hour 16

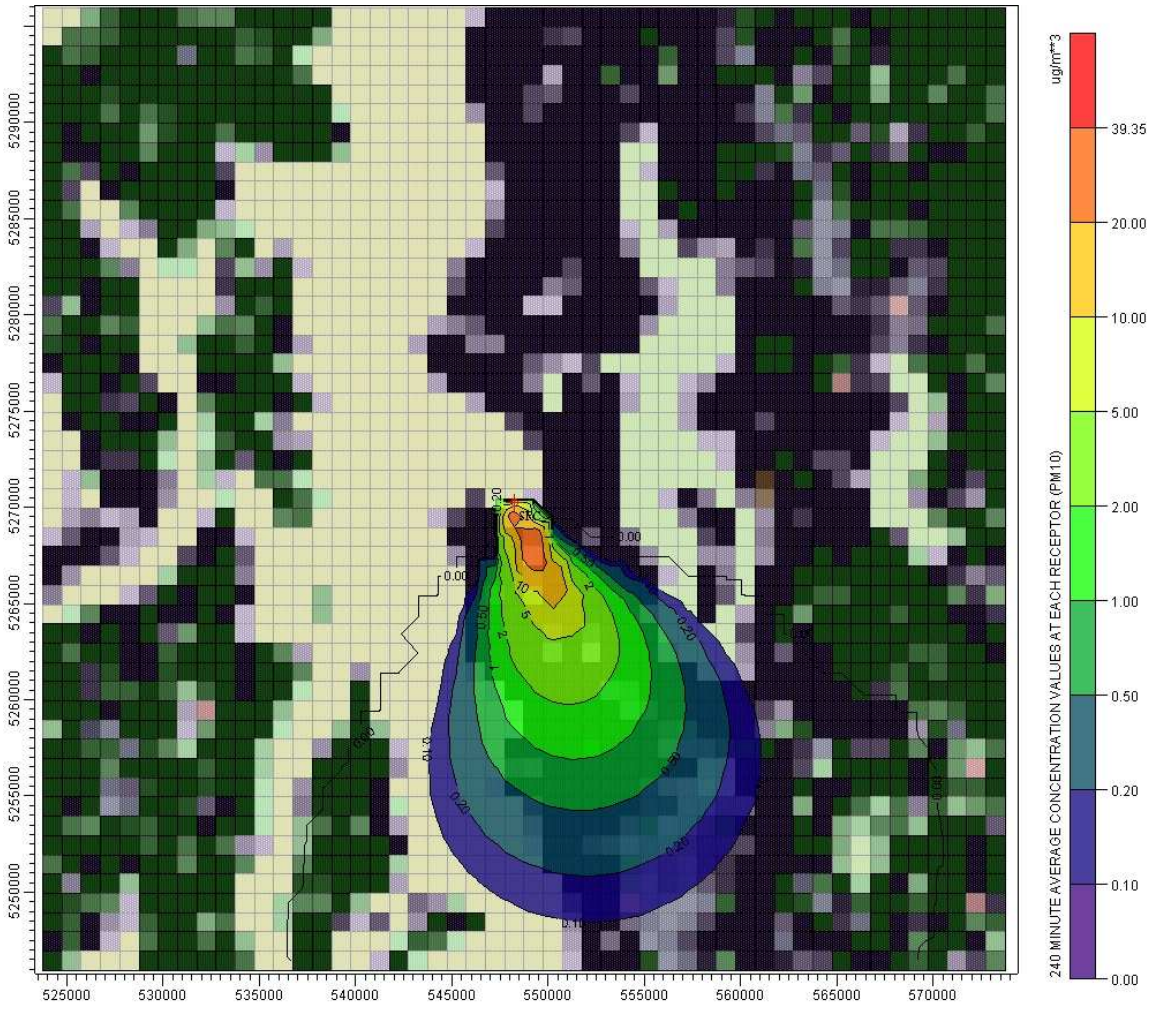

Figure ID	CALPOST Run Period Begins	CALPOST Run Period Ends
W7	Jan 16, hour 12	Jan 16, hour 16

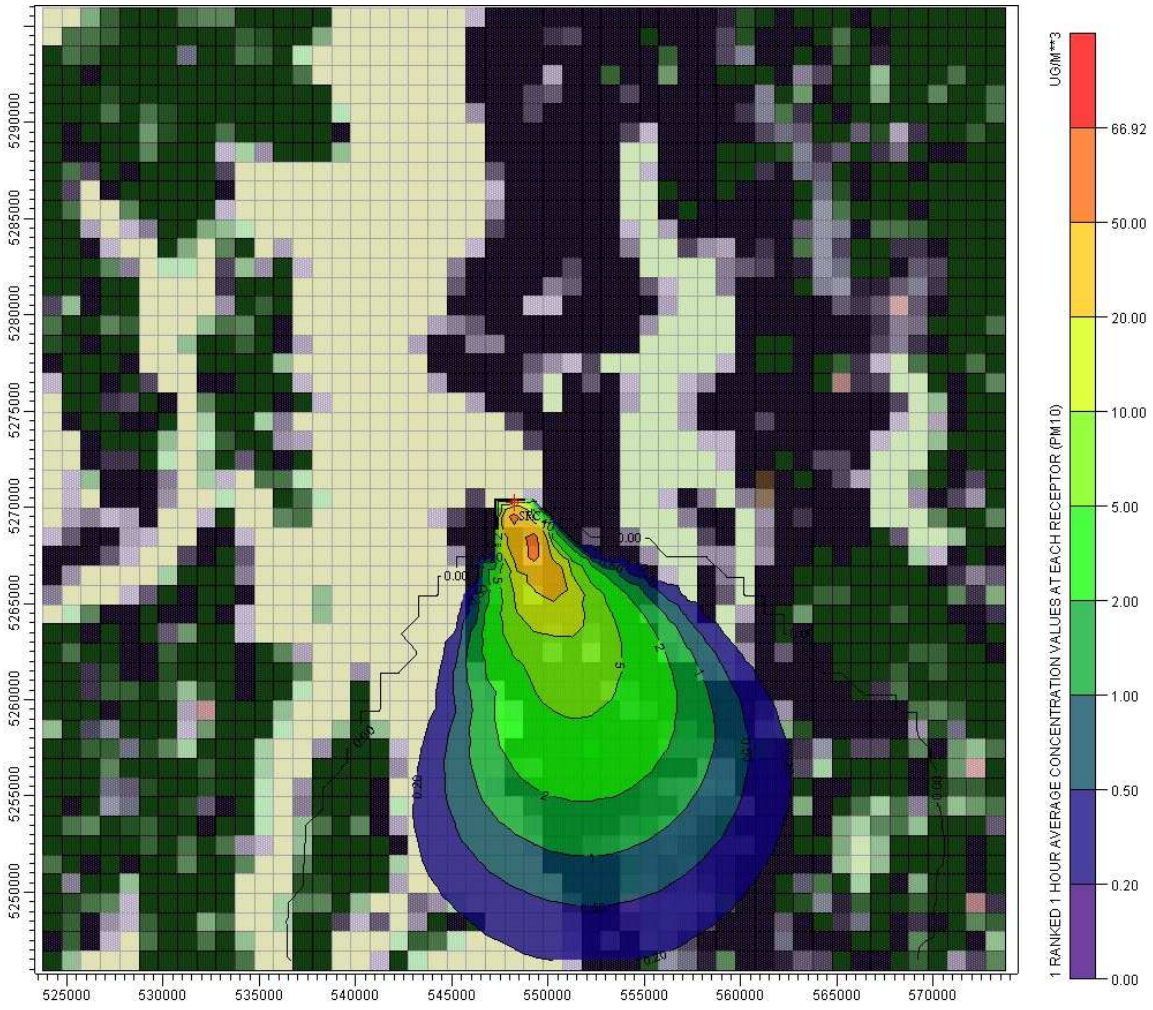

Figure ID	CALPOST Run Period Begins	CALPOST Run Period Ends
W8	Jan 16, hour 12	Jan 16, hour 16

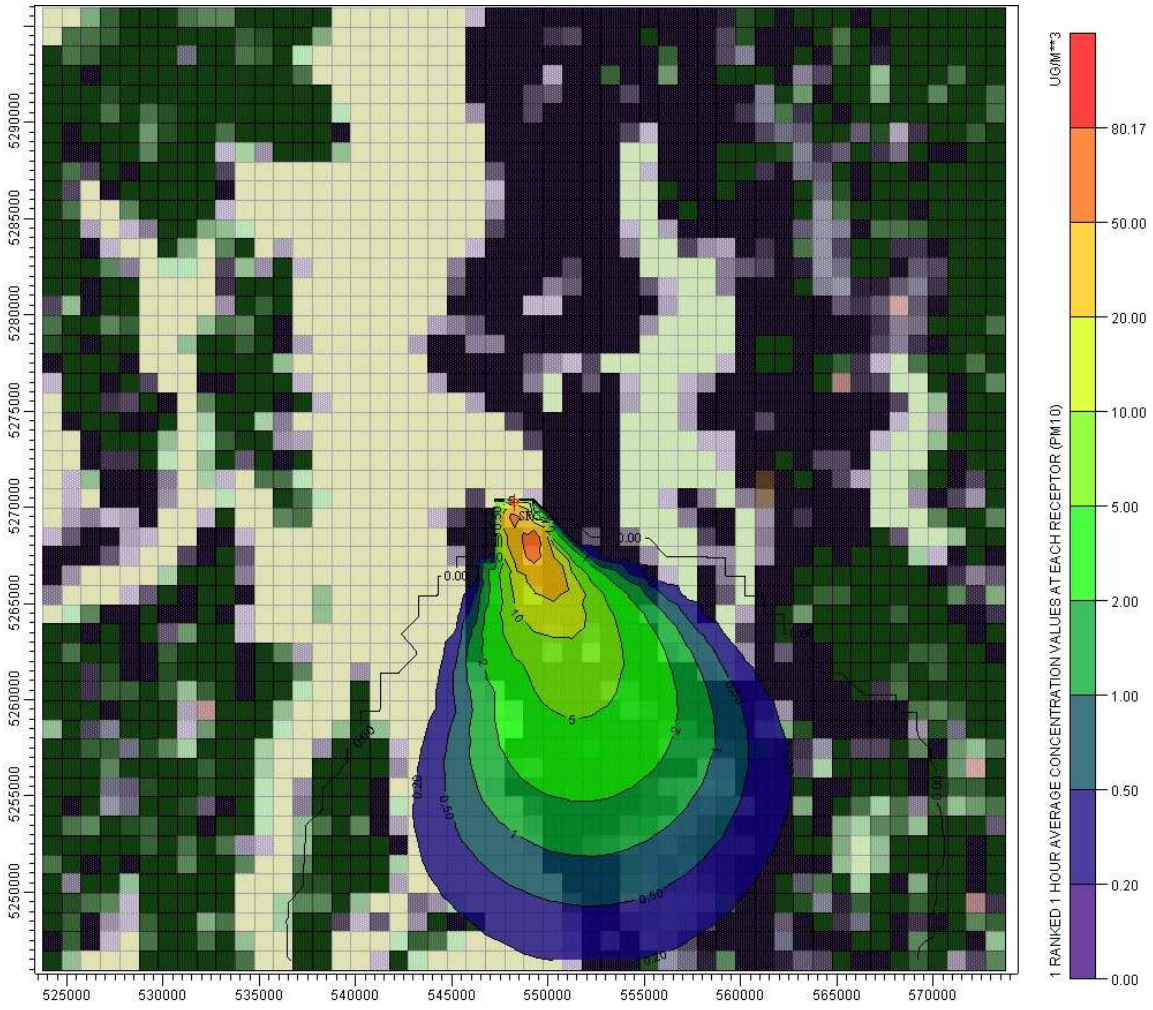

Figure ID	CALPOST Run Period Begins	CALPOST Run Period Ends
SP1	April 23, hour 16	April 25, hour 2

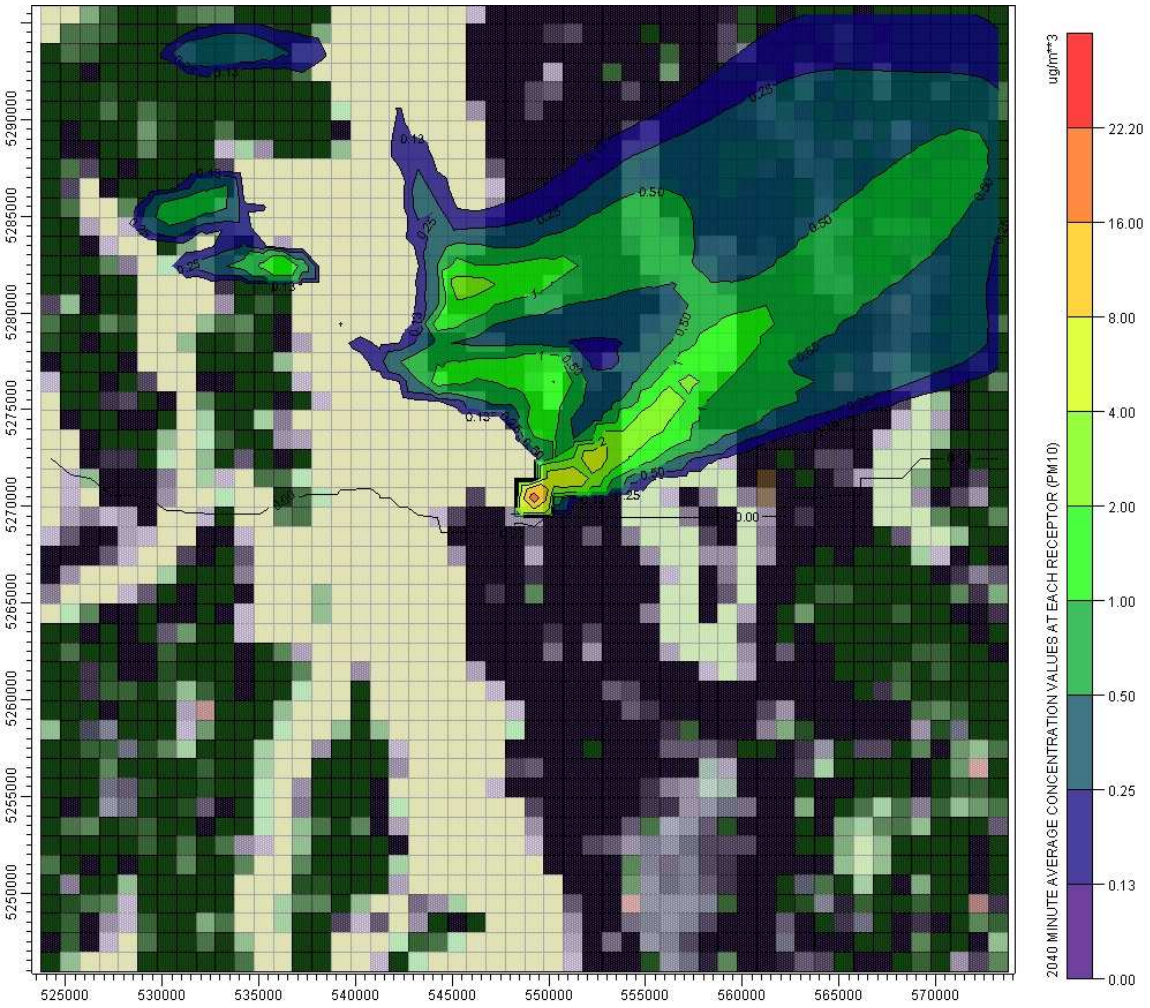

Figure ID	CALPOST Run Period Begins	CALPOST Run Period Ends
SP2	April 23, hour 18	April 25, hour 0

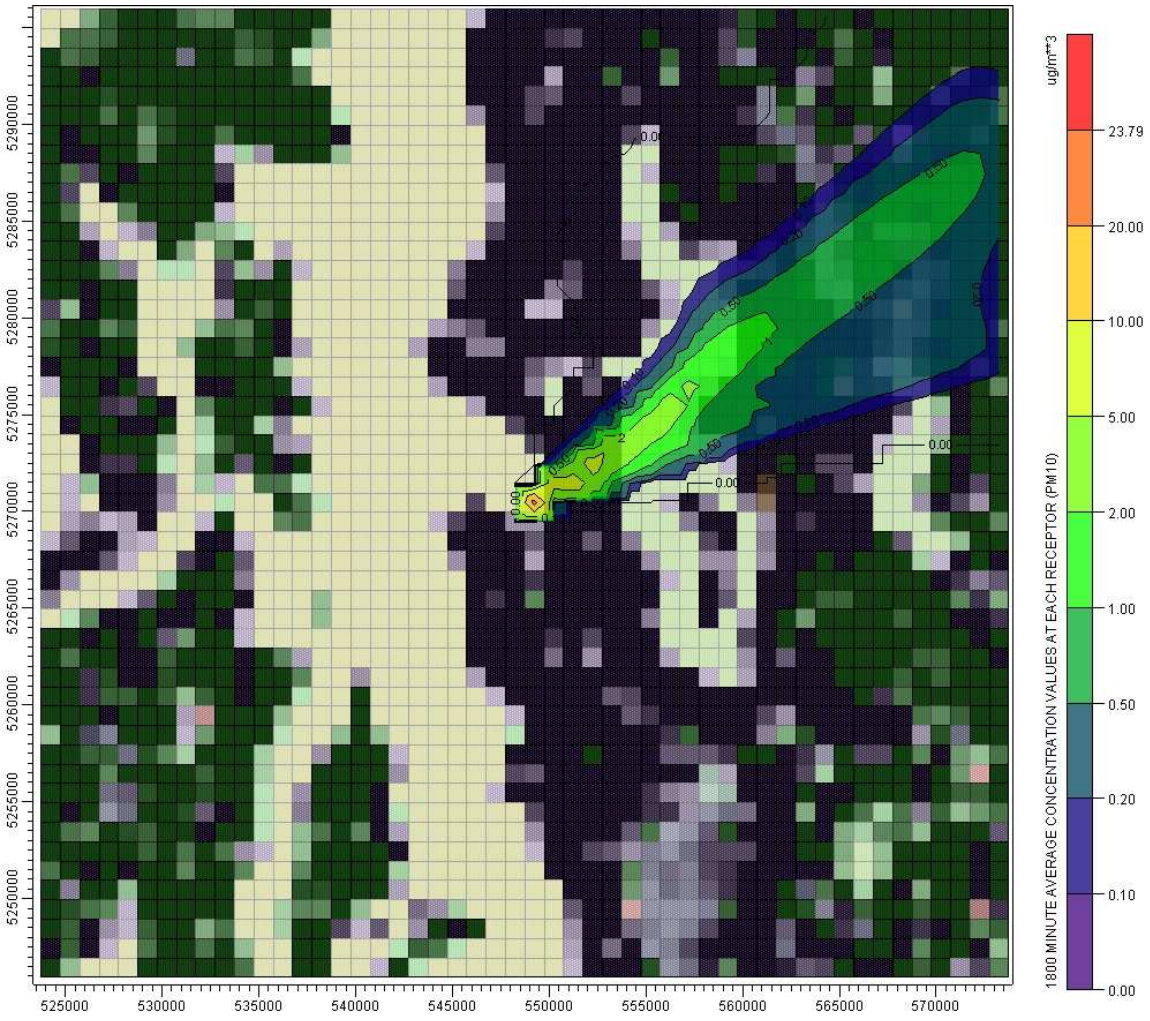

Figure ID	CALPOST Run Period Begins	CALPOST Run Period Ends
SP3	April 23, hour 18	April 25, hour 0

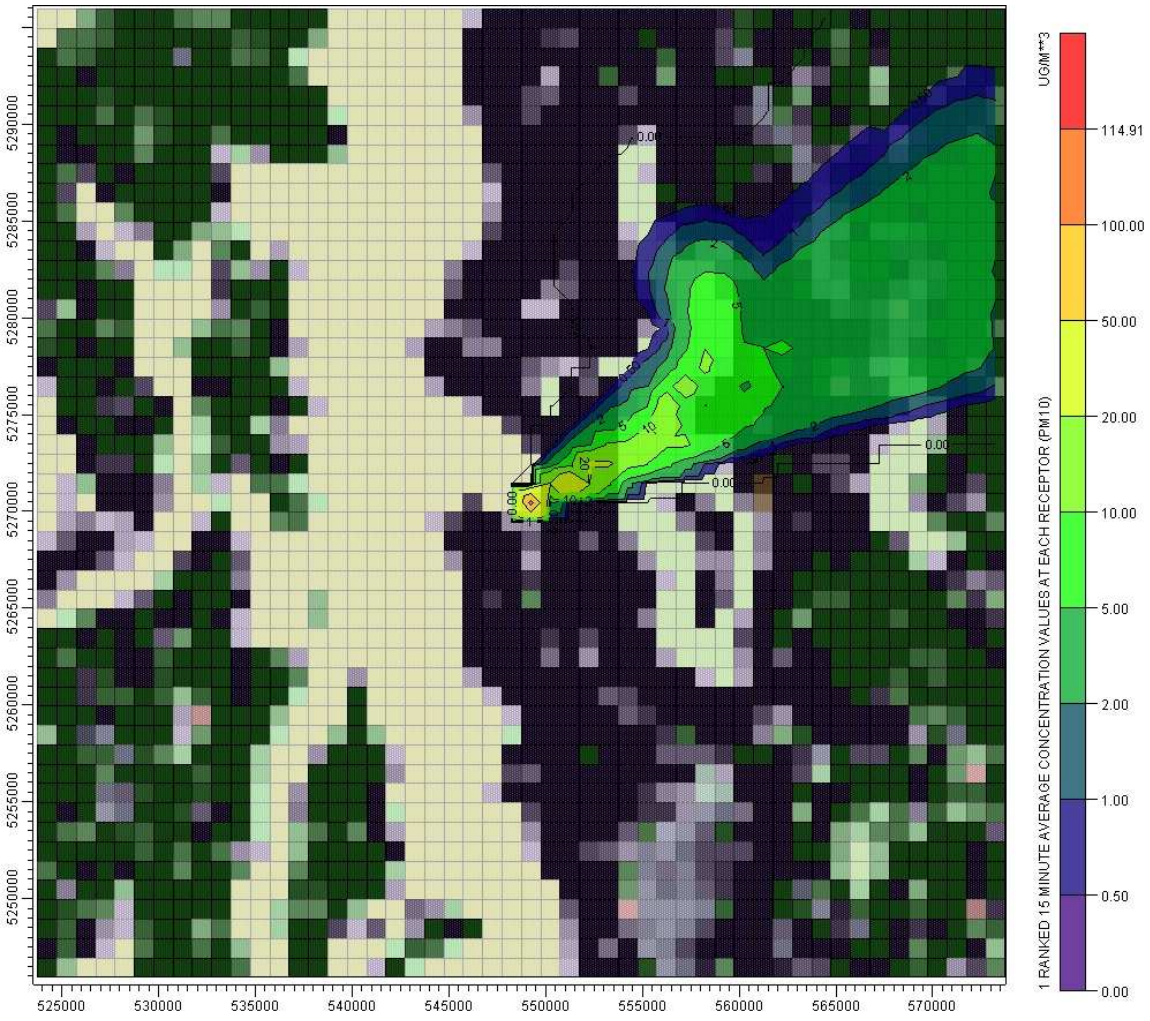

Appendix C: Meteorological Conditions of the Modeling Periods Chosen for Each Season

The following figures display, for each half hour during the CALPOST run periods specified in Figures S1, A1, W1 and SP1, the ambient temperature (color coded), wind speed (color coded), and wind direction at several layers in the atmosphere. The maximum height displayed was set to 2 km, and wind speeds are given in knots. These figures serve to illustrate the ways in which the meteorological conditions were different for each modeling period, and how those conditions changed over time. They were obtained from the National Oceanic and Atmospheric Administration Earth Systems Research Laboratory-Global Systems Division/Meteorological Assimilation Data Ingest System Cooperative Agency Profiler (NOAA ESRL-GSD/MADIS CAP) CAP website (http://www.madis-fsl.org/cap/profiler.jsp), which displays up to date information of several meteorological variables. This particular data was collected by instruments measuring the temperature lapse rate (Radio Acoustic Sounding System (RASS)) and wind profiles in the Seattle area (Sand Point) at the following GPS coordinate: Lat: 47.69 N, Long: 122.26 W, Elevation: 11 m.

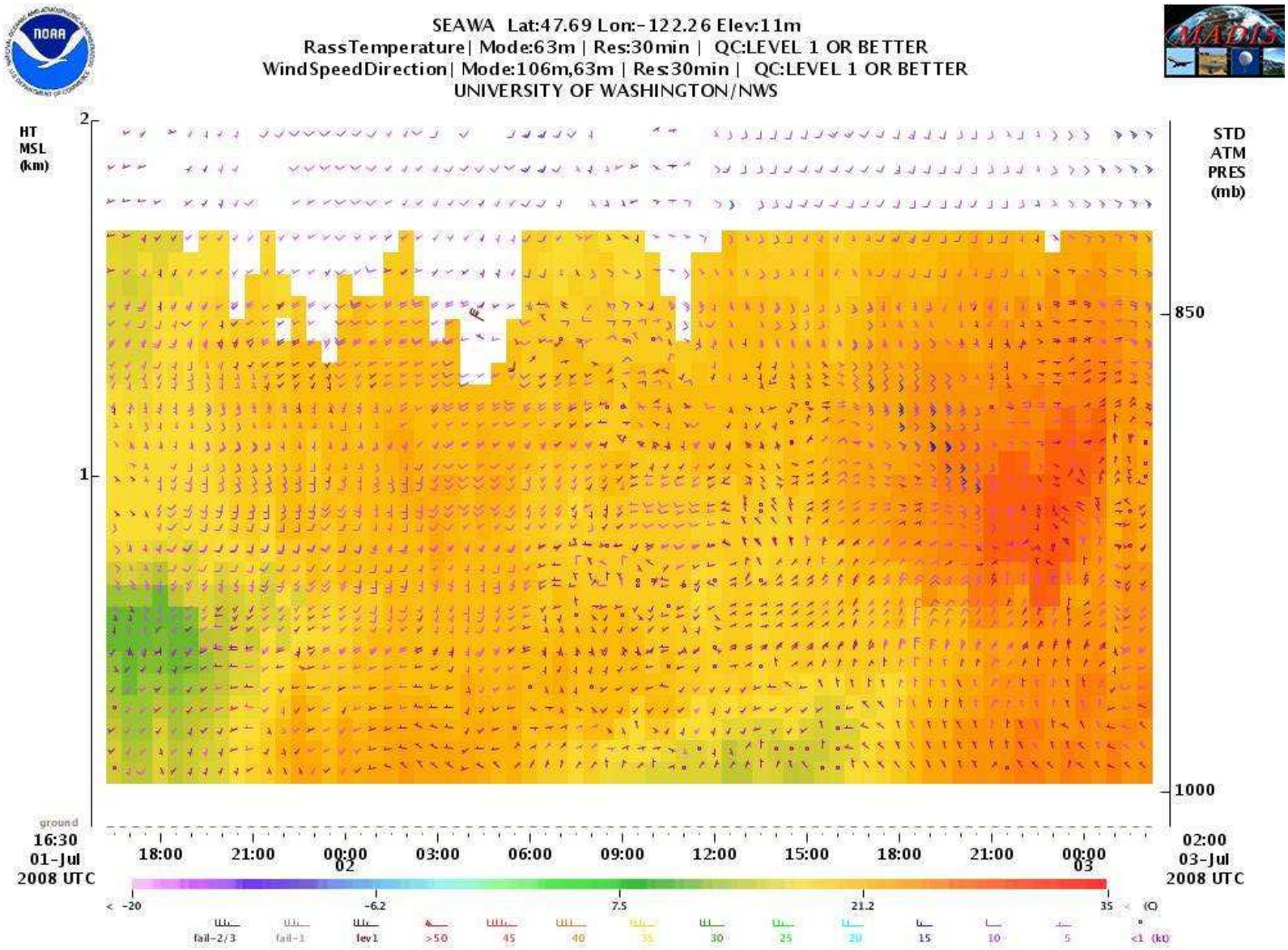

Summer Run (Pertains to Figure S1)

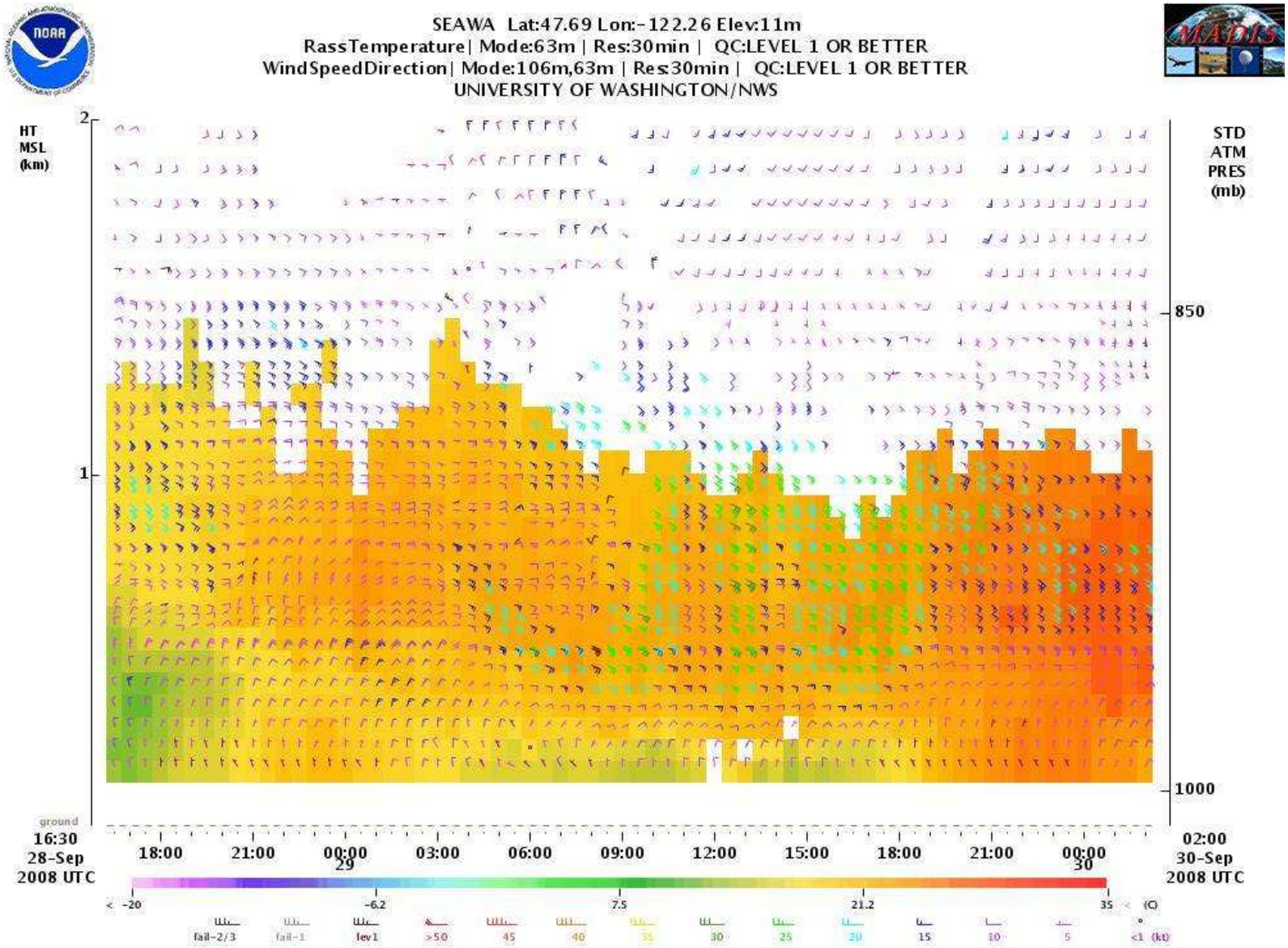

Autumn run (Pertains to Figure A1)

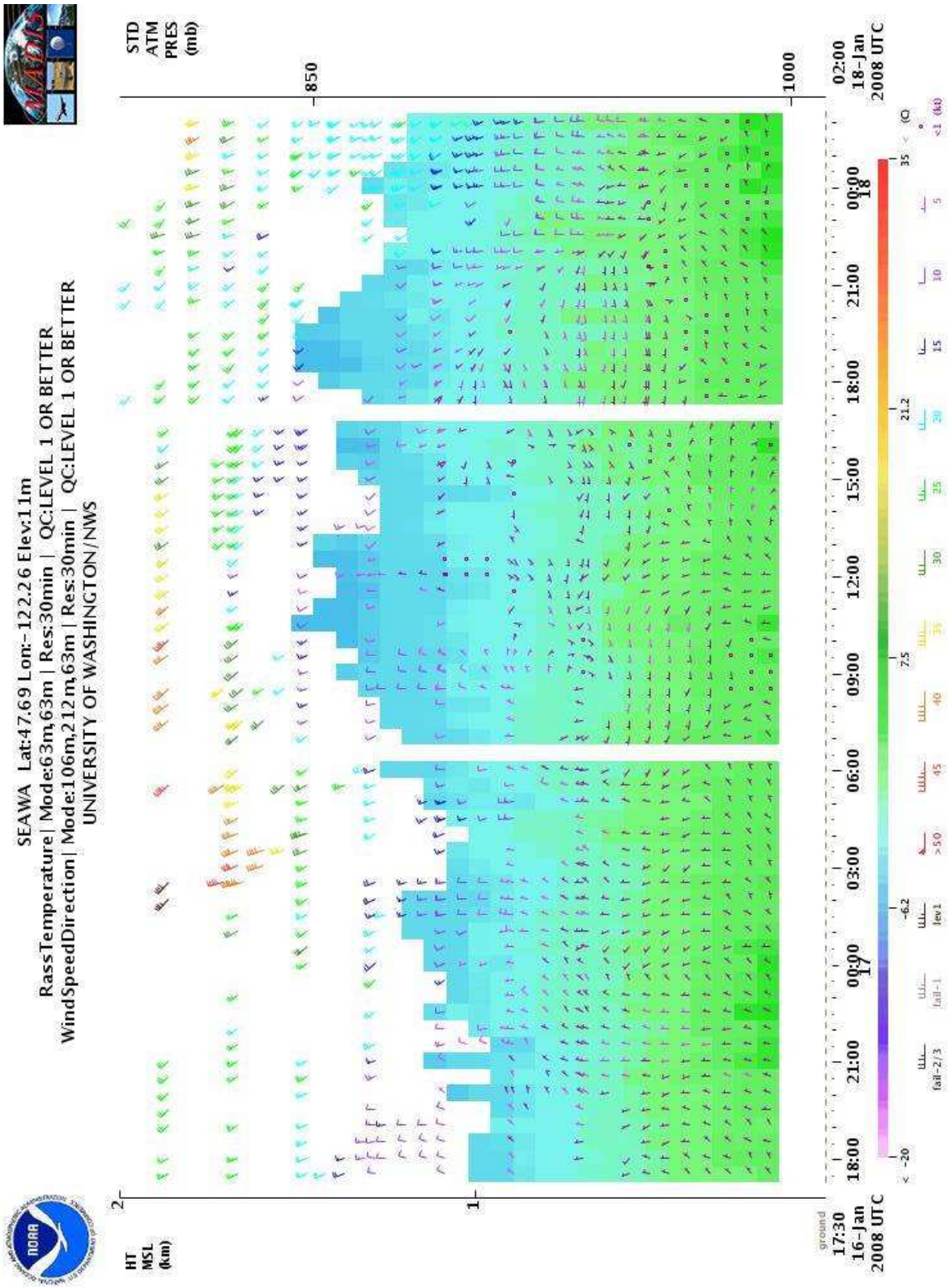

Winter Run (Pertains to Figure W1)

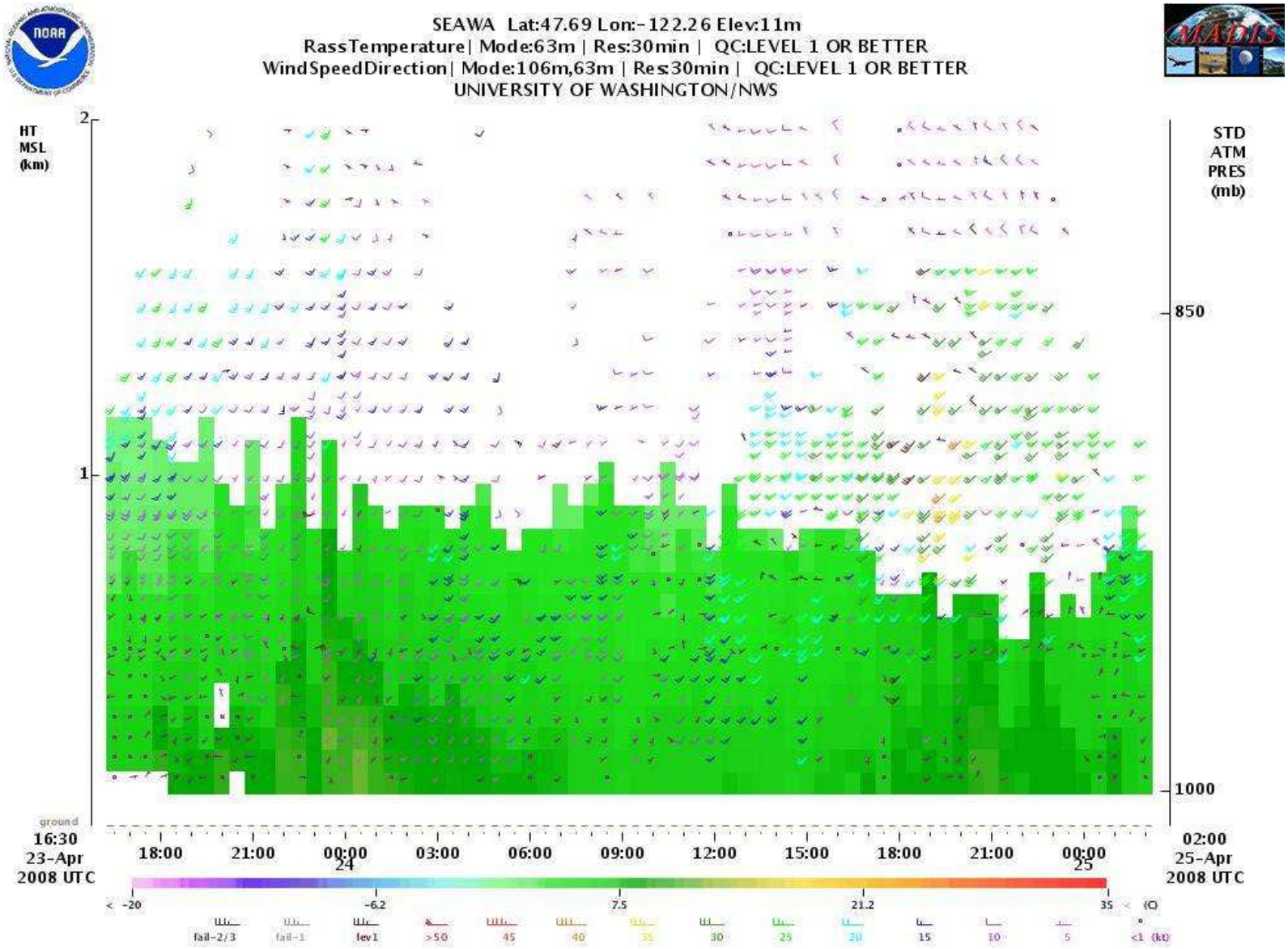

Spring Run (Pertains to Figure SP1)